Investigating the effects of N-methyl-D-aspartate receptor autoantibodies on cortical oscillations *in vitro*

Anaïs Chiara Thouin

Institute of Neuroscience

Newcastle University

Thesis submitted for the degree of Doctor of Philosophy at Newcastle University

January 2017

Abstract

N-methyl-D-Aspartate receptors (NMDARs) play a key role in memory formation and learning, and modulate gamma-frequency oscillations (γ-: 30-80Hz). Gamma-oscillations are important in perception, cognition and memory formation. They are disrupted in patients with schizophrenia, in whom NMDAR hypofunction has been posited, and in animal models of schizophrenia. Furthermore, NMDAR antagonists reduce γ-oscillation power and frequency *in vitro*.

NMDA receptor antibody (NMDAR-Ab) encephalitis recapitulates some of the features seen with blockade or ablation of NMDARs, including anterograde memory loss and psychiatric symptoms.

We hypothesised that patients' autoantibodies against NMDARs could disrupt neuronal network activity and that this may be responsible for the neuropsychiatric symptoms experienced by patients. We examined the effect of acute and subacute NMDAR-Ab exposure on γ-frequency oscillations in the medial entorhinal cortex (mEC), using an *in vitro* rat brain slice preparation. We also performed the first comparison of four different diagnostic assays used for the detection of NMDAR-Abs.

We found that:

1. Cell-based assay using live cells was 100% sensitive but poorly specific in the detection of NMDAR-Abs. Immunohistochemistry was 100% specific and also sensitive (85%). Two cell-based assays using fixed cells produced significant non-specific staining and had intermediate sensitivity and specificity values.
2. Acute exposure to purified IgG from patients with NMDAR-Ab encephalitis reduced the power of γ-frequency oscillations in the mEC but not in the hippocampus.
3. Immunoglobulin deposition was not found in the slices acutely exposed to patient or control IgG.

4. Subacute exposure to IgG by single intracerebral injection of either patient or control IgG did not alter mEC γ-oscillations *ex vivo.* No change in NMDAR-mediated responses was detected.
5. IgG uptake into presumed neurons was detected in slices from these animals, but it was not possible to co-localise the IgG to either excitatory neurones or inhibitory interneurones with certainty.

Acknowledgments

I would like to start by thanking my supervisors, Dr Mark Cunningham and Professor Angela Vincent for the tremendous support they have given me through the last three years and their patience and kindness.

I am also indebted to my post-doctoral and postgraduate colleagues in Newcastle, Drs Georgia Rentesi, Stephen Hall, Natalie Adams, Katherine Newling, Faiza Ben Mabrouk, Anupam Hazra, and (soon to be Dr) Felix Chan for teaching me all I know about electrophysiology, immunohistochemistry, and good lab work generally. Thank you also for being such good friends to me, you were always there when I needed you. Thank you also to my very friendly and efficient undergraduate student Cameron Clemence.

In the lab in Oxford, I am very grateful to Drs Philippa Pettingill, Sukhvir Wright, Theresa Moloney, Inga Konezcky, Leslie Jacobson, Mark Woodhall, Patrick Waters and Miss Sian Peach for their help with immunoglobulin preparations, all the great advice they gave me and the time they spent training me in cell-based assay. I am also indebted to Dr Louise Upton for all her advice and help and her very generous trip to Newcastle to teach me how to perform intracerebral injections. A special thanks to Dr Matteo Gastaldi for his hard work on the CBA/IHC project – it wouldn't have been the same without you. Thank you also to Matteo and Maria-Pia for their kind friendship, which made what would have otherwise been a rather stressful time in Oxford a lot of fun.

A large number of other people very generously gave me their time and allowed me to use their equipment, for which I am very grateful: Drs Gavin Clowry, Andrew Trevelyan, Fiona Le Beau, Gavin Falkous, Trevor Booth, and Claudia Racca.

Finally I would like to thank my family and my husband Adam for their unwavering support and encouragement, and for putting up with me throughout this long and arduous process.

List of Abbreviations

Ab	Antibody
ABC	Avidin-Biotin Horseradish peroxidase complex
AChR	Acetylcholine receptor
ACSF	Artificial cerebrospinal fluid
ADP	Afterdepolarisation
AHP	Afterhyperpolarisation
AMPA	α–amino-3-hydroxy-5-methylisoxaazole-4-propionic acid
ANOVA	Analysis of variance
BBB	Blood-brain barrier
BSA	Bovine serum albumin
CA	Cornu Ammonis
CASPR2	Contactin-associated protein 2
CBA	Cell-based assay
CGP55485	(2S)-3-[[(1S)-1-(3,4-Dichlorophenyl)ethyl]amino-2-hydroxypropyl](phenylmethyl)phosphinic acid
CNS	Central nervous system
DAB	3,3'-diaminobenzidine tetrahydrochloride
D-AP5	D-2-amino-5-phosphonopentanoic acid
DC	Disease control
DC	Direct current
DG	Dentate gyrus
DMEM	Dulbecco's modified Eagle's medium
EC	Entorhinal cortex
EEG	electroencephalogram
EPSC	excitatory Postsynaptic Current
EPSP	Excitatory postsynaptic potentials
Fab	Fragment antibody-binding region

Fc	Fragment crystallisable region
FFT	Fast Fourier transform
GABA	γ–aminobutyric acid
GAD67	Glutamate decarboxylase isoform 67
GluR	Glutamate receptor
HC	Healthy control
HEPES	4-(2-hydroxyethyl)-1-piperazineethanesulfonic acid buffer
HPC	Hippocampus
Hz	Hertz
IgA-M	Immunoglobulin (A-M)
IQR	Interquartile range
ING	Interneuronal network gamma
IPSC	Inhibitory postsynaptic current
IPSP	Inhibitory postsynaptic potential
ivIG	intravenous immunoglobulin
KA	Kainic acid (kainate)
KO	Transgenic knockout
LE	Limbic encephalitis
lEC	lateral entorhinal cortex
LGI1	Leucine-rich glioma inactivated 1
LTP	Long term potentiation
mEC	medial entorhinal cortex
MGluR	Metatropic glutamate receptor
MTL	Medial temporal lobes
NBQX	1,2,3,4,-tetrahydro-6-nitro-2,3-dioxo-benzo[f]quinoxaline-7-sulfonamide
NGS	Normal goat serum
NMDA	N-methyl-D-aspartic acid

NR1/2	
PBS	Phosphate buffered saline
PCP	Phencyclidine
PEI	polyethylenimine
PFA	Paraformaldehyde
PHR	Parahippocampal region
PING	Principal-Interneuronal network gamma
PlEx	Plasma exchange/plasmapheresis
Pt	Patient
PV+	Parvalbumin-positive
R	Receptor
RM ANOVA	Repeated measures ANOVA
sACSF	Sucrose-modified artificial cerebrospinal fluid
sAHP	Slow afterhyperpolarisation
SEM	Standard error of the mean
SD	Standard deviation
TBS	Tris-buffered saline
VGCC	Voltage-gated calcium channel
VGKC	Voltage-gated potassium channel
WT	Wild type

Table of Content

List of Tables

List of Figures

Chapter 1 Introduction

1.1 Antibody-mediated diseases of the central nervous system

Some diseases of the peripheral nervous system are antibody-mediated, and this has been recognised for some time. The role of autoantibodies against acetylcholine receptors (AChR) in myasthenia gravis was established in the 1970's (reviewed in Vincent (2002)), and the experimental approaches used still define the paradigm used to determine the autoimmune basis of a disease. In the 1980's and 90's, pathogenic antibodies to voltage-gated calcium channels (VGCC) and voltage-gated potassium channels (VGKC) and their effects at the neuromuscular junction in Lambert-Eaton myasthenic syndrome and acquired neuromyotonia respectively were described, and similar approaches were used to demonstrate their pathogenicity.

The association of cancer and central nervous system (CNS) syndromes such as encephalomyelitis, cerebellar degeneration or sensory neuronopathy, had been observed since the 1960s and it was clear that they were not related to the primary tumour itself or to its metastases but rather to an as yet unexplained immune response (reviewed in Voltz (2002); and Dalmau and Rosenfeld (2008)). In 1985, Posner and colleagues (Graus *et al.*, 1985) defined the first paraneoplastic antibody, named anti-Hu, directed against a neuronal nuclear antigen. Since then many more paraneoplastic antibodies have been described. Most are directed against intracellular nuclear targets that are ectopically expressed by the patients' tumour. Several lines of evidence, including the intracellular location of the antigen, the failure of passive transfer or active immunisation experiments, and the lack of efficacy of treatments that reduce circulating antibody concentration, counter a pathogenic role for these antibodies. Instead, these antibodies are useful diagnostic markers for paraneoplastic disorders that are felt to be T-cell-mediated (see Dalmau and Rosenfeld (2008) for review). Paraneoplastic limbic encephalitis has been linked in particular with lung cancer (usually small cell lung carcinoma), testicular cancer and breast cancer. The usual paraneoplastic antibodies found in such patients are anti-Hu (mainly lung cancer), anti-Ma/Ta (mainly in testicular cancer patients), ANNA-3 and CRMP-5 (Voltz, 2002).

The recognition of antibody-mediated CNS diseases lagged behind, however, and such disorders were felt to be less common partly because of the immune privilege accorded to the CNS by the blood-brain-barrier (BBB). Up to the beginning of the 21st century subacute non-viral limbic encephalitis (LE) was thought to represent a paraneoplastic syndrome with poor prognosis. However, by then, it was becoming clear that there were cases of non-infectious immune-mediated limbic encephalitis not associated with neoplasms. Bien *et al.* (2000) published a series of four patients with intractable temporal lobe seizures, cognitive and memory deficits, and psychiatric symptoms. They all had changes in one or both medial temporal lobe on MRI as well as lymphocytic infiltrates and astrogliosis on brain biopsy histology. They were hence clinically indistinguishable from paraneoplastic LE. However, they did not have paraneoplastic antibodies and repeated detailed tumour searches were negative. Also, all four improved significantly with immunomodulatory treatment with steroids and/or intravenous immunoglobulin, leading the authors to speculate that a primary or secondary autoimmune mechanism may have caused this non-paraneoplastic LE. The symptoms of LE are summarised in Table 1.1.

Simultaneously, Vincent's team in Oxford in collaboration with neurologists in Bologna asked whether VGKC antibodies were present in Morvan's syndrome (Liguori *et al.*, 2001). This is a condition characterized by peripheral nerve hyperexcitability and consequent neuromyotonia, but also associated with CNS features such as insomnia, hallucinations, confusion and memory loss. As in isolated acquired neuromyotonia, antibodies to voltage-gated potassium channels (VGKC-Abs) are present in some patients with Morvan's syndrome and are thought to be pathogenic (Liguori *et al.*, 2001; Irani *et al.*, 2012). Following the success of plasma exchange in the first patient, and some similarities between symptoms of Morvan's syndrome and LE, they examined whether VGKC antibodies were also present in LE, identifying two patients with high serum VGKC Ab titres. In both cases, improvement in LE symptoms correlated with a decrease in VGKC Ab titre, which resulted from treatment with plasmapheresis in the first patient and occurred spontaneously in the second patient (Buckley *et al.*, 2001).

Shortly thereafter, the same group published a case series of fifteen patients with LE (Pozo-Rosich *et al.*, 2003). Of these, 4 had VGKC Abs, 8 had either anti-Hu or anti-Ma Abs and three had no detectable antibody. Of the 4 patients with VGKC Abs, two had tumours (both lung) and two did not. All the other patients in that study had cancer. Again, the authors found that symptomatology as well as MRI appearances were more likely to improve after immunomodulating treatment if the patient harboured VGKC Ab, particularly in the two patients with non-paraneoplastic LE.

Unlike intracellularly directed onconeuronal antibodies such as anti-Hu or anti-Ma/Ta, the pathogenic potential of VGKC Abs, which were at that time thought to target the VGKC itself, expressed on the cell membrane of neurons, was easier to envisage. Furthermore the reduction in VGKC Ab titre achieved by steroids, plasmapheresis and intravenous immunoglobulin treatments with concurrent improvement in all symptoms of LE suggested a direct role for this autoantibody in the causation of symptoms.

Two further case series confirmed the treatment-responsiveness of VGKC-Ab LE (Thieben *et al.*, 2004; Vincent *et al.*, 2004). In Vincent's (2004) series, the ten cases were non-paraneoplastic. Again, there was improvement in neuropsychological function in line with reductions in Ab titre following treatment.

More recently, it has become clear that most VGKC-Abs are in fact directed against proteins that complex with VGKC *in situ*, most commonly Leucine-rich glioma inactivated 1 (LGI1) and contactin-associated protein 2 (CASPR2) (Irani *et al.*, 2010a). LGI1 antibodies are found predominantly in patients with LE, whilst CASPR2 and Contactin-2 antibodies prevail in neuromyotonia and Morvan's syndrome, although there is some overlap (Irani *et al.*, 2010a).

Subsequently, a number of different antibodies directed against cell-surface antigens have been reported in patients with autoimmune forms of encephalitis, including antibodies against the N-methyl-D-aspartate receptor (NMDAR), the α-amino-3-hydroxy-5-methyl-4-isoxazolepropionic acid receptors (AMPAR), the γ-aminobutyric acid B and A receptors ($GABA_BR$, $GABA_AR$), and glycine receptors. Tumours are found in some of these patients, but much less

frequently than in the classical onconeural paraneoplastic antibodies and the proportions vary for each antibody (Leypoldt *et al.*, 2015).

1.2 Pathogenic mechanisms in autoantibody-mediated diseases

Antibodies, or secreted immunoglobulins (Igs), are produced by plasma cells, B-lymphocytes that have to be activated by exposure to a specific antigen within a pro-inflammatory milieu. They are Y-shaped structures that consist of two identical polypeptide heavy chains (named α, δ, ε, γ, and μ in mammals) and two identical light chains (see Figure 1.1). There are therefore five Ig isotypes with differing biological properties and named according to the heavy chain they contain (IgA, IgD, IgE, IgG and IgM). IgG is the most abundant Ig molecule and exists as four different subclasses (IgG1-4) numbered after their relative abundance in serum. The different IgG subclasses have different complement activating properties and Fc receptor binding affinities. IgM and IgD (which is bound to B-cells) are important in the initial immune response. After B-cell activation, heavy-chain class-switching occurs, allowing production of IgA (mucosal regions), IgE (involved in allergic reactions and parasitic infections) or IgG (serum) without affecting the antigen-specificity.

The heavy and light chains consist of a constant and variable region each. The two antigen binding sites are formed by the combination of the variable regions of the heavy and light chains. Together, they are known as the Fragment antigen-binding region (Fab). The stem of the Y-shaped Ig molecule, consisting only of two heavy chains, is called the Fragment crystallisable region (Fc) and is responsible for triggering effector mechanisms of the immune response, for example by binding to Fc receptors on effector cells or triggering the complement system.

Autoantibodies can cause tissue damage and functional changes by several different mechanisms, some of which are related to the normal function of antibodies in the presence of a pathogen, such as cell-mediated cytotoxicity and complement-mediated lysis. In antibody-dependent cell-mediated cytotoxicity, natural killer cells (NK cells) are activated by interaction of the Ig molecule with their Fc receptors. Other immune effector cells can also be activated by antibody binding to Fc receptors. Activation of the complement

cascade, eventually leading to osmotic lysis of the targeted cell(s), occurs through binding of the first protein complex of the cascade to the Fc-region of antigen-bound antibodies.

Antibodies do not only cause cellular damage. Other mechanisms include internalisation after cross-linking of the antigen (see Figure 1.2) and direct effects on the target protein or target-expressing tissue. The two antigen-binding sites on the arms of the Y-shaped antibody molecules allow binding of two adjacent antigens. If the antigenic sites for any antibody are present in multiple copies on each macromolecule, cross-linking between antigens can be substantial. This promotes clustering of the antigen resulting in internalisation and degradation of the antigen-antibody complexes and therefore reduces surface availability of the protein. This has been shown to take place with AChR in myasthenia gravis (Vincent, 2002). The requirement for divalency for internalisation is demonstrated by the fact that single Fab fragments do not cause internalisation unless the Fabs are cross-linked by an anti-Fab antibody. In addition, some antibodies have been shown to have direct effects on their targets: for example, thyroid-stimulating immunoglobulins activate thyroid-stimulating hormone receptors in the thyroid gland, causing excessive thyroid hormone synthesis and hyperthyroidism in Grave's disease.

Table 1.1 Symptoms of limbic encephalitis

Amnesia	Seizures	Affective disturbance
Anterograde amnesia Can present initially as confusion	Complex partial and secondarily generalised seizures of limbic origin	Change in behaviour or personality Agitation Anxiety or change in mood Psychotic features including delusions and hallucinations

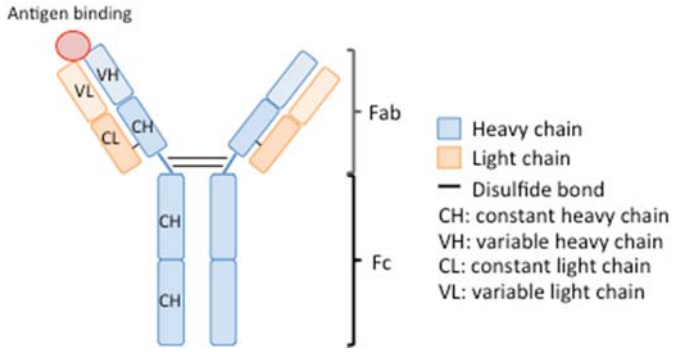

Figure 1.1 Schematic representation of an IgG molecule.
IgG molecules consist of two heavy (blue) and two light (orange) chains connected by disulphide bonds. The antigen binding sites are in the antigen-binding fragment (Fab), which can be cleaved enzymatically from the crystallisable fragment (Fc), which binds to effector cells and complement factors to mediate the effect of IgG.

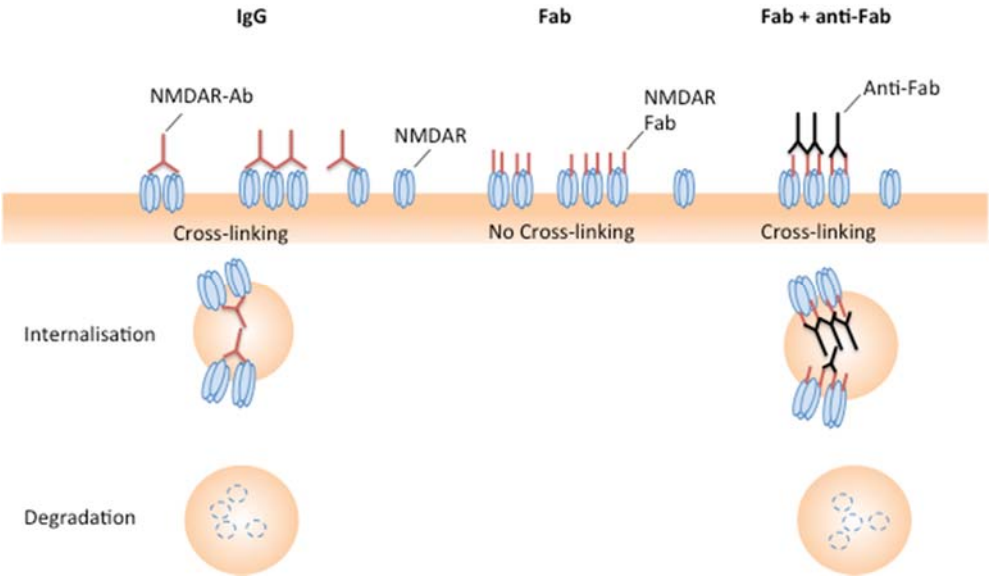

Figure 1.2 Cross-linking of antigen by antibodies and internalisation followed by degradation.
NMDAR-Abs cause the internalisation of NMDAR, reducing their surface density. This effect is specific to the full divalent IgG molecules as incubation with NMDAR-Fab, which is monovalent, does not cause internalisation of NMDAR. The requirement of divalency for this mechanism of action has been demonstrated by rendering the NMDAR-Fab divalent by adding anti-Fab antibody. In that situation, NMDAR are internalised.

1.3 Anti-NMDA Receptor antibody encephalitis (NMDAR-Ab encephalitis)

1.3.1 First description of NMDAR-Ab encephalitis

The description of VGKC-complex LE prompted the recognition of other cell membrane antigen-directed treatment-responsive LE syndromes. In the 1990's, a number of case reports described treatable limbic encephalitis in young women with ovarian teratomas (Nokura *et al.*, 1997; Okamura *et al.*, 1997; Taylor *et al.*, 1999), but it was not until 2005 that the remarkable similarity in presenting symptoms - marked psychiatric features resembling acute psychosis - and the presence in each patient of an antibody in serum and CSF that bound to the molecular layers of the hippocampus, that the idea of a separate treatable paraneoplastic syndrome associated with teratoma took form (Vitaliani *et al.*, 2005). Another remarkable feature of this syndrome was the involvement of extra-limbic areas: abnormal choreiform and dystonic movements developed in most of these patients, as did central hypoventilation. The patients also manifested a broad range of seizure types, some of which localised to non-temporal lobe structures. Although the target of the antibodies was not found, the authors demonstrated that this was a cell-surface antigen by showing binding to the cell membrane and dendrites of live cultured hippocampal neurons. A prospective study then showed that 44% of 39 patients with limbic encephalitis investigated at a single institution had this same novel antibody, and presented with a similar multi-focal encephalitic syndrome (Bataller *et al.*, 2007). They were overwhelmingly women, and in the majority of cases, had teratoma of the ovaries or thymus. Marked improvement was seen in most of these patients with steroids, plasma exchange, immunoglobulin infusion or a combination of these.

Later in the same year, Dalmau and his colleagues (2007) were able to determine that the antigen in this condition was a subunit of the NMDA receptor (NMDAR) expressed most strongly in the molecular layer of the hippocampus but also present in forebrain cortical areas. The epitope was likely to be conformational as patients' sera and CSF did not react with immunoblots prepared from cultured hippocampal neurons or cell lines recombinantly expressing subunits of the NMDAR, which present linear epitopes. The epitope

was eventually shown to be in the extracellular region of the NR1 subunit of NMDARs (Dalmau *et al.*, 2008). More recent studies using mutant NR1 subunits demonstrated that the NMDAR antibody epitope is within the amino terminal domain (ATD) of NR1 (Gleichman *et al.*, 2012). This region is important functionally as it provides the binding sites for NMDAR allosteric modulators. Within the ATD, a small region in the vicinity of the hinge between the two lobes of the ATD was found to be important for antibody binding. Mutations that increased the size of this region progressively reduced the intensity of antibody binding and also pushed the receptor into a closed conformation, suggesting that the antibodies bind preferentially to receptors in an open-cleft configuration. Binding of patient NMDAR-Abs to the wild-type NR1 subunit after brief exposure (six minutes) to patient CSF also prolonged receptor opening time, though it did not increase the likelihood of channel opening, suggesting it may stabilise the open configuration (Gleichman *et al.*, 2012) rather than cause it to open. The authors did not indicate the magnitude of the prolongation of the channel opening time and whether this was significant compared to baseline. Furthermore, the functional implications of the prolonged open time were not investigated.

1.3.2 The NMDA receptor

NMDA receptors are a subset of glutamatergic receptors. Glutamate is the main excitatory neurotransmitter in mammalian CNS and acts through two classes of receptors: ligand-gated ion channels and G-protein coupled metabotropic receptors. The ligand-gated ion channels, also called ionotropic receptors, are channels that become permeable to ions once activated by their agonist. They are named after the agonist they bind most strongly, i.e. AMPA, kainate or NMDA (for review, see Dingledine *et al.* (1999)). All glutamatergic ionotropic receptors share basic structural similarities. They are multimeric constructs consisting of four subunits. These subunits are formed of four hydrophobic transmembrane regions, one of which is re-entrant in order for the subunits to carry an extracellular N-terminal and an intracellular C-terminal. The ligand-binding domain consists of the N-terminal and part of the loop between the third and fourth transmembrane regions. The NMDA receptor is mostly made up of two families of subunits, NR1 and NR2. The NR1 subunits are obligate to the formation of NMDA receptors, although they cannot by themselves form

functional receptors as they do not contain glutamate binding sites. Instead, it contains a glycine binding site. Functional NMDA receptors are formed by two NR1 subunits and two NR2 subunits. There are four subtypes of NR2 subunits (A-D), affording NMDA receptors pharmacological variability.

The expression of NR2 subunits changes during foetal and neonatal development and varies by region in the adult brain, suggesting a role in functional specialisation (Monyer *et al.*, 1992; Monyer *et al.*, 1994). In rats, NR2B and D are expressed pre-natally and decrease post-natally into adulthood, whilst NR2A and C mRNAs appear after birth. In adulthood, NR2A and NR2B are expressed throughout the cortex and particularly strongly in the pyramidal layers of the hippocampus. NR2C is chiefly expressed in the cerebellum and NR2D expression declines dramatically. Interestingly, NR2A and NR2B subunit expression localises to hippocampal pyramidal cells and dentate gyrus granule cells, whilst NR2C and NR2D expression occurs in interneurons. Further functional differentiation is reflected in the different electrophysiological properties of the different NR2-subunit containing receptors: NR1-NR2A channels have much faster decay times than receptors containing either NR2B or C, and NR2D-containing receptors have very protracted time constants (Monyer *et al.*, 1994). A final NMDAR subunit named NR3 was identified somewhat later. Like NR1, it has a glycine binding site rather than a glutamate binding site but its physiological role is not well understood at present (Low and Wee, 2010).

There are a number of differences between NMDA receptors and AMPA and Kainate receptors (AMPAR and KAR), which have significant functional implications. AMPA and kainate receptors are involved in fast glutamatergic neurotransmission (Dingledine *et al.*, 1999). They are rapidly activated by glutamate, but have relatively low affinity for glutamate and therefore de-activate rapidly as well. Activation leads to Na^+ influx, but most AMPAR and KAR are impermeable to Ca^{2+}, which limits their involvement in excitotoxicity. Furthermore, AMPAR and KAR desensitise rapidly. The NMDA receptor is characterised by its slow kinetics (Dingledine *et al.*, 1999). Although it has a 500 times higher affinity for glutamate, it activates and de-activates much more slowly (time constants in the tens of milliseconds). Additionally, in the continued presence of glutamate, NMDARs desensitise slowly and by several different

complex mechanisms. It is also unusual in that three conditions must be fulfilled in order for the NMDA receptors to activate: its two co-agonists, glutamate and glycine, must bind and a voltage-gated block must be lifted. Glutamate binds to the NR2 subunits and the glycine binding site is found on NR1.

A voltage-dependent block is imposed on the NMDAR ion channel by magnesium (Mg^{2+}) ions. This renders NMDA receptors inactive at resting membrane potential. If the postsynaptic cell is depolarised at the same time as glutamate release is occurring pre-synaptically, however, the channel block is released and receptor activation leads to calcium-influx into the postsynaptic cell. This mechanism of activation ideally places the NMDA receptor as a coincidence detector and explains its role in synaptic response modulation. AMPARs and NMDARs are usually co-expressed at synapses and this distribution allows participation of NMDAR in synaptic transmission: postsynaptic cell depolarisation and displacement of the Mg^{2+} block in NMDAR channels is provided by the rapid activation of AMPARs following glutamate release. The slow de-activation time of NMDAR, which often exceeds the presence of glutamate in synaptic clefts, can then control the duration of the synaptic current (Dingledine *et al.*, 1999). Various forms of activity-dependent synaptic plasticity, such as long-term potentiation, have been shown to be NMDAR-dependent (Bliss and Collingridge, 1993), and are thought to underlie learning and memory.

These same mechanisms, as well as the very slow desensitisation process, also make the NMDA receptor a major mediator of excitotoxicity. Indeed, prolonged NMDA receptor activation leads to rising intracellular calcium concentration and eventually cell death through complex downstream steps including mitochondrial dysfunction and changes in kinase, protease and phosphatase signalling (Waxman and Lynch, 2005).

1.3.3 Clinical course of NMDAR-Ab encephalitis

Since 2007, there has been a cascade of case reports and case series describing patients with NMDAR-Abs. Initial reports suggested the condition was overwhelmingly paraneoplastic and affected mainly young women (Dalmau *et al.*, 2007; Sansing *et al.*, 2007; Tonomura *et al.*, 2007; Dalmau *et al.*, 2008; Iizuka *et al.*, 2008; Kataoka *et al.*, 2008; Seki *et al.*, 2008). Indeed, in a case

series of 100 patients, Dalmau et al (2008) found that 91% of the patients were female and 59% had tumours. These were mainly mature ovarian teratomas, and all examined tumour tissue stained strongly for NMDA receptors. However, as recognition of the new disease grew, the phenotype widened. Irani *et al.* (2010b) described the characteristics and clinical course of 44 European patients with NMDAR-Abs. In this series, 70% of patients were female and only 20% were found to have a tumour. The tumours consisted solely of ovarian teratomas, except for one male who suffered a recurrence of a previously treated Hodgkin's lymphoma. A recent retrospective observational cohort consisting of all 577 patients whose serum and/or CSF tested positive for NMDAR-Abs in Professor Dalmau's laboratory in Barcelona included 19% male patients, with greater prevalence of male patients in children under the age of twelve and adults over the age of 45 (Titulaer *et al.*, 2013). In this study, paraneoplastic cases were in the minority again, with 38% of patients having underlying neoplasm.

Recognition of NMDAR-Ab encephalitis in children has also grown. 37% of the patients in the Titulaer *et al.* (2013) cohort and 32 of 80 patients in a separate American cohort were under the age of 18 (Florance *et al.*, 2009).

The clinical course of NMDAR-Ab encephalitis evolves over two distinct stages (Irani *et al.*, 2010b). The majority of patients present with symptoms of higher cognitive dysfunction, such as confusion and amnesia, and/or psychiatric symptoms (Dalmau *et al.*, 2008; Irani *et al.*, 2010b; Titulaer *et al.*, 2013). The psychiatric symptoms described include anxiety, depressive symptoms, obsessive thoughts and behaviours, agitation, delusions and other psychotic phenomena, and visual and auditory hallucinations. Seizures, which can be generalised tonic-clonic, complex partial or simple partial, affect up to 82% of patients at initial presentation. Five to twenty days later, an increasingly sub-cortical picture emerges, progressing to reduced levels of consciousness, frequently with central hypoventilation that often requires intubation and ventilation (Irani *et al.*, 2010b). Abnormal movements become prominent. These are most often choreoathetoid but parkinsonian features with rigidity, myoclonus, oculogyric crises and opisthotonus have all been described. During this time autonomic dysfunction is also frequent, affecting up to 72% of patients and often requires treatment in its own right.

Seizures are less frequent and less persistent in NMDAR-Ab encephalitis than in other types of autoimmune encephalitis. Indeed, seizures are a very prominent feature of limbic encephalitis with antibodies to GABARs (Lancaster *et al.*, 2010), LGI-1 (Irani *et al.*, 2010a), and GAD (Malter *et al.*, 2010). Additionally, the two published animal models of NMDAR-Ab encephalitis did not report spontaneous seizures even with prolonged administration of antibodies and strong hippocampal binding (Planagumà *et al.*, 2014; Wright *et al.*, 2015b). Whilst this could reflect a species difference in the role of NMDAR in epileptogenesis, it is also possible that the seizures seen in patients with NMDAR-Ab encephalitis are not a direct result of the effects of NMDAR-abs on NMDARs in limbic and cortical areas. Instead, they may be a downstream effect of alterations of the balance of excitation and inhibition in cortical networks as seen in NR1 knock-down mice (Gary E. Duncan *et al.*, 2010; Gandal *et al.*, 2012), or could result from cortical damage caused by the inflammatory reaction.

Implicating loss of surface NMDAR in epileptogenesis is not straightforward: many studies point to a protective effect of NMDAR hypomorphism/antagonism in seizures (Kalev-Zylinska *et al.*, 2009; Wasterlain *et al.*, 2013), with NMDAR antagonists displaying anticonvulsant properties in many animal models of epilepsy (Chapman, 1998). Furthermore, it is noteworthy that one common animal model of epilepsy is to use low/no magnesium aCSF to perfuse slices (for example, see Anderson *et al.* (1986). This removes the Mg^{2+} block of NMDARs and therefore potentiates NMDAR-mediated glutamatergic transmission, and leads to the development of epileptiform activity in slices. Nevertheless, there is also evidence that NMDAR hypomorphism increases susceptibility to kainate-induced seizures by sensitizing kainate receptors to endogenous glutamate (Gary E. Duncan *et al.*, 2010). Altering surface and synaptic NMDAR density is therefore associated with wide-ranging and occasionally opposing effects (protection from seizures as well as increasing susceptibility to seizures by secondary mechanisms as seen above), suggesting that individual clinical outcomes such as seizures, may depend on multiple factors including antibody titre, location and duration of exposure, and accompanying inflammation, in each patient.

Similar arguments can be made for other characteristic features of NMDAR-Ab encephalitis, such as the movement disorders observed, which so far have not been directly linked to an NMDAR-mediated effect.

1.3.4 Clinical investigations in NMDAR-Ab encephalitis

CSF and scalp electroencephalogram (EEG) are abnormal in the majority of patients (79-95% and 90-100% respectively (Dalmau *et al.*, 2008; Titulaer *et al.*, 2013)). Irani *et al.* (2010b) found that investigation results follow a biphasic

pattern that mirrors the clinical presentation. At presentation, CSF findings are mostly that of lymphocytic pleocytosis with leucocyte counts ranging from just above normal to well into the hundreds (normal range <5/ml). CSF protein is sometimes mildly elevated and oligoclonal bands are rarely found. In CSF collected later in the course of the illness however, leucocytosis is usually absent and oligoclonal bands unmatched in the serum are more often seen (Irani *et al.*, 2010b). Epileptiform EEG changes on a normal background are more often seen in the early stages of the disease, whereas diffuse slowing with delta and theta activity is a common late feature.

Magnetic Resonance Imaging (MRI) is surprisingly often normal in NMDAR-Ab encephalitis. Dalmau *et al.* (2008) found that 45% of patients had no imaging findings and this proportion was even higher in Irani *et al.* (2010b). The most common abnormalities were high signal in the medial temporal lobes on Fluid Attenuation Inversion Recovery (FLAIR) sequences or T2 sequences, contrast enhancement in the cerebral cortex and overlying meninges or basal ganglia, and white matter hyperintensity.

1.3.5 Treatment and outcome in NMDAR-Ab encephalitis

One of the features that initially differentiated NMDAR-Ab encephalitis from classical paraneoplastic encephalitis syndromes was the response to immunomodulatory treatments. Although experience with the treatment of NMDAR-Ab encephalitis has increased dramatically recently, the condition is still rare and relatively new, and no prospective trials of different immunomodulatory drugs or regimes exist at present. The three largest cohorts of NMDAR-Ab encephalitis patients (Dalmau *et al.*, 2007; Irani *et al.*, 2010b; Titulaer *et al.*, 2013) have found that patients with paraneoplastic NMDAR-Ab encephalitis who undergo tumour resection tend to do better than patients with non-paraneoplastic NMDAR-Ab encephalitis. This is likely to be related to the probable role played by the teratomas in triggering the immune response. Indeed, all tumours examined histologically were found to contain neurons that expressed NMDA receptors, and these were bound by patient antibodies. Considerable improvement is seen after surgical resection and first-line immunotherapy in around 80% of patients (Seki *et al.*, 2008; Florance *et al.*, 2009; Irani *et al.*, 2010b; Alexopoulos *et al.*, 2011; Dalmau *et al.*, 2011).

In the non-paraneoplastic group of patients, various forms of immunomodulation and immunosuppression have been used alone or in combination. A combination of glucocorticoid treatment with other immune therapies is more successful than glucocorticoids alone (Dalmau *et al.*, 2008; Irani *et al.*, 2010b; Titulaer *et al.*, 2013). Early treatment is also a significant factor in the outcome (Irani *et al.*, 2010b; Titulaer *et al.*, 2013). However, first-line immunotherapies fail in nearly half of patient with non-paraneoplastic NMDAR-Ab encephalitis (Titulaer *et al.*, 2013) and such patients are often treated with second-line agents such as rituximab or cyclophosphamide. Substantial improvements are seen in around 75% of patients treated with second-line immunotherapy (Titulaer *et al.*, 2013).

While cyclophosphamide is able to cross the blood-brain-barrier, it is not clear that rituximab can. Rituximab is a monoclonal antibody targeting CD20 positive B cells, that is naïve and memory B cells, but not the long-lived plasma cells that are likely to be responsible for the intrathecal production of NMDAR-abs. Cyclophosphamide reduces both B and T-cell populations. B cells are abundant in the perivascular infiltrates in patients with NMDAR-Ab encephalitis (Martinez-Hernandez *et al.*, 2011) where they may perpetuate the inflammatory environment required for maturation of plasma cells. Significant selective B cell expansion has been described in the CSF of patients with NMDAR-Ab encephalitis during active disease (Dale *et al.*, 2013), but whether rituximab or other therapies can deplete CSF B-cell in this condition has not been studied. In blood, rituximab-induced $CD20^+$ B-cell depletion at one month after treatment was accompanied by a reduction in $CD20^-$ plasma blasts, short-lived cells that are able to secrete antibodies (Hachiya *et al.*). Rituximab, and perhaps cyclophosphamide too, may therefore be useful both in terms of reducing the supply of B cells to the CNS and depleting short-lived plasma blasts.

A minority of mostly non-paraneoplastic NMDAR-Ab encephalitis patients suffer relapses (12-25%, (Dalmau *et al.*, 2008; Florance *et al.*, 2009; Irani *et al.*, 2010b; Gabilondo *et al.*, 2011; Titulaer *et al.*, 2013)). Relapses may occur months to several years after the initial episode and are often less severe than the initial event. They usually occur in patients who received no or limited treatment for the initial episode and are rare in patients exposed to second-line

immunotherapy (Dalmau *et al.*, 2008; Florance *et al.*, 2009; Irani *et al.*, 2010b; Gabilondo *et al.*, 2011; Titulaer *et al.*, 2013).

The case reports and case series described above all report very encouraging recovery rates (75-81%), especially when the duration of coma and intensive care unit stay is considered. However, more careful analysis shows that up to 85% of patients described as having fully recovered or experiencing mild deficits only do show signs of frontal lobe dysfunction on cognitive testing (Dalmau *et al.*, 2008). Long-term cognitive outcome has only been reported in one small study. Patients classified as having good outcome were found to have deficits in executive function and memory testing, more severe in those with delayed treatment (Finke *et al.*, 2012). Overall, this does suggest that the initial part of the illness may be critical in terms of neuronal damage and long-term outcome.

1.3.6 NMDA Receptor antibodies in NMDAR-Ab encephalitis

NMDAR-abs are found in the serum and CSF of patients with NMDAR-Ab encephalitis and are predominantly of the IgG1 subtype (Tuzun *et al.*, 2009; Irani *et al.*, 2010b). Intrathecal production of antibodies has been demonstrated in most patients with CSF antibodies (Dalmau *et al.*, 2008; Irani *et al.*, 2010b) but absolute titres of NMDAR-abs are higher in serum than CSF (Irani *et al.*, 2010b). Serum IgG concentration is about 400 times higher than CSF IgG concentration. Once IgG concentration in CSF is normalised to that in serum, however, the relative NMDAR-Ab concentration in CSF will be higher in the majority patients (Dalmau *et al.*, 2008). This explains the apparent discrepancy in relative serum and CSF titres reported by Dalmau's group in their original study (2008) and the Oxford laboratory, as the former were expressed after normalisation to serum IgG concentration.

CSF NMDAR-Ab titres, and to a lesser extent serum titres, correlate with disease course: one study found that CSF titres fell markedly and rapidly in patients with a monophasic illness and good outcome, whereas the reduction was slower in those with poor outcome (Gresa-Arribas *et al.*, 2014). Similarly, serum titres remained elevated in patients with poor outcome or death in another study (Irani *et al.*, 2010b). It is noteworthy that both serum and CSF antibodies remain detectable in a proportion of patients after recovery from

NMDAR-Ab encephalitis (Irani *et al.*, 2010b; Finke *et al.*, 2012; Gresa-Arribas *et al.*, 2014), posing questions about the significance of continued antibody production. Few studies have systematically studied the effect of immunotherapy on antibody levels. Case reports occasionally describe reduction (Kurian *et al.*; Turkdogan *et al.*; Seki *et al.*, 2008; Irani *et al.*, 2010b) or eradication (Batra *et al.*; Ishiura *et al.*, 2008) of NMDAR-abs in serum following 1st-line immunotherapy in patients with good outcome, with concomitant decrease in CSF titres (Kurian *et al.*; Turkdogan *et al.*; Ishiura *et al.*, 2008; Seki *et al.*, 2008). Reductions in CSF titres with 2nd-line treatments have also been demonstrated (Frechette *et al.*, 2011; Hachiya *et al.*; Thomas *et al.*, 2013), but for obvious practical reasons are less commonly reported.

Two long-term follow-up case reports may shed some light on the relative importance of CSF and serum Abs. Indeed, both case reports describe patients with very prolonged clinical courses. Frechette *et al.* (2011) describe an 18-year-old man with a severe clinical course. He was comatose with dyskinetic facial and limb movements for nearly one year. No tumour was found on repeated searches. He was treated with a combination of ivIG, cyclophosphamide and rituximab and had monthly serum and CSF Ab titre measurements. His serum antibodies remained low (within the control range for the ELISA used) throughout the course of his illness whereas CSF titres were initially elevated. CSF titres fell gradually over the course of the hospitalisation with concomitant improvement in clinical state. It is worth noting that antibody titres in serum and CSF were measured using an ELISA, which is no longer in routine use as it is less sensitive than cell-based assays (Dalmau *et al.*, 2008; Irani *et al.*, 2010b) and this might explain the apparent negativity of the serum samples.

Alexopoulos *et al.* (2011) describe a 42-year-old woman with a very severe syndrome in whom a mature ovarian teratoma was only found one year after admission to hospital, after repeated tumour searches. Her CSF Ab titre had initially been higher than the serum titre. She had been treated with monthly intravenous immunoglobulin up until oophorectomy with no improvement in clinical state. She started to improve after oophorectomy but serum NMDAR-Ab persisted. CSF Abs were not rechecked. Her recovery was very slow and at four years post-admission she still had significant cognitive difficulties, at which

point serum Abs were still present. Unfortunately, the antibody titres are not available. As described above, the relationship between serum and CSF antibodies is unclear and the titre of one is not predictive of the other. It is difficult therefore to determine whether the persistent and slowly improving cognitive difficulties are related to the persistent serum Abs, the potential presence of CSF Abs as in the previous care report (Frechette *et al.*, 2011), or to cortical damage in the early stages of her prolonged admission. It should be noted that the comparisons in Alexopoulos *et al.* (2011) were made using different assays which adds another potential confound to their conclusions.

Post-mortem studies and biopsy findings have been quite variable with some studies finding areas of intense immunoglobulin deposition and extensive microgliosis (Dalmau *et al.*, 2008; Tuzun *et al.*, 2009), whilst others found very little in the way of parenchymal lymphocytic infiltration or gliosis (Camdessanché *et al.*, 2011; Martinez-Hernandez *et al.*, 2011). Reduced NR1 staining intensity was measured in the hippocampus of patients with NMDAR-Ab encephalitis at autopsy compared to controls, suggesting a specific effect of the antibodies (Hughes *et al.*, 2010). All studies were remarkable for the lack of neuronal damage and loss reported and no complement deposition was found despite NMDAR-abs being of the IgG1 complement-activating subtype (Martinez-Hernandez *et al.*, 2011). The most common feature was perivascular lymphocytic cuffing with infiltrates including antibody-secreting plasma cells (Dalmau *et al.*, 2008; Tuzun *et al.*, 2009; Camdessanché *et al.*, 2011; Martinez-Hernandez *et al.*, 2011), the likely source of intrathecally-produced antibodies. Pathological studies have however generally been conducted late in the disease and after some immunotherapy (Tuzun *et al.*, 2009; Martinez-Hernandez *et al.*, 2011), and therefore cannot exclude complement or cell-mediated toxicity as important pathogenic mechanisms in the early stages of disease.

A recent paper (Kreye *et al.*, 2016) has demonstrated the presence of IgG directed against a multiplicity of non-NR1 targets in the CSF of patients with NMDAR-Ab encephalitis, both patients with active disease and those in remission. Having observed binding to astrocytic and neuronal antigens outside of NMDAR-rich areas in 6 of 8 CSFs tested, the authors isolated the antibody-secreting cells and memory B-cells from the CSF of these patients and

investigated their monoclonal antibody repertoire by cloning their immunoglobulin genes. In total, they found 170 monoclonal antibodies across the 8 patients' CSF samples, and only 9 of these (from three patients) were directed against the NR1 subunit of NMDARs. The NR1 monoclonal antibodies behaved as expected from previous studies using CSF from patients with NMDAR-Ab encephalitis (Dalmau *et al.*, 2011) – causing reduction in synaptic NMDAR density and reduced NMDAR currents in neuronal cultures – confirming that these effects were solely related to the NR1 antibodies and that these are sufficient to cause the changes (Kreye *et al.*, 2016).

The specific antigenic targets of the remaining 161 monoclonal antibodies await investigation, but the truly surprising findings of this study are the breadth of the antibody repertoire in these patients and the low frequency of NMDAR-Ab-producing cells. If Kreye *et al.* (2016) succeeded in isolating all the antibody-producing cells from the CSF samples provided, and if the sampled cells represented a true reflection of the intracerebral/intrathecal antibody-secreting cells *in vivo* in the patients, then the results of this study would suggest that the CSF NMDAR-Abs in most patients have originated in the periphery. This is in contrast with findings of intrathecal antibody production in most patients (Dalmau *et al.*, 2008; Irani *et al.*, 2010b). Furthermore, and as pointed out in a vehement letter to the editor of Brain (Dalmau, 2017), previously reported immunohistochemical findings with patient CSF are not in keeping with the presence of non-NR1 directed antibodies, and some studies have specifically ruled this out by performing NR1-Ab pre-absorption studies (Pettingill, 2013), showing abrogation of brain reactivity with removal of NMDAR-Abs.

The presence and extent of a significant non-NMDAR-directed antibody response in NMDAR-Ab encephalitis therefore remains controversial at present.

1.3.7 The origin of the immune response in NMDAR-Ab encephalitis

In patients with paraneoplastic NMDAR-Ab encephalitis, the teratomas contain nervous tissue strongly expressing NMDARs (Dalmau *et al.*, 2007; Dalmau *et al.*, 2008; Seki *et al.*, 2008; Hara *et al.*, 2011). This may well be responsible for the breakdown of immune tolerance to NR1 subunits and the initiating step in NMDAR-Ab encephalitis. This would account for the peripheral production of NMDAR-Abs. It is still unclear how these antibodies subsequently gain access

to the CNS in sufficient quantity to cause disease. The CSF:serum IgG ratio under normal circumstances is around 1:400 to 1:500 (Reiber, 1998), but diffusion of antibodies would increase through areas of blood-brain-barrier (BBB) disrupted by the systemic inflammation accompanying the neoplastic process or by preceding or prodromal infections. Additionally antibody-secreting B-cells also enter the CNS, as intrathecal NMDAR-Ab synthesis has been demonstrated (Dalmau *et al.*, 2008; Irani *et al.*, 2010b). Dalmau *et al.* (2008); (2011) state that the BBB is intact in most patients at the time that paired serum and CSF samples were studied. However, both the increased protein concentration in the CSF and contrast enhancement on brain MRI of patients with NMDAR-Ab encephalitis suggest that the BBB is disrupted.

In non-paraneoplastic cases it is not clear how the immune response is initiated. Irani et al (2010b) suggest that the much higher serum than CSF antibody titres signify that the antigenic stimulus is to be found peripherally rather than in the CNS. Some, usually monophasic, autoimmune disorders such as Guillain-Barre syndrome or Sydenham's chorea are caused by antibodies formed in response to bacterial agents cross-reacting with nervous system epitopes. A significant proportion of patients with NMDAR-Ab encephalitis describe a prodromal viral-like illness with headache, fever and occasionally vomiting or diarrhoea (75% in Dalmau *et al.* (2007), 72% in Dalmau *et al.* (2008), but only 25% in Irani *et al.* (2010b)) and in very few of these has an IgM response been demonstrated (indicating a true infectious event rather than an inflammatory event). When the temporal association with the onset of the neurological syndrome has been examined in detail (Irani *et al.*, 2010b), only two of eleven patients suffered their infectious prodrome sufficiently early for the development of cross-reactive antibodies to occur, and extensive immunological studies of CSF and serum argue against cross-reactivity with bacterial epitopes (Dalmau *et al.*, 2008). It is of note that both patients with or without tumours suffer infectious-like prodromes (fever and headache), suggesting these may be inflammatory in nature rather than infectious. This systemic inflammation may disrupt the blood-brain-barrier resulting in passive diffusion of antibodies into the CNS. However, intrathecal production of antibodies needs to be explained and its contribution evaluated. In fact, Irani et al (2010b) suggested that intrathecal antibody production might occur later in the disease process and be responsible for the

appearance of oligoclonal bands in the CSF and the more global encephalitic process with basal ganglia and brainstem features.

Intrathecal antibody production has significant implications for treatment, as most first line immunotherapies reduce serum antibody concentration whilst the effects on CSF antibodies are not clear. It remains to be shown whether agents such as rituximab or cyclophosphamide, which appear efficacious in the treatment of NMDAR-Ab encephalitis, can affect intrathecal antibody production.

1.3.8 Are NMDAR-Abs pathogenic?

Evidence for a pathogenic role of NMDAR-Abs is accumulating but has not yet been proven beyond doubt. The extracellular nature of the epitope recognised by NMDAR-Abs, the correlation between disease course and CSF and serum NMDAR-Ab titres, and the effectiveness of treatments that reduce serum antibody concentrations are appealing arguments in favour of the pathogenicity of the antibodies. Below, *in vitro* and *in vivo* work pointing to an effect of NMDAR-Abs on NMDAR function will be reviewed.

In vitro effects of NMDAR antibodies

There is good evidence that CSF and purified serum IgG from patients with NMDAR-Ab encephalitis alter synaptic NMDAR content and function in cultured hippocampal neurons. Dalmau et al (2008) showed that numbers of NMDAR clusters on postsynaptic dendrites were reduced after 3 and 7 days of incubation with CSF from patients with NMDAR-Abs compared to control patient CSF. This reduction was reversible, as substituting patient CSF with control CSF after 3 days' incubation led to normalisation of NMDAR cluster numbers at day 7. The same effect was seen with purified IgG. These effects appeared to be NMDAR-specific, as the number of clusters of PSD95, another post-synaptic protein, was unaltered by patient CSF application.

More detailed *in vitro* studies showed that incubating cultured HPC neurons with patient CSF or purified IgG decreased the total amount of NR1 protein as well as the cell-surface expressed fraction of NR1 protein (Hughes *et al.*, 2010). Purified patient IgG reversibly and selectively reduced synaptically located NMDAR without affecting the number of excitatory synapses. AMPA receptors

and GABA receptors were not affected and dendritic branching and complexity remained unaltered. Also, cell density and the number of cells expressing markers of apoptosis were similar in cultures exposed to patient or control CSF. Thus NMDAR-Abs appear non-toxic to cultured neurons. Later, the reduction in surface NMDAR clusters was shown to be significant only after twelve hours of exposure to patient CSF (Moscato *et al.*, 2014).

Experiments using the isolated Fab fragments of the NMDAR Ab showed no effect on NMDAR cluster density (see Figure 1.2) (Hughes *et al.*, 2010). Using anti-Fab antibodies to cross-link the individual Fab fragments restored the effect, suggesting that antibody capping and cross-linking of the antigen followed by internalisation and degradation underlie the change in density and localization of NMDARs described above (Hughes *et al.*, 2010). Finally, the decrease in surface and synaptic NMDAR was accompanied by reduced NMDAR-mediated currents, whilst AMPAR-mediated currents remained intact, in whole cell patch-clamp recordings of cells exposed to NMDAR-Ab positive CSF (Hughes *et al.*, 2010). The reduction in NMDAR-mediated currents was shown to be related to receptor internalisation rather than an acute antagonistic effect on NMDAR by demonstrating the lack of effect of acute application of patient CSF (30 minutes, at which time surface NMDAR density in essentially unchanged) and the chronic (24 hours) application of patient Fab (Moscato *et al.*, 2014).

On the other hand, three small electrophysiological studies have proposed that NMDAR-Abs can have an acute antagonistic effect on NMDAR function. In cultures of cerebellar neurons exposed to the CSF of a single patient with NMDAR-Ab encephalitis, calcium influx after addition of NMDA to the medium was prevented (Rubio-Agustí *et al.*, 2011). However, it is worth noting that the clinical history of the patient was atypical for NMDAR-Ab encephalitis and that little detail of the diagnostic technique, which had been carried out in-house rather than at an experienced diagnostic laboratory, was given.

Spike rate and burst rate recorded by multi-electrode array in spontaneously bursting *in vitro* neuronal networks obtained from dissociated rat cortical cultures were reduced 15 minutes after application of patient CSF and recovered after removal of patient CSF (Jantzen *et al.*, 2013). The synchrony of

the remaining activity was unaffected however. Unfortunately, it is not possible to directly attribute the reduction in global network activity to the effects of NMDAR-Abs or even to changes in NMDAR function in this study, and the effect of other factors, such as the anticonvulsant and neuroleptic drugs given to the patient whose CSF was used were not controlled for.

Another paper demonstrated altered synaptic plasticity in mouse hippocampal slices briefly exposed to NMDAR-Ab positive CSF (Q. Zhang *et al.*, 2012). The authors examined the effect of the CSF of four patients with NMDAR-Ab encephalitis on long-term potentiation (LTP) in the Cornu Ammonis 1 (CA1) area of the hippocampus. LTP occurred in slices exposed to artificial CSF and CSF from patients with viral encephalitis or other neurological conditions. However, 5-minute exposure to NMDAR-Ab positive CSF prevented LTP from taking place. LTP was not prevented if NMDAR-Abs had been pre-absorbed from CSF prior to application to slices, confirming that the effect was NMDAR-Ab-mediated.

As mentioned above, there is evidence to suggest that NMDAR-Abs may prolong the open time of NMDARs (Gleichman *et al.*, 2012). One might hypothesise that this could increase the rate of desensitisation of NMDARs and thus depress NMDAR-mediated transmission. However, NMDARs have long open times, a low open probability and presynaptic stimuli cause opening of only about 50% of the NMDAR channels that bind glutamate, suggesting that NMDAR-mediated neurotransmission has significant “functional reserve” (Rosenmund *et al.*, 1995). Although stimuli that induce LTP probably recruit significantly more NMDAR than the stimulation protocol in the latter study, thus increasing the likelihood of receptor desensitisation by prolonged opening, it still seems difficult to reconcile a potential prolonged opening time with the depressing effect on LTP seen in Zhang et al’s study (2012). Overall, a different mechanism of action seems likely to have been invoked here.

Finally, the time frame within which significant NMDAR internalisation, or at least sequestering by the antibodies, takes place has been challenged by Mikasova *et al.* (2012). Like Hughes *et al.* (2010) and Moscato *et al.* (2014), they found significant reductions in surface NMDARs in cultured hippocampal neurons after 20-hour incubation with patient CSF. By contrast, the reduction

was already significant at two hours' incubation for extrasynaptic NMDARs (NR2B-containing NMDARs). Unfortunately, they did not examine if this was the case for synaptic NMDARs as well. Furthermore, by using quantum dot imaging to label and follow individual NMDARs, they were able to show that patient antibodies removed synaptic NR2A-containing NMDARs from synapses and caused the internalisation of extrasynaptic NR2B-containing NMDAR after two hours' incubation with patient CSF. No effect was seen in the first 10 minutes or so of incubation, indicating that these effects took 20-120 minutes to occur (Mikasova *et al.*, 2012). This time frame is still not compatible with that seen in the study by Q. Zhang *et al.* (2012), but a significant loss of NMDARs from synapses within a short time frame is of great interest as it could foreseeably acutely depress NMDAR-mediated transmission.

In conclusion, bar one well-controlled study demonstrating an acute electrophysiological effect of NMDAR-Abs in patient CSF (Q. Zhang *et al.*, 2012) suggestive of a direct antagonistic or blocking effect on NMDARs, most of the evidence would suggest that NMDAR-Abs exert their effect by causing NMDAR internalisation, both at the synapse and extrasynaptically, without causing toxicity to cultured neurons (Dalmau *et al.*, 2008; Hughes *et al.*, 2010; Moscato *et al.*, 2014). The time-frame within which the internalisation occurs is not yet clear, with evidence both for a relatively rapid effect within two hours of exposure (Mikasova *et al.*, 2012), and for a slow process requiring at least 12 hours of exposure (Moscato *et al.*, 2014).

In vivo effect of NMDAR-antibodies

Evidence for an *in vivo* effect of NMDAR-Abs is much sparser. Currently, there are five studies reporting such effects. Dalmau's group (Hughes *et al.*, 2010) showed that infusing NMDAR-Ab-positive patient CSF into rat hippocampus *in vivo* for two weeks resulted in selectively decreased NMDAR cluster density and NR1 immunostaining in the hippocampus. In accordance with this, autopsy studies of patients with NMDAR-Ab encephalitis showed diminished NMDAR immunolabeling in hippocampus compared to control brains.

Manto *et al.* (2011) studied the effect of patient CSF and purified IgG on corticomotor responses in anaesthetised rats. They infused 5μL of patient CSF (at 1μL/min) into the prefrontal area, which is known to modulate the excitability

of the motor cortex. Motor evoked potential (MEP) amplitudes before and after afferent facilitation were not affected. However, after trains of high-frequency stimulation (HFS) to the premotor cortex, which are known to enhance afferent facilitation in motor cortex, both unconditioned (no afferent facilitation) MEP amplitudes, and post-afferent facilitation MEP amplitudes were significantly greater in rats treated with NMDAR-Ab positive CSF than in those of control rats and rats treated with control CSF. So, although the antibodies did not increase cortical excitability by themselves, they appeared to enhance the LTP-like effect of HFS. The effect on afferent facilitation was much greater in forelimb MEPs compared to hindlimb MEPs. The effect was restricted to the area into which the CSF had been infused as spinal cord excitability was unchanged. The reason for the marked asymmetry of effect on forelimbs and hindlimbs is unclear. Overall, the authors conclude that NMDAR-Abs markedly enhance motor cortex excitability and postulate that this hyperexcitability could result from loss of inhibitory tone from GABAergic interneurons due to NMDAR-Ab-related inhibition of NMDAR on these interneurons.

In another study by the same group (Manto *et al.*, 2010), CSF and purified serum IgG from patients with NMDAR-Ab encephalitis and control patients were infused into the hippocampus of anaesthetised rats (5μL at 1μL/min). Levels of extracellular glutamate were then measured by microdialysis over a period of at least one hour. Patient CSF caused a significant increase in the extracellular glutamate concentration. The increased extracellular glutamate concentration is likely to be related to impaired glutamatergic auto-regulation and reduced inhibitory drive from interneurons.

The results of these two studies would be consistent with NMDAR-Abs having an acute effect on NMDAR-mediated transmission. That would be in contrast to the most recent *in vivo* study, in which mice were administered NMDAR-Ab-positive CSF or control CSF intracerebroventricularly over 14 days (Planagumà *et al.*, 2014). Recapitulation of disease features in experimental animals with transfer of antibodies is required for definitive proof of the pathogenicity of autoantibodies. In this study, the authors found that the mice that received NMDAR-Abs developed progressively worsening memory deficits on the novel object recognition test during the infusion period and up to four days after the end of the infusion, as well as some anhedonic behaviours. The impairments

recovered in the following week. Increases in the intensity of staining for human IgG deposited in the hippocampus and decreases in density of NMDAR clusters and total NMDAR protein mirrored the memory deficits observed in the mice during the infusion period, and normalised after the cessation of the infusion. Although only a limited phenotype was obtained (no seizures, movement disorder or reduction in conscious level), this finding is still an important demonstration that the effects of the patient antibodies *in vitro* do translate to relevant behavioural changes, and does substantiate the removal of antibodies with immunomodulatory treatments.

Finally, another study (Wright *et al.*, 2015b)was able to demonstrate increased seizure susceptibility 48 hours after mice were given a single bolus of purified NMDAR-Ab IgG intracerebroventricularly, with pentylenetetrazole (PTZ) as a pro-convulsant. Surprisingly, there was no apparent loss of NMDARs in this acute model and thus the mechanisms by which seizure threshold was reduced are not known.

In summary, there is good evidence for a pathogenic role for NMDAR Abs in NMDAR-Ab encephalitis. The published findings so far provide potential partial mechanisms of action for the Abs at a cellular and synaptic level (internalisation, although which cell types are predominantly affected is not clear) but no mechanistic link to the devastating deficits in memory and behaviour seen in this condition has yet been established. These deficits are likely to be caused by changes in neuronal network function in the medial temporal lobe and this is what this thesis proposes to investigate further.

1.4 NMDAR in memory and learning and behaviour

The slow kinetics and double-gating of NMDARs underlie their ability to integrate pre- and postsynaptic activity and thereby change synaptic efficiency. The latter was long thought to underlie learning and memory (Hebb, 1949) and the role of NMDARs in this process was confirmed when NMDAR antagonists were shown to block the induction of long-term potentiation (LTP), one of the most prevalent forms of activity-dependent synaptic plasticity (Bliss and Collingridge, 1993). A number of pharmacological and NMDAR knockout studies have demonstrated the importance of NMDAR-dependent LTP in certain forms of memory. Impaired spatial memory, but not non-spatial learning,

together with loss of CA1 LTP were demonstrated in mice lacking NR1 (and therefore NMDARs) in CA1 of the hippocampus by Tsien *et al.* (1996). CA3 NR1 knock-out mice were found to have impaired acquisition of spatial memory during one-time experiences, but normal spatial memory acquisition and retrieval for repeated experiences (Nakazawa *et al.*, 2003). Similarly, dentate gyrus granule cell NR1 knockout mice with deficient LTP in the dentate gyrus inputs, were shown to have spatial working memory but not reference memory impairments (Niewoehner *et al.*, 2007). NMDARs also appear important for the consolidation of long-term contextual memories stored in the frontal cortex rather than hippocampus (Wiltgen *et al.*, 2004). Selective ablation of NR1 in parvalbumin-positive interneurons, a subtype of GABA-ergic interneuron that plays a critical role in network synchronisation (see later), also led to deficits in spatial working memory and spatial recognition memory (Korotkova *et al.*, 2010).

In addition to their role in memory, NMDARs have been implicated in several neurological and psychiatric disorders (for review see Waxman and Lynch (2005)). The most relevant to this thesis is the NMDAR hypofunction model of schizophrenia. This was formulated on the basis of the similarity of symptoms experienced by individuals taking NMDAR antagonists and both the positive and negative symptoms of schizophrenia. Indeed, healthy volunteers receiving a single low dose of intravenous ketamine reported transient alterations in perception, including illusions, perceptual distortions and occasionally simple auditory hallucinations such as popping noises (Krystal *et al.*, 1994; Lahti *et al.*, 2001). Disturbance of thought content and organisation, and experiences similar to dissociative states were also reported. The subjects' performance on the social withdrawal subsection of the Brief Psychiatric Rating Scale as well as several tests of executive function and memory was also disrupted, suggesting that the negative symptoms of endogenous psychoses could also be elicited by ketamine. Furthermore, when ketamine was administered to volunteers with schizophrenia, they reported a brief increase in positive symptoms including delusions similar to those they had experienced in a previous psychotic phase, formed visual or auditory hallucinations and thought disorder (Lahti *et al.*, 1995; Lahti *et al.*, 2001). This led to the development of several animal models of NMDAR hypofunction, each exhibiting some cellular, anatomical or behavioural

correlate of schizophrenia in humans. For example, Mansbach and Geyer (1989) found that injections of the NMDAR non-competitive antagonists phencyclidine and MK-801 in rats caused increased startle responses and reduced pre-pulse inhibition indicating a deficit in sensorimotor gating, which is also found in patients with schizophrenia (Parwani *et al.*, 2000). Rujescu *et al.* (2006) found changes in NR2B subunit expression and a reduction in parvalbumin-positive interneuron numbers in the hippocampus of rats administered low-dose MK-801 chronically, similar to those seen in humans with schizophrenia (Gao *et al.*, 2000; Z. J. Zhang and Reynolds, 2002). Keilhoff *et al.* (2004) also found reduced density of parvalbumin-positive cells in the hippocampus of rats treated with low doses of ketamine.

The first genetic model of NMDAR hypofunction was developed by Mohn *et al.* (1999). They generated mice with 5-10% of normal NR1 expression. These mice exhibited several behaviours similar to those seen in rodents treated with NMDAR antagonists and relevant to patients with schizophrenia, including increased locomotion and stereotypic movements during habituation to a new environment, and social and sexual interaction deficits. These behaviours improved with treatment with antipsychotic drugs. NR1 knock-down mice were further shown to have deficient sensorimotor gating on the pre-pulse inhibition test (G. E. Duncan *et al.*, 2004), as well as reduced numbers of parvalbumin-positive interneurons and reduced parvalbumin expression in the prefrontal and sensorimotor cortices (Gandal *et al.*, 2012). Further implicating GABA-ergic interneurons, Belforte *et al.* (2010) found schizophrenia-like behaviours similar to those seen in the NR1 knock-down mice above in mice with selective NR1 deletion from 40-50% of corticolimbic GABA-ergic interneurons. GAD67 and parvalbumin expression were reduced in the GABAergic interneurons targeted by the NMDAR deletion, and cortical pyramidal cells were found to have increased firing rates and reduced cross-correlation of firing with nearby neurons, suggesting less efficient inhibition and synchronisation by surrounding interneurons.

In summary, there is evidence for NDMAR dysfunction in schizophrenia, and this is of particular interest here, in view of the prominent psychotic symptoms seen in NMDAR-Abs encephalitis and the demonstrable reduction in surface NMDAR in this condition. What mechanism link disrupted NMDAR signalling

and the behavioural deficits described in this section? One of the many potential mechanisms is hinted at by the decrease in parvalbumin-positive interneurons found in a number of the studies discussed above. These interneurons are crucial for synchronisation of brain oscillatory activity in the gamma-frequency range, which in turn underlies several cognitive and sensory processes. The evidence for this is discussed below.

1.5 Gamma-frequency oscillations

Since Hans Berger discovered that he could record brain electrical activity from electrodes placed on the scalp in 1923 it has become clear that such activity tends to be organized into oscillatory patterns (Buzsaki and Draguhn, 2004). Several frequency bands of oscillations exist, spanning 50 orders of magnitude, and each correlates with a particular brain state. Low frequency oscillations tend to involve large and widespread cortical networks, allowing for long-range synchronization of cortical areas, whereas high-frequency oscillations recruit smaller more localized neuronal assemblies. It has also become clear that oscillation frequency bands and their behavioural correlates are well preserved throughout mammalian evolution (Buzsaki and Draguhn, 2004) allowing reasonable conclusions to be drawn from animal data where human studies are difficult or unacceptable.

Slow-wave (<1Hz) and low frequency (delta, 1-4Hz) oscillations are predominantly seen during deep sleep and anaesthesia (Steriade *et al.*, 1993), and are important for memory consolidation (Castro-Alamancos and Connors, 1996). Theta-frequency oscillations (4-12 Hz) are prominent in the limbic system during low-level brain activity such as exploration in rodents and probably define the active state of the hippocampus. They are thought to represent a computational process allowing linking of activity in different areas activated by sensory stimuli and also areas involved in memory retrieval, thus allowing the organisation of segregated cell assemblies dealing with and integrating new and old information. In the hippocampus, theta rhythms are intrinsically linked with gamma-frequency rhythms (30-80 Hz), with increased power of gamma-rhythms during theta-associated behaviours and modulation of gamma amplitude by the theta cycle (Bragin *et al.*, 1995). Beta-frequency oscillations are intermediate to theta and gamma rhythms with frequencies

ranging from 13-30Hz. They occur prior to directed motor function following a sensory cue and also in response to novel stimuli, when their interplay with gamma-frequency oscillations appears important for encoding the information (Tallon-Baudry *et al.*, 1999; Haenschel *et al.*, 2000; Roopun *et al.*, 2006). Finally, rhythms with frequencies over 80 Hz are collectively termed very fast oscillations (VFOs). They are implicated in memory consolidation (Chrobak and Buzsaki, 1996; Ego-Stengel and Wilson, 2010) but also in seizure onset and epileptogenesis (Traub *et al.*, 2001; Grenier *et al.*, 2003).

Gamma-frequency oscillations (γ-oscillations, 30-80Hz) have been recorded in several cortical areas in humans and other animals and can be transiently elicited by sensory stimuli (for example (Gray and Singer, 1989; Pantev *et al.*, 1991; Llinas and Ribary, 1993; Haenschel *et al.*, 2000; Howard, 2003; Hanslmayr *et al.*, 2009)). Evoked γ-oscillations occur within the first 100 ms following a stimulus and are phase-locked to it. Although they do not appear to have a direct role in the object representation, evoked γ-oscillations provide a mechanism to process the different features of a stimulus by temporally synchronising the activity of spatially separate cortical areas (Gray and Singer, 1989; Tallon-Baudry and Bertrand, 1999; Tallon-Baudry *et al.*, 1999). Fractionally later (200-400ms after a stimulus), induced γ-oscillations appear. These oscillations are not phase-locked to the stimulus and play a role in binding observed features together into a coherent perception (“bottom-up” processing and object representation) (Singer and Gray, 1995; Tallon-Baudry *et al.*, 1999). They also appear to play a role in the “top-down” processes that allow percepts to be compared with memorised internal representations (Tallon-Baudry and Bertrand, 1999; Tallon-Baudry *et al.*, 1999). γ-oscillations carry out these roles by acting as a precise temporal structure for neuronal firing. This way, the binding problem of how to establish which perceived features belong together in active distributed systems, where potentially large numbers of neurons might be responding to individual features of the percept, is bypassed (Singer and Gray, 1995); by synchronising action potential firing in distributed groups of neurons (or cell assemblies) responding to a stimulus defined in time, γ-oscillations mediate the integration of information carried by the neurons activated by different aspects of a perceived stimulus into a coherent perception (Miltner *et al.*, 1999; Rodriguez *et al.*, 1999). This mechanism is also efficient in

that it allows cells to be part of any number of assemblies through modulation of their output (Singer, 2001).

In addition to this central role in perception, γ-oscillations are associated with selective attention (Tiitinen *et al.*, 1993), and a specific role in memory formation has been confirmed by a number of human scalp and intracranial electroencephalogram studies. γ-oscillations have been shown to increase with memory load in working memory tasks (Howard, 2003) and to be increased in the hippocampus and left frontal cortex during successful memory formation (Sederberg *et al.*, 2007) and during associative learning (Miltner *et al.*, 1999). Increased rhinal-hippocampal γ-oscillation synchronisation occurs with successful memory formation (Fell *et al.*, 2001).

Gamma-oscillations have been found to be impaired in individuals with schizophrenia. Delayed γ-band synchronisation during steady-state auditory stimulation using click trains (Kwon *et al.*, 1999), and absent stimulus-locked visual cortex γ-oscillations in response to viewing of illusory squares (Spencer *et al.*, 2004), have been demonstrated in patients with schizophrenia. Furthermore, individuals with schizophrenia produced a much slower reaction time phase-locked Beta-band oscillation in response to the illusory square than the healthy controls, who demonstrated a γ-band response, suggesting that neural networks in the brains of individuals with schizophrenia were less able to support high-frequency synchronisation (Spencer *et al.*, 2004). Deficits in evoked γ-oscillations have been demonstrated in first episode psychosis patients as well as patients with a chronic course and first-degree relatives of patients with schizophrenia (Uhlhaas *et al.*, 2008), suggesting that these deficits are likely to be related to the pathophysiology of the disease rather than be a result of medication or other consequences of the syndrome. Reductions in induced γ-oscillations during perception tasks and decreased γ-power during executive and working memory tasks have also been demonstrated in patients with schizophrenia (Uhlhaas *et al.*, 2008).

In summary, γ-oscillation power and synchronisation are associated with perception and cognition and deficits appear linked to the pathophysiology of schizophrenia, where reductions in parvalbumin-positive interneuron numbers and NMDAR dysfunction also appear to play a role. The elucidation of the

mechanisms underlying γ-oscillations *in vitro* has provided a convincing link between these entities, and is discussed below.

There are now several *in vitro* models of γ-oscillations. In each case the oscillation is an emergent property of neuronal networks involving phasic inhibitory post-synaptic potentials onto local principal cells at γ-frequency (30-80Hz). The models vary in terms of the role attributed to principal cells. All forms have been extensively studied in the hippocampus and the studies discussed below have all been performed in the hippocampus.

1.5.1 Interneuron Network Gamma-Frequency Oscillations (ING)

In the earliest *in vitro* model of γ-oscillations, oscillations were seen in networks of interconnected interneurons isolated from ionotropic glutamatergic excitation (Whittington *et al.*, 1995) in the hippocampus. Intracellular recordings were made from pyramidal cells in hippocampal slices where ionotropic glutamate receptors (AMPA, KA and NMDA) were blocked pharmacologically. Upon electrical stimulation, 40 Hz trains of inhibitory post-synaptic potentials (IPSPs) were recorded in pyramidal cells. These were blocked by a $GABA_A$ receptor antagonist, suggesting they were generated by networks of interconnected tonically activated inhibitory interneurons. Similar results were obtained using pressure ejection of glutamate and a metabotropic glutamate receptor agonist, the latter highlighting the role of tonic excitation of the interneurons. The IPSP trains were felt to entrain pyramidal neuronal firing at the frequency of the IPSP train (with firing occurring on the ascending/depolarising phase of the IPSP). This form of γ-oscillation is transient only, limited by metabotropic receptor desensitisation. Its frequency is controlled by the decay kinetics of inhibitory postsynaptic currents in interneurons, the amplitudes of which are related to the magnitude of tonic excitation received by interneurons. One of the shortcomings of this model is the non-physiological conditions in which ING is seen.

1.5.2 Pyramidal- Interneuron Network Gamma-Frequency Oscillations (PING)

The non-physiological conditions under which ING is seen experimentally led to the investigation of the role of principal neurons and ionotropic glutamatergic neurotransmission in the generation of γ-frequency oscillations. Computer modelling of networks of excitatory and inhibitory cells showed that excitatory

input to interneurons via ionotropic glutamate receptors also established γ-frequency rhythms. These rhythms combined aspects of ING (slow excitation via NMDA receptor activation acting like tonic excitation in ING model) and a frequency-modulating role provided by AMPAR-driven fast excitation of the interneurons (Traub *et al.*, 1997). It remained to be shown that such rhythms could occur in cortical structures. The hippocampus is known to receive strong cholinergic inputs and the ability of cholinergic activation to induce oscillations in the hippocampus was therefore investigated. Carbachol, a muscarinic acetylcholine receptor agonist, elicited γ-frequency field oscillations *in vitro* (A Fisahn *et al.*, 1998). These were blocked by $GABA_A$ receptor antagonism, suggesting, as in ING, that the oscillation is dependent on rhythmic IPSPs from inhibitory interneurons to synchronise the activity of pyramidal neurons. The decay kinetics of the $GABA_A$ receptor mediated IPSPs controlled the precise frequency of the oscillatory activity. In contrast to ING however, it was the phasic excitatory synaptic ionotropic glutamate receptor activation onto interneurons that generated and maintained the oscillation. Indeed, blocking AMPA and kainate receptors using 6-nitro-7-sulphamoylbenzo(f)-quinoxaline-2,3-dione (NBQX) abolished the oscillation. Blockade of NMDA-type ionotropic glutamatergic receptors and metabotropic glutamate receptors did not affect the oscillation, supporting a role for fast phasic glutamatergic excitation in these oscillatory rhythms. Thus, in this model, pyramidal cells provide sufficient excitatory input to inhibitory interneurons to produce IPSPs, which in turn rhythmically modulate principal cell output (see Figure 1.3). Support for the physiological relevance of this rhythm comes from two genetic knock-out models with neurotransmitter receptor deletions on parvalbumin-positive (PV+) interneurons only: mice that lack the AMPAR on PV+ interneurons had dramatically reduced γ-oscillations in keeping with the loss of fast synaptic excitation in these interneurons (Fuchs *et al.*, 2007), whilst mice lacking the $GABA_A$ receptor on PV+ interneurons still displayed γ-oscillations (Wulff *et al.*, 2009). This is in keeping with the preserved ability of interneurons, synaptically activated through ionotropic glutamatergic receptors, to synchronise the activity of excitatory principal cells via $GABA_A$ receptors on these cells.

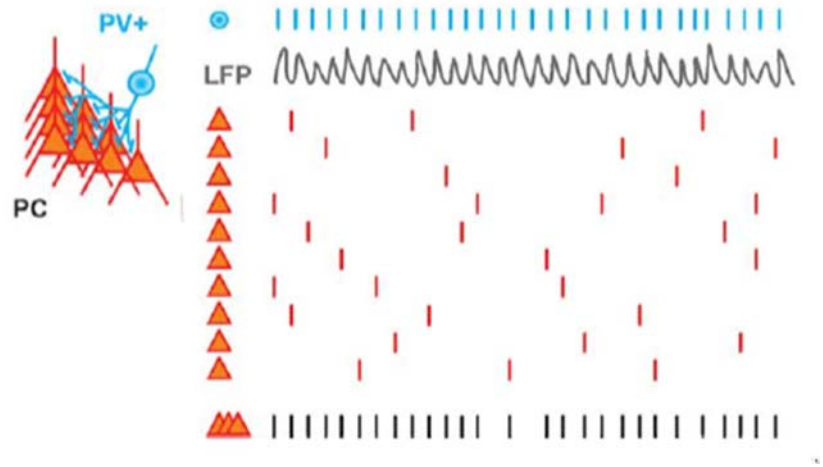

Figure 1.3 Schematic representation of the interplay of principal cells and interneurons during γ-oscillations.
Parvalbumin-positive fast-spiking interneurons produce a rhythmic output at γ-frequency (30-80Hz) (first line, blue) upon stimulation. This evokes rhythmic inhibitory postsynaptic potentials (IPSPs) in principal cells, which is reflected as rhythmic negative potentials (oscillation) in the local field potential (LFP, second line). This powerful peri-somatic inhibition of the principal cells (in this case hippocampal pyramidal cells, PC, orange triangles) allows principal cells to fire only in a brief window as inhibition wanes. Each principal cell involved in the γ-oscillation does not fire on every cycle, but if the population of principal cells involved is considered as a group, action potentials at γ-frequency, locked to the oscillation phase can be seen (bottom line), allowing precise information processing by the network. The additional excitatory drive to interneurons is provided via the axonal plexus (not shown). The inset illustrates the fact that a single interneuron contacts several principal cells. Taken from Kann *et al.* (2014).

1.5.3 PING and the axonal plexus

The PING model described above requires high principal cell spike rates with no phase lag with interneurons to provide interneurons with sufficiently strong input to produce phasic IPSP trains. Fisahn et al (A Fisahn *et al.*, 1998), however, found that the pyramidal cells they recorded from in CA3 during carbachol-induced PING fired on only 5% of the cycles of the oscillations. The same has been shown in kainate-induced oscillations in cortical areas (Cunningham *et al.*, 2003a; Cunningham *et al.*, 2004). This cannot provide sufficient excitatory input to the interneurons to generate rhythmic firing and thus rhythmic IPSPs in their postsynaptic principal cells. The observation that high-frequency activity (>100Hz) was present in the axon-containing CA3 stratum oriens that was of axonal origin, gap-junction transmission-dependent and phase-locked to the field γ-oscillation in the pyramidal cell layer (Traub *et al.*, 2003), provided an explanation for this discrepancy: indeed, a gap-junctionally coupled principal cell axonal plexus can propagate non-somatically produced action potentials very rapidly and, therefore, in addition to the somatic spiking of principal cells, provide the strong phasic drive required to excite the interneurons and produce a γ-oscillation. This ectopic activity is thought to result from GABA overspill from synapses, as GABA has been shown to have an excitatory action on non-somatic sites, and/or from kainate-induced axonal excitation (Traub *et al.*, 2003). In some neocortical areas, including the entorhinal cortex, fast rhythmic bursting cells have been described, whose intense spiking behaviour populates the axonal plexus with ectopic action potentials, thereby playing an essential role in γ rhythm-generation (Cunningham *et al.*, 2004).

There are two widely used models of persistent hippocampal γ-oscillations *in vitro*: oscillations can be generated in acute brain slices using either carbachol as described above, or kainic acid (KA), an agonist at the kainate receptor, one of the ionotropic glutamatergic receptor subtypes. Both oscillations are abolished by $GABA_AR$ antagonism, and AMPAR antagonism blocks carbachol-induced hippocampal oscillations (A Fisahn *et al.*, 1998) but not KA-induced oscillations (A. Fisahn *et al.*, 2004). This highlights that, whilst they both rely on inhibition for their generation and maintenance, they differ in the excitatory mechanisms invoked. Carbachol-induced oscillations also rely on phasic

excitation, mediated by AChR activation of pyramidal cells and consequent glutamate release. In KA-induced hippocampal oscillations, the direct activation of KAR on interneurons is sufficient to generate the oscillation.

1.5.4 The role of PV+ interneurons in γ-oscillations

As discussed above, *in vitro* models of γ-oscillations have revealed a reliance on $GABA_AR$-mediated inhibition. There are several types of inhibitory interneurons, classified according to their intrinsic properties, such as fast-spiking or non-fast spiking, whether they preferentially target the soma or the dendrites of other cells, and further subdivided using their expression of intracellular proteins such as calcium-binding proteins (parvalbumin, calbindin, calretinin) and neuropeptides (e.g. somatostatin). Fast-spiking parvalbumin-positive interneurons that target the perisomatic region of pyramidal cells (also called basket cells) have been shown to play a crucial role in the generation and maintenance of γ-oscillations in both hippocampus and cortical areas *in vivo* and *in vitro* (Buhl *et al.*, 1994; Klausberger *et al.*, 2003). Several of their intrinsic properties place them in an ideal position to fine-tune the activity of pyramidal cells. Their axons arborize extensively in the pyramidal layer of the hippocampus and innervate the soma and proximal dendrites of pyramidal cells, with around twelve synapses onto each pyramidal cell, as well as other PV+ interneurons (Buhl *et al.*, 1994; Klausberger *et al.*, 2003). The somatic location of the synaptic contacts controls the spiking of pyramidal cells and shortens the window for input integration by pyramidal cells, enforcing precise coincidence detection and thus reducing noise in the soma (Pouille and Scanziani, 2001). It has been estimated that each basket cell synapses with up to 2,500 principal cells (Kann *et al.*, 2014). Together with the mutual connections, this allows synchronisation of activity in interneuron networks as well as large and spatially distributed pyramidal cell populations (Strüber *et al.*, 2015). These cells are able to fire action potential trains up to 100Hz in frequency and are the most active interneuron subtype during γ-oscillations when their firing is phase-locked to the oscillation, with action potentials occurring rhythmically at every cycle of the oscillation (Hájos *et al.*, 2004; Mann *et al.*, 2005; Gulyás *et al.*, 2010). In addition to the genetic knock-out models described in section 1.5.2 that strongly implicate PV+ interneurons in γ-rhythmogenesis, recent optogenetic experiments *in vivo* using mice with channelrhodopsin-2 expression on PV+

fast-spiking cells demonstrated an increase in γ-band activity of the local field potential with activation in the γ-frequency range in somatosensory cortex (Cardin *et al.*, 2009) and even with non-rhythmic drive in neocortex, whilst inhibiting PV+ cells suppressed γ-frequency rhythms (Sohal *et al.*, 2009). Additionally, γ-oscillations modulated sensory stimulus response such that temporal precision of spike-timing was enhanced (Cardin *et al.*, 2009) and improved the signal-to-noise ratio during transmission (Sohal *et al.*, 2009).

1.5.5 The role of NMDAR in γ-frequency oscillations

In the sections above, we have seen that γ-oscillations are dependent upon $GABA_AR$ kinetics and phasic drive to interneurons through AMPA receptors. The putative roles of NMDA receptors as coincidence detectors and mediators of synaptic plasticity, and of γ-oscillations as a mechanism to strengthen synapses between co-active cells would predict that NMDAR should have a role in modulating γ-oscillations. However, several *in vitro* experiments have indicated that blocking NMDAR has no effect of hippocampal γ-oscillations (A Fisahn *et al.*, 1998; Mann *et al.*, 2005). Whilst some studies have demonstrated preferential inhibition of interneurons by NMDAR antagonists and consequent pyramidal cell disinhibition with increased firing rate in several cortical areas *in vitro* (Li *et al.*, 2002) and *in vivo* (Homayoun and Moghaddam, 2007) - which would be predicted to impair γ-oscillations - the specific interneuron subtype affected by the NMDAR antagonism was not determined. On the other hand, the contribution of NMDAR activity to synaptic excitation of PV+ fast-spiking basket interneurons has been shown to be relatively weak: in the hippocampus, the NMDAR content of glutamatergic synapses on PV+ interneurons is remarkably low (NyÍri *et al.*, 2003). NMDAR-mediated currents are present only in the minority of fast-spiking interneurons in the adult rat prefrontal cortex (Wang and Gao, 2009). Similarly, AMPAR-mediated currents are three times larger than their NMDAR counterparts at the thalamocortical synapses onto fast-spiking interneurons in the rat somatosensory cortex, and individual NMDARs passed less charge at fast-spiking cell synapses than at regular-spiking interneuron synapses (Hull *et al.*, 2009).

Nevertheless, it is possible that this apparent lack of NMDAR contribution to PV+ fast-spiking cells is region-specific. Indeed, marked region-specific

differences in the effect of ketamine on KA-induced γ-oscillations have been described: ketamine had no effect on hippocampal, somatosensory cortex and insular cortex oscillations, but reduced entorhinal cortex oscillations and increased auditory cortex oscillations in one study (Roopun *et al.*, 2008). Cunningham *et al* (Cunningham *et al.*, 2006) showed that ketamine reduced the power of kainate-induced γ-oscillations in the superficial layers of the medial entorhinal cortex (mEC). The frequency of the oscillation also decreased (from 45Hz to 39Hz) but this reduction was not statistically significant. Intracellular recordings from pyramidal cells during the field γ-oscillation revealed less frequent IPSPs and more frequent action potentials in the presence of ketamine, suggesting that the principal cells were disinhibited in the presence of ketamine, in keeping with a preferential effect of ketamine on the local layer II PV+ fast-spiking interneurons. Further support for a strong contribution of NMDAR to PV+ interneuron activity in the EC comes from the finding that stimulus-evoked synaptic responses of basket-like fast-spiking interneurons in layer II mEC are dominated by NMDAR-activity, with only a small fast component of the excitatory post-synaptic potential abolished by AMPAR blockade (Jones and Buhl, 1993). Spontaneous EPSPs also appeared mediated by NMDAR: they were abolished by the selective NMDAR antagonist D-AP5 but not by an AMPAR antagonist, indicating that NMDARs may be tonically activated in interneurons in the mEC

Further to this, it was shown that ketamine reduced both the frequency (this time from an average of 41 Hz to 31Hz) and power of γ-oscillations in superficial mEC layers (Middleton *et al.*, 2008). Here it was shown that basket-type interneurons significantly reduced their firing rate from a γ-frequency to about 3Hz in the presence of ketamine, suggesting they were no longer participating in γ-rhythmogenesis. Instead, goblet-type interneurons were found to fire at the new field oscillation frequency, indicating that tonic NMDAR activation on basket-type interneurons is essential in maintaining γ-oscillations above 40Hz in the superficial mEC layers. This is likely to be of functional significance as the different hippocampal areas to which the mEC projects preferentially oscillate at different frequencies, suggesting that changes in mEC oscillations could affect information flow by altering synchronization ability (Middleton *et al.*, 2008).

Further evidence for a modulating role of tonic NMDAR activation on gamma oscillations comes from a study by Mann and Mody (2010). Here, the authors sought to explain why *in vivo* hippocampal oscillations can have frequencies up to 200 Hz whereas *in vitro* oscillations seem restricted to around 40 Hz. They found that *in vitro* carbachol-induced hippocampal oscillations in mice lacking the delta-subunit (δ) of the $GABA_AR$ were significantly faster than in slices from wild-type mice, and that the oscillation frequency was reduced by the NMDA receptor antagonist D-AP5 in the knock-out mice. The δ-$GABA_AR$ subunit mediates tonic inhibition in interneurons. In slices obtained from δ-subunit knock-out mice, the hippocampal interneurons were therefore less inhibited and this exposed an NMDAR-dependent excitatory drive to the interneurons, resulting in increased frequency oscillations. In further experiments, they showed that NMDA increased the oscillation frequency in hippocampal slices from juvenile δ-subunit knock-out mice. This was reflected in increased phasic inhibitory currents in pyramidal cells, mediated by an increase in the amplitude of IPSPs but not a change in frequency of IPSPs.

Several important conclusions can be drawn from this work: firstly, tonic inhibition via extrasynaptic $GABA_ARs$ controls the activation of NMDAR in hippocampal interneurons. This is consistent with the fact that NMDAR are voltage- as well as ligand-gated. Secondly, network activity frequency in the gamma-range is modulated by a balance between NMDAR-mediated excitation and $GABA_AR$-mediated inhibition in the hippocampus. This balance is of likely functional importance, because network activity frequency will dictate which neurons are active simultaneously and therefore what connections undergo synaptic plasticity. Finally this work also suggests, on a more general level, that oscillation power and frequency respond differently to changes in neuronal excitability.

By contrast, NMDAR antagonism *in vivo* has been shown to increase the power of basal γ-oscillations in several cortical areas and in awake as well as anaesthetised rodents (Hakami *et al.*, 2009). It is important to note that it is difficult to tease out the mechanisms for this increase in the whole brain, but this generalised increase in γ-activity was felt to represent diffuse network noise rather than cognitively important activity. The development of a mouse model

with a selective loss of NMDAR from PV+ fast-spiking interneurons has provided a more useful approach to the study of the role of NMDAR in γ-oscillations and supports a role for NMDAR in the generation of normal, behaviourally-relevant γ-rhythms. These mice displayed increased power in the γ-frequency band of the local field potential recorded in the hippocampus during awake exploration (Korotkova *et al.*, 2010) and somatosensory cortex during anaesthesia (Carlen *et al.*, 2011). Theta-modulation of the hippocampal γ-rhythms was impaired and positional firing of pyramidal cells was less precise in the knock-out mice (Korotkova *et al.*, 2010), supporting the idea of reduced signal-to-noise ratio. When the PV+ interneurons were selectively optogenetically stimulated at either γ-frequency or non-rhythmically (Carlen *et al.*, 2011), there was no further increase in γ-activity in the knock-out mice, suggesting an inability to produce stimulus relevant γ-oscillations. This deficit in γ-induction was related to less well-synchronised firing of PV+ interneurons in the knock-out mice. Furthermore, the knock-out mice performed poorly on spatial working memory, short and long-term recognition memory (Korotkova *et al.*, 2010), habituation and associative learning tasks (Carlen *et al.*, 2011).

The evidence discussed above supports a role for NMDAR on PV+ interneurons in the modulations of normal γ-oscillations and suggests that the mEC, with its exquisitely NMDAR-sensitive basket interneurons, might provide an ideal region to study the effects of NMDAR antagonism on γ-oscillations.

1.6 The medial entorhinal cortex (mEC)

In rats, the HPC and the EC-containing parahippocampal region lie in the caudal part of the brain. The hippocampus consists of three subregions: the dentate gyrus (DG), the Cornu Ammonis areas 1-3 (CA1, 2 and 3) and the subiculum. The PHR borders the subiculum and consists of the presubiculum, the parasubiculum, the entorhinal cortex, the perirhinal cortex and the postrhinal cortex (see Figure 1.4).

The hippocampus is a three-layered cortex, therefore classified as “allocortex”. From superficial to deep, the layers consist of the molecular layer, the cell layer and finally a layer consisting of axons and interneurons, whose name varies by subregion. The molecular layer is referred to as the stratum moleculare in the

DG and subiculum. In the CA areas, it is further subdivided into stratum lucidum, radiatum (containing apical dendrites of neurons in the cell layer), and lacunosum-moleculare (containing the apical tufts of the apical dendrites), although stratum lucidum is not present in CA1. The cell layer is composed of principal cells and interneurons and is called stratum pyramidale in CA areas and subiculum, and granule layer in the DG. The deepest layer is named hilus in the DG and stratum oriens in the CA areas (van Strien *et al.*, 2009).

The EC is classed as a transitory zone, in that its laminar structure can be viewed as a transition from three-layered allocortex to six-layered neocortex. Indeed, the EC has six distinct layers, although no cell bodies are visible in layer IV (lamina dissecans).

Up until recently it was felt that the EC functioned mainly as an input-output station for the HPC. Research into memory formation had resulted in the development of a standard model for the circuitry of the PHR and HPC, which is depicted in Figure 1.5. In this model, information flows from unimodal or polymodal neocortical association areas to the postrhinal (POR) and perirhinal (PER) cortices in functionally distinct pathways, with the POR cortex receiving input from visual association areas whereas input to the PER cortex originates from all other association areas. The peri-and postrhinal cortices project to the lateral and medial EC respectively, keeping the two streams segregated. The EC then relays the input to the HPC, projecting to all its subregions through the perforant pathway. Layer II of the EC projects to the DG and CA3, and layer III of the EC to CA1 and the subiculum. In the HPC, a polysynaptic pathway connects all the HPC subregions sequentially. The mossy fibres project from the DG to CA3, which in turn targets CA1 through the Schaffer collaterals. CA1 is connected to the subiculum, and both project to the deep layers of the EC. The EC then projects back out to neocortical areas via the rest of the PHR (Kandel *et al.*, 2000).

It has since then become clear that the connectivity between the PHR and HPC, as well as within each area, is far more complex and intricate (van Strien *et al.*, 2009). A lengthy discussion of these connections is outwith the scope of this review. Suffice it to say that significant overlap in POR and PER projections to the EC as well as reciprocal connections between the mEC and lEC suggest

that visuospatial and non-visuospatial information may be integrated at the level of the EC, a role classically left to the HPC.

A role for the medial temporal lobe (MTL) structures in memory was first suggested in the 1940s by Penfield. He had found that, by stimulating the MTL electrically in awake surgical patients, he could occasionally elicit memories (Penfield, 1947). In the 1950s, his findings were confirmed when the now famous patient H.M. was studied (Squire, 2009). H.M. had had both MTLs excised for intractable epilepsy. After the surgical procedure he was found to have severe anterograde amnesia, although his memory of past events was unaffected. This suggested that the HPC and PHR were necessary to form new declarative memories, but that storage of memories took place elsewhere, namely in association cortices. Further animal and human lesion studies established that lesions to PHR and in particular the EC caused more severe memory deficits than lesions to HPC (Kandel *et al.*, 2000). The mEC has been shown to play an important role in spatial navigations and contains grid cells that are spatially modulated and accurately predict animal location in a two-dimensional test environment (Fyhn *et al.*, 2004; Hafting *et al.*, 2005). Interactions between mEC and lateral EC appear important to link encoding of stimuli and their context, with lesions of lEC leading to impairment of item recognition in animals whilst lesion of the mEC were associated with loss of object-location recognition (Eichenbaum *et al.*, 2007). Studies of the function of the entorhinal cortex in humans are still in their infancy, and it is not clear if the human entorhinal cortex can be divided into medial and lateral areas as in rodents, but activation of the parahippocampal region (containing the medial aspect of the entorhinal cortex) and the perirhinal cortex (containing the lateral aspect) have been demonstrated during tasks involving examination of spatial scenes and object processing respectively (reviewed in (Eichenbaum *et al.*, 2007)). Reductions in entorhinal cortex volume have also been demonstrated in very early Alzheimer's disease and mild cognitive impairment, with conversion to Alzheimer's disease predicted by loss of entorhinal volume (de Toledo-Morrell *et al.*, 2000). In keeping with the presumed role of the entorhinal cortex in memory, a more recent study has shown that γ-frequency oscillations in EC and HPC are more strongly synchronised during successful memory formation,

suggesting that rhinal-hippocampal cooperation is required for declarative memory formation (Fell *et al.*, 2001).

Furthermore, temporal lobe epilepsy in humans is associated with changes in the histology of the entorhinal cortex, with marked loss of pyramidal cells in layer III (Du *et al.*, 1993). Many lines of evidence suggest the EC might be an important site of seizure generation, and its connectivity might play a role in seizure propagation (reviewed in Vismer *et al.* (2015)).

In summary, its position at the interface between neocortical areas and hippocampus suggest a computational and integrational role for the entorhinal cortex in spatial and memory domains that are beginning to find support in animal and human studies. γ-oscillations can be induced pharmacologically in the mEC in rodent brain slices and these have a number of attributes, different from hippocampal oscillations, that make them useful to study the effects of NMDAR antagonism on this cognitively-relevant rhythm.

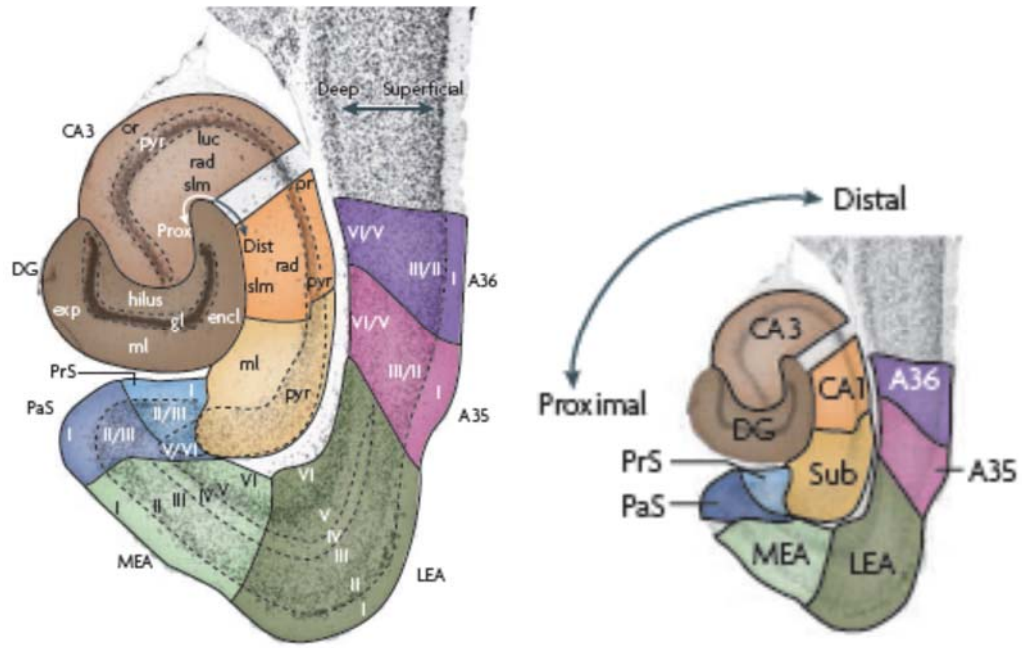

Figure 1.4 The anatomy of the Hippocampus and parahippocampal region.
A Nissl-stained horizontal cross-section of the hippocampus and parahippocampus with superimposed colour codes indicating the location of the different subregions. Postrhinal cortex: pink and purple; lateral entorhinal area of EC: dark green; medial entorhinal area of EC: light green; parasubiculum: dark blue; presubiculum: light blue; subiculum: yellow; CA1: orange; light brown: CA3; dentate gyrus: dark brown. The roman numerals indicate cortical layers.
Encl, enclosed blade of the DG; exp, exposed blade of the DG; gl, granule cell layer; luc, stratum lucidum; ml, molecular layer; or, stratum oriens; pyr, pyramidal layer cell layer; rad, stratum radiatum; slmstratum lacunosum-moleculare. Taken from van Strien et al 2009 (van Strien *et al.*, 2009).

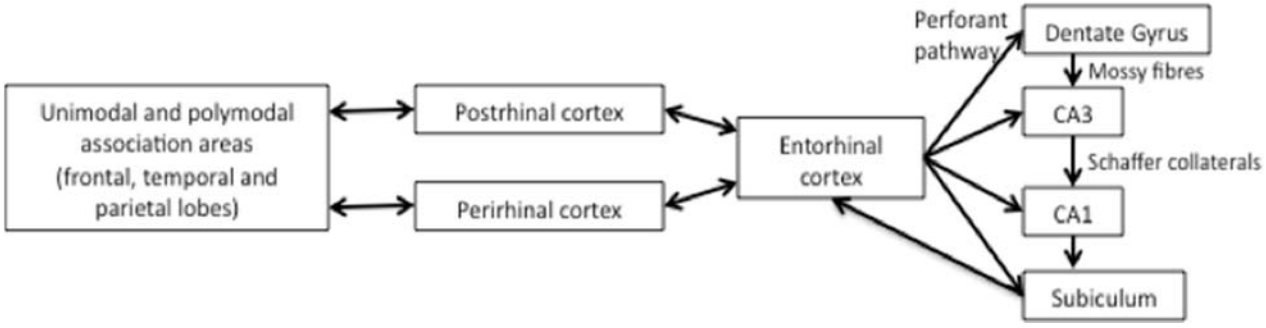

Figure 1.5 Standard view of PHR-HPC circuitry.
Adapted from (Kandel *et al.*, 2000)

1.7 Aims and hypotheses

NMDAR-Ab encephalitis is a recently described autoimmune encephalitis presenting with psychiatric symptoms, amnesia, seizures, central hypoventilation, dyskinesia and autonomic features (Dalmau *et al.*, 2008; Irani *et al.*, 2010b). There is now good evidence that the NMDAR-Abs found in the blood and CSF of patients can have an effect on NMDAR density and function (Dalmau *et al.*, 2007; Dalmau *et al.*, 2008; Hughes *et al.*, 2010), and a recent study found that passive transfer of NMDAR-Abs to mice induced memory deficits (Planagumà *et al.*, 2014), supporting the pathogenicity of the antibodies. However, most of the studies investigating the mechanism of action of NMDAR-Abs were conducted in neuronal cell cultures, which lack the connectivity seen *in vivo* or in the *in vitro* slice preparation. The *in vivo* studies performed so far were either short (Manto *et al.*, 2010; Manto *et al.*, 2011) or did not record electrophysiological data (Hughes *et al.*, 2010; Planagumà *et al.*, 2014). It is therefore not clear if these antibodies alter or disrupt neuronal network activity, which forms the basis of perception and cognition.

The hypothesis in this thesis is that NMDAR-Abs are able to disrupt cortical network activity in the form of γ-oscillation in the medial entorhinal cortex through effects on parvalbumin-positive interneurons. γ-oscillation deficits in this region are likely to translate to memory and cognitive deficits as seen in NMDAR-Ab encephalitis**.**

Firstly, a comparison of the available diagnostic assays for NMDAR-Abs will be carried out to determine the most sensitive and specific method of NMDAR-Ab detection. Currently, different diagnostic laboratories use different assay methods and these have not been fully compared.

The aim of this project is then to contribute to the demonstration of the pathogenic nature of the antibodies by providing a network-level mechanism for the observed cognitive deficits seen in the presence of reduced NMDAR density. To achieve this, three different approaches will be used:

- Investigate if NMDAR-Abs acutely alter organised cortical rhythms when applied to live rodent brain slices *in vitro* and explore the mechanisms by which this occurs.

- As acute exposure to NMDAR-Abs may be insufficient to cause changes in network activity, the effect of sub-acute exposure to NMDAR-Abs by passive transfer will also be examined.
- Determine the effect of exposure to NMDAR-Abs on other measures of inhibition in the entorhinal cortex using immunostaining techniques

Chapter 2 Materials and Methods

2.1 Purified Immunoglobulin G preparation

Purified IgG was prepared from the serum or plasma of patients with NMDAR-Ab encephalitis (3), VGKC-Ab encephalitis (1), and healthy controls (2). Other than 1 patient sample (Patient 3), all purified IgG and the purified Fab samples were gifts of Professor Angela Vincent and the Neuroimmunology laboratory at the Nuffield Department of Clinical Neurosciences, Oxford University. Patient 3 IgG was purified from the plasma obtained following plasmapheresis as treatment for NMDAR-Ab encephalitis using the same protocol used for the other patient and control samples as follows: 20mLs of patient plasma were incubated overnight with 5mls of washed protein G Sepharose beads (Sigma, UK) and 20mLs of Hartman's solution at 4°C on a shaker, to allow IgG of all subclasses to bind to the protein G beads. The solution was then loaded into a chromatography column and allowed pass through the column until only the beads remained. The column was washed with 50mLs Phosphate-buffered saline (PBS 0.1M, ThermoFisher-Oxoid, UK) to remove non-specifically bound proteins. To separate the IgG from the protein G beads, 1 mL of eluting solution (0.1M Glycine at pH 2.3) was then allowed to quickly drip through the bead pellet and collected in Eppendorf tubes containing 200μL 1M Tris-buffer at pH 8.0 to neutralise the solution and avoid denaturation of the molecules. Protein concentration was measured using a spectrophotometer (OD 280nm measured by NanoDrop 2000, Thermo Scientific, UK). The four elution fractions with the highest protein concentration were pooled and sealed in snakeskin dialysis tubing (10, 000 kDA cut-off, ThermoScientific, UK), and dialysed overnight in 2 L of Hartman's solution. The purified IgG remaining within the snakeskin was then filter-sterilised, and protein concentration determined as above. Purified IgG was stored at 4°C until use.

2.2 Animal provision

For acute slice experiments, male Wistar rats aged 40-60 days were obtained from Charles River UK and housed in a pathogen-free environment in the Comparative Biology Centre at Newcastle University for at least one day prior to use to allow acclimatisation. They were housed in standard non-ventilated cages enhanced with environmental enrichment, provided with food and water *ad libitum*, and subjected to a 12-hour light/dark cycle.

For experiments on slices from animals injected with purified IgG, male Wistar rats weighing 230-250 g were obtained from Charles River UK and housed as described above in cages of four or five animals for at least a week prior to surgery to allow acclimatisation.

2.3 Animal procedures

All procedures were performed in accordance to the UK Animals (Scientific Procedures) Act 1986 and were covered by the following personal and project licenses granted by the UK Home Office:

- Anaïs Thouin 60/12991 (personal license)
- Mark Cunningham: PPL 60/4455 (project license)

2.3.1 Intracerebral injections

For the experiments investigating the effect of sub-acute exposure to NMDAR-Abs, male Wistar rats weighing 260-280g received a single intra-entorhinal injection of 5μL of purified human IgG (10-12.5 mg/ml). The tails of animals were marked for identification using a marker pen. The animals were anaesthetised using 4% isofluorane in O_2 at a flow rate of 4 L/min in a specially built anaesthetic chamber. Once breathing rate had slowed to about 1 breath/second and righting reflex was abolished, the scalp was shaved and the animal transferred to a heating blanket placed on the stereotactic frame. Anaesthesia was maintained using 3% isofluorane at an oxygen flow rate of 2L/min. The animal was positioned in the stereotactic frame (Digital New Standard Stereotaxic Frame, Stoelting Europe, Dublin, Ireland) using the tooth bar and non-traumatic ear bars. The rat was covered with bubble wrap to maintain body temperature, paraffin eye cream was applied to the eyes for protection during the procedure, body temperature was monitored using a rectal probe (Harvard Apparatus, UK), blood O_2 saturation and pulse rate were monitored using a rodent digital oxymetry meter (DRE veterinary, USA), and analgesia and further sedation were given by intraperitoneal injection (Buprenorphine 0.05 mg/kg, and meloxicam 1mg/kg, diluted 1 in 10 in 0.9% Saline). The scalp was then cleaned with chlorhexidine. The rest of the procedure was performed under aseptic conditions with the help of an assistant. The scalp was infiltrated with ca. 1 mL 0.25% Bupivacaine along the line of the

incision and a central incision was made from ear level to the caudal aspect of the skull. The skull was exposed by dividing any subcutaneous tissue and allowed to dry for 1-2 minutes. Isofluorane concentration was then reduced to 1.5% (O_2 at 2 L/min) to avoid respiratory depression. Bregma was identified and set as point 0 on the digital stereotactic frame. The stereotaxic coordinates used for the injection were -8.4 mm in the anteroposterior direction, +4.8 mm laterally to left and -3.4 to -3.9 below the brain surface. A small hole was drilled into the skull at the injection site using a dental drill (Stoelting Europe, Ireland) and cleared of debris using sterile cotton wool. IgG was drawn up into a 25μL Hamilton syringe (700 Series, removable needle, Sigma-Aldrich, UK) as follows: A 33 gauge custom length of 35mm needle was attached to the Hamilton syringe and cleaned three time in pure ethanol. 5μL Ethanol were drawn up followed by 5μL air then 6μL IgG and a minute amount of fluorescent beads (so just visible above in the syringe, <1 μL). The needle was lowered into the craniotomy and IgG was injected in a staged fashion using a microdriver (Harvard Apparatus, UK): 2.5 μL were injected at 0.5μL/min at -3.9 mm below brain surface. The needle was then left in this position for 1 minute before being retracted to -3.4 mm below the brain surface. A further two minutes were allowed to elapse before the remaining 2.5μL were injected at 0.5μL/min. The needle was again left in place for 1 minute, then retracted by a further 1mm and another pause of three minutes was made before withdrawing the needle completely. This was to avoid the injected IgG tracking up along the path of the needle. The scalp was closed using subcuticular uninterrupted sutures and the knot buried before applying a small amount of superglue (Vetbond, WPI, UK) to the caudal aspect of the wound. The isofluorane was stopped and rats were observed until awakening. They were then placed in a single cage in a heated cabinet (25°C) and given a soaked diet and water *ad libitum*. The following day, they were returned to their home-cage together with their similarly injected cage-mates. The syringe was washed with 100% ethanol and sterile PBS. The rats were observed and examined daily post-operatively and welfare score sheets (see Appendix) were completed daily until used for experiments.

2.3.2 Preparation of brain slices

Rats were killed by terminal anaesthesia followed by intracardiac perfusion before decapitation. Rats were anaesthetised by inhalation of isofluorane (1-

2ml, Abbott Laboratories Ltd., Kent, UK). When the righting reflex was abolished, an intramuscular injection of 0.3mls 2% xylazine (≈10mg/kg, Millpledge Veterinary, Retford, UK) and 0.3 mls ketamine (≈100 mg/kg, Fort Dodge Animal Health Ltd., Southampton, UK) was given. When the pedal withdrawal response and the corneal reflex were abolished, the heart was surgically exposed and an intracardiac perfusion of 50ml chilled (4°C) oxygenated sucrose-containing artificial CSF (composition: 25mM sucrose, 3mM KCl, 1.25mM NaH_2PO_4, 24mM $NaHCO_3$, 2mM $MgSO_4$, 2mM $CaCl_2$ and 10mM glucose) at a rate of 25ml/min using a perfusion pump (Harvard Apparatus, UK) was performed. Pressure damage to organs was avoided by incising the right atrium. The animal was decapitated and the brain dissected. Horizontal slices 450 micrometres thick were cut using a Leica VT1000 microtome (Leica Microsystems, Germany) and trimmed to contain only HPC and entorhinal, as well as auditory, cortex, in sucrose-modified aCSF. The use of sucrose-modified aCSF for perfusion and slicing is known to protect interneurons and GABA-ergic transmission in slices by preventing excessive action potential firing (sucrose aCSF does not contain Na^+).

Slices were transferred to a holding chamber, and maintained on a nylon mesh at the interface between artificial CSF (aCSF; composition: 126mM NaCl, 3mM KCl, 1.25mM NaH_2PO_4, 24mM $NaHCO_3$, 1mM $MgSO_4$, 1.2mM $CaCl_2$ and 10mM glucose) and humidified 95% O_2/5% CO_2 for one hour at room temperature to allow death-related processes at the cut surfaces to occur. Slices were then transferred to a recording chamber, where they were placed on lens paper (Whatman, UK) soaked in oxygenated aCSF. The lower Mg^{2+} concentration in this aCSF was used to potentiate NMDAR-transmission. The slices were maintained at the interface between humidified 95% O_2/5% CO_2 and aCSF at 32°C constantly circulated using a peristaltic pump (Watson-Marlow, UK) at a rate of 1.3 ml/min. The slices were left to equilibrate for at least thirty minutes prior to the addition of any drug or IgG. Slices were exposed to drugs and IgG by dissolving these in the circulating aCSF. Additional slices were maintained in the holding chamber at room temperature until use and were found to be viable for up to 8 hours.

2.4 Recording techniques

2.4.1 Extracellular field recordings

Extracellular field recordings were obtained using micropipettes of borosilicate glass (Harvard Apparatus GC120TF 1.2mm outer diameter x 0.94mm inner diameter) filled with aCSF. Micropipette resistance ranged between 2 and 5 megaOhms. The field potential was recorded in current-clamp mode, amplified using AXOprobe-1A amplifiers (Axon instruments Inc, USA), and filtered at 0.1-300Hz. Mains noise was filtered from the signal using Humbugs (Quest Scientific Instruments Inc., Canada). The signal was then digitized at 5-10 kHz. Data were recorded and analysed using Axograph 4.6 software (AxoGraph Scientific Software, Axon Instruments, Sydney, Australia).

2.4.2 Intracellular recordings

Intracellular recordings were made using borosilicate glass micropipettes containing an inner filament (Harvard Apparatus, UK; GC120F 1.2mm O.D. x 0.69mm I.D.) with very sharp tips capable of impaling single cells. The micropipettes were pulled using a P-97 Flaming-Brown horizontal puller and filled with 2M potassium acetate at pH 6.8-7, with resistances between 70 and 170 MΩ. The signal was filtered between DC and 1 KHz and the remaining data acquisition process was as for extracellular field potential recordings. Biocytin-HCl (Sigma-Aldrich, UK) was diluted in the potassium acetate to a 2% solution to slowly fill the recorded cells during recording for post-hoc visualisation by immunohistochemistry. Only cells with a resting membrane potential of less than -50mV and action potentials overshooting 0mV were used in these experiments. Cell type was determined electrophysiologically using their membrane and action potential characteristics (see later chapters). Hyperpolarising cells to a membrane potential of -70mV using DC current revealed invading excitatory post-synaptic potentials (EPSPs). Evoked EPSPs were recorded by placing a bipolar stimulating electrode made of silver wire and connected to a stimulating box capable of delivering stimuli ranging from 0.1-100V (Constant Voltage Isolated Stimulator, Digitimer Ltd., UK) in the most medial portion of layer II/III of entorhinal cortex whilst recording from a cell more laterally in the same layer. Stimuli of up to 20V and of 25μs duration were given singly or at 1Hz frequency for 10 seconds.

2.5 Experimental protocol

Slices were allowed to equilibrate to the rig temperature (32°C) for 30 minutes prior to the start of experiments. Extracellular or intracellular recording electrodes were then placed in layers II or III of the medial entorhinal cortex or stratum radiatum of CA3 (Figure 2.1 B). It is not possible to visually determine whether the recording electrode is in layer II or III of the mEC, and the recordings are therefore describes as being from layers II/III. Baseline activity was observed and recorded as control recordings to ensure that there was no spontaneous oscillatory or epileptiform activity (Figure 2.1 Ai). Slices displaying spontaneous epileptiform activity were not used for experiments. Gamma-frequency oscillations were generated by adding kainic acid (KA) to the perfusing aCSF to a concentration of 400nM KA (Figure 2.1 Aii) for the mEC and 50nM for the HPC. Oscillations developed in power and frequency over 45 minutes to 1 hour (Figure 2.1 Di). Oscillation parameters (peak power, frequency at peak power and area power (the overall power within the 20-80Hz range)) were determined by applying a fast-Fourier transform (FFT) to a 60-second epoch of activity (see below 2.5.2 for discussion and Figure 2.1 Ci). The power and frequency of oscillations were assessed 1 hour after addition of KA, and if found to be outside the gamma-frequency range (i.e. below 30Hz) or to be too small or to large in amplitude (corresponding to a peak power less than 5 $\mu V^2/Hz$ or greater than 100 $\mu V^2/Hz$), the electrode was moved to a new location within layer II/III of mEC. These power values were chosen as oscillations with peak powers outside these limits were rare and tended to collapse over 1-2 hours. Much larger power values were accepted for hippocampal γ-oscillations as these are known to be much stronger due to the simple laminar organisation of the hippocampus (Bartos *et al.*, 2007). Oscillations were then observed every ten minutes until the values obtained for peak power, frequency at peak power, and area power were within 20% of each other for four consecutive readings (30 minutes of stability, Figure 2.1 Di and ii). The drug or IgG under investigation was then dissolved into the circulating KA-containing aCSF and allowed to perfuse the slices for 1 hour before being washed out with KA-containing aCSF for at least 30 minutes (Figure 2.1 Dii). Drug and IgG concentrations are given in the relevant chapter. Drug concentrations were as used in relevant literature.

2.5.1 Blinding of experiments

In order to reduce bias, experiments were carried out blind to the IgG preparation applied. Blinding was achieved by preparing aliquots containing the volume of purified IgG required for dilution into 25ml of aCSF as well as aliquots with similar volumes of aCSF only. A colleague was then asked to label the aliquots randomly using numbers or letters, and kept a record of the labels for future identification of the samples. Experiments to include in the analysis were chosen whilst still blind to the IgG preparation used. Experiments were accepted for analysis based on the stability of the γ-frequency oscillation before IgG perfusion, and also the quality of the recording during the experiment: if strong mains noise was present or if sudden wide variations in oscillation power occurred or the electrode was found to have exited the slice, as can happen when a drop of condensation runs down the electrode and falls onto the slice, the experiment was excluded.

Blinding was applied in a similar fashion for the intra-entorhinal injections in the subacute exposure experiments, except the aliquots were kept in batches, such that all rats injected in one week received the same IgG preparation. Here, all experiments were included in the first analysis focussing on baseline γ-power and frequency, unless epileptic activity or mains noise were present. Analysis was performed by grouping recordings by week, i.e. IgG preparation, and calculating all relevant information before removing the blinding.

2.5.2 Fast Fourier Transforms and the meaning of their results

A fast Fourier transform (FFT) is a mathematical method transforming a function of time into the frequency domain. Complex signals, such as LFP recordings, are composed of simple waves of different amplitude, frequency and phase, and these can be extracted from the signal using the Fourier analysis. Fourier Transforms use the Fourier analysis to express this same signal in terms of the frequencies of each component wave, by giving a measure of “how much” of each frequency component is required to make up the original signal. In other words, an FFT plots the power of each component frequency.

The FFT provides three important parameters to describe the recorded field potential oscillation: the area power, peak power and the frequency at peak power (see Figure 2.1). The area power, sometimes called total power, is a

measure of the size of the population of neurons within the area recorded by the electrode, whose membrane potential is oscillating in the γ-range (30-80Hz). The peak power and frequency at peak power must be looked at together as they define each other. The peak power is a measure of the strongest frequency within the γ-range; that is the size of the population of neurons whose membrane potential is oscillating at the strongest frequency.

In a persistent γ-oscillation generated pharmacologically in a slice preparation, area power reflects the level of activation in the slice, but also the health of the slice, as a slice with a large proportion of dead or damaged cells has less cells overall to participate in any oscillation. Changes in peak power, on the other hand, also give a measure of changes in the synchronicity of oscillations within the area recorded by the electrode. Indeed, a new lower peak power with little change to area power in response to a pharmacological intervention, would suggest that the strongest synchronous oscillation in the slice has lost a proportion of the population previously engaged in it in favour of the pool of on-going frequencies. On the other hand, an increase in peak power at the expense of area power would suggest an increased synchronicity as more cell assemblies in the slice would be oscillating at the same frequency. A change in peak power frequency suggests either a change in the output of γ-generating interneurons or a change in the subtype of interneuron responsible for the strongest oscillation recorded (Middleton *et al.*, 2008).

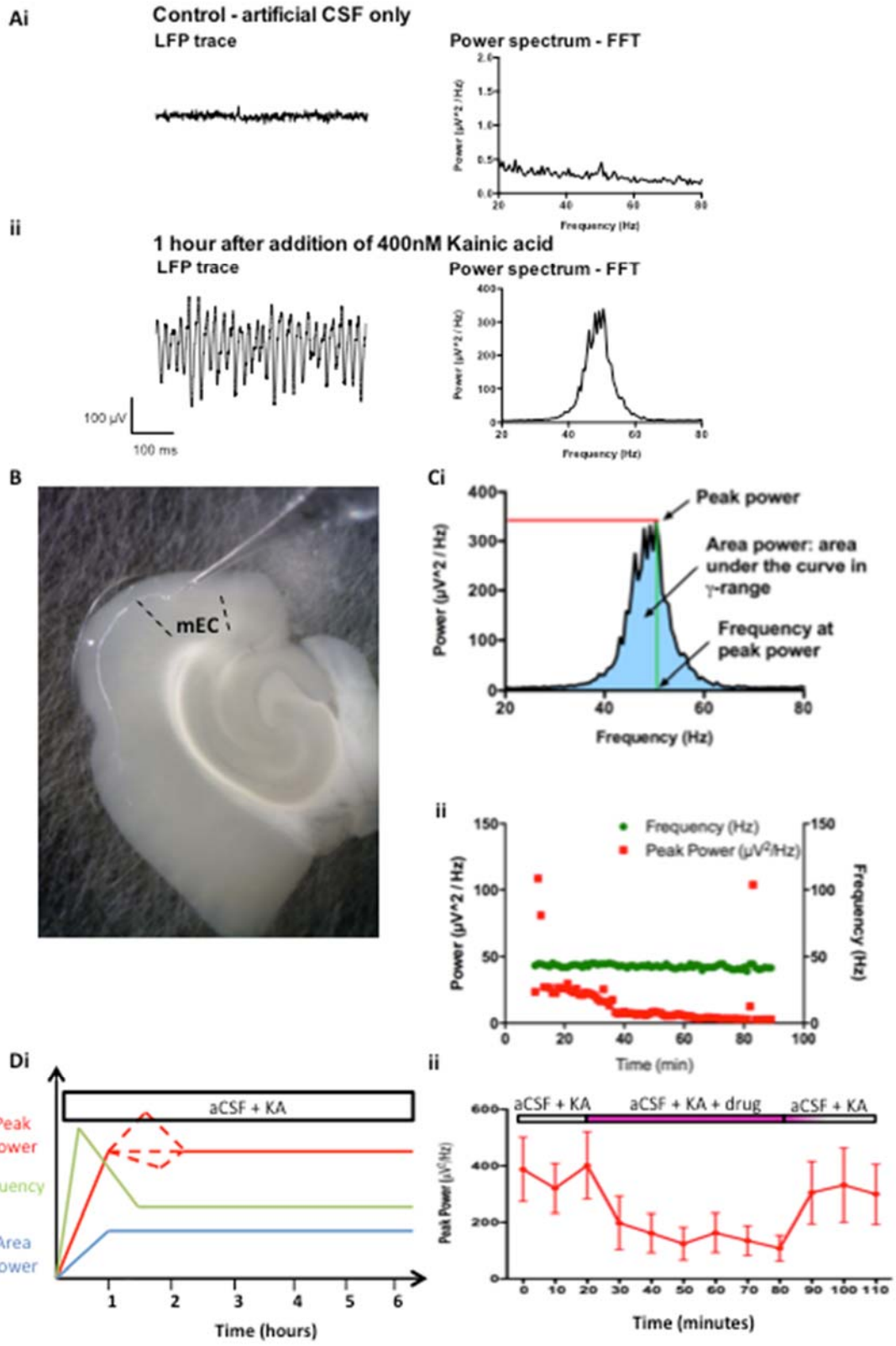

Figure 2.1 Generating and quantifying gamma-frequency oscillations in mEC. The glass recording electrode is placed in layer II/III of mEC (B) and baseline activity in aCSF in the local field potential (LFP) is recorded (Ai). Kainate is then added to generate γ-oscillations (Aii). A fast Fourier tansform is applied to 1-minute epochs of recording to obtain a power spectrum, which allows determination of the peak power, frequency at peak power and area power of the activity (Ci). IF these values vary by <20% over 40 minutes, oscillations are deemed stable (e.g. from 2.5 hours in Di). Once stable, drugs can be applied to the circulating aCSF and KA (Dii). A washout period is used to ensure the effect is specific to the drug and not simply due to deterioration of the slice.

2.6 Data Analysis

For each experiment, data from at least five to six slices were used. Data were analysed off-line using Microsoft Excel (Microsoft Inc., USA) and Prism 6.0 (GraphPad Software, San Diego, California). For γ-oscillations, either the raw values (slices from injected animals) or the normalised values (acute exposure experiments) for power and frequency at baseline (average of last three recordings in stable period), after 60 minutes of drug/IgG application, and at 30 minutes of washout were used for analysis. For normalisation, the average of the last three values during the stable baseline was defined as 100% for each individual slice. The power and frequency values for subsequent measurements were then converted to percentages of the baseline value. This allowed more accurate comparisons of the change in power or frequency by reducing the variability introduced by the highly variable baseline power. The normality of the results was determined by performing D'Agostino & Pearson's omnibus normality test. This suggested that raw values for peak power, area power and frequency were mostly normally distributed in the larger groups of slices. When a sample size in an experiment was too small for the normality test to be valid, it was assumed that the data were likewise parametrically distributed. Results were therefore expressed as mean plus and minus standard deviation of the values at baseline, 60 minutes after addition of drug/IgG, and 30 minutes after the beginning of washout. In small experiments, this sometimes resulted in a standard deviation larger than the mean, because one oscillation had a much larger power than others and skewed the distribution within that group. However, to maintain consistency, it was assumed that the sample was part of a normally distributed population as in the larger groups. Means were compared using repeated measure ANOVAs. If data failed the normality test, they were expressed as median and interquartile range and compared with a Friedman test. The percentage change in power and frequency between groups (patient IgG, control IgG, vehicle, etc.…) were also compared using ordinary one-way ANOVAs or Kruskal-Wallis tests depending on normality. A p value of <0.05 was considered significant. For data from the injected slices, two-way ANOVAs were used with IgG type (control or patient) and drug as factors. Correction for multiple comparisons was applied in most cases, unless it was clear that each comparison was independent of the other comparisons.

The choice of statistical test was not always straightforward. Non-parametric tests such as the Friedman or Kruskal-Wallis test have lower power to detect differences in groups that are actually present. This is because they compare ranks rather than means. There are therefore arguments to use parametric tests to compare results among the IgG preparations used. Firstly, peak and area power measurements were sometimes found to be normally distributed and other times not, suggesting that the result of the normality test was more likely related to the small sample sizes in this thesis than the real distribution of the measurements. Indeed, normality tests do not have much power in small sample sizes. Also, parametric tests such as t-tests and ANOVAs are relatively robust to violations of the parametric distribution of the groups compared. However, this only holds true for large sample sizes. The sample sizes compared here are relatively small, comprising n=5 to n=13. Additionally, many observations in the natural world are not normally distributed and it may be that oscillation power and frequency in slices similarly are not. A compromise position was therefore chosen of using non-parametric tests were when normality tests failed to demonstrate parametric distribution of the groups compared, in order to avoid type I error.

2.7 Histological reconstruction of cells and immunohistochemical techniques

Following the end of intracellular recording experiments, cells were filled with 2% biocytin according to a standard protocol, giving 200ms hyperpolarising current pulses (-0.2 nA) every 100 ms for 15-20 minutes. The intracellular electrode was then carefully withdrawn, the slices was washed in aCSF for 10-20 minutes and then placed in 4% paraformaldehyde in PBS and stored at 4°C until used for IHC.

For cell reconstruction, no re-sectioning was carried out. The slices were washed in PBS, then incubated in 1% H_2O_2 in 10% methanol for 15 minutes. Following further PBS washes, the sections were permeabilised in 2% Triton X-100 in PBS for 1 hour at room temperature. The slices were then incubated overnight in 1:200 Avidin-Biotin Complex (ABC Elite kit, Vector Labs, UK) in 1% Triton X-100 in PBS. The following day, slices were washed extensively in PBS and the chromogenic reaction was performed by incubating the slices in 3,3'-Di-

aminobenzidine tetrahydrochloride (DAB, SigmaAldrich, UK) prepared in PBS for 5-10 minutes. Once the cells were visible under a microscope, the reaction was stopped by washing in PBS. The slices were mounted onto poly-lysine coated glass slides (VWR, UK) and allowed to air-dry before dehydration and coverslipping (see below).

For immunohistochemistry for interneuron markers, slices were placed in 4% PFA in PBS at the end of electrophysiological recordings and stored at 4°C. On the day of use they were cryoprotected in 40% sucrose in TBS until sunk and resectioned to 40 μm on a freezing stage microtome. Any remaining PFA and sucrose were washed off in TBS. Antigen retrieval was performed by two 5-minute incubations in just-boiled 50mM Na^+ citrate at pH 6.00, followed by TBS washes. Endogenous peroxidase activity was quenched with a 30-minute incubation in 70% methanol and 3% hydrogen peroxide (H_2O_2) at room temperature. This was followed by TBS washes and non-specific binding block by 1 hour incubation with 10% normal goat, horse or rabbit serum (Vector Labs, UK) depending on the secondary antibody being used. The primary antibody was diluted in TBS with 3% normal serum and 0.05% Tween as below:

- Parvalbumin: 1:1500
- Calretinin: 1:1000
- Calbindin 1:10000
- Somatostatin 1: 500
- GAD67 1:1000
- GABA 1:1000

Slices were incubated in primary antibody overnight at 4°C then washed in TBS. Secondary antibodies were diluted to 1:200 in TBS with 0.05% Tween. Secondary antibodies used were:

- Biotynilated horse anti-mouse
- Biotynilated rabbit anti-goat
- Biotynilated goat anti-rabbit

Slices were exposed to the secondary antibody for 2 hours at room temperature on a rocker then washed in TBS and incubated in horseradish peroxidase (Ready-to-Use Streptavidin Horseradish Peroxidase, VectorLabs, UK) for 1

hour at room temperature followed by three TBS washes. The chromogenic reaction was then developed using DAB (Sigma-Aldrich, UK) for 5 minutes. Slices were then washed and mounted onto poly-lysine coated glass slides (VWR, UK). After air-drying overnight, sections were briefly re-hydrated in distilled water, followed by dehydration in increasing ethanol concentrations. Slides were bathed in 70%, 90%, 100% and a further 100% ethanol for 5 minutes each. They were then bathed in Histoclear I and Histoclear II for 5 minutes each before being coverlipped using Histomount.

For slices undergoing double-labelling with anti-human IgG, antigen retrieval was performed as above. A 1-hour blocking step in 10% normal goat serum was performed and the sections were then incubated overnight with the primary antibody as above. The next day, the sections were incubated with 1:200 fluorescently-labelled secondary antibodies (Goat anti-human IgG H+L antibody AlexaFluor 488, goat anti-mouse IgG AlexaFluor 568 and goat anti-rabbit AlexaFLuor 568, all Invitrogen, UK) for 2-3 hours at room temperature. The sections were then washed and mounted using DAKO fluorescent mounting medium containing DAPI.

2.8 Cell-based assay

The cell culture techniques described below were performed in a class II tissue culture hood under sterile conditions in the Neuroimmunology laboratory at the Nuffield Department of Clinical Neurosciences in Oxford.

Human embryonic kidney 293 (HEK293) cells were grown in Corning T175cm^2 tissue culture flasks (APPW) in Dulbecco's Modified Eagle Medium (DMEM, Sigma, UK) supplemented with 10% fetal calf serum (FCS, Sigma, UK) and 1% penicillin + streptomycin + amphotericin (PSA, Invitrogen, UK), maintained at 37°C in a humidified atmosphere with 5% CO_2 in an incubator. Cells were split at day 3-4, when 80-95% confluent, by aspirating the medium, and adding 2mls of 1% trypsin in PBS to the flasks. This separated the cells from the flask surface. Cells were then resuspended in DMEM-FCS-PSA, counted, and centrifuged at 1000RPM for 5 minutes. The supernatant was aspirated and the cells were partly re-seeded into new culture flasks or resuspended in DMEM-FCS-PSA and seeded onto poly-L-lysine (PLL, Sigma, UK) coated 13mm glass coverslips (VWR, UK; briefly, this was done by placing four 13mm glass

coverlips in each well of a 6-well plate, adding 2 mls of PLL solution (0.01% in PBS) for 15-20 minutes, then aspirating the PLL solution and allowing the coverlips to air-dry inside the tissue culture hood) at a concentration of 4.6 x 10^5 cells/well in 2mls of medium in 6-well plates. The plates were then incubated overnight. Transfection occurred the following day and was different for live and fixed cell assays.

2.8.1 Live cell-based assay

The cells in each well were transfected by adding a transfection mixture containing 2.1 μg of NR1 cDNA, 0.7μg of NR2B cDNA (i.e. 3:1 NR1: NR2B), 0.2μg of EGFP cDNA, 1.25μL of 20% glucose and 1.5μL of polyethylenimine (PEI) to 2mls of fresh DMEM-FCS-PSA. At 16 hours, the transfection medium was aspirated and replaced with fresh DMEM-FCS-PSA containing 500μM ketamine to avoid glutamate-mediated cytotoxicity. The cell-based assay was performed the next day. First, the patient sera and CSF samples were diluted in DMEM containing 4-(2-hydroxyethyl)-1-piperazineethanesulfonic acid buffer (HEPES, Sigma, UK) and 1% bovine serum albumin (BSA, Sigma, UK) for blocking. Serum was diluted 1:40 and CSF 1:10 to a total volume of 250μL per sample. Further dilutions were done in steps of 3 (i.e. for serum 1:40, 1:120, 1:360 etc.). Samples were transferred into 24-well plates and one transfected coverslip was added cell-side up to each well and incubated for 1 hour at room temperature. The supernatant was aspirated and the coverslip washed three times in DMEM-HEPES. The cells were then fixed in 4% formaldehyde in PBS for 10 minutes at room temperature, and the coverlips then washed again in DMEM-HEPES three times. The coverlips were then incubated in 250μL/well of secondary antibody (goat anti-human IgG H+L, AlexaFluor 568, Invitrogen, UK) diluted 1:750 in DMEM-HEPES-1% BSA for 45 minutes at room temperature in the dark. Following aspiration of the secondary antibody, the coverslips were washed three times in DMEM-HEPES and 3 times in PBS prior to being mounted onto glass microscope slides (VWR, UK) using DAKO fluorescent mounting medium containing DAPI (Invitrogen, UK). Slides were allowed to dry for at least 30 minutes before being examined under a fluorescent microscope. Positive and negative controls were included in each assay.

Binding was assessed semi-quantitatively using the CBA scoring system developed by the Oxford group (Irani *et al.*, 2010b). It is important to note that co-localisation of IgG surface binding with EGFP expression in the live cell assay was not frequent and that EGFP expression was mainly used as a marker to determine the success of the transfection. When no cell surface IgG-binding was detected, a score of 0 was given. A score of 0.5 was given if a small number of cells were faintly bound. Scores of 1-4 denoted increasing number and intensity of fluorescence of IgG surface-binding.

2.8.2 Fixed cell CBA

There were a few notable differences in the preparation of the fixed CBA. The process of establishing the assay is discussed in Chapter 3, and the differences between the final form of the fixed CBA and the live CBA are described here. HEK293 cells were cultured and seeded as above. They were transfected using 1.5μL of NR1 DNA and 1.5μL of NR2B DNA with glucose and PEI as above. No EGFP was used. On the day of the assay, the cells were fixed using 4% PFA in PBS for 5 minutes at room temperature and then washed 6 times in PBS. The coverslips were then incubated with PBS containing 10% BSA and 0.1% Triton-X100 for permeabilisation and block for 1 hour at 37°C. The serum and CSF samples were diluted (1:40 and 1:10 respectively) in PBS with 1% BSA and coverlips incubated for 2 hours at room temperature. The coverslips were washed 3 times in PBS before incubating for 1 hour at room temperature with a commercial antibody against NR1 (IgG_{2a} mouse monoclonal antibody against NR1 extracellular loop at amino acids 660-811, BD pharmingen) diluted 1:1000 in PBS-1% BSA This is the same antibody used by Gresa-Arribas *et al.* (2014). This was followed by a further three washes in PBS and a 90-minute incubation with the secondary antibodies diluted in PBS-1% BSA at room temperature in the dark (AlexaFluor 568 goat anti-human IgG H+L antibody and AlexaFluor 488 goat anti-mouse IgG_{2a} antibody, Invitrogen). The coverlips were washed again in PBS and mounted, examined and scored as for live CBA.

2.8.3 Euroimmun cell-based assay

Euroimmun slides (Euroimmun, Lübeck, Germany) were used as per instructions, using the reagents provided in the diagnostic kit. Serum and CSF were diluted 1:10 (instructions suggest using undiluted CSF) using the PBS-

tween supplied in the pack. 30μL diluted sample was applied to each reaction field on the reagent tray and the biochip slides placed on the reagent tray. Once the biochips had been incubated with the samples for 30 minutes they were washed in PBS-tween and incubated with 25μL of the ready to use fluorescein-labelled anti human globulin provided for 30 minutes. Following a final wash in PBS tween they were cover-slipped in fluorescent mounting medium containing DAPI to visualise nuclei and examined under a fluorescent microscope. Results are normally reported as positive or negative, but here, a visual scoring system similar to the one for live CBA was used in order to correlate Euroimmun results with live CBA and fixed CBA results. Some samples were diluted further to determine endpoint titration. The procedure for Euroimmun immunohistochemistry was exactly the same.

2.9 Immunohistochemistry for NMDAR-Ab

IHC was performed as described in the most recent publications from Dalmau's group (Gresa-Arribas *et al.*, 2014; Planagumà *et al.*, 2014). Female Wistar rats were anaesthetised in isofluorane and killed by CO2 inhalation. The brain was removed without perfusion, sagitally bisected and immersed in 4% PFA at 4°C for one hour. The brain halves were then cryoprotected by immersion in 40% sucrose until sinking followed by embedding in freezing medium and snap-freezing in isopentane chilled in dry ice. Attempts at cutting 7μm thick section were abandoned in favour of slightly thicker slices (10-12μm), as the cryostat slicing was technically very difficult. Sections were air-dried overnight and then stored at -20°C until use. When ready to use, slides were thawed for 30 minutes at room temperature and washed once in PBS. They were then serially incubated in 0.25% hydrogen peroxide at 4°C for 10 minutes, 10% normal goat serum (NGS) for 1 hour at room temperature, and patient serum (1:120 in PBS with 3% NGS) or CSF (1:10 in PBS with 3% NGS) overnight at 4°C. The next day, slides were washed and incubated with 1:2000 biotinylated goat anti-human IgG antibody in PBS for 1 hour at room temperature. Reactivity amplification was performed by incubation with avidin-biotin complex for 1 hour at room temperature as per the "Vector lab" instruction manual and colour developed with diaminobenzidine for 5 minutes. Staining was scored visually from 0 to 4 as for live CBA at 1:120 for serum and 1:10 for CSF. Some samples were diluted further to determine endpoint titration.

Chapter 3 Refining diagnostic assays for optimal definition of patients with NMDAR antibody encephalitis

3.1 Introduction

When “anti-NMDAR encephalitis” was first described, it appeared to be a striking clinical syndrome of rapidly progressive neuropsychiatric symptoms followed by encephalopathy, autonomic instability and characteristic movement disorders, occurring almost exclusively in young women, most of whom had ovarian teratomas (Dalmau *et al.*, 2007; Dalmau *et al.*, 2008). Rapidly, the phenotype widened: the proportion of female patients decreased, as did the proportion of paraneoplastic cases, and the disorder was increasingly diagnosed in children of both sexes (Florance *et al.*, 2009; Irani *et al.*, 2010b; Titulaer *et al.*, 2013). Partial phenotypes were reported. For example, Irani *et al.* (2010b) reported a cohort of 44 NMDAR-Ab positive patients, of whom 4 had seizures as the only symptom. Then, NMDAR-Abs were detected in the serum of 3 out of 47 patients presenting to an early intervention in psychosis service with psychiatric symptoms and without encephalopathy throughout the follow-up period (Michael S. Zandi *et al.*, 2011), and also in two patients with subsequently pathologically confirmed sporadic Creutzfeldt-Jakob disease (Mackay *et al.*, 2012). Although both patients had a clinical course typical for sCJD, negative CSF NMDAR-Abs and low serum titres, the results were surprising: no NMDAR-Abs had been reported in the serum of 32 healthy controls or 138 disease controls (including patients with autoimmune encephalopathy, chronic psychosis, multiple sclerosis, systemic lupus erythematosus, opsoclonus-myoclonus, herpes simplex encephalitis and epilepsy) using the same diagnostic assay (Irani *et al.*, 2010b).

These cases raised questions about the clinical specificity of the NMDAR-Abs, and the positive predictive value of the diagnostic assay used. For the purposes of this thesis and the work that follows in Chapters 4 to 6, it was important to better understand the nature of the assays performed, and their relationship with the well-defined clinical syndrome of “anti-NMDAR encephalitis” or NMDAR-Ab encephalitis as it will be called here.

3.1.1 NMDAR-Ab assays currently in use

Dalmau and co-workers originally detected NMDAR antibodies by immunohistochemistry on fixed rat brain sections (Vitaliani *et al.*, 2005; Bataller *et al.*, 2007; Dalmau *et al.*, 2007), as used previously by the same group for

detecting paraneoplastic antibodies. What was striking in this case was the predominance of hippocampal neuropil staining. They then established a diagnostic approach based initially on CSF (and serum) binding to rodent brain sections in this pattern, together with binding of antibodies to fixed and permeabilised human embryonic kidney cells (HEK293 cells) transfected with equimolar NR1 and NR2B cDNA (f-CBA). To confirm that the antibodies were against cell surface epitopes of the NMDAR, they also used binding to live non-permeabilised hippocampal neurons cultured from E18 rat foetuses, and modified the immunohistochemistry (IHC) technique to optimise the detection of cell-surface antigens (Dalmau *et al.*, 2008; Gresa-Arribas *et al.*, 2014).

More recently they have reported that the live neurons are unnecessary as they cannot distinguish between different surface antigens, and that IHC and the f-CBA are sufficient (Gresa-Arribas *et al.*, 2014). In their experience, all patients who have NMDAR-Abs in either serum or CSF detected by these methods suffer from the characteristic NMDAR encephalitis syndrome they initially described (Dalmau *et al.*, 2007; Dalmau *et al.*, 2008; Gresa-Arribas *et al.*, 2014). Conversely, antibodies were not detected in a 250-strong control group consisting of healthy blood donors and disease controls (limbic encephalitis, Morvan's syndrome, paraneoplastic disorders, Rasmussen's encephalitis, epilepsy, viral encephalitis, and cancer with no neurological symptoms (Dalmau *et al.* (2008)). However, they found that serum testing in their hands missed 7% of positive results (f-CBA and IHC combined) in serum-CSF pairs, and claimed that CSF should always be tested (Gresa-Arribas *et al.*, 2014).

Although all NMDAR-Ab assays used elsewhere follow on from these initial studies, there are two alternative approaches. A commercially available Biochips mosaic test has been developed by Euroimmun (Lübeck, Germany) and is widely used throughout the world. This contains 1mm^2 chips of fixed cells expressing the NR1 and NR2 subunits or untransfected cells (Euf-CBA), with or without additional chips containing 4μm thick sections of rat hippocampus and cerebellum (Eu-IHC). The advantage of the Euroimmun chip assay is its convenience and ease of use without the need for a laboratory with in-house molecular biology proficiency and maintenance of cell-cultures. However, interpretation of results is not straightforward (discussed later) and

requires expertise. Results are reported as positive or negative but semi-quantitative reporting is possible by dilutions of samples.

By contrast with the two techniques above, the Oxford laboratory uses a cell-based assay consisting of live HEK293 (l-CBA) transfected with NR1 and NR2B cDNA at a 3:1 ratio, with addition of cDNA for enhanced green fluorescent protein (eGFP) expression to confirm transfection efficiency and visualise the cells expressing the NMDAR subunits. A visual scoring system has been developed to report the results, with scores of 0 to 1 reported as negative, 1.5 as low positive and 2-4 as positive (Irani *et al.*, 2010b; M. S. Zandi *et al.*, 2015). The advantage of using live cells is that the assay should only detect the pathologically relevant antibodies directed against the extracellular NR1 epitope (although antibodies to NR2, if present, could be detected). In the experience of the Oxford service, testing for antibodies in serum is sufficient as CSF is sometimes negative for NMDAR-Abs in paired serum and CSF samples (Vincent and Bien, 2008; Irani *et al.*, 2010b; M. S. Zandi *et al.*, 2015) whereas the reverse has never been identified.

3.1.2 Comparisons of current assays

Limited comparisons of some of these diagnostic assays have been published. After finding that f-CBA was negative in 13.2% of sera with a paired positive CSF sample (about half of these serum samples were positive by IHC) and that IHC was negative in 8.4% of sera with a paired positive CSF sample (1.2% positive on f-CBA), Gresa-Arribas *et al.* (2014) investigated whether l-CBA could improve detection of NMDAR-Abs in serum. Instead, they found that l-CBA was less “sensitive” than f-CBA. It is worth noting that they introduced a permeabilisation step in the l-CBA, which is not present in the Oxford L-CBA, such that their results may not reflect the findings using the Oxford L-CBA. The general conclusion was that CSF was more sensitive and easier to use because of reduced background/non-specific binding, and sufficient in all cases.

However, in that study, NMDAR encephalitis was defined as the “new onset of neuropsychiatric symptoms with positive serum or CSF antibodies” by the Barcelona methods. The samples, and therefore patients, used in the study were chosen from a larger cohort of positive serum-CSF sample pairs known to belong to patients with NMDAR encephalitis. The diagnosis was not

independent of the antibody result, and unsurprisingly therefore, they found that one of their methods (CSF f-CBA and/or IHC) was 100% sensitive (Gresa-Arribas *et al.*, 2014), and negative results were obtained in the 100 control patients. There is no gold standard for the diagnosis of NMDAR-Ab encephalitis at present. This makes it difficult to assess the sensitivity and specificity of any of the established tests, or the relevance of the presence of positive results in potentially related conditions, such as isolated psychosis or isolated focal epilepsy.

The sensitivity of a test refers to the proportion of positive results in those who have the disease, and therefore requires an antibody-independent definition of the disease and acknowledgement of the false-negative rate of the test. This has not been reported for any of the tests. Additionally, the Barcelona group exemplify the high specificity of their method by pointing out that no NMDAR-Abs were found in the serum of 80 patients with schizophrenia during their first psychosis episode (Masdeu *et al.*, 2012) (cf. Michael S. Zandi *et al.* (2011) above). However, CSF studies, which they consider more sensitive, were not undertaken in that study. It would be more correct to say that the positive predictive value (PPV) rather than the sensitivity of CSF f-CBA and IHC was 100% in Gresa-Arribas *et al.* (2014), whilst serum f-CBA and IHC had PPVs of 86.8% and 91.6% respectively.

Another notable difference between using l-CBA and f-CBA combined with IHC is the results of paired CSF and serum samples: negative CSF in the presence of positive serum has reportedly never been found in the Barcelona laboratory (Gresa-Arribas *et al.*, 2014), whilst this is sometimes the case with l-CBA (Irani *et al.*, 2010b; M. S. Zandi *et al.*, 2015). The reason for this difference is not clear: it could be caused by non-specificity of the l-CBA or because the fixation used in both IHC and f-CBA masks some epitopes bound by a population of serum antibodies which are not present in the CSF.

There was a comparison of Euf-CBA and Eu-IHC with results from the Barcelona laboratory f-CBA and IHC (Wandinger *et al.*, 2011). 100% concordance between Euf-CBA and the Barcelona f-CBA and IHC was found in a study of 66 serum and CSF NMDAR-Ab-positive samples and 381 control samples (Wandinger *et al.*, 2011). The same result was obtained with Eu-IHC,

although the control samples from patients with other antibody-mediated encephalitides also produced hippocampal and cerebellar staining, albeit in a different pattern to NMDAR-Abs. However, previous experience in the Oxford laboratory (Vincent, unpublished) did not support the 100% sensitivity of the Euf-CBA even in patients with definite disease and high titres with l-CBA.

Other large studies using the Euf-CBA have found much higher prevalence of NMDAR-abs (about 10%) in the serum of healthy controls and patients with a number of neurological or psychiatric conditions including schizophrenia, affective disorders, Parkinson's, stroke, and motor neurone disease (Steiner *et al.*, 2013; Dahm *et al.*, 2014; Steiner *et al.*, 2014). However, IgA and IgM subclass antibodies, which are not specific to the NMDAR encephalitis syndrome and are of doubtful pathological relevance even when present in the CSF, were far more common than IgG (0.5% in schizophrenia and 0.6% in healthy controls in Steiner *et al.* (2014); 0.6% in schizophrenia and 1.2% in healthy controls in Dahm *et al.* (2014)). This rate of positivity in healthy and disease control populations has not been found in any of the Barcelona group studies discussed above using f-CBA and IHC, or in the original Oxford study using l-CBA (Irani *et al.*, 2010b).

These studies were large serum screening studies and did not investigate any differences in disease presentation or severity among the disease controls. Furthermore, the prevalence amongst healthy controls matched that of disease controls, arguing against a pathological role even of the IgG subclass antibodies. Indeed, the authors felt the detected antibodies were some of a large number of constitutively expressed antibodies against brain epitopes, which form a sort of "physiological autoimmunity", which may modulate brain function in both health and disease (Dahm *et al.*, 2014). The titres of IgG subclass NMDAR-Ab in these studies are also unclear but may have been rather low, so it is difficult to comment on whether a cut-off for pathogenicity could be established, or whether substantial CSF presence of NMDAR-abs could be predicted from the basic transfer rate of IgG across the BBB of 1:400 of the serum IgG concentration.

There are two other interesting observations to note from the Dahm *et al.* (2014) study: firstly, over 50% of the seropositive cases for each antibody investigated

(they also quantified seropositivity for 24 other brain antigens including CASPR-2, LGI-1, GAD-65, amphiphysin, MOG, AQ4, AMPA and GABA R) were male, including in the healthy controls, whereas a female preponderance is usually expected in most autoimmune diseases or autoimmune diathesis. Secondly, seropositivity for any antibody of any Ig subclass was greater in the group of patients with schizophrenia compared to those with borderline personality disorder or those whose diagnosis was reclassified from schizophrenia to "mental illness not yet specified". Is this relevant to schizophrenia pathophysiology in terms of its association with variations in Major Histocompatibility Complex (MHC) locus? Similarly, seropositivity was high for all antibodies in the group of patients with stroke, perhaps suggesting a secondary antibody response following the insult of the stroke and subsequent neurodegeneration (as perhaps seen in the patients with sporadic CJD discussed above).

Overall, these studies suggest that IgG NMDAR-Ab, which is what hospital laboratories would test for upon receiving a request for NMDAR-Ab testing, are present in at most 1% of patients who do not appear to have NMDAR-Ab encephalitis using the Euf-CBA. It is not yet clear if this is the false-positivity rate of the Euf-CBA in serum caused by difficulties in reading it (see later discussion), which could be resolved by re-testing these same samples using l-CBA/f-CBA and IHC, or whether it reflects the rate of presence of these antibodies in the general population. In the latter case further information regarding titres and presence in CSF would need to be obtained in order to determine if a cut-off for pathogenicity exists, as is the case with some other autoantibodies.

3.1.3 Aims

The arguments put forward by the Barcelona group would suggest that l-CBA is both less sensitive and less specific than f-CBA or IHC. Furthermore, Euf-CBA and Eu-IHC have not been compared to l-CBA directly.

A comparison of l-CBA, f-CBA, ICH and Euf-CBA was therefore undertaken using serum and paired CSF samples, when available, stored at the Oxford Neuroimmunology laboratory. L-CBA-positive serum samples or negative serum samples from previously positive patients were chosen with no knowledge of

the final diagnosis, as well as a number of control samples from patients with other diagnoses including limbic encephalitis syndromes. Once all assays had been performed and scored, clinical data acquisition (still on-going) commenced, with the aim of correlating test results with final diagnosis.

This sampling method was chosen as it offered some advantages over the methods in Gresa-Arribas *et al.* (2014). Firstly, by not limiting the study to clinically clear cases of NMDAR encephalitis, the presence of NMDAR-Abs in other conditions, and whether these can be detected by f-CBA, IHC or Euf-CBA, might be highlighted. Secondly, it would allow inclusion of l-CBA false-positives and comparison of the false-positive rates across tests. Thirdly, the results of repeat samples from previously NMDAR-Ab-positive patients might provide a hint at the detection thresholds of each test. Finally, whether different detection thresholds for CSF NMDAR-Abs for each test explain the discrepancy in published CSF-serum pairs between Oxford and Barcelona might also be addressed.

This study was performed in the Neuroimmunology laboratory at the Nuffield Department for Clinical Neuroscience in Oxford with the assistance of Dr Matteo Gastaldi, a visiting clinical fellow from Pavia, Italy.

3.2 Methods

3.2.1 Live CBA

L-CBA was performed according to the Oxford neurosciences group protocol described in Chapter 2 (Irani *et al.*, 2010b). Cells were transfected with untagged NR1 and NR2B cDNA at a 3:1 ratio as well as a eGFP expression vector to visualise transfection using polyethylenimine (PEI). Serum samples were diluted 1:40 in DMEM-HEPES with 1% bovine serum albumin (BSA; note Oxford standard protocol for clinical diagnosis uses 1:20 dilution but 1:40 dilution was used to standardise across tests). CSF samples were diluted 1:10 (Oxford uses CSF diluted 1:2, but only small quantities of CSF were available and had to suffice for 4 diagnostic tests so dilution had to be increased). After incubation with patient samples, cells were fixed with 4% PFA in PBS. Binding of human IgG to surface NMDAR was detected using goat anti-human IgG H+L antibody AlexaFluor 568. Coverslips were examined using a fluorescent

microscope and scored independently by Dr Gastaldi and myself, using the semi-quantitative scoring system devised by Oxford. Some samples were diluted further to determine endpoint titration.

CBA scoring

The semi-quantitative scoring system used here was developed at the Oxford Neuroimmunology service (Leite *et al.*, 2008). Scores from 0-4 are given as follows:

- 0: no labelling
- 0.5: weak labelling of a few transfected cells with no obvious GFP co-localisation
- 1: weak labelling of some of the transfected cells with precise co-localisation
- 2: moderate labelling of some (~20-50%) of the transfected cells, with precise co-localisation
- 3: moderate/strong labelling of 50-80% of the transfected cells, with precise co-localisation
- 4: strong labelling of virtually all transfected cells with precise co-localisation

This scoring system is not linear, and scores depend on transfection efficiency as well as NMDAR-Ab concentration in the sample assayed. To more accurately compare NMDAR-Ab concentration between different samples, serial dilutions of samples to determine end-titres would be more useful. Our early assays were also independently scored by experienced research assistants usually responsible for scoring diagnostic assays. This allowed us to validate our scores.

3.2.2 Fixed CBA

The Barcelona f-CBA was performed as closely as possible to the method described in Gresa-Arribas *et al.* (2014). Only the differences from l-CBA are noted here: HEK293 cells were transfected with NR1 and NR2B cDNA in equimolar ratio with no EGFP (rather than 3:1 with untagged EGFP). Cells were fixed with 4% PFA and permeabilised in 0.1% Triton-X100 before the start of the assay (rather than fixation occurring after exposure to patient samples).

1:40 serum or 1:10 CSF diluted in PBS with 1% BSA were used (rather than using DMEM-HEPES with 1% BSA). Coverlips were also incubated with a mouse monoclonal antibody against the extracellular loop of NR1 to allow colocalisation with any bound human IgG, before incubation with the two secondary antibodies. Scoring was done as above. Some samples were diluted further to determine endpoint titration.

3.2.3 Euroimmun CBA

Euroimmun slides were used according to the instruction manual supplied (EUROIMMUN Medizinische Labordiagnostika AG, 2011) as described in Chapter 2. Serum was diluted 1:10 using the PBS-tween supplied in the pack, and CSF was not diluted as suggested in the instructions. Results are normally reported as positive or negative, but here, a visual scoring system similar to the one for l-CBA was used in order to correlate Euroimmun results with l-CBA and f-CBA results. Some samples were diluted further to determine endpoint titration. The procedure for Eu-IHC was exactly the same.

3.2.4 Immunohistochemistry

IHC was performed as described in the most recent publications from the Barcelona group (Gresa-Arribas *et al.*, 2014; Planagumà *et al.*, 2014) except that TBS was used instead of PBS. Patient serum was diluted to 1:120 in TBS with 3% NGS and CSF to 1:10 in TBS with 3% NGS. Staining was scored visually from 0 to 4 as for l-CBA at 1:120 for serum and 1:10 for CSF. Some samples were diluted further to determine endpoint titration.

3.3 Results

3.3.1 Comparison of l-CBA with original l-CBA results

Ninety-one serum and twenty-six CSF samples sent to the Neuroimmunology laboratory at Oxford from 2012-2014 were selected by AV for use in this study. For some patients, samples were available from different time points such that the serum of 80 patients and the CSF of 25 patients were tested (see Figure 3.1). Of the 25 patients with available CSF, 8 had no serum available for study. The total number of patients in the study was therefore 88. For the CSF samples, 10 were paired with serum samples, 8 had been obtained separately

from serum (2 samples from 1 patient), and 8 were from patients for whom there were no serum samples available. The major barrier to finding paired serum and CSF samples was the number of empty or insufficient CSF samples available after routine diagnostics since the amounts provided by the referring laboratories are highly variable.

L-CBA was repeated in all serum (1:40) and CSF (1:10) samples, and scored independently by AT and MG blind to the original result (done at 1:20 serum; 1:2 CSF by Dr Jacobson, Oxford University). Examples of serum and CSF samples scoring 0-4 are shown in Figure 3.2. Although the cells were co-transfected with eGFP as well as the NMDAR subunits, there was often poor co-localisation of human IgG with eGFP in l-CBA, since the NR1, NR2B and EGFP are on independent plasmids and the eGFP is mainly used to demonstrate successful overall transfection. In the l-CBA, scores of 0.5 and 1 are given when only a few cells are weakly labelled, with some co-localisation with eGFP required for a score of 1. These scores are reported as negative, but they can indicate emerging or decreasing positivity. L-CBA reporting has been under continuous review by the Oxford laboratory, and the cut-off for positivity was adjusted to 1.5 based on audits of the clinical relevance of positive results (M. S. Zandi *et al.*, 2015). Similar information or qualitative data have not been reported for the other assays. This does not apply to CSF, however, and any score of 0.5 or above is reported as positive.

The results of the original l-CBA were positive for 70 serum samples (61 patients) and negative in 21 serum samples (20 patients; one patient had 1 positive and one negative serum sample in this study). For CSF, 9 samples were positive in the original l-CBA and 17 were negative.

Among the sera positive on the original l-CBA, scores on the new l-CBA were lower (see Table 3.1 and Figure 3.3 A), with twelve samples scoring 0, and 29 samples now scoring below the usual cut-off for positivity (1.5). A small reduction in scores was expected as a higher dilution was used in this study, but the range of reduction varied widely, consistent with a loss of reactivity caused by antibody degradation during the prolonged storage period (-20°C). The 12 serum samples whose scores had decreased from an original threshold score of 1.5 or more to 0 were therefore excluded from further analysis, leaving

58 sera from 50 patients. No serum samples originally scoring 0.5 or 1 were excluded however, as although these would have been reported as negative when originally tested, we wished to investigate the possibility that other techniques might be more sensitive than l-CBA. Moreover, a difference of 0.5 points in the scoring at such low levels of binding can be hard to detect and it cannot be ruled out that our relative inexperience may have played a role in the variability in the lower scores obtained, as well as the higher dilution used.

Despite excluding the 12 serum samples that had lost reactivity, the new serum scores remained lower than the original scores (see Figure 3.3 B). Most of the sera originally reported as negative (n=21) scored 0 in the new l-CBA, except for two samples, which scored 1.5 and 2, and had originally scored 1 (Figure 3.3 C). Among the 9 originally positive CSF samples, scores on the current l-CBA were generally lower, with three samples scoring 0, but this did not reach statistical significance (Table 3.1 and Figure 3.3 D). As these samples had originally scored 1, and the reduction in score may have been related to the increased dilution of the samples, they were not excluded from the study. All CSF samples scoring 0 in the original l-CBA remained negative in the new l-CBA.

Table 3.1 Comparison of original and new l-CBA scores among originally positive samples (>1.5 for serum; >0 for CSF)

	Original l-CBA score (serum 1:20/ CSF 1:2)		New l-CBA score (serum 1:40/ CSF 1:10)		Paired t-test	
	Mean	**S.D.**	**Mean**	**S.D.**	**T, df**	**P**
Serum[1] (n=70)	2.27	0.947	1.5	1.129	7.556, 69	<0.0001
Serum[2] (n=58)	2.38	0.957	1.81	0.986	5.902, 57	<0.0001
CSF (n=9)	1.83	1.00	1.11	1.14	1.982, 8	0.083

1 all originally positive serum samples
2 originally positive serum samples that have lost reactivity completely excluded

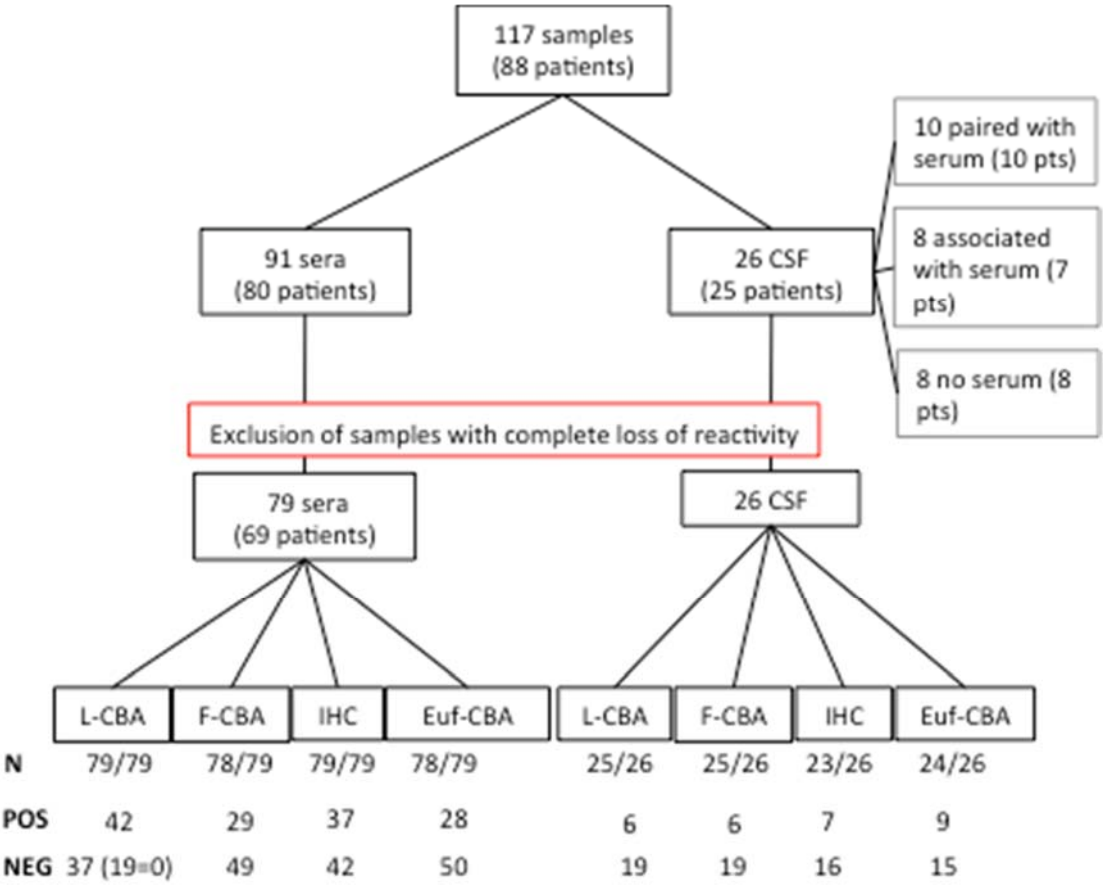

Figure 3.1 Serum and CSF samples included in present study
L-CBA: live cell-based assay; F-CBA: fixed cell-based assay; IHC: immunohistochemistry on frozen rat brain sections; Euf-CBA: Euroimmun biochip cell based assay. Numbers in brackets on bottom row for L-CBA denote the number of samples scoring 0, as serum scores of 0.5 and 1 are reported as negative. In all other tests any score above 0 was considered positive.

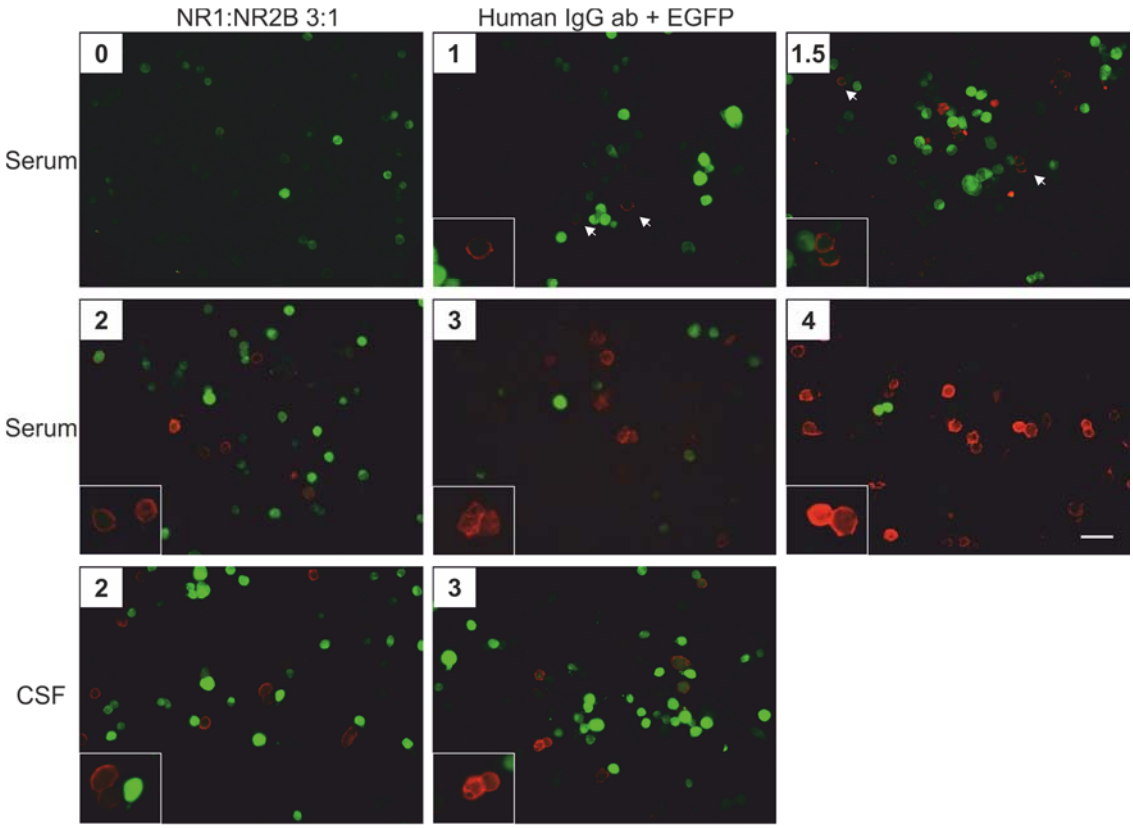

Figure 3.2 Examples of scores 0-4 on L-CBA
Pictures in the first two rows illustrate serum samples scoring from 0-4 on live cell CBA. Magnification is x40 and scale bar represents 50μm. Magnified (x2) insets are included for detail. The photographs show merged EGFP and AlexaFluor 568 anti-human IgG fluorescence. Coverslips with no human IgG-bound cells scored 0. If weak red fluorescence was present in isolated cells, a score of 0.5 was given, and if this weak labelling co-localised with EGFP a score of 1 was given. 1.5 was given in cases where the anti-human IgG fluorescence was weak but present in about 20% of cells, with some co-localisation with EGFP. Scores from 2-4 were assigned on the basis of increasing intensity of anti-human IgG immunofluorescence and increasing number of labelled cells. The criteria for co-localisation with EGFP was not strictly applied as only the minority of cells binding anti-human IgG also expressed EGFP. On l-CBA, non-specific background staining with both serum and CSF (see bottom row for examples) was minimal, and the same scoring rules applied for both.

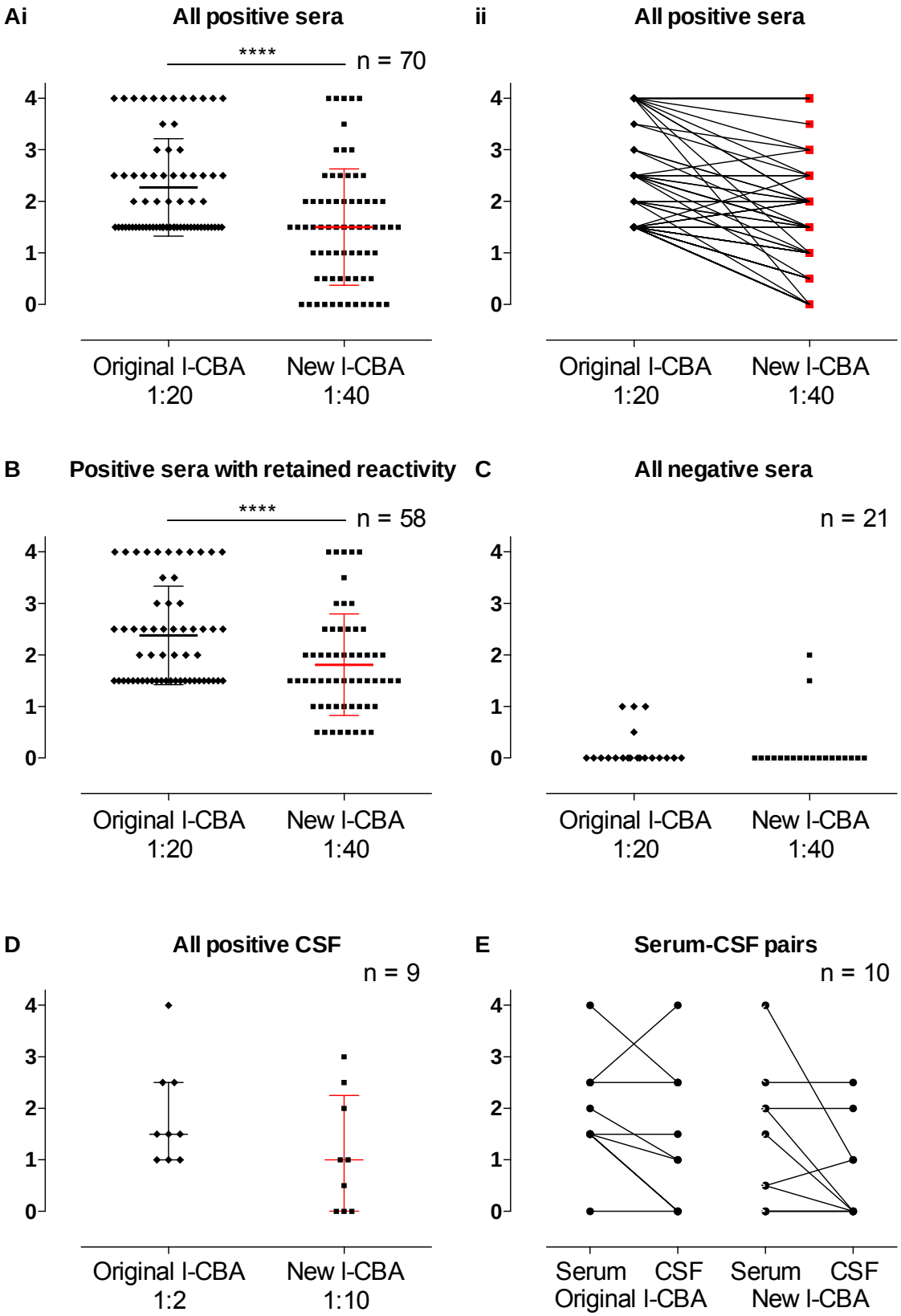

Figure 3.3 Comparison of scores in original I-CBA and current I-CBA
The originally positive serum scores (1:20) were higher than the new serum scores (1:40), when compared before (Ai, mean ± S.D) and after (B, mean ±SD) exclusion of samples with loss of reactivity. The variability of change is shown in Aii. Originally negative serum samples remained so in the new I-CBA (C). There was no difference between original and new scores for positive (D) or negative (not shown) CSF samples. E shows the scores of serum and CSF pairs in the original and repeat I-CBA. CSF scores were usually lower than serum scores.

Inter-observer agreement was high on first-pass scoring (92.5%, *CI* 84.39-97.2 %; scores > 2 within 1 point of each other, and scores 0-1.5 within 0.5 of each other). If scores differed, the assay was re-scored independently. If this did not resolve the inter-observer variability the sample was re-tested.

In the original l-CBA, six of the 10 serum-CSF pairs had lower scores in CSF than serum (of which three were 0 in CSF) and three had equal CSF and serum scores. Only one CSF scored higher than the paired serum. That CSF had been obtained from an intraventricular catheter in a patient with a very severe disease course. The distributions were similar in the new l-CBA (see Figure 3.3 E). Four of the eight CSF samples that were associated but not paired with a serum sample had lower CSF scores (two were negative) and the remaining four had equal serum and CSF scores. These scores, however, do not take into consideration the different dilutions used here.

3.3.2 Developing the Barcelona fixed cell CBA

In order to compare the results obtained with l-CBA with those that would be obtained with the Barcelona methods, a f-CBA protocol was developed based on the methods published by this group. This was not straightforward as the description of their CBA methodology was always brief and clearly evolved over publications (Table 3.2).

In the first attempts the 3:1 NR1:NR2B ratio was maintained and EGFP was used to visualise transfection as this allowed transfection success to be rapidly checked prior to starting the CBA. Samples and secondary antibody were diluted in DMEM-HEPES with 1% BSA as in the l-CBA. Non-specific background staining was very high with serum samples in all these trials (Table 3.3 and Figure 3.4 top panel), such that it was not possible to differentiate positive samples and negative controls.

Background appeared much reduced once the dilutant had been switched to PBS with 1% BSA, and a 1-hour block with permeabilisation at 37°C had been introduced, suggesting that DMEM-HEPES was perhaps more difficult to wash away in fixed and permeabilised cells, and that access of the 1% BSA as blocking agent to the intracellular compartment was helpful (Figure 3.4 middle panel).

Table 3.2 Comparison of f-CBA methods published by Dalmau's group over time and with l-CBA.

	Dalmau 2007	Dalmau 2008	Gleichman 2012[1]	Gresa-Arribas 2014	Honnorat 2015 Unpub-lished	L-CBA
NMDAR subunits	NR1 = NR2A/B	NR1 = NR2A/B	NR1=NR2B	NR1=NR2B	NR1-EGFP and NR2B	NR1:NR2B 3:1+EGFP
Plasmids	N/R	N/R	N/R	N/R	N/R	NR1: pCDNA 3.1+ NR2B: pCDNA 3.1 hygro Invitrogen
Total DNA concen-tration	N/R	N/R	2μg/ml medium	N/R	N/R	1.5μg/ml medium
Transfec-tion method	N/R	N/R	Calcium Phosph-ate	N/R	Lipofect-amine	Polyethyle-nimine
Post-transfec-tion	Up to 24h 500μM ketamine	Up to 24h 500μM ketamine	Up to 24h 500μM ketamine	Up to 24h 500μM ketamine	Up to 24h 500μM ketamine	Up to 24h 500μM ketamine
Fixation	**Post** incubation 4% PFA-PBS	Pre incubation 4%PFA-PBS	Pre incubation 4%PFA-PBS	Pre incubation 4%PFA-PBS	Pre incubation 4% PFA-PBS	**Post** incubation 4% formalde-hyde-PBS
Duration	N/R	N/R	10 min RT	5 min RT	10 min	10 min RT
Permea-bilisation	N/R	0.3% Triton after fix	0.3% Triton after fix	0.3% Triton after fix	0.1% Triton + block	No
Duration		N/R	10 min RT	5 min RT	1h	N/A
Block	N/R	N/R	10% BSA-PBS 1h RT	N/R	0.2% gelatin-PBS +triton 1h RT	Samples diluted in DMEM-HEPES w.1% BSA
Samples						
Serum	Max 1:400	1:200	N/A	1:40	1:5	1:20
CSF	Max 1:10	1:10	1:10-100	1:2	1:5	1:2
Dilutant	N/R	N/R	PBS w.1% BSA	N/R	Saturation buffer	DMEM-HEPES w. 1% BSA
Duration	N/R	N/R	ON 4°C	2h RT	90 min	1h RT
NMDAR	N/R	Anti-NR1	Anti-NR1	Anti-NR1 Ab[4]	NR1+EGFP	EGFP-not

labelling		Ab[2]	Ab[3]		conjugated	conjugated
Duration	N/R	N/R	ON 4°C	1h RT	N/A	N/A
2° antibody	N/R "appropriate fluorescent secondary abs"	N/R	AlexaFluor 488 goat anti-human IgG 1:1000 in PBS w.1% BSA	Goat AlexaFluors: 488 anti-human IgG, 1:1000 + 594 anti-mouse IgG, 1:1000	cy3-conjugated anti-human IgG containing DAPI	AlexaFluor 568 goat anti-human IgG 1:750
Duration	N/R	N/R	2h 37°C	1h RT	N/R	45 min
Dilutant	N/R	N/R	PBS w. 1% BSA	N/R	N/R	DMEM-HEPES w. 1% BSA
Medium for washes	N/R	N/R	PBS	PBS	PBS likely	DMEM-HEPES

1 not diagnostic assay protocol, research protocol
2 rabbit monoclonal anti NR1 1:10000, AB9864, Chemicon, C-terminus aa 909-938.
3 mouse monoclonal anti-NR1 1:1000, 556308, BD Biosciences, against TM3-4 loop aa 660-811.
4 mouse monoclonal anti-NR1 1:20000, MAB363 Millipore, against TM3-4 loop aa 660-811.
N/A not applicable; N/R not recorded; ON overnight; RT Room temperature; PBS phosphate buffered saline; BSA bovine serum albumin; DMEM-HEPES Dulbecco's modified Eagle's medium with HEPES.

Non-specific background staining appeared to improve further when cells were transfected with equal concentrations of NR1 and NR2B with no EGFP (Table 3.3, and Figure 3.4 bottom panel). However, it was noted that cells fixed more than 48 hours prior to CBA were generally in poor condition with very few cells adhering to the coverslips and a number of apparently lysed cells present, suggesting that storage of fixed cells in PBS at 4°C was not advisable. There was no non-specific background with CSF samples in any of the methods tested, as for the l-CBA.

Table 3.3 Results of initial trials of f-CBA

Trial	NR1:NR2B EGFP	Dilutant	Permeabilisation and block	Result
1	3:1 + EGFP	DMEM-HEPES + 1% BSA	0.3% Triton 10min, no block	Background ++ unreadable
2	3:1 + EGFP	DMEM-HEPES + 1% BSA But PBS washes	½ permeabilised with 0.1% Triton at each step; 10% BSA block 1 h in ½	Background ++ unreadable
3	3:1 + EGFP	PBS-1% BSA PBS washes ++	0.3% Triton 10 min	Background ++ and no effect of 2°Ab dilution No background if omit serum
4	3:1 + EGFP	PBS-1% BSA	5% BSA + 5% NGS 1h 0.1% Triton in 1/2	↓↓background readable perm=no perm NB: few cells
5	3:1 + EGFP ½ coverslips untransfected	PBS-1% BSA	5% BSA + 5% NGS + 0.1% Triton 1h	Untransfected cells aided interpretation
6	1:1	PBS-1% BSA	10% BSA + 0.1% Triton 1 h	Anti-NR1 Ab labels ++ cells with minimal background ↓↓background with serum easy readable
7	1:1	PBS-1% BSA	10% BSA + 0.1% Triton 1 h	Fixed cells stored for 5 days: in poor condition
8+9	3:1+EGFP vs. 1:1	PBS-1% BSA	10% BSA + 0.1% Triton 1 h	Much less background in 1:1 w/o EGFP

The final protocol used for the f-CBA was as follows:

- Growing and seeding of HEK293 cells as for l-CBA
- Transfection on day 2 with 1.5μg each of NR1 and NR2B cDNA per well (total 1.5μg/ml of medium).

- Change to medium containing 500μM ketamine 16 hours after transfection
- CBA performed on day four:
    - Cells fixed with 4% PFA in PBS for 5 minutes at room temperature followed by 6 rapid PBS washes
    - Cells incubated with 10% BSA and 0.1% TritonX-100 in PBS for 1 hour at 37°C followed by a single PBS wash
    - Serum samples diluted 1:40 and CSF 1:10 in PBS with 1% BSA (and further dilutions in steps of 3 if required) and transferred into 24-well plates
    - Single coverslip added to each well (cell side up) and incubated for 2 hours at room temperature
    - 3 PBS washes
    - 1 hour incubation at room temperature with commercial anti-NR1 antibody at 1:1000 in PBS with 1% BSA
    - 3 PBS washes
    - 90-minute incubation with fluorescently-labelled secondary antibodies at 1:1000 in PBS with 1% BSA at room temperature
    - 3 PBS washes
    - coverslips placed on microscope slides cell-side down in mounting medium with DAPI

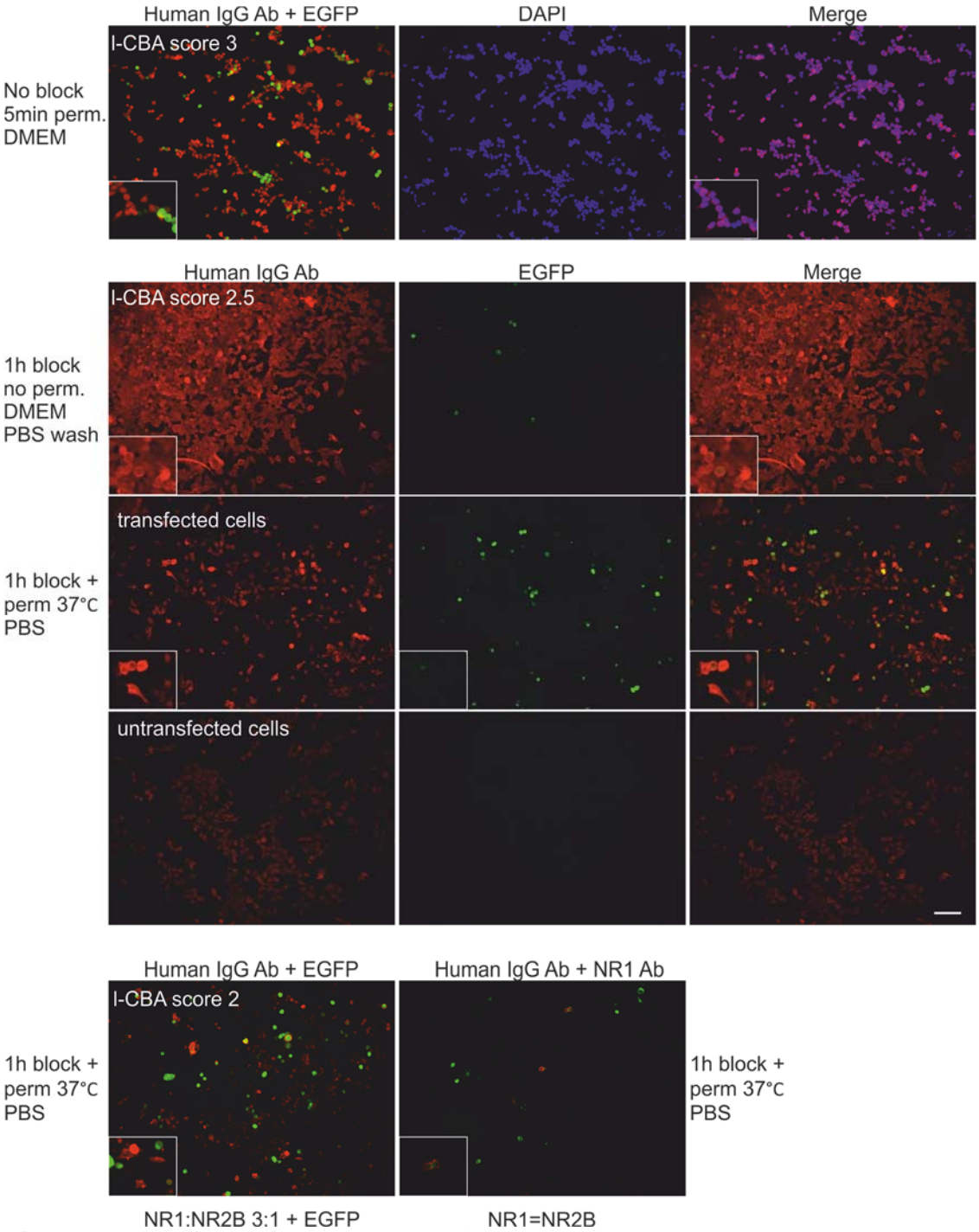

Figure 3.4 Results of first attempts at f-CBA

The first attempts at f-CBA, using 3:1 NR1:NR2 with untagged EGFP transfection and no specific blocking step yielded very high non-specific background (see 1st panel), with every cell (denoted by blue DAPI stain) being bound by anti-human IgG fluorescent antibody (red) such that no specific NMDAR staining could be detected. The introduction of a blocking step alone was not sufficient to reduce the background (1st row of second panel), but changing the dilutant for serum and CSF to PBS and permeabilising and blocking simultaneously for 1 hour at 37°C appeared to markedly reduce background staining (middle and bottom row of second panel) such that specifically IgG-bound were detectable above background. Not using EGFP transfection and instead co-localising with a commercial NR1 antibody appeared to further reduce non-specific staining. Scale bar is 50μm, pictures taken at x20 magnification.

Despite optimisation of the developed protocol, non-specific staining with serum was much stronger than in the l-CBA; nevertheless, detection of NMDAR-antibody binding was still possible after optimisation, as this appeared in a very specific cell-membrane pattern, whilst the background staining was present at a lower intensity throughout the cytoplasm of the cells (see Figure 3.5). Additionally, there was good co-localisation with the commercial anti-NR1 antibody (see bottom panel of Figure 3.5). The non-specific staining sometimes made interpretation of low-positives difficult at 1:40 dilution, in which case a higher dilution (1:120) helped clarify the results, as background staining was considerably weaker (Figure 3.5). Therefore, serum was always tested at both these dilutions for the f-CBA. For the analysis, the score at 1:40 was used.

There was no background staining with CSF, as in the l-CBA, and CSF was therefore tested at 1:10 only and any value of 0.5 and above considered positive. Examples of serum and CSF scores 0 to 4 are shown in Figure 3.6 and Figure 3.7.

All observed binding (scoring from 0.5) was considered positive. This was because, unlike for l-CBA results' reporting, which has been under continuous review by the Oxford laboratory as was described above, f-CBA scoring and reporting information is not available in the literature. Additionally, co-localisation of human IgG with commercial NR1 antibody staining was very consistent in the f-CBA, improving the confidence with which the result could be stated as positive, once non-specific binding to all cells has been taken into consideration.

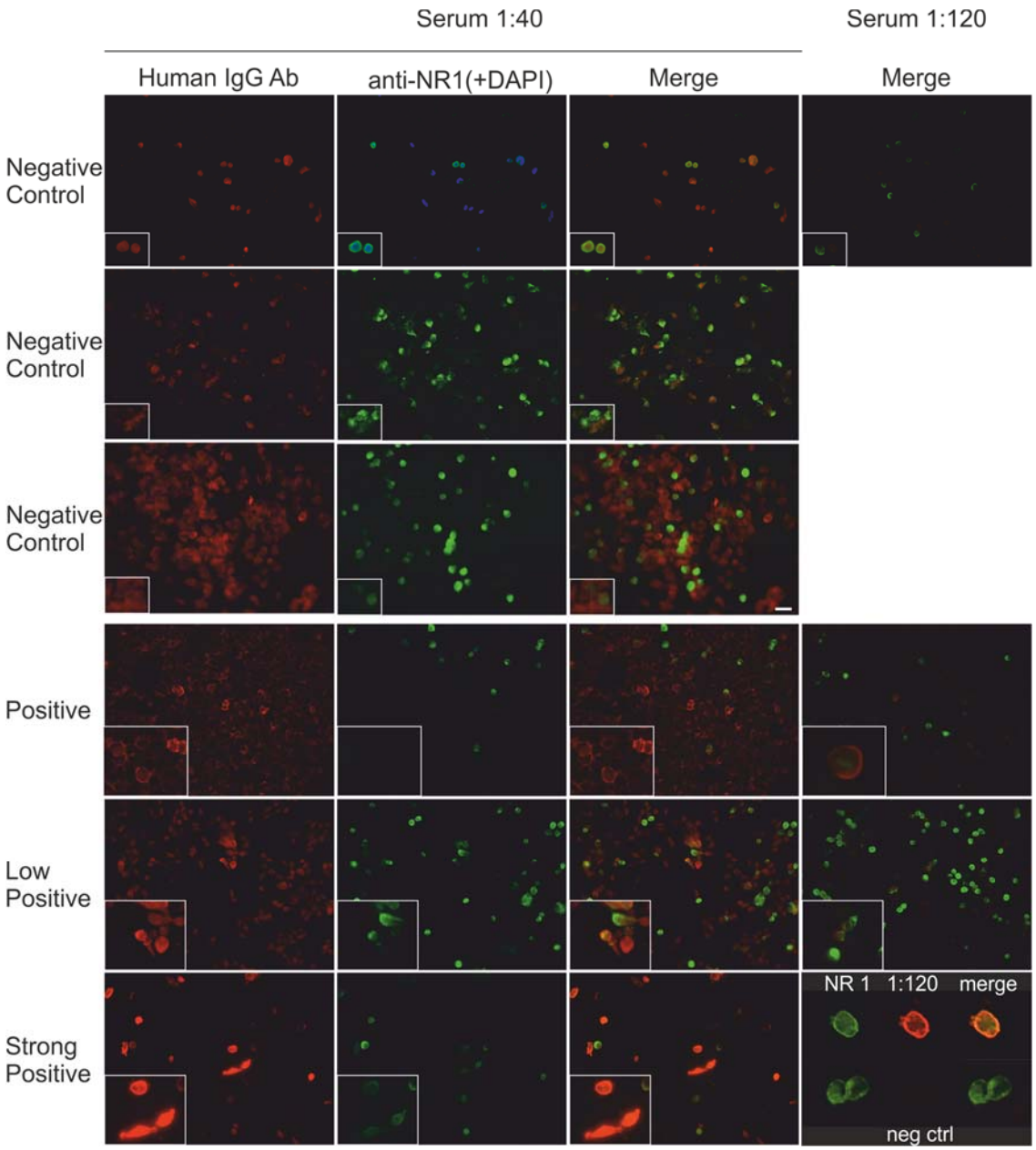

Figure 3.5 Non-specific background staining with serum in f-CBA.
Non-specific background staining of cells in f-CBA with serum was marked in comparison to l-CBA (see Figure 3.2). The top panel shows three examples of results obtained with negative control serum samples. Background staining is present throughout the cytoplasm of all the cells (red), sometimes with variable intensity (e.g. middle and bottom row). Background staining reduced markedly at 1:120 dilution of serum. This pattern of staining can be distinguished from NMDAR-specific IgG binding (red, bottom panel), which is present in a cell-membrane pattern similar to that seen in l-CBA. NMDAR-specific human IgG binding (red) co-localised well with anti-commercial NR1antibody-binding (green), which appeared more diffusely present throughout the cytoplasm as well as in the cell membrane. NMDAR-specific human IgG binding remained present at 1:120 in the majority of samples tested, whilst non-specific background diminished markedly. Scale bar 50 μm, pictures taken at x40 magnification.

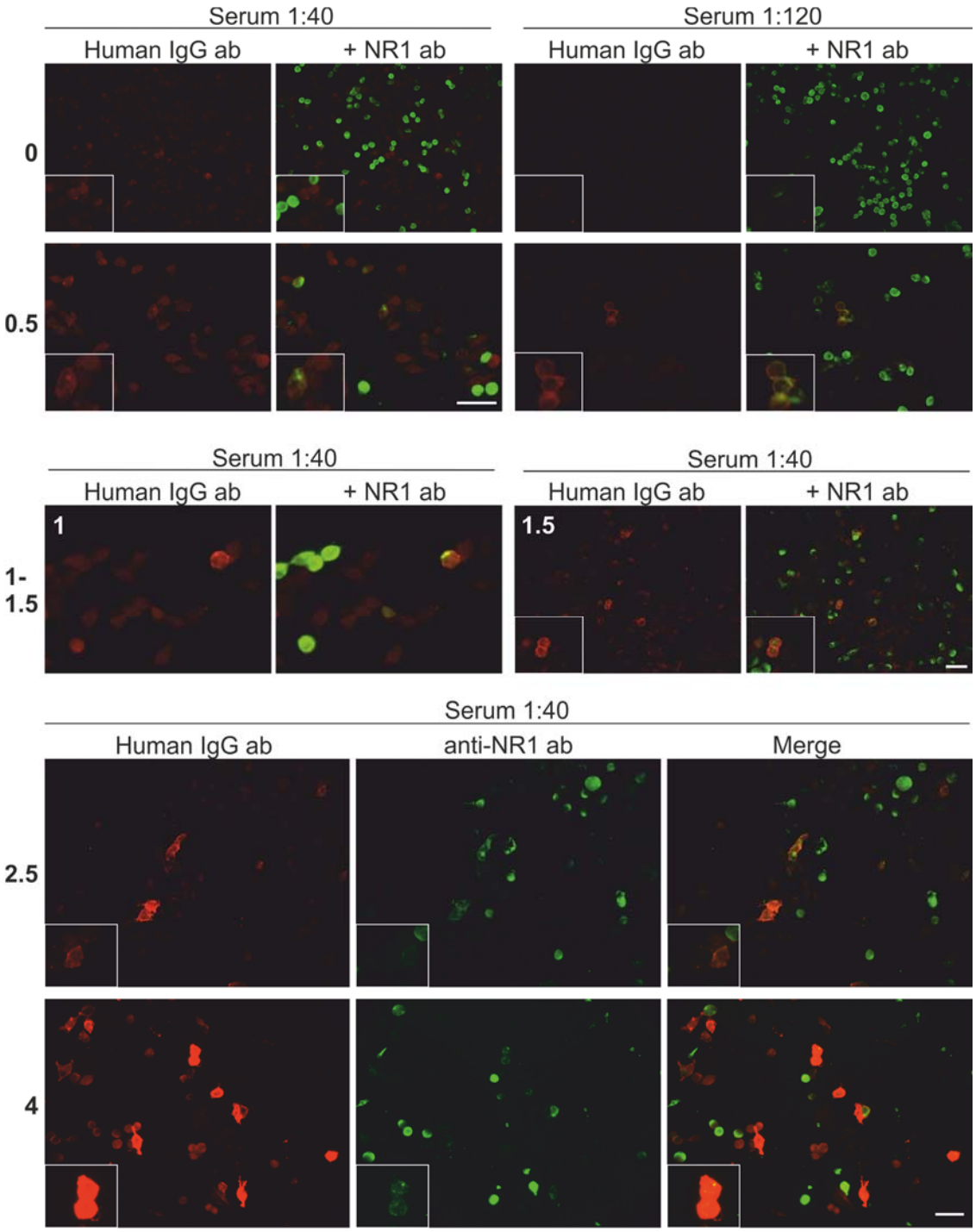

Figure 3.6 Scoring of f-CBA results for serum samples
Pictures illustrate serum samples scoring from 0-4 on fixed cell CBA. Magnification is x20 in the top panel and x40 in the middle and bottom panels. Scale bar represents 50μm. Magnified (x2) insets are included for detail. The photographs show anti-human IgG staining alone (red) followed by merged anti-human IgG and anti-NR1 antibody (green) binding. Coverslips with background staining only scored 0. If weak red fluorescence was present in isolated cells in the correct pattern (confirmed by increasing signal:noise ratio at 1:120 dilution), a score of 0.5 was given (same sample shown at both dilutions here). Scores of 1-4 were given based on increasing intensity and density of bound cells. Unlike for l-CBA, colocalisation was important to determining the specificity of the binding.

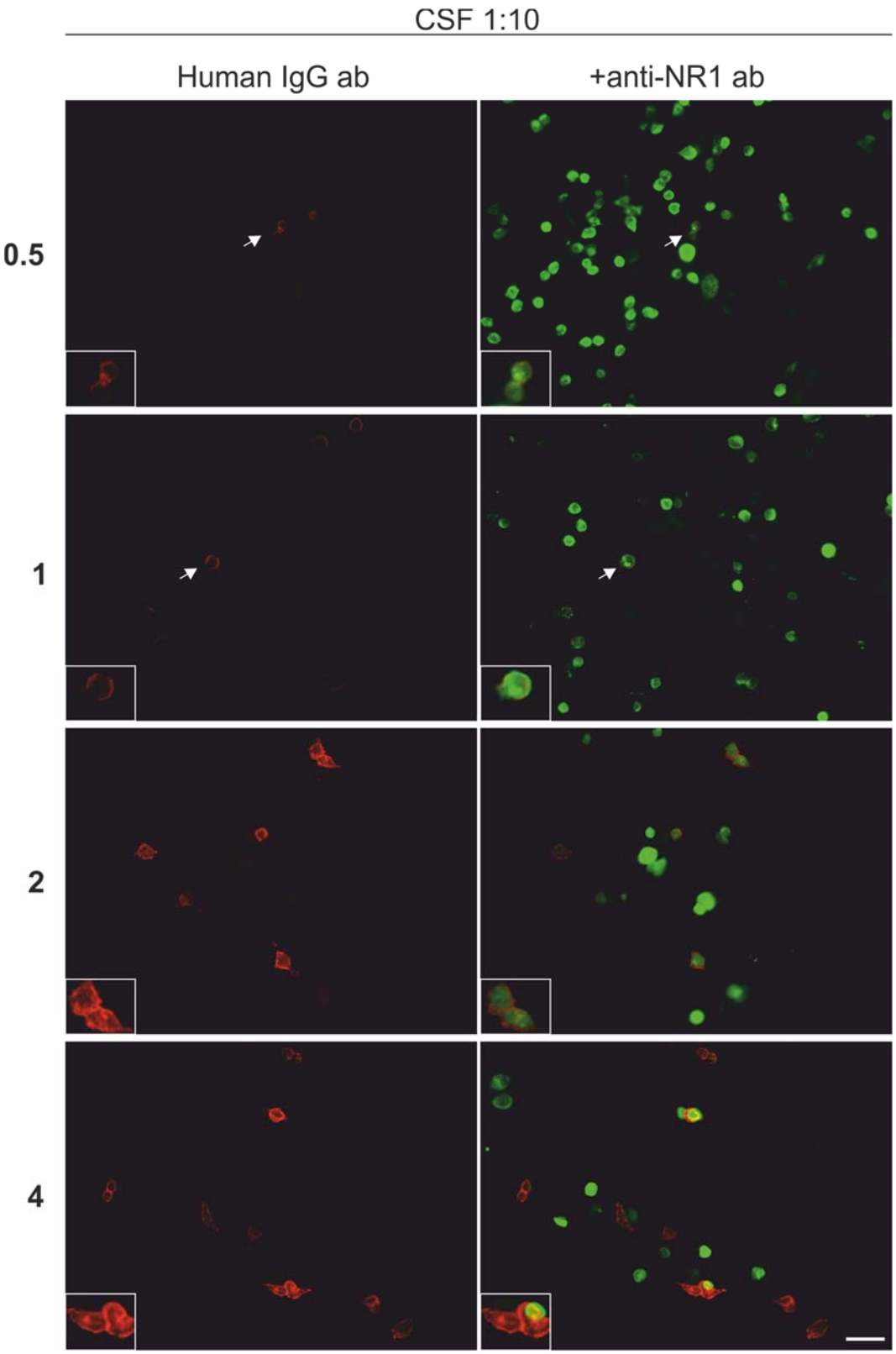

Figure 3.7 Scoring of f-CBA results for CSF samples
Magnification is x40. Scale bar represents 50μm. Magnified (x2) insets are included for detail. The photographs show anti-human IgG staining alone (red) followed by merged anti-human IgG and anti-NR1 antibody (green) binding. Unlike with serum, there was no non-specific background staining. Coverslips with no binding scored 0. If weak red fluorescence was present in isolated cells in the correct cell-membrane pattern, a score of 0.5 was given. Scores of 1-4 were given based on increasing intensity and density of bound cells. Unlike for l-CBA, colocalisation was important to determining the specificity of the binding.

3.3.3 Developing the Barcelona immunohistochemistry protocol used in this thesis

The IHC protocol used here was based on the IHC methods optimised for cell-surface antigens published by the Barcelona group (See Table 3.4 (Dalmau *et al.*, 2007; Höftberger *et al.*, 2013; Gresa-Arribas *et al.*, 2014; Planagumà *et al.*, 2014)).

Obtaining 7μm sections after this brief fixation protocol proved difficult, with sections often crumpling or folding when collected onto microscope slides. Reducing the cryostat temperature to -25°C alleviated the problem in some half brains but not others. Ensuring that freshly made PFA was used, careful washing after immersion in PFA and removal of excess sucrose solution prior to embedding in freezing medium did not improve slicing ease. A range of section thicknesses (7-12 μm) was used here.

Table 3.4 Published IHC methods

	Dalmau 2007	Gresa-Arribas 2014	Höftberger 2013	Planaguma 2015
Kill Method	Not given	Not given	CO2	CO2
Perfusion	No	No	No	No
Fixation	Immersion 24h in 4% PFA	Immersion in 4% PFA at 4°C for 1h	Immersion in 4% PFA at 4°C for 1h	Immersion in 4% PFA at 4°C for 1h
Freezing	Immersion 40% sucrose 24h and snap frozen in isopentane chilled with liquid nitrogen (l-N_2)	Immersion in 40% sucrose for 24h at 4°C, then embedded in freezing medium and snap frozen in isopentane chilled with l-N_2	Immersion in 40% sucrose for 48h at 4°C then embedded in freezing medium and snap frozen in isopentane chilled with l-N_2	Immersion in 40% sucrose for 48h 4°C, embedded in freezing medium then snap frozen in isopentane chilled with l-N_2
Section thickness	7μm	7μm	7μm	7μm
Antigen retrieval	Yes (?only for paraffinised tissue)	No	No	No
Endogenous peroxidase block	0.3% H_2O_2 for 20min	N/R	0.3% H_2O_2 for 15 min	0.25% H_2O_2 for 10 min at 4°C
Protein block	10% normal goat serum 1h	N/R	5% NGS for 1 h	5% NGS for 15min at room T°
Primary	Serum 1:250 CSF 1:10 Overnight 4°C	Serum 1:200 + dilutions CSF 1:2 + dilutions Overnight 4°C	Serum 1:200 in PBS-5% NGS; CSF 1:2 Overnight 4°C	Animals received biventricular infusion of patient or control CSF for up to 14d
Secondary	"Appropriate" secondary Ab; 1:2000 no time indication	Biotinylated goat anti-human IgG Ab 1:2000 1h at RT	Biotinylated goat anti-human IgG Ab 1:2000 in PBS-5% NGS 1h at RT	Biotynilated goat anti-human IgG Ab 1:2000 overnight at 4°C
Development	Avidin-biotin-peroxidase	Avidin-biotin-peroxidase (Vector Labs)	Avidin-biotin-peroxidase 1h RT	Avidin-biotin-peroxidase
Chromogen	N/R	N/R	DAB 7 min	DAB

Initial trials revealed high levels of non-specific background, making the interpretation of results difficult. Substituting PBS with 0.1M Tris-buffered saline markedly reduced the background staining and was particularly helpful in

negative samples as background staining often appeared somewhat stronger in HPC when PBS was used. The protocol was otherwise as described in Höftberger *et al.* (2013), except serum samples were diluted 1:120 and CSF 1:10. For serum, a further dilution of 1:360 was also always tested. As expected, non-specific staining was higher with serum samples than CSF samples and decreased with increasing dilution.

Positivity was defined as neuropil binding in the HPC with sparing of the granule cell layer in DG and CA1-3 pyramidal layers, according to the pattern previously described (see also Dalmau *et al.* (2007); Dalmau *et al.* (2008); Gresa-Arribas *et al.* (2014)). Cerebellar granule cell layer staining has not clearly been reported with positive samples in Dalmau's papers but is defined as a specific finding by Euroimmun (Wandinger *et al.*, 2011). It was therefore included in our criteria for positivity, albeit only if associated with the typical hippocampal distribution of binding, as nuclear staining with some samples occasionally gave rise to marked cerebellar granular layer staining. Faint staining was also seen in cerebral cortex and basal ganglia. Examples of scores 0-4 for serum and CSF samples are shown in Figure 3.8.

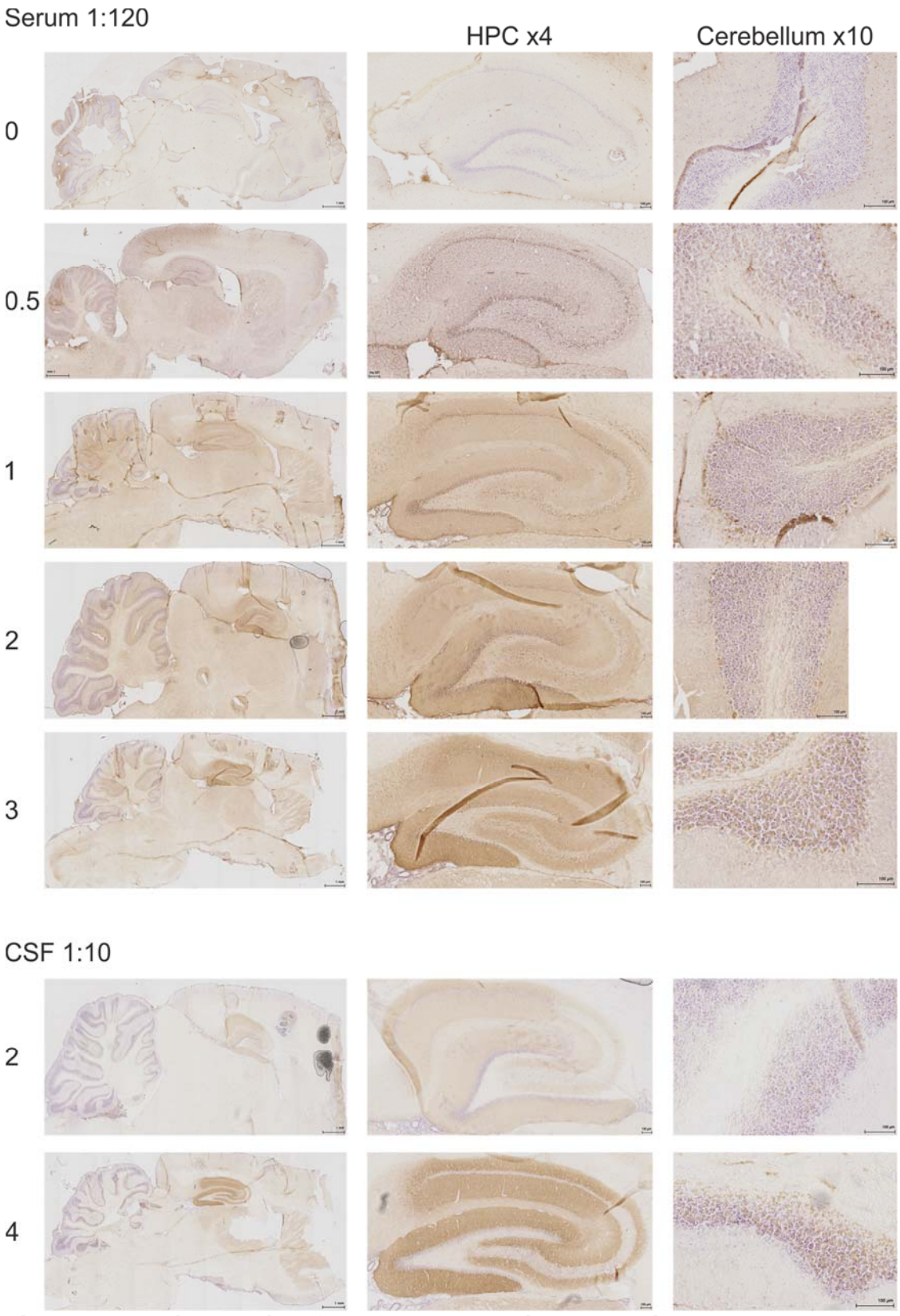

Figure 3.8 Scoring results of IHC for serum and CSF samples
Results were scored visually, based on the strongest staining obtained from 0-1. Scale bar in the photographs in the first column is 1mm. Magnification is otherwise as indicated and scale bars represent 100μm. The most marked anti-human IgG binding is found in the HPC, and dominates in the molecular layer of the dentate gyrus, sparing the hilus of the DG and the cell layers of CA1-3. Punctate staining was also present in the granule cell layer of the cerebellum in positive samples, with variable non-specific staining of the Purkinje cells. Background staining is more prominent with serum than CSF.

3.3.4 Gaining experience with the Euroimmun Biochips

Cell-based assays for serum and CSF were carried out according to Euroimmun instructions. A visual scoring system similar to the one used in l-CBAs was used, with the maximum score of 4 defined by the positive control provided by Euroimmun, which produced intense cytoplasmic punctate staining in most cells in the biochip. All scores over 0 were considered positive. Examples of scores 1-4 are shown in the top and middle panel of Figure 3.9. Unlike the cell-surface staining seen in l- and f-CBA, the binding pattern in Euf-CBA was always cytoplasmic.

Some serum samples produced ambiguous bright staining in a pattern not seen with the positive control provided by Euroimmun or other clearly positive samples. This staining was not punctate and present throughout the cytoplasm as with the positive samples, but also not entirely nuclear as was seen, for instance, in some negative samples with anti-nuclear antibodies (see Figure 3.9 lower panel). In the case of these ambiguous samples, the neighbouring non-transfected biochip, included by the company as a control, was not always helpful for determining positivity or negativity. This pattern of staining also led to the incorrect reporting of the presence of NMDAR-Abs in 2 of 319 (0.6%) patients with schizophrenia (de Witte *et al.*, 2015); when the two sera were re-tested by f-CBA and on a different batch of the Euroimmun biochips, NMDAR-Abs were not detected.

Adding a further brief incubation with mouse anti-NR1 antibody, and then double-staining with the human IgG antibody provided by Euroimmun and a goat anti-mouse IgG antibody eliminated the uncertainty, as the pattern of staining with the NR1 antibody replicated that seen with the positive control and allowed determination of co-localisation with the anti-human IgG antibody (Figure 3.9 lower panel). As expected, CSF samples produced clear, background-free results.

Euroimmun slides containing rodent hippocampal tissue biochips were used for 65 of 79 serum samples and 18 of 26 CSF samples. Surprisingly, incubating hippocampal tissue biochips with the specific anti-NR1 antibody used above did not produce any binding. There was a striking lack of consistency between the scores on the fixed cell biochips and hippocampal tissue biochips for the serum

samples (Spearman's correlation r = 0.415 (moderate), p= 0.0006, n=65 pairs) although this was much better for CSF samples (Spearman's correlation r = 0.874 (very strong), p< 0.0001, n= 18 pairs). The typical pattern of hippocampal staining obtained with NMDAR-Abs in unfixed or PFA-fixed tissue described in section 3.3.3 above was not consistently seen in the hippocampal tissue biochips. The hilus of the dentate gyrus also appeared stained with some positive samples, and bright fluorescence sometimes appeared throughout the HPC (including the dentate gyrus hilus) of some negative samples (see Figure 3.10). The Euroimmun tissue scores were therefore excluded from further analysis.

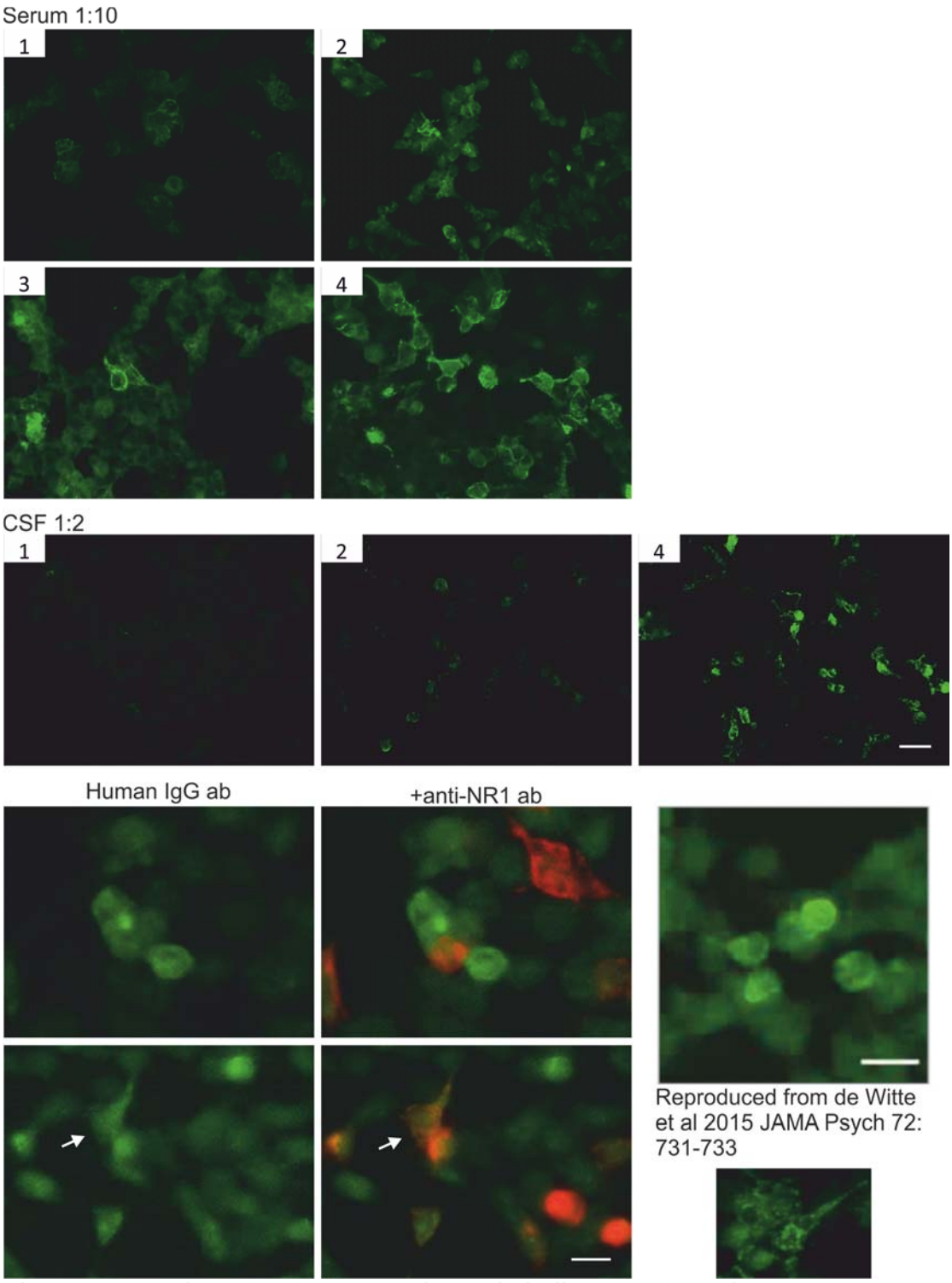

Figure 3.9 Scoring of Euf-CBA results and challenges of scoring
The top two panels show examples of serum (top) and CSF (middle) samples scoring 1-4 on Euroimmun CBA. If there was no difference between the chip with the transfected cells and the untransfected cells, a score of 0 was given. Positive scores were given if punctate cytoplasmic staining was present (see bottom right inset in lower panel). Increasing scores were given based on the number of cells bound and the intensity of the fluorescence. The bottom panel illustrates the challenges of scoring Euf-CBA: sometimes brightly stained cells could be seen, but the staining was not punctate as seen in the small bottom right picture, and did not extend throughout the cell cytoplasm as seen in the bottom left picture. An additional incubation with anti-NR1 and a red fluorescent secondary allowed determination of colocalisation, which helped determine positivity (bottom right) or negativity (top right). Magnification x40 (x20 in middle panel). Scale bar 50μm.

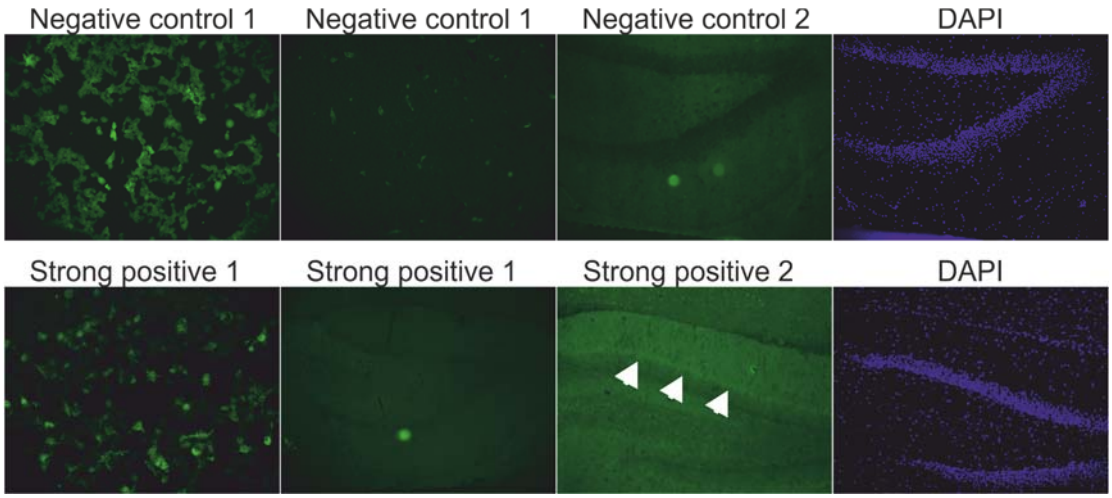

Figure 3.10 Results obtained with biochips containing fixed hippocampal tissue. Variable results were obtained with the biochips containing fixed hippocampal tissue. Incubation with negative controls either gave rise to no binding as expected (negative control 1) or to a pattern that looked indistinguishable from some positive samples with apparent fluorescent present in the molecular and hilar layers of the dentate gyrus (e.g. negative control 2). Some samples that gave strongly positive results on the biochips containing cells were not associated with any detectable hippocampal staining (e.g. strong positive 1). Other positive samples gave rise to detectable fluorescence, but the pattern was not always clearly similar to that seen by IHC, with only subtly increased molecular layer binding compared to hilus (e.g. strong positive 2).

3.3.5 Comparison of scores in all assays

To compare score results across assays, the scores in the current l-CBA were used as these were obtained contemporaneously to the other assays. The samples that were positive in the original l-CBA were analysed separately from the originally negative samples, and the samples that had lost reactivity were excluded.

Samples positive in original l-CBA

There were 58 serum samples from 50 patients with a positive score in the original l-CBA, but 2 serum samples had to be excluded as the result of one of the assay methods was missing for each of these (due to insufficient sample volume). This therefore left full data from 56 positive samples from 49 patients (one of the excluded samples was from a patient with 2 samples available).

The serum scores in the repeat l-CBA were generally higher than with the other assay methods (Friedman test, F=39.11, $p< 0.0001$, n=56 originally positive samples, Figure 3.11 A). As mentioned above, only the f-CBA was performed at the same dilution as the l-CBA (1:40), the IHC having been scored at the 1:120 dilution and Euf-CBA at 1:10. Nevertheless, the IHC score median was slightly higher than that of f-CBA, and the Euf-CBA scores were the lowest despite being done at the lowest dilution. 27, 24 and 28 samples scored 0 in f-CBA, IHC, and Euf-CBA respectively, whilst none scored 0 in the repeat l-CBA. Most of the samples that scored 0 in the f-CBA and IHC had scored from 0.5-1.5 in the l-CBA, whilst a similar proportion of samples scoring 0.5-1.5 and 2-4 in l-CBA scored 0 in Euf-CBA (Figure 3.11 Bi), perhaps suggesting lower sensitivity of this method.

Among previously positive serum samples, scores in f-CBA were strongly correlated to l-CBA scores (Spearman $r= 0.681$, $p<0.0001$), and scores in IHC were moderately correlated with l-CBA scores (Spearman $r=0.412$, $p=0.002$). As would be expected from the results above, Euf-CBA only correlated weakly with l-CBA scores (Spearman $r=0.287$, $p=0.032$, Figure 3.11 Bii)).

Nine CSF samples were positive in the original l-CBA, but three of these scored 0 in the repeat l-CBA. There was no difference between scores on the four assays (RM one-way ANOVA, $F(2.39, 16.72)=2.22$, $p=0.133$, Figure 3.12 A).

Four scored 0 in the f-CBA (scores of 0-0.5 in l-CBA), only one scored 0 in IHC (scored 0 in l-CBA and f-CBA and 1 in original l-CBA), and two scored 0 in Euf-CBA (both scored 0 in l-CBA).

Samples negative on l-CBA

21 serum samples from 20 patients had been negative on the original l-CBA (three scores of 1, one score of 0.5, seventeen score of 0). There was a significant difference in scores between the four different assays (Friedman test, F=9.57, p = 0.023) although Dunn's multiple comparisons test could not determine which groups were different (Figure 3.11 C). All but two of the negative samples remained negative in the repeat l-CBA (both had scored 1 in original l-CBA). All 21 samples were negative in f-CBA and Euf-CBA, but 5 were positive in IHC (all scored 0 in both original and new l-CBA, and in f-CBA and Euf-CBA) and this is likely to be the cause of the statistical difference. It is possible that these IHC-positive samples were from patients with other neuronal cell-surface antibodies and alternative LE diagnoses. The pattern of binding was consistent with NMDAR-Abs however, and the clinical details that became available for two of these five samples revealed the samples had been taken following clinical recovery from NMDAR-Ab encephalitis. No clinical information is available for the other three samples.

Seventeen CSF samples were negative in the original l-CBA. All but two remained negative in all other assays (one score of 1 in f-CBA; one score of 2 in Euf-CBA, Figure 3.12 B).

3.3.6 Effect of dilutions in the four assay methods

Serial titration was performed in four serum samples and two of their paired CSF samples (Figure 3.13 A and B). The last dilution at which reactivity was visible was recorded for each assay as the end-titration for that sample (Figure 3.13 C). For serum, the highest end-titres were found with IHC, and Euf-CBA reactivity was lost earliest. In CSF, IHC and Euf-CBA gave the highest end-titres. The number of samples studied is too small to draw any firm conclusions.

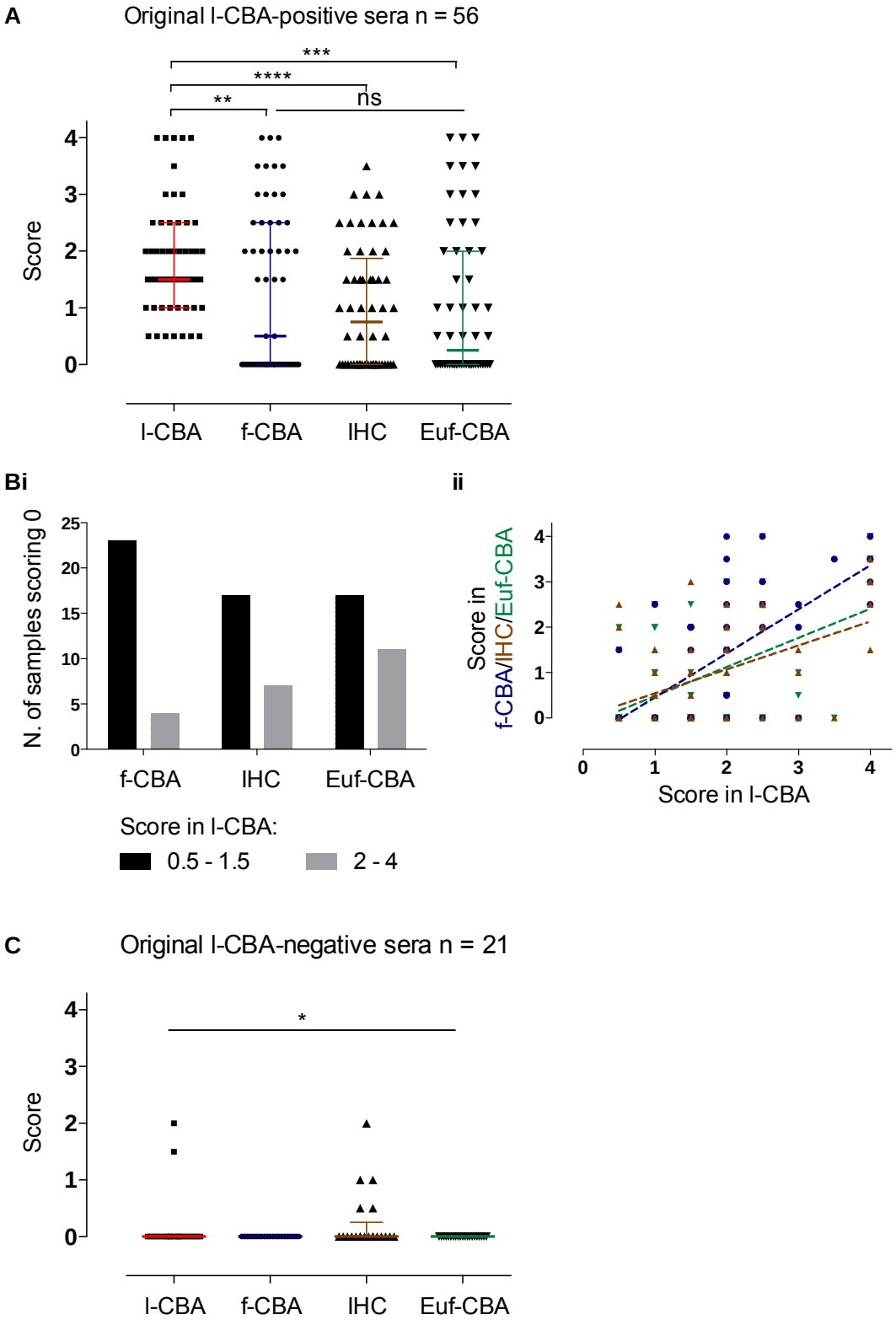

Figure 3.11 Comparison of serum sample scores in all assays.
L-CBA (1:40) scores were higher than f-CBA (1:40), IHC (1:120) and Euf-CBA (1:10) scores in samples that had previously been reported as positive by l-CBA (A, Friedman test with Dunn's multiple comparisons test). 27 of these samples scored 0 on f-CBA, 24 on IHC and 28 on Euf-CBA. For f-CBA and IHC, most of the samples scoring 0 had scored 0.5-1.5 on the new l-CBA, but many of the Euf-CBA-negative samples had scored positively in l-CBA (Bi). F-CBA scores were strongly correlated to l-CBA scores, IHC scores moderately correlated and Euf-CBA weakly correlated (Bii). Originally negative serum samples generally remained negative on all assays, except for 5 samples, which scored positively on IHC.

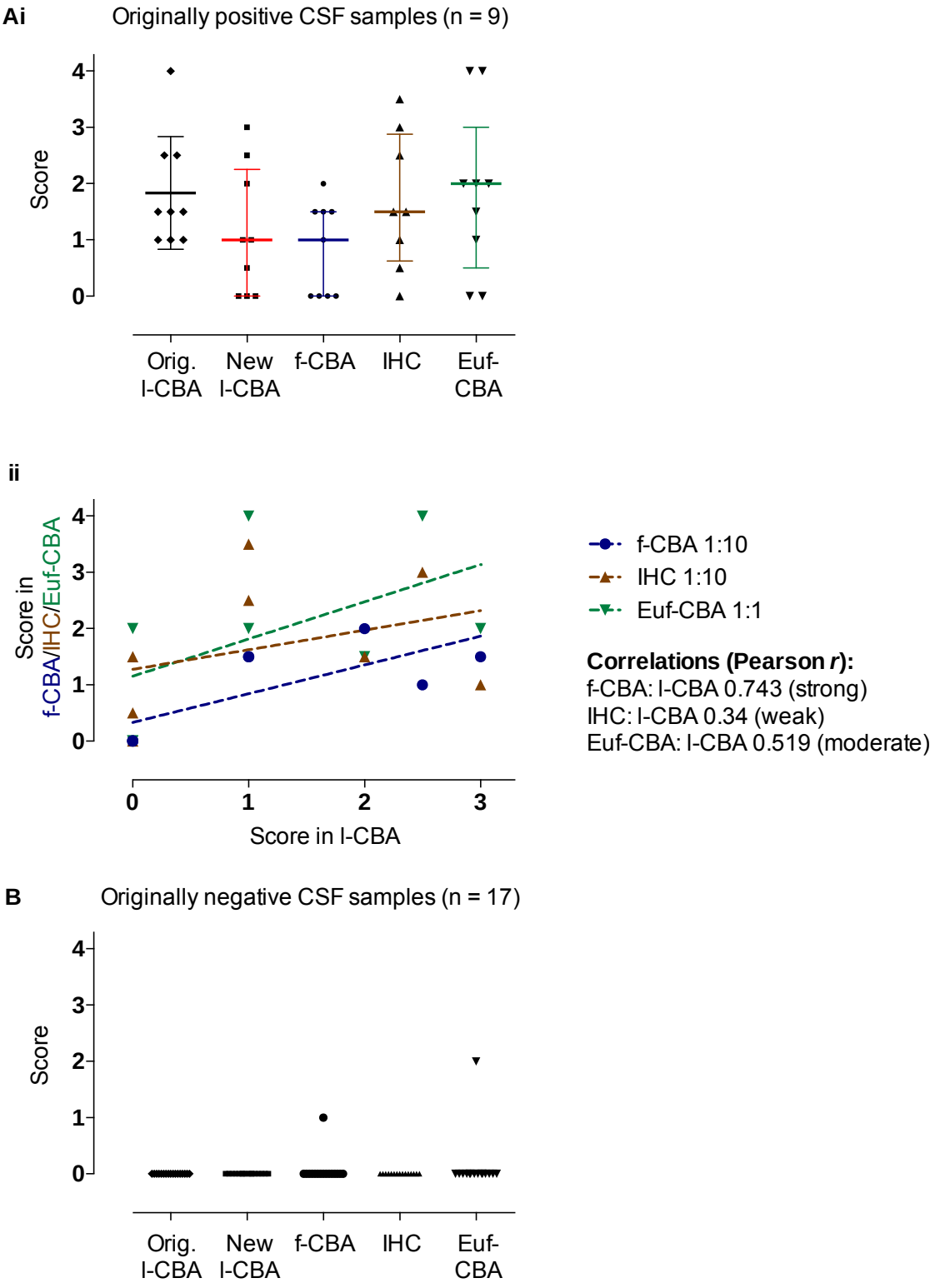

Figure 3.12 Comparison of CSF sample scores in all assays
There was no difference between scores on the repeat l-CBA (1:10), f-CBA (1:10), IHC (1:10) and Euf-CBA (1:1) in CSF samples that scored positively (>0) on the original l-CBA (1:2) (Ai). Only f-CBA and l-CBA scores were strongly correlated, with IHC scores weakly and Euf-CBA scores moderately correlated to l-CBA scores (Aii). Two samples scoring 0 in the original l-CBA scored positively in other assays (one each in f-CBA and Euf-CBA) but the remaining 15 samples scored negatively in all assays.

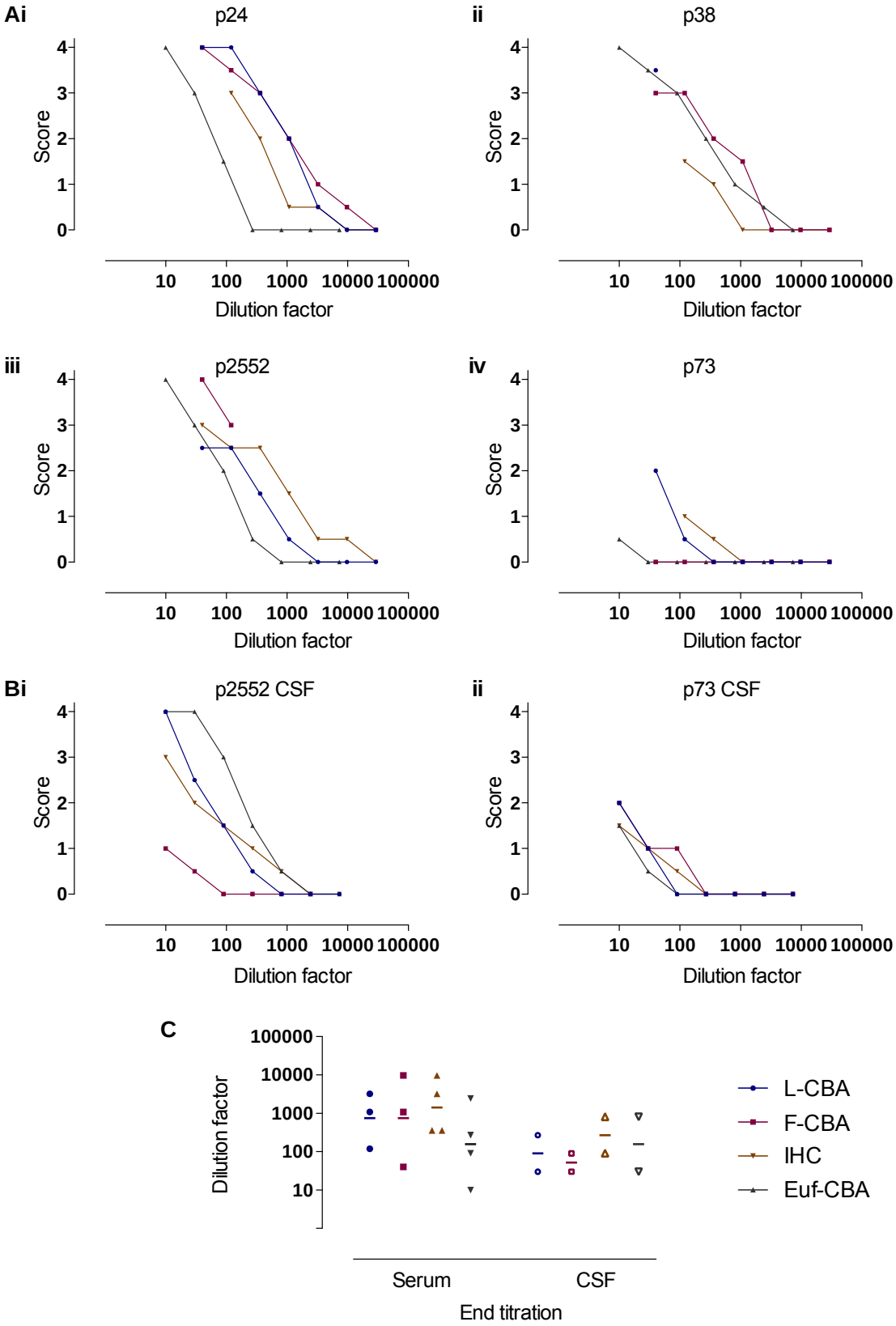

Figure 3.13 End-titration results in serum and CSF for the four assay methods. The scores for each dilution of four serum samples and two CSF samples are graphed in Ai-iv and Bi-ii respectively for each method. The end-titration (the last dilution at which binding was still visible) for each assay method is shown in C.

3.3.7 Correlation with clinical details

Clinical details have so far been obtained on 44 of the 88 patients whose serum and/or CSF samples were included in the study, and the results of their assays are shown in Table 3.5. Treating physicians were contacted and asked to define the patients' illness as definite, probable, possible, or unlikely NMDAR-Ab encephalitis based on their clinical syndrome and response to immunotherapy. No antibody-independent criteria are available at present; the clinician was therefore asked to give their diagnosis based on their experience with treating similar patients. The diagnoses included 23 definite, 1 probable, 6 possible and 14 unlikely. The range of scores obtained in each diagnostic classification are shown in Figure 3.14 (A, B, C, left panel) for serum samples (n=49 samples from 40 patients, 3 "definite" and 1 "possible" patients excluded as samples taken after recovery and therefore negative), and for CSF samples from patients with definite NMDAR-Ab encephalitis (n=6, Figure 3.15). Clinical details were available for a further 3 patients with CSF samples (2 possible NMDAR-Ab encephalitis and 1 unlikely NMDAR-Ab encephalitis) and all 3 scored 0 in all assays and hence have not been shown.

In serum, in the "definite" category, the highest scores were obtained using l-CBA (original l-CBA median 2.5, *IQR* 1.5-4, new l-CBA median 2.0, *IQR* 1-2.88), followed by f-CBA (median 2.25, *IQR* 0-3), and then IHC (median 1.5, *IQR* 1-2.5) and Euf-CBA (median 1.5, *IQR* 0-3, Figure 3.14 A left panel). Statistical comparison was not carried out as different dilutions were used in different assays. A similar trend was noted in the "possible"/"probable" (Figure 3.14 B left panel) as well as "unlikely" categories (Figure 3.14 C left panel), where l-CBA tended to score positively whilst f-CBA, IHC and Euf-CBA scored negative in the majority of the samples

Table 3.5 Results of each assay in patients with available clinical diagnosis

Patient identifier	CSF or serum	Paired or unpaired CSF	Original I-CBA (serum 1:20; CSF 1:2)	Current I-CBA (serum 1:40; CSF 1:10)	IHC (serum 1:120; CSF 1:10)	f-CBA (serum 1:40; CSF 1:10)	Euf-CBA (Serum 1:10; CSF 1:1)	Final Clinical Diagnosis	Comment
41	Serum 1		4	1	0.5	2.5	1	Definite	
83	*Serum 2*		*3*	*2*	*1.5*	*3.5*	*0*		*Further sample*
26	Serum 1		4	2	2.5	4	3	Definite	
10	*Serum 2*		*2.5*	*2.5*	*2.5*	*4*	*2.5*		*Further sample*
38	*Serum 3*		*4*	*4*	*1.5*	*2.5*	*4*		*Further sample*
12	Serum	Unpaired	4	3	1.5	2	0	Definite	
12A	CSF	Unpaired	1	3	1.5	1	2		
47	Serum 1	Paired	4	4	2.5	3.5	3.5	Definite	
47A	CSF	Paired	2.5	1	2.5	1.5	4		
88	*Serum 2*		*4*	*4*	*3.5*	*3*	*3.5*		*Further sample*
110	*Serum 3*		*4*	*4*	*3*	*3.5*	*3.5*		*Further sample*
24	Serum		4	4	3	4	4	Definite	
25	Serum 1		4	2.5	2	3	3	Definite	
68	*Serum 2*		*1.5*	*0.5*	*0*	*0*	*Insufficient*		*Further sample*
50	Serum		3.5	3	1	0	1	Definite	
9	Serum 1		2.5	2.5	2	2.5	0	Definite	
61	*Serum 2*		*1.5*	*1.5*	*1.5*	*2*	*0.5*		*Further sample*
2552	Serum	Paired	2.5	2.5	2.5	2	4	Definite	

2150	CSF	Paired	4	2.5	1	3	4		
53	Serum 1		2.5	1	0.5	0	2	Definite	
76	*Serum 2*		*1.5*	*1*	*1.5*	*0*	*2*		*Further sample*
11	Serum	Paired	2	2	0	2.5	0	Definite	
11A	CSF	Paired	1	0	0	0	2		
56	Serum	Unpaired	1.5	2	1.5	1.5	1.5	Definite	
27	CSF	Unpaired	1.5	0	0	1.5	0		
108	Serum		1.5	1	1.5	0	1	Definite	
105	Serum		1.5	2	1	2	0	Definite	
36	Serum		1.5	2.5	2.5	3	0	Definite	
66	Serum		1.5	0.5	0	0	0	Definite	
78	Serum		1.5	2	1.5	3	0.5	Definite	
67	Serum		1.5	1.5	3	0	1	Definite	
69	Serum		1.5	0.5	0	1.5	1.5	Definite	
13	Serum	Paired	1.5	0.5	2.5	0	2	Definite	
13A	CSF	Paired	1.5	1	1.5	3.5	2		
71§	*Serum*		*1*	*0*	*0*	*0*	*0*	*Definite*	*post treatment*
93§	*Serum*		*0*	*0*	*0.5*	*0*	*0*	*Definite*	*other samples +*
104§	*Serum*		*0*	*0*	*1*	*0*	*0*	*Definite*	*Post-recovery*
40	Serum		2	1.5	0	0	0	Probable	
18	Serum		2.5	1.5	0	0	0.5	Possible	

51	Serum		2.5	2	0	1.5	0	Possible	
23[§]	*Serum*	*Unpaired*	*2.5*	*0.5*	*0*	*0*	*0*	*Possible*	*Post-recovery*
23A[§]	*CSF*	*Unpaired*	*0*	*0*		*0*		*Possible*	*Post-recovery*
44	Serum		2	1.5	0	0	0	Possible	
79	Serum		1.5	1	0.5	0	1	Possible	
65[†]	Serum 1	Paired	1.5	0	0	0	0	Possible	
65A	CSF	Paired	0	0	0	0	0		
89	*Serum 2*		*0*	*0*	*0*	*0*	*0*	*Possible*	*Further sample*
39	Serum		3.5	2.5	0	0	0	Unlikely	
42	Serum		3	2	0	0	0	Unlikely	
48	Serum		2.5	3	0	2.5	0.5	Unlikely	
37	Serum		2	2	0	0.5	0	Unlikely	
45	Serum		2	1	0	0	0	Unlikely	
8	Serum		1.5	1.5	0	0	0	Unlikely	
4	Serum	Paired	1.5	1.5	0	0	0	Unlikely	
4A	CSF	Paired	0	0	0	0	0		
77	Serum		1.5	0.5	0	0	0	Unlikely	
70	Serum		1.5	1.5	0	0	0	Unlikely	
98	Serum		1	2	0	0	0	Unlikely	
92	Serum		0	0	0	0	0	Unlikely	
99	Serum		0	0	0	0	0	Unlikely	

100	Serum	0	0	0	0	0	Unlikely
21	Serum	0	0	0	0	0	Unlikely

§ excluded from analysis as samples taken after clinical recovery/post-treatment and would therefore introduce bias by increasing false-negative rate.
† excluded as reactivity lost during storage (score 1.5 or above in original I-CBA and 0 in new I-CBA).

The CSF samples from patients with definite NMDAR-Ab encephalitis were all positive in the original l-CBA (1:2 dilution, Figure 3.15 A). Two of these samples scored 0 in the new l-CBA (1:10 dilution) and both scored 0 in two of three other assays (one in IHC and f-CBA, and the other in f-CBA and Euf-CBA), suggesting the higher dilution and prolonged storage were perhaps the cause of the loss of reactivity.

Contingency tables were then built for each diagnostic classification listing the outcome of each serum assay as positive or negative (Figure 3.14 A, B, C right panel). For the original l-CBA, the cut-off of 1.5 for positivity in serum was maintained, but for all other assays (including the new l-CBA) samples scoring 0.5 and above were considered positive in order not to bias the results as a consequence of loss of reactivity over time. The small number of CSF samples with diagnostic information rendered statistical analysis futile, and thus, similar contingency tables were not built.

Twenty-eight serum samples were available from 20 patients with definite NMDAR-Ab encephalitis (4 patients with 2 samples and 2 patients with 3 samples). Seven serum samples were available from 7 patients with possible (n=6) or probable (n=1) NMDAR-Ab encephalitis. Fourteen patients (14 samples) had been classified as unlikely to have NMDAR-Ab encephalitis.

For samples from patients with definite NMDAR-Ab encephalitis, f-CBA and Euf-CBA were more likely to be negative than l-CBA (Fisher's exact test, p= 0.004 for both, Figure 3.14 A right panel), and there was no difference in rates of positivity and negativity between l-CBA and IHC (Fisher's exact test, p= 0.11).

In patients felt not to have NMDAR-Ab encephalitis, f-CBA, IHC and Euf-CBA were all more likely to be negative than l-CBA (Fisher's exact tests, p= 0.006, 0.0002, and 0.001 respectively, n=14, Figure 3.14 C right panel). For those patients with a possible or probable diagnosis of NMDAR-Abs encephalitis, l-CBA appeared more likely to be positive and the other assays more likely to be negative (Figure 3.14 B right panel, no statistical analysis due to low numbers).

Contingency tables were then built for each diagnostic assay to determine their sensitivity and specificity. For this, the patients classified as probable or

possible NMDAR-Ab encephalitis were excluded. The results are listed below in Table 3.6. It is worth noting that the population for which these data were available was biased: some of the positive serum samples included were known to be from patients who did not have NMDAR-Ab encephalitis. When compared to a more naturalistic control group or to the referral population, such patients were over-represented in the small sample of patients for whom clinical details were available.

Table 3.6 Sensitivity and specificity of the three diagnostic approaches studied.

	l-CBA		**f-CBA**		**IHC**		**Euf-CBA**	
	+	**-**	**+**	**-**	**+**	**-**	**+**	**-**
Definite NMDAR-Ab encephalitis	28	0	20	8	24	4	20	7
Unlikely NMDAR-Ab encephalitis	10	4	2	12	0	14	1	13
Sensitivity[1] (95% CI)	100% (87.7-100)		71.43% (51.33-86.78)		85.71% (67.33-95.97)		74.04% (53.72-88.89)	
Specificity[2] (95% CI)	28.57% (8.39-58.1)		85.71% (57.19-98.22)		100% (76.84-100)		92.86% (66.13-99.82)	
PPV[3] (95% CI)	73.68% (56.9-86.6)		90.91% (70.84-98.88)		100% (85.75-100)		95.24% (76.18-99.88)	
NPV[4] (95% CI)	100% (39.76-100)		60% (36.05-80.88)		77.78% (52.36-93.59)		65% (40.78-84.61)	

[1] Probability that a test result will be positive when the disease is present (true positive rate)
[2] Probability that a test result will be negative when the disease is not present (true negative rate)
[3] Positive predictive value: probability that the disease is present when the test is positive
[4] Negative predictive value: probability that the disease is not present when the test is negative

Serum l-CBA was the most sensitive test but had poor specificity, with a high rate of “unlikely” diagnoses scoring positively. The calculated specificity value for l-CBA is, however, an underestimate. As mentioned above, patients known to have non-immune pathology but positive (usually low-positive) NMDAR-Abs by l-CBA were over-represented in the sample of patients for whom clinical details were available, and in this study population as a whole. The specificity of l-CBA would be better if an unselected referral population had been used. IHC, by comparison, was the next most sensitive test in serum and was also 100%

specific, meaning that, in the patients tested, IHC was negative in all patients who were unlikely to have NMDAR-Ab encephalitis. F-CBA and Euf-CBA both had moderate sensitivity, but good specificity.

Sensitivity and specificity for CSF were not calculated, as the number of samples with available clinical data was too small.

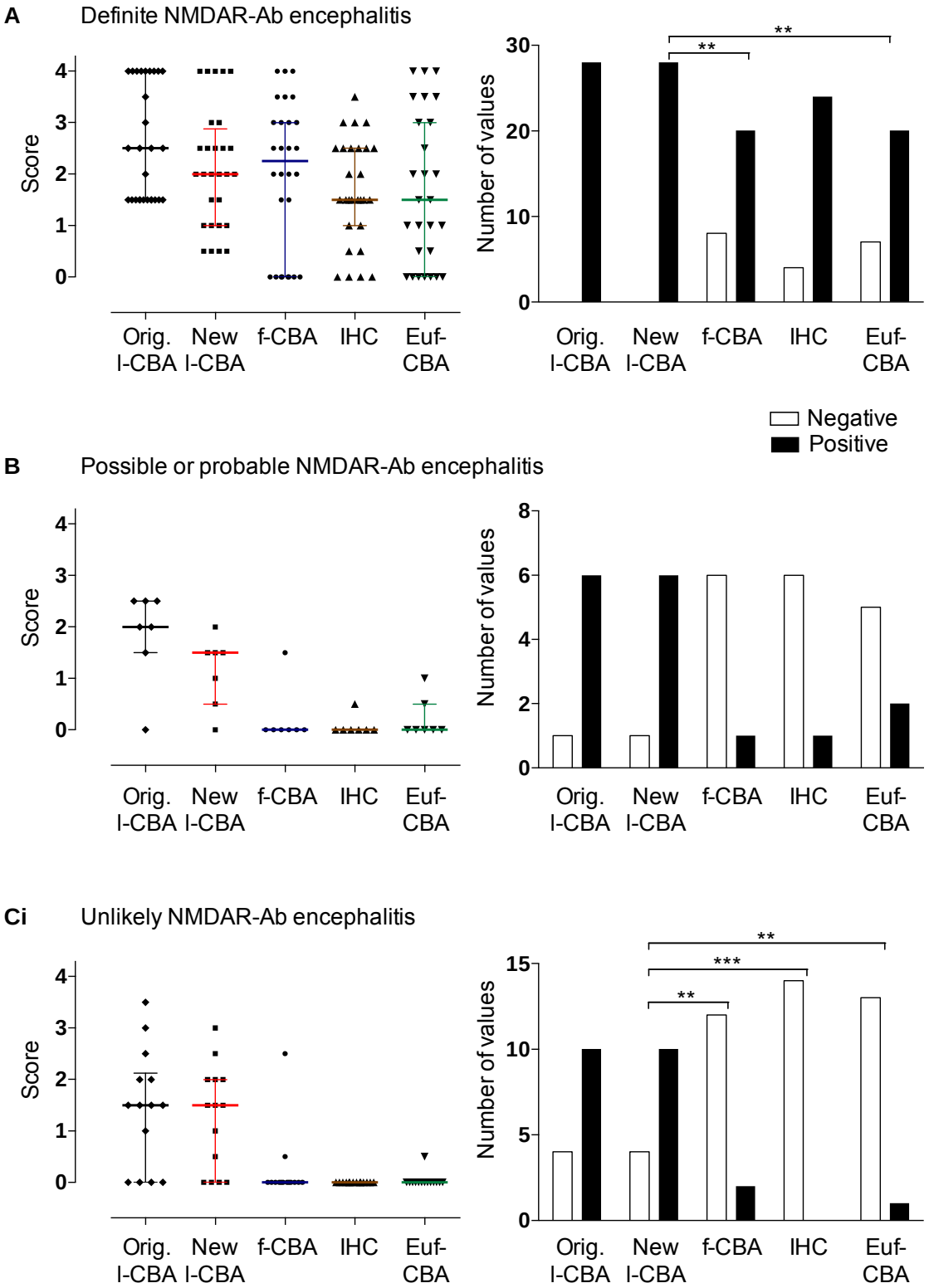

Figure 3.14 Score range in the four assays for serum samples in each diagnostic category.
The serum samples from patients with clinically definite NMDAR-Ab encephalitis (n=28, A) all scored positively in l-CBA (black and red) although the scores in the current l-CBA, done at a higher dilution were slightly lower (median ± IQR, red). In the other three assays median scores were comparable but some samples scored negatively. The serum samples from patients with possible (n=6) and probable (n=1) NMDAR-Ab encephalitis (B) scored mostly positively on l-CBA and mostly negatively on the other assays. This was also the case for serum samples from patients unlikely to have NMDAR-Ab encephalitis (n=14, C).

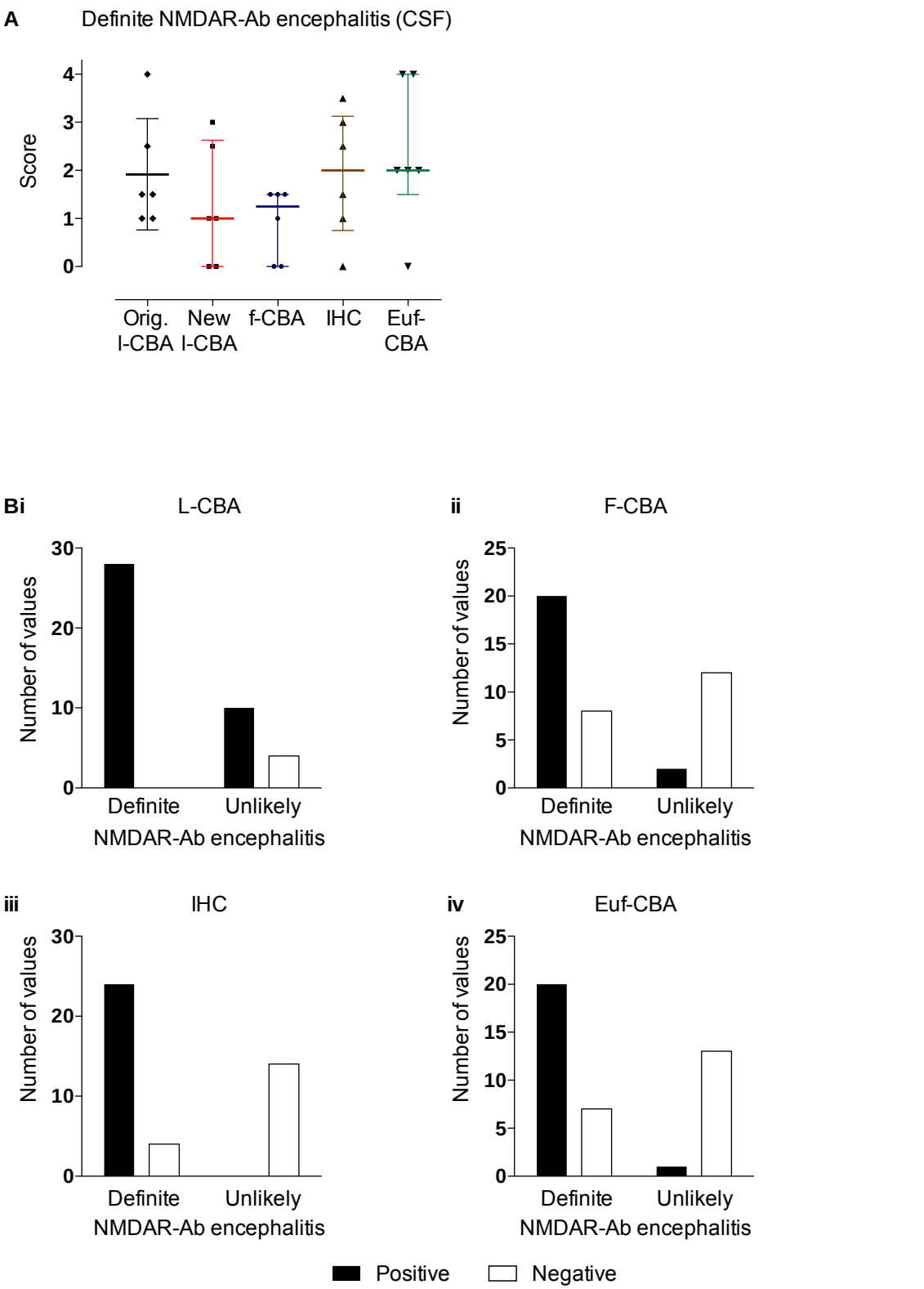

Figure 3.15 Score range in the four assays for CSF samples from patients with definite NMDAR-Ab encephalitis and graphic representation of contingency tables for each assay in serum samples.
The range of scores obtained for CSF samples of patients with definite NMDAR-Ab encephalitis in each assay is shown in A (n=6). All scored positive in the original l-CBA but some samples appeared to have lost reactivity or were negative at the higher dilution used in the current assays. In B, the rates of positivity (≥0.5) and negativity (0) for each assay are compared for serum samples from patients with clinically definite and unlikely NMDAR-Ab encephalitis. These numbers have been used in the sensitivity and specificity calculations in Table 3.6.

3.4 Conclusion

For some time it has been clear that the l-CBA that Oxford has been running since 2008 is sensitive but may identify low positivity in patients who are unlikely to have an antibody-mediated disease (Mackay *et al.*, 2012; M. S. Zandi *et al.*, 2015). By contrast, the Barcelona CBA and the Euroimmun CBA use fixed cells, raising concerns about sensitivity and possibly specificity, since the fixative might mask extracellular epitopes and intracellular epitopes might be detected because of permeabilisation. This was the first time that a full comparison between the three CBAs and with the IHC also used by Barcelona has been made. The results confirm the high sensitivity of the Oxford l-CBA with its relative lack of specificity, and some improvement in the specificity could be attempted by using a two-step assay in positive patients as discussed below.

L-CBA scores in the repeat assay, performed contemporaneously with the other assays, were higher than those obtained in f-CBA, IHC, and Euf-CBA (median of 1.5 for l-CBA and around 0.5 for the other assays). The large proportion of l-CBA-positive samples scoring 0 in f-CBA, IHC and Euf-CBA influenced the median scores in these assays. This difference would suggest either a higher sensitivity or a lower specificity of the l-CBA compared to the other tests, both of which were found to be true when the clinical data were analysed. The fact that most of the samples scoring 0 in f-CBA and IHC scored 0.5-1.5 in l-CBA would also support this conclusion. Looking at the diagnostic classification in the samples scoring positively in l-CBA but negatively in IHC (the second-most sensitive method in this study) suggests these low positive results are more likely to be false-positives: there were 16 patients with clinical details (23 in total) whose samples scored positive in l-CBA and negative in IHC, and 8 of these were classified as unlikely to have NMDAR-Ab encephalitis, 5 as possible and only 3 as definite NMDAR-Ab encephalitis (of these, 2 samples were positive by f-CBA ± Euf-CBA). Nevertheless, it also suggests that serum IHC is not positive in all NMDAR-Ab encephalitis patients, as found by Gresa-Arribas *et al.* (2014).

In Euf-CBA, the negative scores came equally from low-positive and high-positive samples, suggesting that this assay may not be very sensitive, and this was confirmed by the analysis of clinical data as well as the findings of the small

dilution study, which showed low end-titres in Euf-CBA. The pattern of binding in Euf-CBA was also different to that seen in the l-CBA and f-CBA. In Euf-CBA, the binding was punctate and intra-cytoplasmic. This difference is presumably related to the fixation protocol used by Euroimmun. Euroimmun uses covalent bonding (aldehyde fixation) to increase adhesion of cells to the glass surface of the biochips. The intensity of the fixation process is not described, but is likely to be high to avoid loss of substrate from the biochips. Formaldehyde fixation breaks down the normally impermeable cell membrane and denatures proteins by forming cross-linking methylene bridges; however, the structure of intracytoplasmic proteins tends to be well-preserved and the proteinaceous network formed in the cytoplasm has relatively low permeability to macromolecules. Overall, this increased permeability also contributes to increased non-specific “background” staining, and fixation is a compromise between preservation and introduction of artefact by denaturing proteins. The duration of formaldehyde fixation is paramount to the quality of the cytological preservation and immunolocalisation, and the longer the contact with the fixative, the more antigen masking is likely to occur (Farmilo and Stead, 2001). It is therefore possible that a portion of the surface epitopes in the Euroimmun biochips are masked and that the cell membranes are relatively permeable, such that the NMDAR-Abs can access NR1 subunits that have not yet been expressed on the cell membrane. This surface epitope loss may be responsible for the lower sensitivity of Euf-CBA.

It is not clear why binding in f-CBA was not intra-cytoplasmic like that seen in Euf-CBA, as cells have been fixed and permeabilised. Perhaps the fixation method used (10 minutes of 4% PFA followed by gentle permeabilisation for one hour) does not cause the same degree of surface epitope cross-linking, and therefore masking and loss, as the Euf-CBA fixation method, leaving enough cell-membrane-expressed NR1 subunits to result in the cell-surface binding pattern observed.

The aim of the study was to compare the l-CBA to the currently used f-CBA as well as other methods. Unfortunately, it was not possible to use the same protocol for f-CBA as that used in Barcelona, putting into question the validity of the comparison performed here. Indeed, results may have been different if samples had been sent to Barcelona for testing instead of developing an in-

house f-CBA. However, we had no experience of using fixed cells in CBAs and no access to the Barcelona protocol other than what could be gleaned from publications. A step-wise approach to replicating the Barcelona protocol was therefore taken. Once a very similar working protocol had been established, it became apparent that the results of serum assays were difficult to interpret because of non-specific background staining. Further steps and variations from the protocol therefore had to be put in place in order to obtain usable results. However, the basic principles of the Barcelona f-CBA (1:1 NR1:NR2 transfection, fixation and permeabilisation of cells, co-localisation with a commercial anti-NR1 antibody) were respected, and it is reassuring that our results in serum from patients with NMDAR-Ab encephalitis are not dissimilar to those of Gresa-Arribas *et al.* (2014) (71.43% sensitivity in our f-CBA and 86.8% in Barcelona f-CBA), bolstering the validity of our comparison.

The analysis performed once the clinical data was available revealed that, in patients with clinically definite NMDAR-Ab encephalitis, l-CBA and f-CBA resulted in similar scores, and lower scores were found with IHC, as expected since it was performed at a higher dilution. Euf-CBA scores were the lowest, despite being performed at the lowest dilution, and this is in keeping with the possible epitope loss and resultant lower sensitivity as discussed above.

Despite the lower scores in IHC, this method still proved to be sensitive (85.71%). Additional support for its good sensitivity comes from the fact that the highest end-titres were found with IHC in both serum and CSF samples in the small titration study performed here. Furthermore, 2 of the 5 serum samples that were positive in IHC but negative in l-CBA were from patients with definite NMDAR-Ab encephalitis (no diagnosis available for the other 3). These samples had been excluded from the sensitivity and specificity analysis as they were taken after full recovery of the patient.

The poor specificity of the l-CBA, albeit partly overestimated by the over-representation of patients with known non-immune pathology and positive NMDAR-Abs by l-CBA in this study, is concerning and implies that serum testing alone using l-CBA in patients with suspected NDMAR-Ab encephalitis is not necessarily helpful. The results of this study would preliminarily support testing CSF as well, as maintained by Gresa-Arribas *et al.* (2014): all available

CSF samples of patients with definite NMDAR-Ab encephalitis were positive in the original l-CBA. However, the number of CSF results available was small and not all were from the patients at first presentation of their disease when the test is most commonly requested. Thus, further comparisons of serum and CSF at presentation of “definite” disease will be required to answer this issue.

The poor specificity of the l-CBA is unexplained at present. One possibility is that non-specific or low-affinity antibodies (IgG and IgM) bind more readily to the membrane of live cells. Another possibility is that the fluorescent secondary antibody, which is directed against human IgG heavy and light chains and therefore reacts with other immunoglobulin classes as these share common light chains, is also binding to IgM antibodies present in the serum. The use of a secondary antibody with improved specificity for IgG, for example those directed at the Fcγ portion of IgG, would mitigate this effect, and this has now been adopted in the Oxford laboratory. However, this would be expected to cause non-specific binding to be present in all the cell-based assays studied here. Another possibility is that low levels of serum NMDAR-Abs do occur in some individuals with other diagnoses, as in the sCJD study (Mackay *et al.*, 2012). Finally, a further control step for positive samples in the l-CBA may improve specificity: demonstration of colocalisation of anti-human IgG binding with binding to a commercial anti-NR1 antibody, as used in the f-CBA, would allow greater certainty in the reporting of positive results.

In conclusion, a two-step protocol for the detection of NMDAR-Abs in serum may be proposed based on the results of this study. L-CBA was the most sensitive test and was also the least time-consuming assay (except for Euf-CBA but this has very poor sensitivity), and should therefore be part of the diagnostic assay, especially if improved specificity can be demonstrated by adding a step to demonstrate co-localisation with commercial anti-NR1. It should nevertheless be supplemented with IHC, which was also very sensitive and 100% specific. Whether CSF testing is necessary to make a diagnosis was not clear in this study, because of the low number of CSF samples, and this requires further study.

The findings of this study require confirmation in a prospective study using a representational control group or a naturalistic referral population. Additionally,

the prolonged storage of some of the samples used here and consequent reduction in reactivity probably caused some of the variability of the results in the different assays. This may underlie the lower sensitivity values found here for serum f-CBA and IHC in comparison to the Gresa-Arribas *et al.* (2014) study (f-CBA: 71.43% versus 86.8%; IHC: 85.71% versus 91.6%). However, this study clearly does not support the proposition that the commercially available assay from Euroimmun is as sensitive and specific as the combination of f-CBA and IHC (Wandinger *et al.*, 2011). Insufficient CSF samples were available for a valid discussion of the requirement for CSF testing, as suggested by Dalmau's group (Gresa-Arribas *et al.*, 2014).

Developing the protocols and learning to interpret the results of the f-CBA, IHC and Euf-CBA was more complex than anticipated. Whilst the relatively consistent co-localisation with anti-NR1 immunofluorescence in f-CBA was an advantage when interpreting the results, a high level of non-specific background persisted despite optimisation at several steps of the protocol. This high background has been acknowledged by other groups that perform in-house f-CBA (J. Honnorat, personal communication), and it is noteworthy that publications by Dalmau's group show the results of f-CBAs performed with CSF, where background staining is absent.

Similarly, IHC results can also be difficult to score for serum samples with low NMDAR-Ab titres, especially if non-specific background is present. Serial dilutions are often helpful in these situations. Finally, Euf-CBA can also be challenging to interpret (see discussion of de Witte *et al.* (2015) above). Differentiating very low positives from background staining with serum was sometimes difficult and necessitated addition of a commercial NR1 antibody for co-localisation. It was essential to pay close attention to the pattern of staining, which had to be punctate, rather than simply relying on the intensity of the staining.

All of these challenges are avoided by use of CSF, which produced essentially background-free results. The other advantage of finding NMDAR-Abs in the CSF of a patient with presumed NMDAR-Ab encephalitis is that this establishes beyond doubt their access to the brain and thus bolsters their claim to pathogenicity. However, the ease with which serum can be obtained is a

definite advantage when designing a diagnostic test. Furthermore, the immune response and antibody production is likely to be initiated peripherally in the great majority of patients with NMDAR-Ab encephalitis (Irani *et al.*, 2010b; Kreye *et al.*, 2016) (with the exception of patients who develop NMDAR-Ab encephalitis after HSV encephalitis), so that antibodies should always be present in blood and at a higher titre than in CSF. Along those lines, the Oxford laboratory experience so far, was that serum assays are sufficient for NMDAR-Ab detection in patients with the suspected disorder (Vincent and Bien, 2008; Irani *et al.*, 2010b). It is also worth noting that intrathecal antibody responses following neurotropic infections such as HSVE and neurosyphilis, tend to persist much longer than systemic responses, often outlasting the infective episode by years (Reiber, 1998). If this is the case for autoimmune disorders as well, then the presence of CSF antibodies against NR1 may not necessarily represent active NMDAR-Ab encephalitis. Insufficient paired serum and CSF samples were available for this study to examine whether serum testing alone is sufficient, but it is interesting that all the CSF samples from patients with definite NMDAR-Ab encephalitis in this study scored positively on the original I-CBA.

High scores on serum assays (scores 3-4) were invariably associated with a clinical classification as “definite” NMDAR-Ab encephalitis. The patient samples used in the electrophysiological studies in the following chapters were all obtained from patients with scores of 4 on initial I-CBA and the samples diluted to demonstrate their titres. The presence of NMDAR-Abs was also confirmed using IHC.

Chapter 4 The effect of acute exposure to NMDA receptor antibodies on field gamma-frequency oscillations *in vitro*

4.1 Introduction

The onset of NMDAR-Ab encephalitis is characterised by the subacute development of confusion, anterograde memory loss, which can become dense, seizures and psychiatric symptoms. The latter range from anxiety and depression-like symptoms to florid psychosis with hallucinations. Such symptoms can be recapitulated in healthy subjects by acute administration of NMDAR antagonists such as ketamine (Krystal *et al.*, 1994; Lahti *et al.*, 2001). Furthermore, in volunteers with schizophrenia, ketamine caused a brief increase in positive symptoms including delusions similar to those they had experienced in a previous psychotic phase, formed visual or auditory hallucinations and thought disorder (Lahti *et al.*, 1995; Lahti *et al.*, 2001). This early evidence in support of the NMDAR hypofunction model of schizophrenia led to the development of several animal models of NMDAR hypofunction, each exhibiting some cellular, anatomical or behavioural correlate of schizophrenia in humans (e.g. (Mohn *et al.*, 1999; Keilhoff *et al.*, 2004; Rujescu *et al.*, 2006; Belforte *et al.*, 2010; Gandal *et al.*, 2012), and for review(Inta *et al.*, 2010)).

One commonly reported effect of NMDAR antagonism or partial NMDAR ablation was a selective reduction in parvalbumin-positive interneurons in several areas including pre-frontal cortex and hippocampus (Keilhoff *et al.*, 2004; Rujescu *et al.*, 2006; Gandal *et al.*, 2012), and resultant deficits in inhibitory synaptic transmission (Rujescu *et al.*, 2006; Gandal *et al.*, 2012).

Gamma-frequency oscillations (γ-oscillations) are associated with sensory processing and memory as discussed in chapter 1. They result from the synchronised interplay of excitatory principal cell and inhibitory interneuron firing. They can be pharmacologically generated in live brain slices, in which case they are stable for several hours (Cunningham *et al.*, 2003b). Parvalbumin-positive fast-spiking interneurons provide the most powerful inhibitory input to principal cells by targeting their perisomatic region and have been shown to be the principal interneuron subtype involved in the generation of γ-oscillations (Pouille and Scanziani, 2001; Hájos *et al.*, 2004; Fuchs *et al.*, 2007; Strüber *et al.*, 2015).

In the hippocampus, both cholinergically and kainate-induced γ-oscillations are dependent on excitatory activity mediated by ionotropic non-NMDA glutamate

receptors, but there is no NMDAR component to the excitatory drive, as shown by the lack of effect of NMDAR antagonists D-AP5 and ketamine on the power or frequency of these oscillations (A Fisahn *et al.*, 1998; Cunningham *et al.*, 2006). This may be related to the remarkably low synaptic NMDA receptor content of parvalbumin-positive interneuron in the hippocampus (NyÍri *et al.*, 2003).

In the superficial layers of the medial entorhinal cortex, however, NMDAR-mediated excitation is an important component of the drive to the fast-spiking interneurons that are generating the γ-rhythms (Jones and Buhl, 1993; Cunningham *et al.*, 2006). Acute application of the NMDAR antagonist ketamine has been shown to reduce both the power and frequency of layer II and III γ-oscillations in the mEC (Cunningham *et al.*, 2006; Middleton *et al.*, 2008).

There is some evidence to suggest NMDAR-Abs may have an acute antagonistic effect on NMDAR-mediated neurotransmission: brief exposure (in the range of minutes) to NMDAR-Ab-containing CSF prevented NMDA-mediated Ca^{2+} entry into cultured cerebellar neurons (Rubio-Agustí *et al.*, 2011) and blocked the induction of hippocampal LTP in mouse slices (Q. Zhang *et al.*, 2012). The effect of acute exposure to NMDAR antibodies on superficial mEC and hippocampus field γ-oscillations *in vitro* will therefore be investigated in this chapter, to test the hypothesis that, in this slice preparation, NMDAR-Abs may selectively impair oscillations in the mEC.

4.2 Methods

Horizontal hippocampal-entorhinal rat brain slices were prepared and maintained as described in the general methods. The extracellular local field potential was recorded using blunt glass electrodes filled with artificial CSF. γ-oscillations were generated by adding 400nM kainate (KA) to the perfusion medium. The peak power, area power and frequency of the observed oscillation were obtained by applying a fast Fourier transform to a 60 second epoch of recording every 10-15 minutes. Oscillations were considered stable once the values obtained for each of these characteristics varied by less that 20% over four consecutive 10-minute periods. Pharmacological experiments were performed by bath application of ketamine or D-AP5 for 40 minutes to1 hour, followed by a 30-minute washout phase in aCSF and KA (vehicle). Purified

immunoglobulin G (IgG) from three patients with NMDAR Ab encephalitis and high titre NMDAR antibodies, two healthy controls, and one patient with voltage-gated potassium channel complex antibodies (VGKC-complex abs) was used to investigate the effect of NMDAR antibodies on superficial mEC γ-oscillations. These were initially diluted to 10μg/ml in vehicle (aCSF+400nM KA) and bath applied to the slices. Because only small volumes of purified IgG were available, it was diluted in no more than 25ml of vehicle. To control for this significant reduction in the volume of the circulating perfusion medium, control experiments using vehicle only were also performed with this lower volume of perfusion medium. The concentration of 10μg/ml was chosen based on findings from a preliminary study by a previous MRes student (Lawley, 2009). A significant effect on both power and frequency of γ-oscillations in mEC had been demonstrated at 5, 10 and 20μg/ml concentrations of IgG from a patient with NMDAR-Ab encephalitis. Later, some experiments with patient IgG were also performed at a concentration of 30μg/ml as discussion with members of the neuroimmunology groups at Oxford University revealed they were using purified IgG diluted 1:250 to 1:500 in their staining experiments (corresponding to 48 and 24μg/ml concentration). Because of time constraints it was not possible to test all IgG samples at both concentrations.

4.3 Results

4.3.1 Pharmacological blockade of NMDA receptors disrupts γ-oscillations in mEC

Ketamine

The effect of bath application of 25μM ketamine was examined in 6 slices from 4 rats. Kainate perfusion (400nM) generated oscillations in mEC layer II or III with a peak power of 48.44 ± 49.29 μV^2/Hz, area power of 0.424 ± 0.535 μV^2/Hz.kHz, and frequency of 43.25 ± 6.45 Hz. Because of the wide variation in baseline power from one slice to the next, the values for power and frequency in each experiment have been normalised to the average of the values recorded during the 40-minute stable period (all values within 20% of each other) prior to addition of ketamine, such that the baseline period always has a power and frequency of 100% in each slice. Ketamine caused a partially

reversible reduction in power and frequency, but only the change in peak power reached statistical significance (see Table 4.1 and Figure 4.1).

Table 4.1 Effect of ketamine on mEC γ-oscillations

	Reduction at 1 hour (%)	RM ANOVA	P value
Peak power	61.07 ± 16.36	F (1.890, 5.671) = 6.293	0.0372
Area power	35.58 ±25.18	F (2.237, 6.712) = 2.980	0.1160
Frequency	8.89 ±4.78	F (2.587, 7.760) = 3.974	0.0581

D-AP5

The effect of bath application of 50μM D-AP5 was examined in 9 slices from 5 rats. The effect of ketamine had been investigated because this was the drug used by most animal and human studies described above, but ketamine also has non-NMDAR-mediated effects. D-AP5, a selective NMDAR antagonist was used to confirm the effects were NMDAR-mediated. Kainate perfusion generated oscillations in mEC layer II or III with a peak power of 137.7 ± 197.9 μV^2/Hz, area power of 1.085 ± 1.435 μV^2/Hz.kHz, and frequency of 45.48 ± 6.8 Hz. As above, the values for power and frequency in each experiment were normalised, with the average of the values at for power and frequency during the stable baseline period being defined as 100%. D-AP5 caused a partially reversible reduction in peak power and frequency (see Table 4.2 and Figure 4.1). These decreases occurred in the first 20 minutes of D-AP5 perfusion and the oscillations then remained stable at the new lower level.

Table 4.2 Effect of D-AP5 on mEC γ-oscillations

	Reduction at 1 hour (%)	RM ANOVA	P value
Peak power	52.7 ± 32.44	F (2.611, 20.89)= 7.529	0.0019
Area power	35.04 ±39.78	F (2.636, 21.09) = 2.711	0.0769
Frequency	10.76 ± 9.74	F (2.730, 21.84)= 3.196	0.047

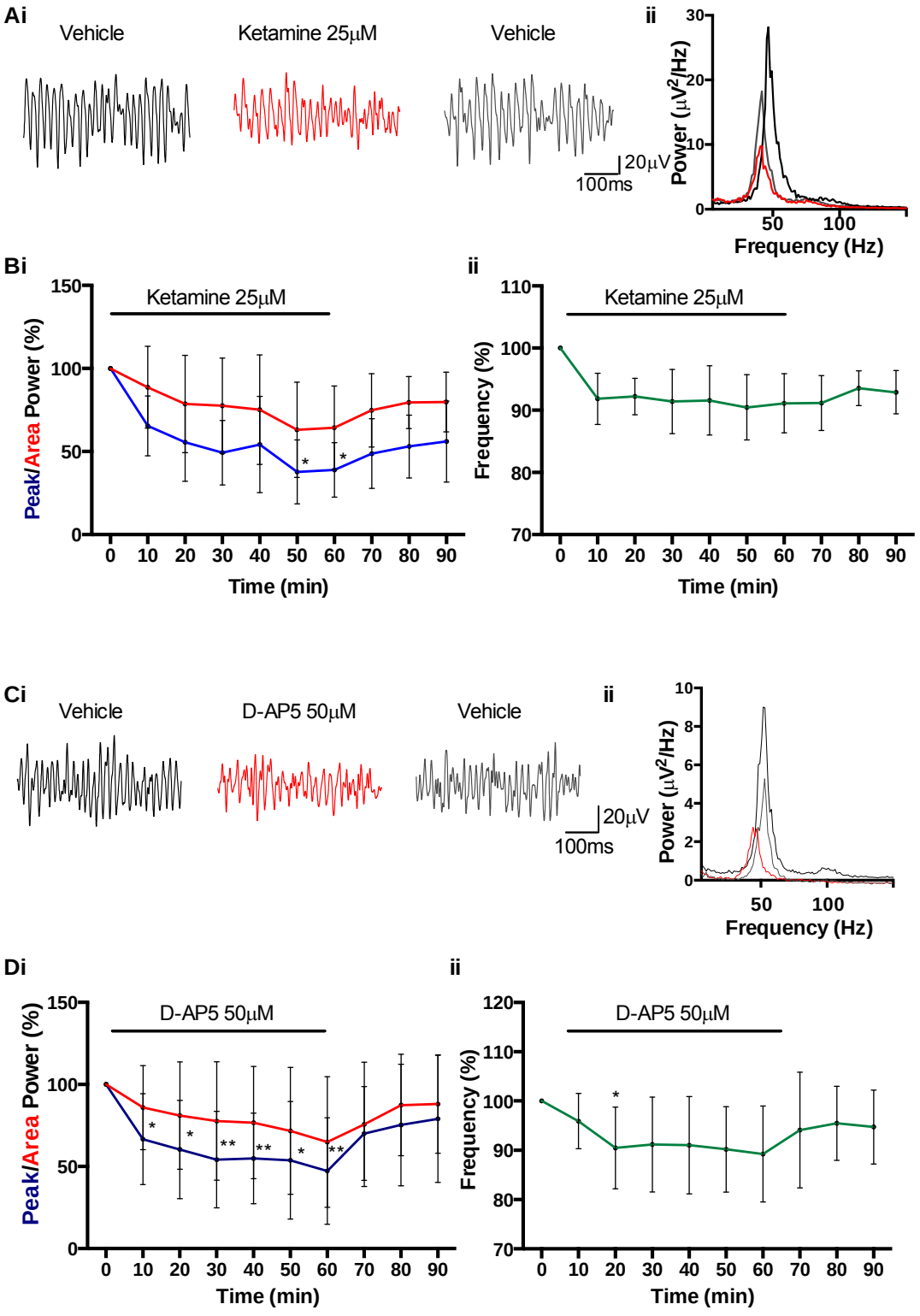

Figure 4.1 The effects of ketamine and D-AP5 on mEC layer II/III γ-oscillation.

Ai and Ci show examples of LII/III mEC extracellular field recording from a single slice during the initial stable period, at the end of the ketamine or D-AP5 perfusion (red) and at the end of a 30-minute washout period (grey). The corresponding power spectra are shown in Aii and Cii, illustrating the marked reduction in power and small reduction in frequency. Bi and ii and Di and ii show the gradual reduction in peak and area power (i) and frequency (ii) over the course of the experiments (mean ± S.D.). Note the apparent partial recovery of power and frequency during the washout period. * $p<0.05$, ** $p<0.01$.

4.3.2 Naïve control

To test the stability of γ-frequency oscillations over time, γ-frequency oscillations deemed stable over the required 40-minute period were followed for the duration of a typical pharmacological experiment, i.e. 90 minutes (60 minutes drug application and 30 minutes drug washout). For these experiments (n=8, 7 animals) the perfusion medium was changed to a smaller container (25ml) of the same perfusion medium to mimic the conditions in other experiments (where drug or immunoglobulin are diluted in a 20-25ml volume of the circulating aCSF).

Kainate perfusion generated oscillations in layer II or III of the mEC with a peak power of 76.54 ± 51.94 μV^2/Hz, area power of 0.58 ± 0.349 μV^2/Hz.kHz, and frequency of 46.08 ± 4.27 Hz. The values for power and frequency in each experiment have been normalised as described above. Oscillation power declined progressively from about 40 minutes into the experiments, reaching significantly lower peak power values after 90 minutes (see Table 4.3 and Figure 4.2 right panel). There were parallel but less marked reductions in area power, whilst frequency remained stable throughout the 90-minute experimental period.

Table 4.3 Change in mEC γ-oscillations over time in vehicle.

	Reduction at 1 hour (%)	Reduction at 90 minutes (%)	RM ANOVA	P value	Significant Dunnett's multiple comparison test	P value
Peak power	17.24 ±35.49	35.47 ±25.72	F(1.735, 12.15) = 5.505	0.0229	90min vs. baseline	0.011
Area power	5.14 ±40.61	17.83 ±32.94	F(1.177, 8.237) = 1.365	0.2844		
Frequency	-0.24 ±4.65	-2.24 ±5.8	F(1.217, 8.518) = 1.191	0.3191		

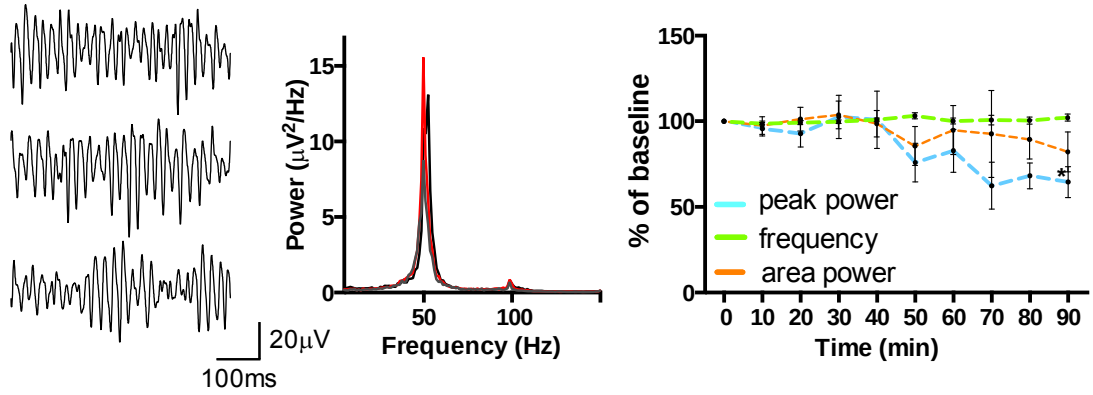

Figure 4.2 Power and frequency of γ-oscillations over time in vehicle in superficial layers of mEC.

The left panel shows examples of extracellular field recordings from LII mEC from a single experiment. The top excerpt is from the baseline period of stability, the middle excerpt from a recording 60 minutes later and the bottom excerpt from a recording 90 minutes after baseline. The corresponding power spectra are shown in the middle panel. The black line corresponds to the baseline oscillation, the red line to 60 minutes and the grey line to 90 minutes after baseline. Note the slight increase in power at 60 minutes, followed by a decrease in power at 90 minutes. The right panel shows the mean ±S.D. for the 8 experiments for peak power (blue), area power (orange), and frequency (green). Peak power decreases gradually after about 40 minutes of the experiments and the reduction is significant after 90 minutes. Area power follows a similar but less pronounced course and frequency remain stable throughout the experiments.

4.3.3 Negative controls – Healthy control IgG

Two healthy control purified IgG samples have been used in this thesis. HC1 IgG was obtained from pooled serum samples from healthy individuals and HC2 IgG was purified from the serum of a single healthy individual with no neurological symptoms. No binding to the surface of HEK293 cells expressing NR1 and NR2B was detected by cell-based assay at either the concentration used in the electrophysiological experiments (10μg/ml) or at a ten times higher concentration (see

Figure 4.3).

Medial entorhinal cortex

Slices exhibiting stable gamma-frequency oscillations were exposed to purified HC1 or HC2 IgG at 10μg/ml for one hour followed by a 30-minute wash.

Kainate perfusion (400nM) generated oscillations in layer II or III with average peak power of 55.61 ± 28.26 μV^2/Hz, area power of 0.57 ± 0.19 μV^2/Hz.kHz, and frequency of 48.08 ± 2.10 Hz in the slices subsequently exposed to HC1 IgG (n=6 slices from 3 animals). In the slices exposed to HC2 (n=7 slices from 6 animals), baseline peak power was 73.30 ±29.47 μV^2/Hz, area power was 0.77 ±0.28 μV^2/Hz.kHz, and frequency was 46.54 ±1.55 Hz. Because of the wide variation in baseline power, the values for power and frequency in each experiment have been normalised as described above.

Over time, there were reductions in peak power and area power very similar to those seen in vehicle. Table 4.4 lists the normalised values obtained from the healthy control experiments.

Table 4.4 Peak power, frequency and area power in slices exposed to HC1 and HC2 IgG at a concentration of 10µg/ml in mEC.

	HC1 10µg/ml (n=6)			HC2 10µg/ml (n=7)		
	Base-line	**60min IgG**	**30 min washout**	**Base-line**	**60min IgG**	**30 min washout**
Peak power (% of baseline)	100 *(55.61 ±28.26 μV^2/Hz)*	82.72 *±14.5*	77.79 *±12.26*	100 *(73.30 ±29.47 μV^2/Hz)*	76.42 *±10.73*	55.89** *±11.75*
Frequen-cy (% of baseline)	100 *(48.08 ±2.10 Hz)*	95.07 *±2.17*	95.21 *±2.15*	100 *(46.54 ±1.55 Hz)*	97.99 *±1.32*	100 *±1.93*
Area power (% of baseline	100 *(0.57 ±0.19 μV^2/Hz.k Hz)*	82.65 *±8.82*	76.67 *±10.68*	100 *(0.77 ±0.28 μV^2/Hz.k Hz)*	75.32** *±6.97*	58.32**** *±4.28*

There was a statistically significant reduction in peak power in slices exposed to HC2 at the end of the washout period (RM ANOVA, F(1.979, 11.87) = 7.674, p = 0.0074; Dunnett's multiple comparisons test 90 minutes vs. baseline p=0.0168, see Figure 4.4). Similarly, the reduction in area power was statistically significant for the HC2 group at both 60 minutes (end of HC2 IgG perfusion) and 90 minutes (end of washout, RM ANOVA, F(1.533, 9.199) = 21.80, p=0.0005; Dunnett's multiple comparisons test baseline vs. 60' p=0.022, baseline vs. 90' p=0.0001).

As for the experiments in aCSF and KA, frequency remained stable over the 90-minute period of observation.

As expected, there were no statistically significant differences between the changes in power and frequency of γ-oscillations in the two healthy control groups at either of the two endpoints (60 minutes of perfusion with IgG and 30 minutes after washout, see Table 4.5 and Figure 4.4 Bii, Cii, Dii) and these were therefore pooled to form a larger control IgG group (cIgG n=13, see Figure 4.5). No significant differences in power or frequency at 60 minutes and 90 minutes (30 minutes washout) were found between the vehicle and cIgG groups (see Table 4.6).

Table 4.5 HC1 and HC2 IgG have similar effects on mEC γ-oscillations

	Mean Difference at 60 minutes (± S.E.M)	Unpaired t-test	P value	Mean Difference at 90 minutes (95% CI)	Unpaired t-test	P value
Peak Power (%)	6.303 ±17.71	T (11) = 0.356	0.729	21.90 ±17.03	T (11) = 1.286	0.225
Area Power (%)	7.33 ±11.09	T (11) = 0.661	0.522	18.35 ± 10.86	T (11) = 1.69	0.119
Frequency (%)	-2.92 ± 2.45	T (11) = 1.190	0.259	-4.82 ± 2.88	T (11) = 1.672	0.123

Table 4.6 The pooled cIgG group of slices behaves similarly to slices exposed to vehicle only.

	Mean Difference at 60 minutes (± S.E.M)	Unpaired t-test	P value	Mean Difference at 90 minutes (95% CI)	Unpaired t-test	P value
Peak Power (%)	-3.438 ± 14.61	t=0.2353 df=19	0.816	1.472 ± 13.24	t=0.1112 df=19	0.913
Area Power (%)	-16.16 ± 15.34	t=1.053 df=9.014	0.319	-15.38 ± 11.70	t=1.315 df=19	0.204
Frequency (%)	-3.603 ± 2.043	t=1.763 df=19	0.094	-4.434 ± 2.536	t=1.748 df=19	0.096

Hippocampus

Bath application of 50nM kainic acid generated oscillations in the CA3 subfield of the hippocampus. These were of somewhat slower frequency than in the mEC (see Table 4.7) but in line with previous published observations. As the baseline power of these oscillations was much less variable than that of mEC oscillations, normalisation of the data was not carried out. Perfusion for one hour with either 10µg/ml HC1 IgG or HC2 IgG did not affect the peak power or area power of hippocampal gamma-frequency oscillations (see Table 4.7 and Figure 4.6). For both IgG samples there was a small reduction in oscillation frequency at peak power over the course of the 90-minute experiment. This is consistent with published observations on the natural history of pharmacologically evoked hippocampal gamma-oscillations (Pietersen *et al.*, 2009). For HC1, this reduction in frequency reached statistical significance at the end of the washout phase (baseline frequency 37.39 ±1.58 Hz vs. WO frequency 34.52 ±1.36Hz, RM ANOVA F(1.470, 8.823)= 13.94, p= 0.003; Dunnett's multiple comparison test baseline vs. 90 minutes p=0.009). However,

in view of the known downward trend in HPC kainate-induced gamma-frequency oscillation, it is unlikely that this reduction was due to the perfusion with IgG.

Table 4.7 Effect of control IgG samples HC1 and HC2 on parameters of hippocampal gamma-frequency oscillations.

	HC1 10μg/ml (n=7)			HC2 10μg/ml (n=6)		
	Base-line (mean ±SEM)	**60 minutes IgG**	**30 minutes washout**	**Base-line (mean ±SEM)**	**60 minutes IgG**	**30 minutes washout**
Peak Power ($\mu V^2/Hz$)	54.92 ±12.58	49.77 ±11.57	56.75 ±13.06	61.34 ±22.12	51.65 ±14.85	48.71 ±16.96
Frequen-cy (Hz)	37.39 ±1.58	36.60 ±1.21	34.52 ±1.36	42.10 ±1.5	40.21 ±2.24	39.20 ±1.96
Area Power ($\mu V^2/Hz.kHz$)	0.606 ±0.162	0.485 ±0.128	0.624 ±0.202	0.933 ±0.357	0.799 ±0.311	0.782 ±0.36

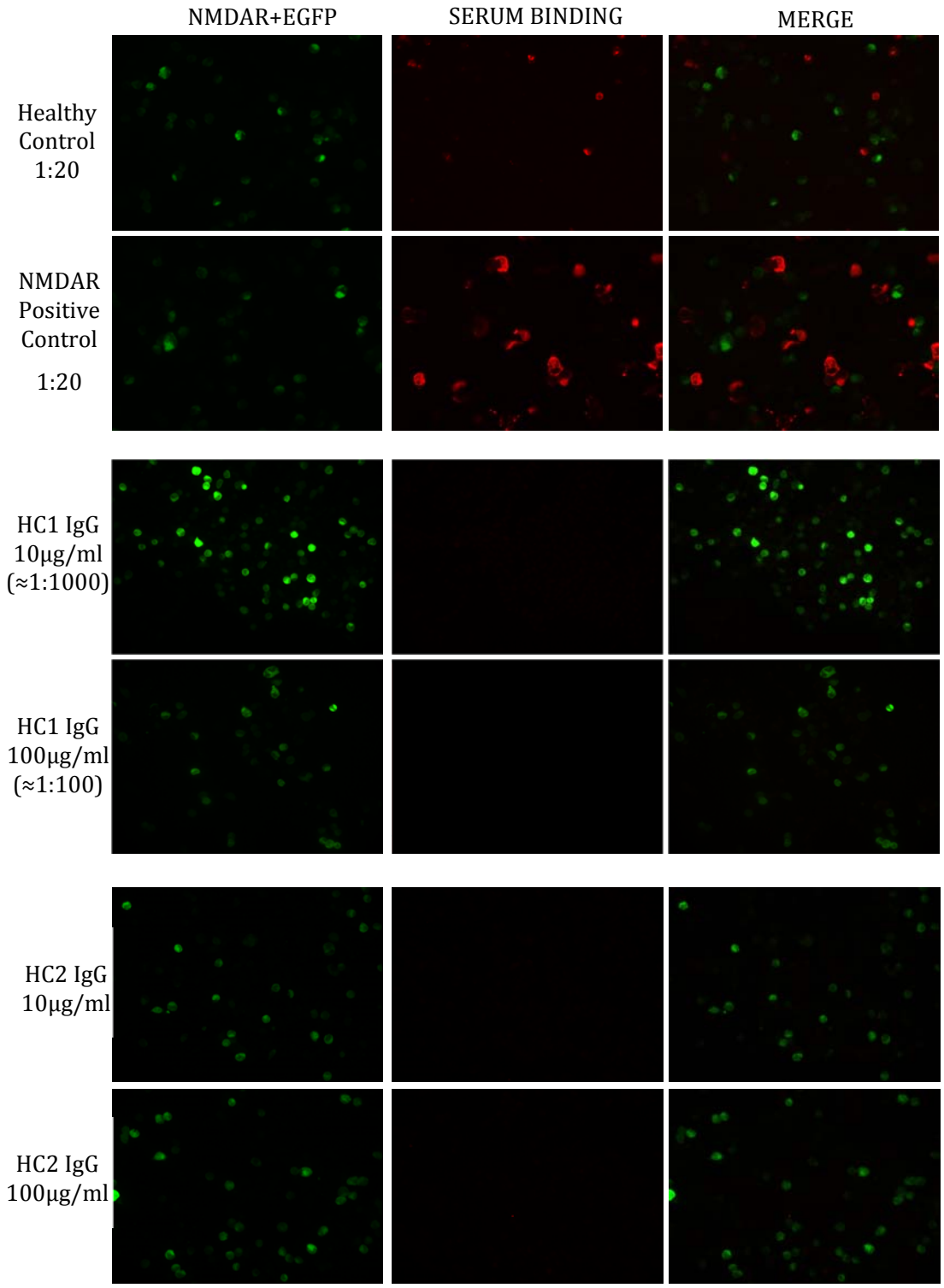

Figure 4.3 Cell-based assay results of HC1 and HC2 IgG
HC1 and HC2 IgG do not bind to NMDAR (NR1 and NR2B subunits coexpressed with EGFP) expressing HEK cells. NMDAR (+EGFP) transfected HEK cells (green) can be visualised in the first column. If serum autoantibodies to NMDAR are present, they bind to NMDAR (+EGFP) transfected cells (red, e.g. row 2) and co-localisation of serum autoantibody binding and NMDAR (+EGFP) expression can sometimes be seen (merge). No red fluorescence is detected on coverslips incubated with HC1 and 2 at 2 concentrations, indicating that no binding to surface NMDAR has occurred.

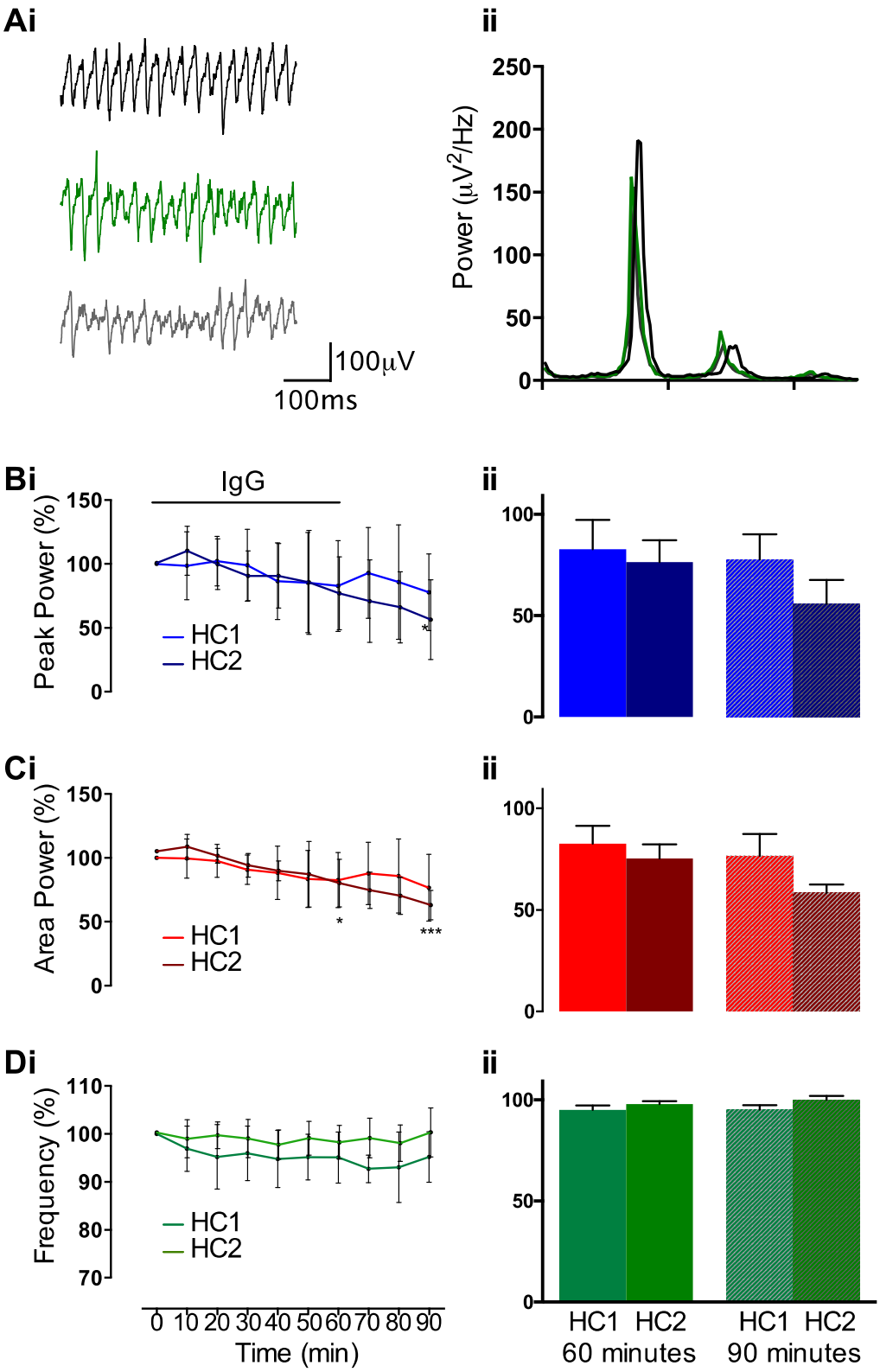

Figure 4.4 The effect of HC1 and 2 IgG on γ-oscillations in mEC.
Examples of field recordings from a single experiment in a slice exposed to HC1 are shown in Ai with the corresponding power spectra in ii, illustrating the small decline in peak power over the course of the experiment. Time course of power and frequency are shown in Bi, Ci, and Di (mean ± SD). Peak and area power decrease significantly in slices exposed to HC2 (Bi and Ci), and frequency remains stable for both IgG preparations (Ci). When power and frequency of the oscillations in the two groups of slices are compared at the relevant time points, no statistical differences are found (Bii, Cii, Dii, mean ± SEM).

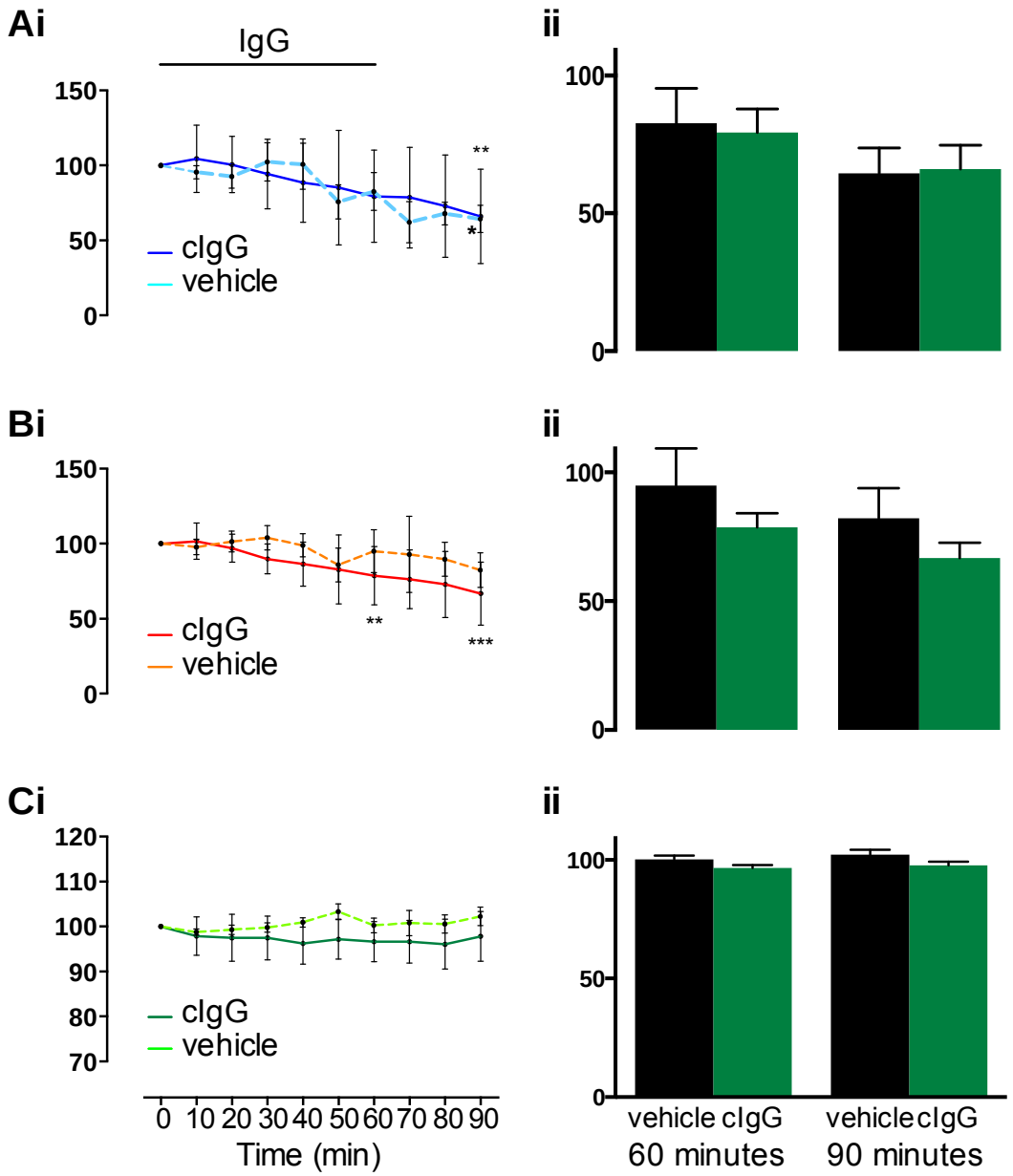

Figure 4.5 Comparison of mEC γ-oscillations in slices exposed to cIgG or vehicle.
There is a decline in peak power in slices exposed to either cIgG or vehicle (Ai, mean ± SD). Although area power also decreases in both groups, only the decrease in cIgG is significant (Bi, mean ± SD). Frequency remains stable in both groups of slices (Ci, mean ± SD). There are no significant differences when power and frequency in the two groups are directly compared at the end of the IgG perfusion period and at the end of washout (mean ± SEM).

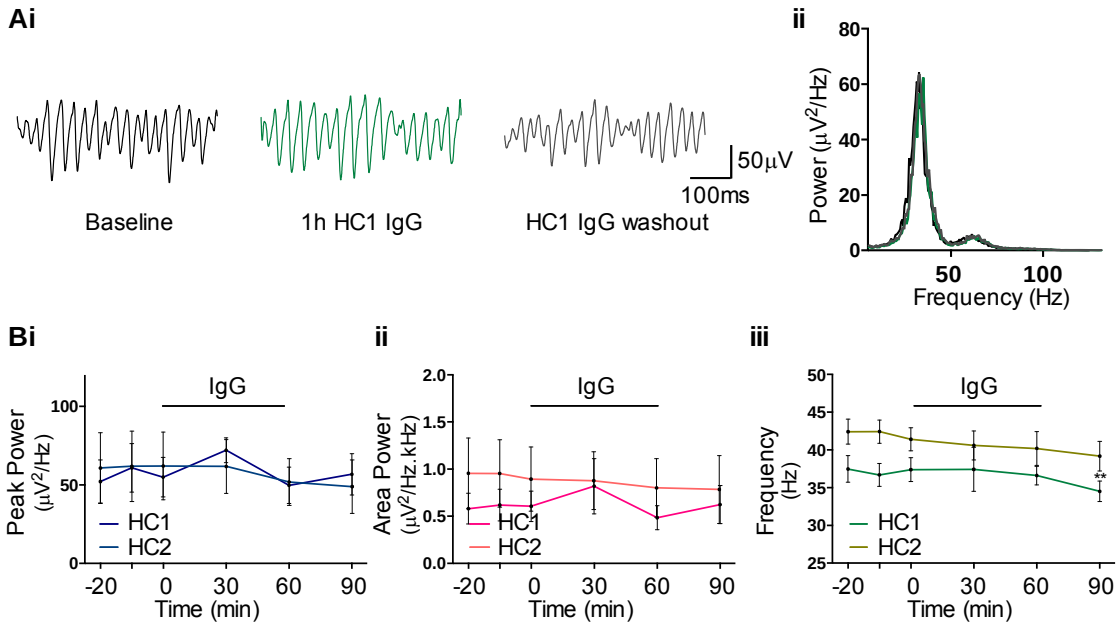

Figure 4.6 γ-oscillation power and frequency in CA3 of slices exposed to HC1 or HC2.

Ai shows examples of extracellular field recordings in CA3 from a single experiment with HC1, and the corresponding power spectra are shown in Aii. Note the very stable appearance of the oscillation with essentially superimposed power spectra at the three time points. The graphs in B show the time course of peak power (i), area power (ii) and frequency (iii) for the two control IgG samples as mean ± S.E.M

4.3.4 Disease Control

IgG purified from the serum of a patient with autoimmune limbic encephalitis and VGKC-complex antibodies was used as a disease control (DC IgG) to ascertain the specificity of any findings with NMDAR-Ab positive IgG. DC IgG did not bind to NR1 and NR2B expressing HEK cells at the concentration used (10μg/ml) or at a tenfold higher concentration (100μg/ml, see Figure 4.7), which was always associated with binding of NMDAR-Ab positive samples, confirming there were no NMDAR antibodies in this IgG sample.

mEC

Slices exhibiting stable gamma-frequency oscillations were exposed to DC IgG at 10μg/ml for one hour followed by a 30-minute wash (n=4 slices from 4 animals). Kainate perfusion generated oscillations in layer II or III with a peak power of 81.61 ± 36.27 μV^2/Hz, area power of 1.016 ± 0.539 μV^2/Hz.kHz, and frequency of 45.08 ± 7.27 Hz. There was no significant change in the normalised power or frequency of mEC γ-oscillations at one hour of exposure to DC IgG or 30 minutes after IgG washout (see Table 4.8 and Figure 4.8)

There was no difference between the change in power and frequency of the oscillations exposed to DC and those in vehicle at 60 minutes or 90 minutes (after 30 minutes of DC washout, see Table 4.8 and Figure 4.8).

Table 4.8 Effect of DC IgG on mEC γ-oscillations and comparison with vehicle

	Reduction at 60 mins (%)	Reduction at 90 mins (%)	RM ANOVA	P value
Peak Power	33.45 ± 42.94	-1.855 ± 30.86	F (1.469, 4.406) = 1.374	0.326
Area Power	27.67 ±48.60	4.377 ± 25.25	F (1.546, 4.639) = 1.150	0.373
Frequency	2.93 ±3.08	-4.106 ± 3.518	F (2.206, 8.826) = 2.328	0.152
	DC IgG 60min – vehicle 60min (%)	**DC IgG WO – vehicle WO (%)**	**ANOVA**	**P value**
Peak Power Mean Difference (95% CI)	-16.21 (-65.68 to 33.26)	33.62 (-15.85 to 83.08)	F (3, 20) = 0.8289	0.494
Area Power Mean Difference (95% CI)	-22.53 (-72.05 to 26.98)	22.21 (-27.31 to 71.72)	F (3, 20) = 0.5986	0.623
Frequency Mean Difference (95% CI)	-3.177 (-9.714 to 3.361)	-6.346 (-12.88 to 0.1918)	F (3, 22) = 1.732	0.19

CA3

DC IgG caused no significant change to γ-oscillation power (mean ± S.E.M.: peak power baseline 80.35 ±19.81 μV^2/Hz vs. 67.63 ±26.34 μV^2/Hz DC 60 minutes, one-way ANOVA *F* (2.120, 8.479) = 0.964, *p*=0.425; area power baseline 0.645 ±0.335 μV^2/Hz.kHz vs. 0.495 ±0.296 μV^2/Hz.kHz DC 60 minutes, *F* (1.34, 5.36)=1.133, *p*=0.358) or frequency (baseline 38.18 ±2.29 Hz vs. 38.34 ±2.16 Hz DC 60 minutes, F(2.68, 10.73)=0.65, *p*= 0.583) in the CA3 subfield of the hippocampus in 5 slices examined (3 animals, see Figure 4.8).

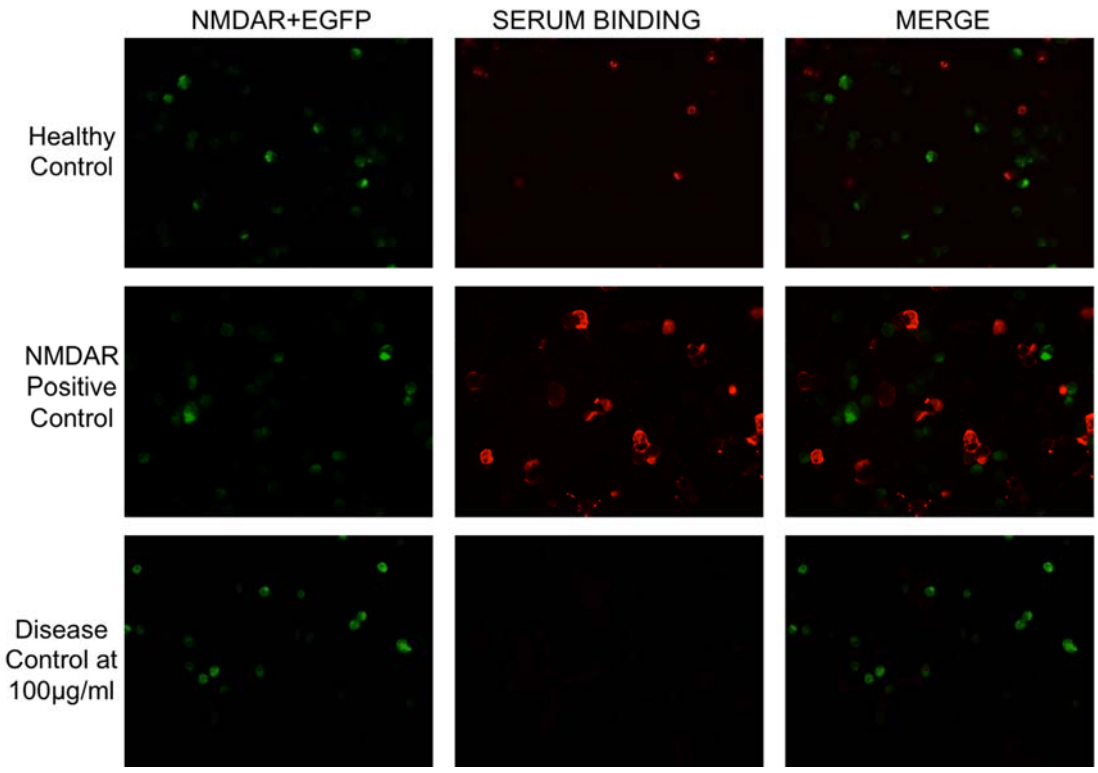

Figure 4.7 DC IgG does not bind to NMDAR (NR1 and NR2B subunits coexpressed with EGFP) expressing HEK cells.
NMDAR (+EGFP) transfected HEK cells (green), serum autoantibodies bound to NMDAR (+EGFP) transfected cells (red) and co-localisation of serum autoantibody binding and NMDAR (+EGFP) expression (merge). The bottom row pertains to the disease control sample. The pictures shown are from coverslip exposed to 100µg/ml DC IgG.

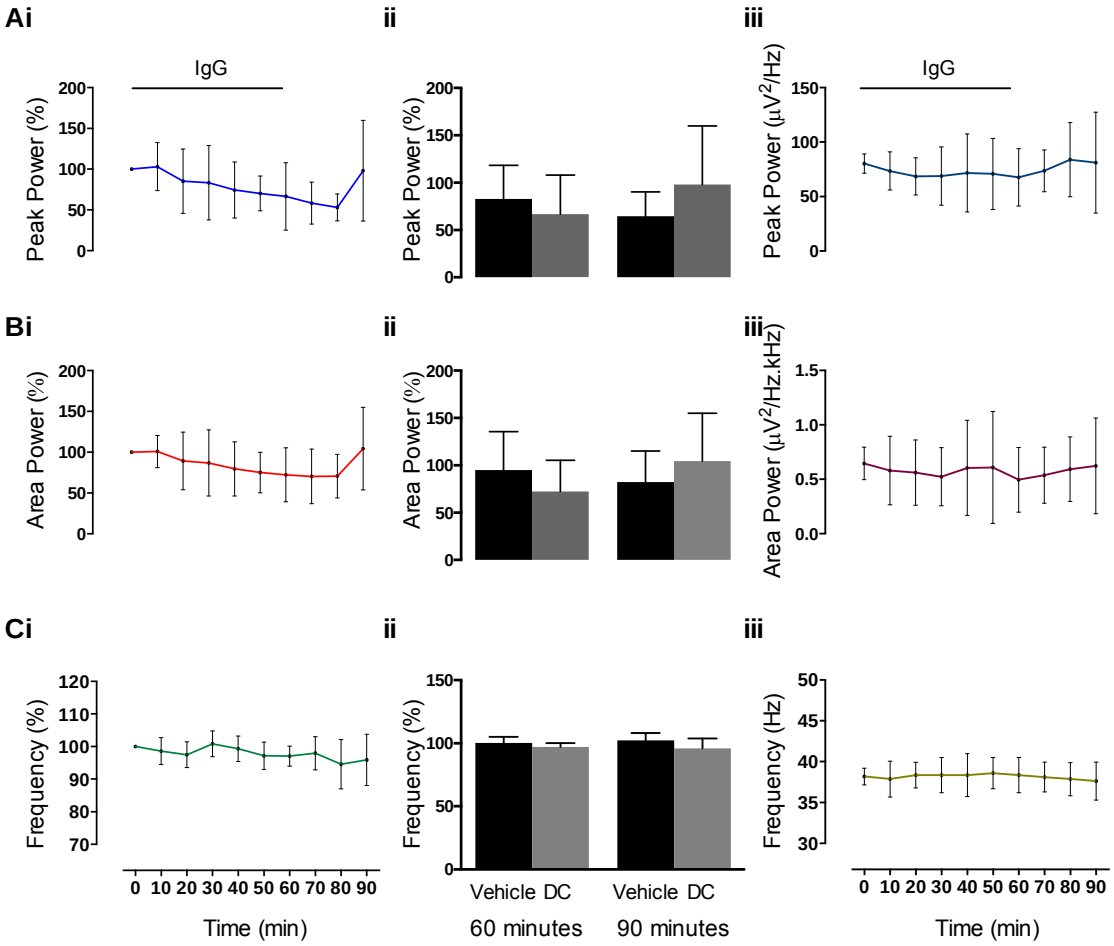

Figure 4.8 Power and frequency of γ-oscillation in mEC and CA3 of HPC in slices exposed to disease control IgG.
In the mEC (n=4, graphs i and ii of each row) there is a gradual decline in power (Ai and Bi, mean ± SEM) comparable to that seen in the vehicle group (Aii and Bii, mean ±SD). Frequency remains stable (Ci and ii). In the HPC (n=5), power (Aiii and Biii) and frequency (Ciii) remain unchanged (mean ± SEM).

4.3.5 Fab fragments from patient IgG

Patient autoantibodies have been shown to cause the internalisation of NMDARs through divalent binding and cross-linking of surface receptors (Hughes *et al.*, 2010). The antigen-binding region of an antibody (fragment antigen-binding or Fab) can be enzymatically cleaved from the immunoglobulin molecule, yielding two Fab fragments for each IgG molecule. Fab fragments prepared from patient IgG bind to surface NMDARs, but unlike the full IgG molecule, they do not cause a reduction in surface NMDAR clusters. Only when an anti-Fab secondary antibody is added, thus restoring the divalent conformation of a normal IgG molecule, is a reduction in surface NMDAR clusters seen (Hughes *et al.*, 2010). This strongly suggests that any effect seen with patient IgG is a result of reduced surface NMDAR availability through internalisation.

Fab fragments (Fab) prepared from NMDAR-Ab-positive patient IgG (gift of Professor Vincent, Oxford University) were used at a concentration of 10μg/ml to determine whether any effect on γ-oscillations was mediated by NMDA receptor internalisation or through an acute antagonistic affect. Kainate perfusion generated oscillations in layer II or III of mEC with average peak power of 70.85 ± 51.69 μV^2/Hz, area power of 0.68 ± 0.32 μV^2/Hz.kHz, and frequency of 46.27 ± 8.39 Hz (n=11 slices from 9 animals). Because of the wide variation in baseline power, the values for power and frequency in each experiment have been normalised as described above. In the presence of Fab, there was a gradual decline in peak and area power similar to that seen in the vehicle group. Frequency remained unchanged (see Table 4.9 and Figure 4.9).

Table 4.9 Effect of NMDAR-Ab Fab on mEC γ-oscillations (mean ± SD)

	Reduction at 60 min (%)	Reduction at 90 min (%)	RM ANOVA	P	Significant multiple comparison test (Dunnett's)	P
Peak Power	17.88 ±27.48	45.08 ± 22.88	F(1.616, 16.16) = 21.43	<0.0001	Baseline vs. 90 min	p<0.001
Area Power	22.02 ± 16.43	33.56 ± 20.31	F(1.554, 15.54) = 22.92	<0.0001	Baseline vs. 60 min	<0.01
					Baseline vs. 90 min	<0.001
Frequen -cy	1.18 ± 5.47	0.87 ± 5.37	F (1.456, 14.56) = 0.368	0.633		

When oscillation power and frequency in the Fab group (n=11), the vehicle group (n=8) and the cIgG group (n=13) were compared at the end of IgG perfusion and the end of washout, there were no significant differences between the groups (see Figure 4.9).

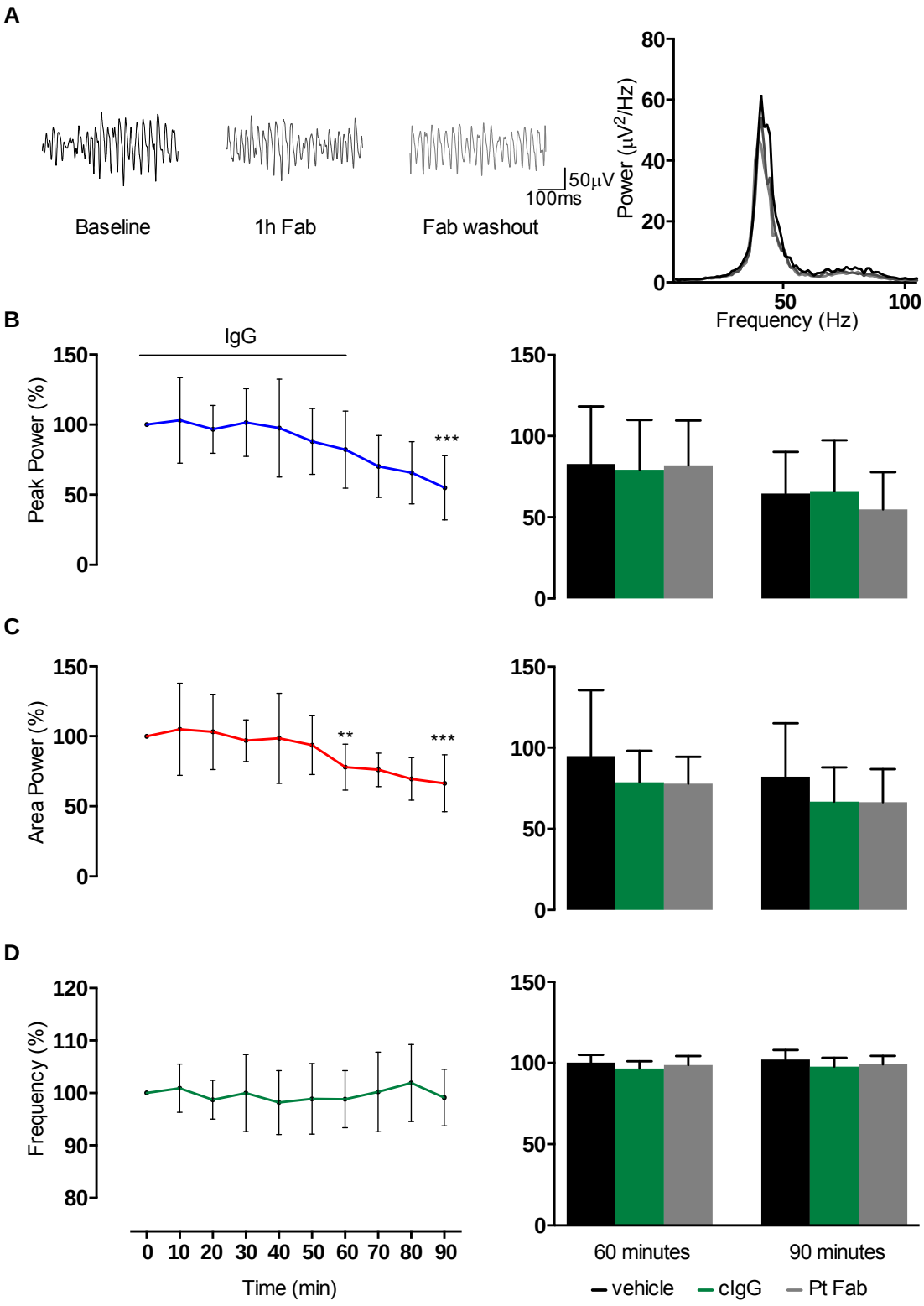

Figure 4.9 Power and frequency of γ-oscillations in the presence of purified Fab fragments from a patient with NMDAR-Abs (10µg/ml).
Examples of extracellular field recordings from three time points during an experiment in a single slice are shown in A. The corresponding power spectra at the far right illustrate the small reduction in peak power that occurs over the course of the 90-minute experiment. The time course of peak power (B), area power (C) and frequency (D) are shown as mean ±S.D. in the left panel. Both peak and area power decline over the course of the experiments. However, these declines are similar to those seen in the vehicle and cIgG groups (right panel).

4.3.6 Patient Immunoglobulin preparations

NMDAR-Ab positive purified IgG was obtained from three patients with NMDAR-Ab encephalitis and strongly positive NMDAR-Ab titres (scores 3-4 on cell-based assay, gift of Professor A. Vincent). Patient 1 IgG was used at 10μg/ml, and patients 2 and 3 at both 10 and 30 μg/ml. Only patients 2 and 3 IgG were tested in the hippocampus due to the limited availability of patient 1 IgG. Clinical details of the three patients can be found in Appendix A

Patient 1

Purified IgG from patient 1 (Pt1) strongly bound to HEK cells expressing NR1, NR2B and EGFP at the standard dilution used for diagnostic cell-based assays (1:20, see Figure 4.10 bottom row). At the concentration used in the electrophysiological experiments below (10μg/ml) binding was present but very subtle (see Figure 4.10 middle row), scoring 1/4. The CBA using Pt1 IgG at 10μg/ml was performed two years after its use for the electrophysiology experiments with an aliquot that had been stored at 4°C and loss of activity may have occurred.

Medial entorhinal cortex

Slices exhibiting stable gamma-frequency oscillations were exposed to purified IgG from Pt1 at 10μg/ml for one hour followed by a 30-minute wash (n=7 slices from 7 rats). Kainate perfusion (400 nM) generated oscillations in layer II or III with a peak power of 56.23 ± 45.78 μV^2/Hz, area power of 0.51 ± 0.35 μV^2/Hz.kHz, and frequency of 43.60 ± 6.79 Hz (mean ± SD). Because of the wide variation in baseline power, the values for power and frequency in each experiment have been normalised as described above. Over time, there were reductions in peak power and area power, which appeared more pronounced than those seen with vehicle or cIgG (see Figure 4.10). Peak power had decreased by 48.01 ±36.36% after 1 hour of perfusion with Pt1 IgG (RM ANOVA, $F(1.918, 11.51)=14.86$, $p=0.007$; Dunnett's multiple comparisons test baseline vs. 1h $p<0.05$). No recovery after washout was seen. In fact peak power continued to decline (change in peak power 67.76 ±34.5% at end of washout, Dunnett's multiple comparisons test baseline vs. 90 minutes $p<0.01$). Area power followed a similar course (decrease of 45.21 ±35.05% at 1 hour and 63.65 ±31.96% at end of washout, $F(1.913, 11.48)=12.08$, $p=0.0016$; Dunnett's

multiple comparisons test baseline vs. 1hr $p<0.05$, baseline vs. 90 minutes $p<0.01$). Frequency remained stable (decrease of 4.4±7.36% at 1 hour and 1.07±14.96% at 90 minutes, $F(1.386, 8.318) = 0.464$, $p= 0.576$).

When compared to the changes seen in vehicle and cIgG, only the change in area power at the end of the washout period was significantly greater in Pt1 IgG slices (one-way ANOVA, $F(2, 25)=5.321$, $p=0.0119$; Dunnett's multiple comparisons test vehicle vs. Pt1 IgG $p<0.01$, cIgG vs. Pt1 IgG $p<0.05$, Figure 4.10).

Patient 2

Purified IgG from patient 2 (Pt2) strongly bound to HEK cells expressing NR1, NR2B and EGFP at the standard dilution used for diagnostic cell-based assays (1:20, see Figure 4.11), scoring 4. At the concentrations used in the electrophysiological experiments below (10 and 30μg/ml) binding was less pronounced but still clearly visible (see Figure 4.11), scoring 1.5/4.

Medial entorhinal cortex

Six slices from 5 animals were exposed to 10μg/ml Pt2 IgG and 8 slices from 5 animals to 30μg/ml. There were significant reductions in power and also frequency of γ-oscillation in mEC after exposure to Pt2 IgG (see Table 4.10 and Figure 4.12).

Table 4.10 Effect of Pt2 IgG on parameters of γ-frequency oscillations in mEC

	Pt2 10μg/ml (n=6)				Pt2 30 μg/ml (n=8)			
	Base-line	**60 min IgG** (mean ±SEM)	**Wash out** (mean ±SEM)	**Significance level** (RM ANOVA)	**Base-line**	**60 min IgG** (mean ±SEM)	**Wash out** (mean ±SEM)	**Significance level** (RM ANOVA)
Peak Power (%)	100	70.3 ±8.43	64.76 ±10.86	F=7.619 **P=0.012**	100	64.45 ±8.99	53.22 ±15.11	F=9.534 **P=0.012**
Area Power (%)	100	67.58 ±6.54	68.46 ±6.9	F=18.08 **P=0.001**	100	71.22 ±7.25	49.37 ±13.48	F=11.14 **P=0.005**
Frequency (%)	100	95.01 ±0.6	93.75 ±1.35	F=20.44 **P=0.003**	100	97.75 ±2.09	89.60 ±5.96	F=2.873 **P=0.127**

There was a significant reduction in peak power over time in the presence of both 10 and 30μg/ml Pt2 IgG. The decrease was significant after 60 minutes (Dunnett's multiple comparisons test IgG vs. baseline p=0.029 for 10μg/ml IgG

and p=0.0099 for 30µg/ml IgG). At both IgG concentrations, peak power continued to drop during the washout phase so that peak power at the end of the washout phase was significantly lower than during the baseline period (Dunnett's multiple comparisons test p=0.039 for 10µg/ml IgG, p=0.031 for 30µg/ml IgG).

Area power also decreased significantly over time in both concentrations of IgG. The reductions were highly significant after 60 minutes of perfusion (Dunnett's multiple comparisons test baseline vs. 60 minutes p=0.0075 for 10µg/ml and p=0.0097 for 30µg/ml) and significant at the end of the washout phase (Dunnett's multiple comparisons test baseline vs. 90 minutes p=0.011 for 10µg/ml and p=0.013 for 30µg/ml).

Unexpectedly, there was a statistically significant decrease in frequency over time in slices perfused with 10µg/ml Pt2 IgG but not 30µg/ml Pt2 IgG (see Table 4.10). The reduction for the slices perfused with 10µg/ml was significant at both time points (Dunnett's multiple comparisons test baseline vs. 60' IgG p=0.0007, baseline vs. washout p=0.0097).

There was no statistical difference between the power and frequency at 1 hour and following washout for the two concentrations (see Table 4.11). Also, the changes were not significant when compared to the vehicle and cIgG groups (see Table 4.11).

Table 4.11 Comparison of Pt2 IgG at 10 and 30 µg/ml with vehicle and cIgG

Peak Power (% of baseline)				
At 60 minutes	**Mean 1**	**Mean 2**	**Mean Diff.**	**Tukey P**
Pt2(10)-60' vs. Pt2(30) -60'	70.31	64.45	5.859	0.983
Pt2(10)-60' vs. vehicle 60'	70.31	82.76	-12.46	0.861
Pt2(10)-60' vs. cIgG -60'	70.31	79.33	-9.019	0.924
Pt 2(30) -60' vs. vehicle 60'	64.45	82.76	-18.32	0.603
Pt2(30) -60' vs. cIgG -60'	64.45	79.33	-14.88	0.676
vehicle 60' vs. cIgG -60'	82.76	79.33	3.438	0.994
At 90 minutes	**Mean 1**	**Mean 2**	**Mean Diff.**	**Tukey P**
Pt2(10)-WO vs. Pt2(30) -WO	64.76	53.22	11.53	0.913
Pt2(10)-WO vs. vehicle 90'	64.76	64.53	0.2250	0.999
Pt2(10)-WO vs. cIgG -WO	64.76	66.00	-1.247	0.999
Pt 2(30) -WO vs. vehicle 90'	53.22	64.53	-11.31	0.89

Pt2(30) -WO vs. cIgG -WO	53.22	66.00	-12.78	0.818
vehicle 90' vs. cIgG -WO	64.53	66.00	-1.472	0.999
Frequency (% of baseline)				
At 60 minutes	**Mean 1**	**Mean 2**	**Mean Diff.**	**Tukey P**
Pt2(10)-60' vs. Pt2(30) -60'	100.2	96.64	3.603	0.315
Pt2(10)-60' vs. vehicle 60'	100.2	95.01	5.236	0.169
Pt2(10)-60' vs. cIgG -60'	100.2	97.75	2.490	0.699
Pt 2(30) -60' vs. vehicle 60'	96.64	95.01	1.633	0.887
Pt2(30) -60' vs. cIgG -60'	96.64	97.75	-1.113	0.948
vehicle 60' vs. cIgG -60'	95.01	97.75	-2.746	0.685
At 90 minutes	**Mean 1**	**Mean 2**	**Mean Diff.**	**Tukey P**
Pt2(10)-WO vs. Pt2(30) -WO	102.2	97.81	4.434	0.711
Pt2(10)-WO vs. vehicle 90’	102.2	93.75	8.487	0.341
Pt2(10)-WO vs. cIgG -WO	102.2	89.60	12.64	0.048
Pt 2(30) -WO vs. vehicle 90'	97.81	93.75	4.053	0.811
Pt2(30) -WO vs. cIgG -WO	97.81	89.60	8.210	0.218
vehicle 90' vs. cIgG -WO	93.75	89.60	4.157	0.838

CA3 hippocampus

Hippocampal γ-oscillations were not affected by perfusion with Pt2 IgG at 10μg/ml for one hour (n=6 slices from 3 animals). There was a gradual and non-significant increase peak power and area power, along with a progressive slow decline in frequency in keeping with findings in Pietersen *et al.* (2009) (see Table 4.12 and Figure 4.12B).

Table 4.12 Effect of Pt2 IgG on HPC γ-oscillations

	Baseline	60 minutes	Washout	RM ANOVA	P value
Peak Power ($\mu V^2/Hz$)	127.2 ±39.61	147.7 ±44.84	160.8 ±38.20	F (1.581, 7.904) = 3.309	0.097
Area Power ($\mu V^2/Hz.kHz$)	1.653 ±0.522	1.603 ±0.462	2.001 ±0.627	F (1.243, 6.214) = 1.217	0.327
Frequency (Hz)	39.44 ±1.35	38.29 ±0.43	37.49 ±0.92	F (1.569, 7.847) = 2.091	0.189

Patient 3

Purified IgG from patient 3 (Pt3) strongly bound to HEK cells expressing NR1, NR2B and EGFP at the standard dilution used for diagnostic cell-based assays (1:20, see Figure 4.13), scoring 4/4. At 10μg/ml binding was barely visible and therefore scored 0.5. At 30μg/ml, the binding scored 1/4.

Medial entorhinal cortex

As for the Pt2 IgG, perfusion of purified Pt3 IgG was accompanied by a significant decline from baseline in peak power and area power of kainate-induced mEC gamma-frequency oscillations, whilst frequency remained unchanged (see Table 4.13: RM ANOVAs: peak power 10μg/ml $F(1.535, 7.677)=37.37$, $p=0.0002$, 30μg/ml $F(1.639, 16.39)=8.331$, $p=0.0047$; area power 10μg/ml $F(1.257, 6.285)=39.07$, $p=0.0005$, 30μg/ml $F(1.773, 15.96)=7.962$, $p=0.005$).

Table 4.13 MEC γ-oscillation parameters after perfusion with Pt3 IgG

	Pt3 10µg/ml (n=6 slices, 5 animals)				Pt3 30 µg/ml (n=10 slices, 6 animals)			
	Base-line	60 min IgG (mean ±S.D.)	Wash-out (mean ±S.D.)	Signifi-cance level (RM ANOVA)	Base-line	60 min IgG (mean ±S.D.)	Wash-out (mean ±S.D.)	Signifi-cance level (RM ANOVA)
Peak Power (%)	100	47.37 ±27.23	22.59 ±16.23	*** 0.0002	100	58.59 ±29.95	64.78 ±42.76	** 0.005
Area Power (%)	100	58.34 ±8.23	39.72 ±20.12	*** 0.0005	100	66.06 ±24.72	66.83 ±34.04	** 0.005
Frequency (%)	100	93.82 ±6.08	95.28 ±3.35	ns	100	98.24 ±12.46	98.88 ±10.65	ns

Peak power had decreased significantly compared to baseline at both 60 minutes of perfusion with Pt3 IgG (Dunnett's multiple comparisons tests baseline vs. 60 minutes 10µg/ml $p=0.0091$ and 30µg/ml $p=0.001$) and after washout (Dunnett's multiple comparisons tests baseline vs. 90 minutes 10µg/ml $p=0.0002$, 30µg/ml $p=0.038$).

Area power had also declined significantly at both time points (Dunnett's multiple comparisons tests: 60 minutes vs. baseline: 10µg/ml $p=0.0001$,

30µg/ml *p*=0.0035; 90minutes vs. baseline: 10µg/ml *p*=0.0013, 30µg/ml *p*=0.024). Interestingly, the reductions are greater in slices exposed to 10µg/ml Pt3 IgG (50-80% reduction from baseline vs. 35-45% in those exposed to 30µg/ml, see Table 4.13). This is likely to be a chance effect caused by two slices demonstrating very large reductions in power in the 10µg/ml Pt3 IgG group.

When compared to equivalent time points in control experiments, peak power at the end of the washout phase in the 10μg/ml group was significantly lower than in the vehicle, cIgG and 30μg/ml Pt3 IgG groups (one-way ANOVA $F(3,34)=2.886$, $p=0.0498$; Uncorrected Fisher's Least Significant Difference $p<0.05$ for Pt3 IgG 10μg/ml vs. each of vehicle, cIgG, and Pt3 30μg.ml (note that correcting for multiple comparisons, e.g. with Dunnett's test, abolished any group differences). Similarly, area power in the Pt3 10 and 30μg/ml groups was significantly lower than in the vehicle group at 60 minutes of IgG perfusion (one-way ANOVA at 60 minutes perfusion $F(3, 33) = 2.905$ $p=0.0493$; Uncorrected Fisher's LSD $p<0.05$ for vehicle vs. Pt3 10μg/ml and Pt3 30 μg/ml; note that correcting for multiple comparisons, e.g. with Dunnett's test, obscured any group differences). Comparisons to area power in the cIgG group and comparisons after washout were not significant. Frequencies throughout the experiments were comparable in all four groups (see Figure 4.14).

CA3 hippocampus

Hippocampal γ-oscillations were not affected by perfusion with Pt3 IgG at 30µg/ml (n= 7 slices from 3 animals, see Figure 4.14).

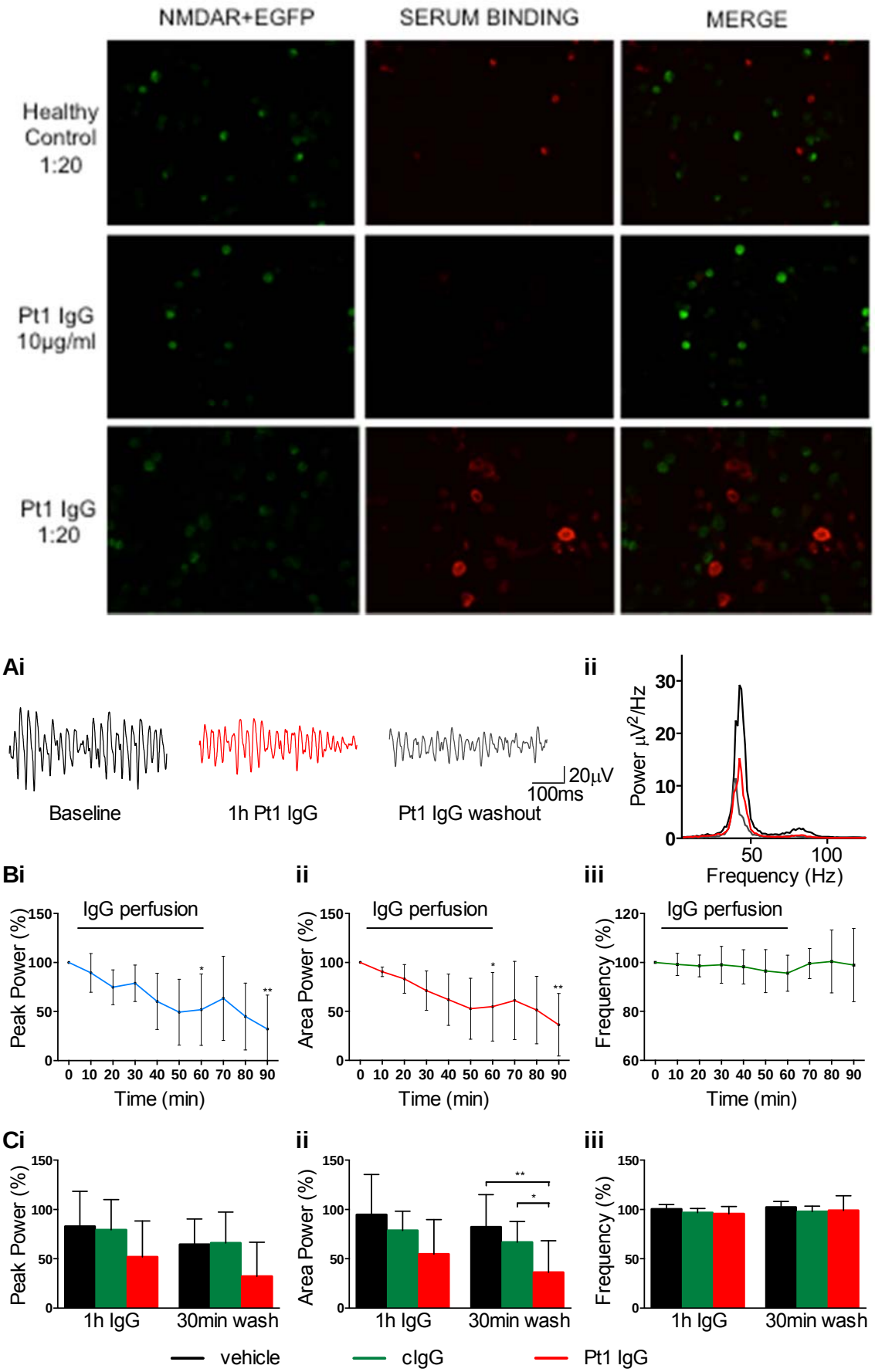

Figure 4.10 Effect of Pt1 IgG on γ-oscillations in superficial mEC.
The top panel shows the results of a CBA performed with Pt1 IgG. When initially tested at standard CBA dilution (1:20, bottom row), there was strong binding to HEK293 cells expressing NR1 and NR2B. Some faint binding could still be detected at 10µg/ml 3

years later (middle row). The bottom panel shows the electrophysiological results. Examples of field recordings from a single experiment are shown in Ai with corresponding power spectra in Aii, illustrating the decline in power at the end of the IgG perfusion period, which also continues during the washout phase. The averaged time-course of peak power, area power and frequency (mean ± S.D.) are shown in Bi, ii, and iii respectively. Despite the apparent marked reductions in peak and area power with Pt1 IgG, there is no significant difference between the peak and area power of vehicle, cIgG and Pt1 IgG oscillations at 1 hour of IgG perfusion. At the end of the washout period there is a significant difference in area power between the vehicle, cIgG and Pt 1 IgG groups.

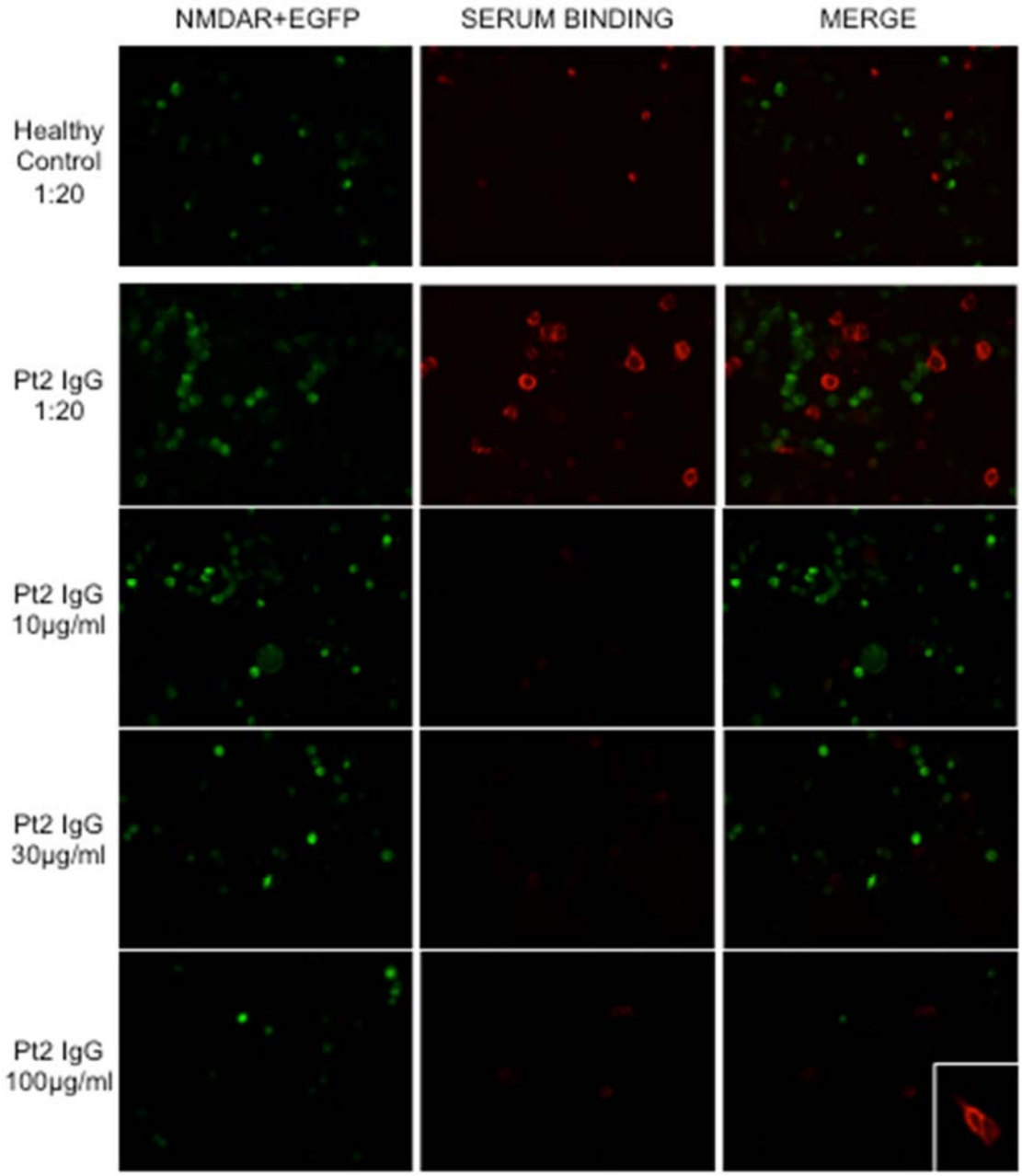

Figure 4.11 Results of CBA using Pt 2 IgG at 10, 30, and 100 μg/ml.
Cell-surface binding of IgG to HEK293 cells expressing NR1 and NR2B (with EGFP) is subtle but definite at both the concentrations used in electrophysiological experiments, scoring 1 and 1.5 on CBA. Stronger binding can be observed at 100μg/ml and at 1:20, the usual diagnostic CBA dilution for serum.

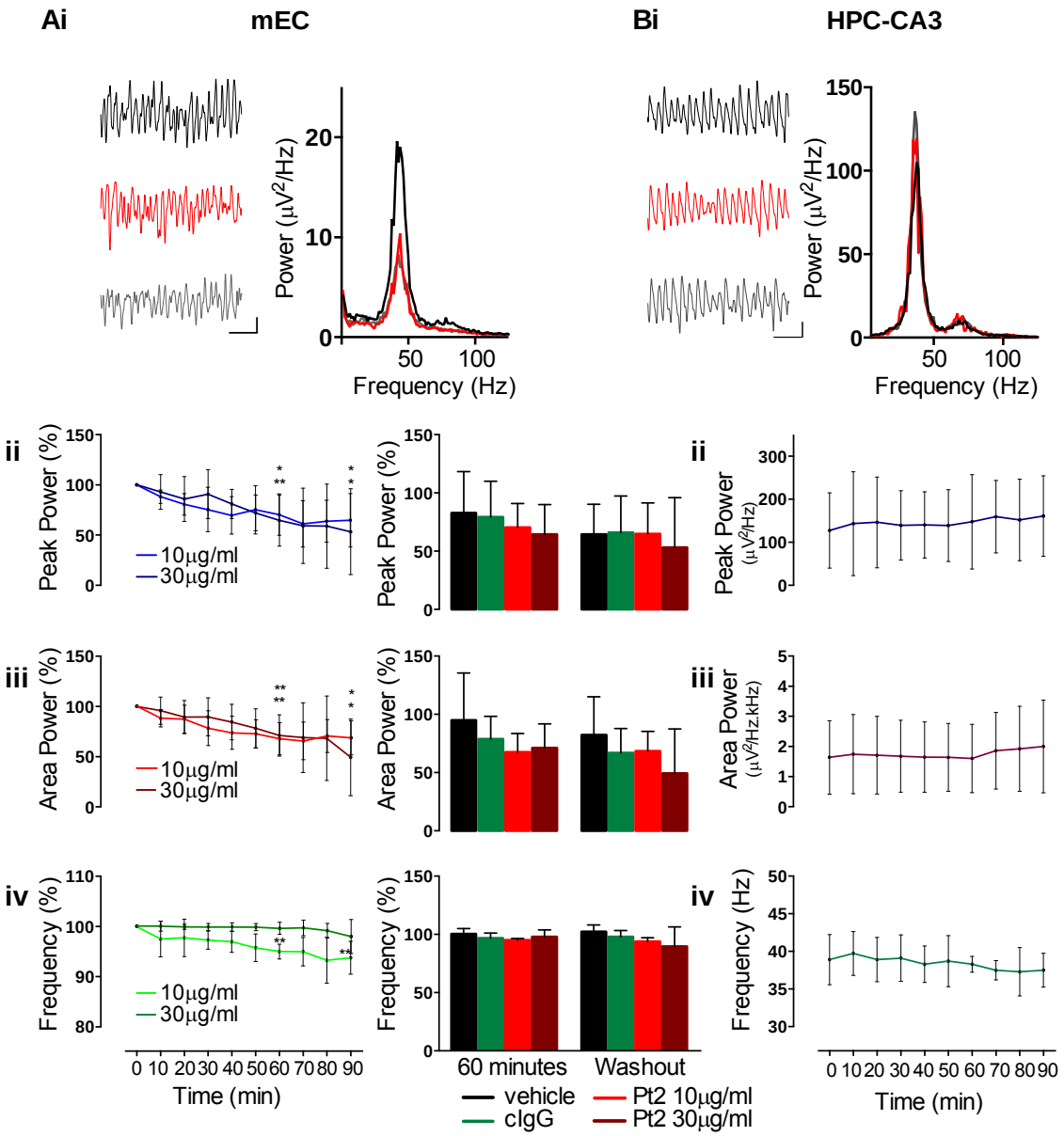

Figure 4.12 The effect of Pt2 IgG on mEC and CA3 γ-oscillations.
Example mEC and CA3 oscillations at baseline (black), 1h after Pt2 perfusion (red) and after 30 minutes IgG washout (grey) are shown in Ai and Bi. Horizontal scale bars : 100ms, vertical scale bars: 20μV in Ai, 50μV in Bi. The corresponding power spectra demonstrate the reduction in power after IgG perfusion in mEC, which is maintained through the washout period. In CA3, there is a gradual increase in γ during the experiment. In the mEC (Ai-iv) Pt2 IgG perfusion was associated with a reduction in peak power (ii) and area power (iii), however these were not significant when compared to vehicle and cIgG data (right panel). Although frequency appears to decrease in the 10μg/ml group (iv, left panel), there is no significant difference when all groups are compared (iv, right panel). 10μg/ml Pt 2 IgG has no effect on CA3 γ-oscillations.

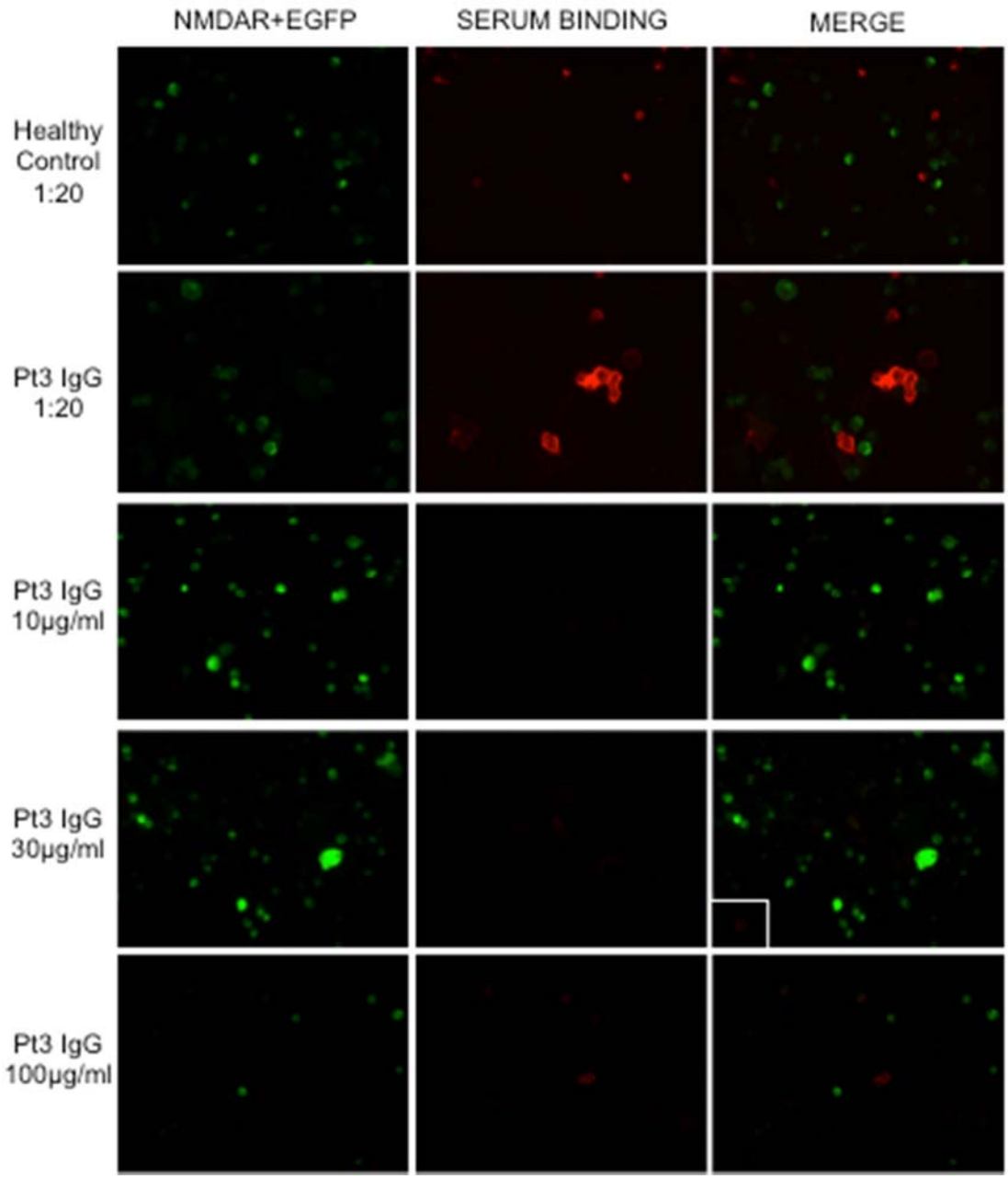

Figure 4.13 CBA results using Pt 3 IgG at 10, 30, and 100μg/ml.
Cell-surface binding of IgG to HEK293 cells expressing NR1 and NR2B (with EGFP) is very subtle at both the concentrations used in electrophysiological experiments, scoring 0.5 and 1 at 10 and 30μg/ml respectively on CBA. Stronger binding can be observed at 100μg/ml and at 1:20, the usual diagnostic CBA dilution for serum.

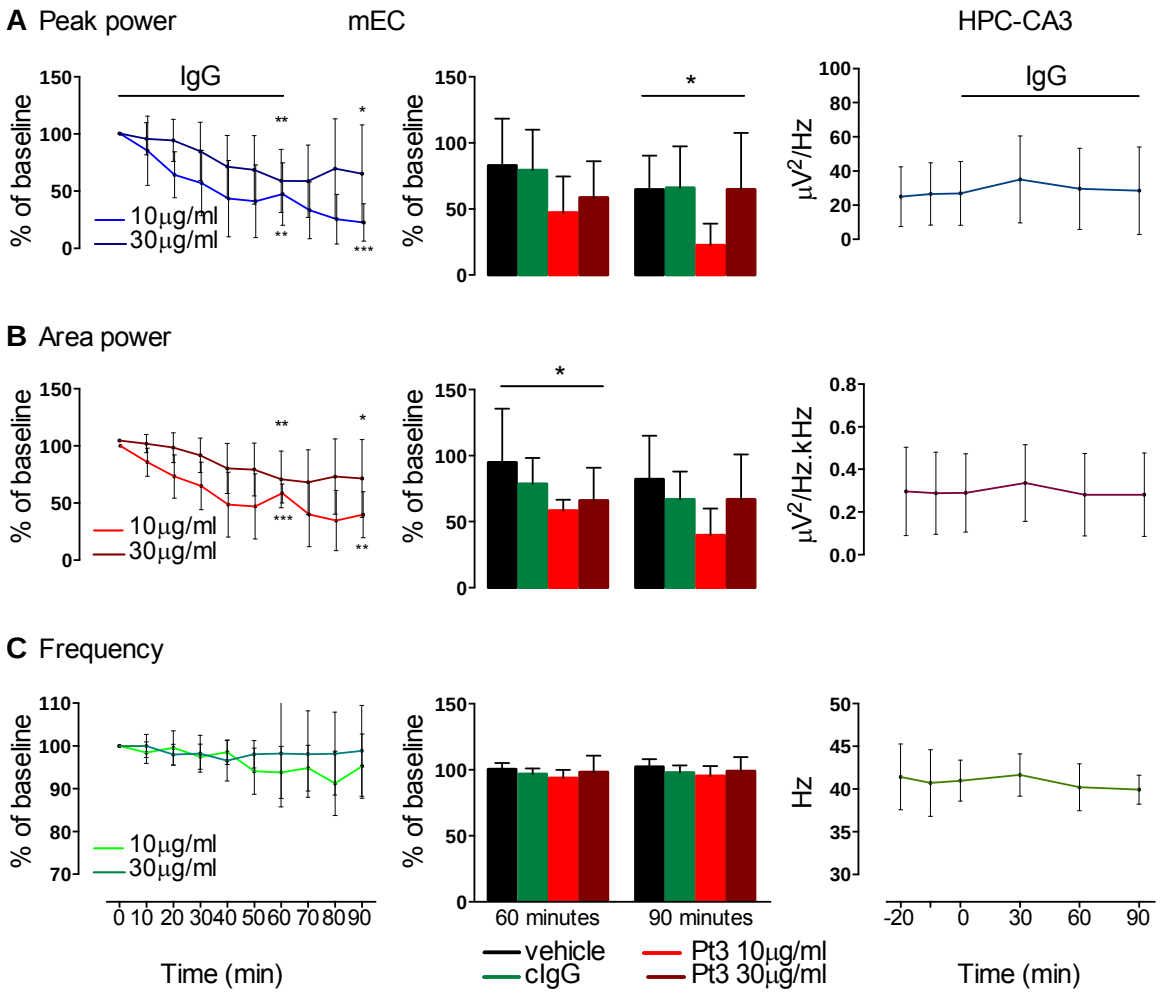

Figure 4.14 The effect of Pt3 IgG on mEC and CA3 γ-oscillations.
In the mEC (first two graphs per row) Pt3 IgG perfusion was associated with a reduction in peak power (A) and area power (B). Peak power in the 10μg/ml group was significantly lower than in the other groups at 90 minutes, and area power in both the 10 and 30 μg/ml groups was lower than in the vehicle group at 60 minutes (A and B middle graphs). Although frequency appears to decrease in the 10μg/ml group (C, first graph), there is no significant difference when all groups are compared (middle graph). 30μg/ml Pt3 IgG has no effect on CA3 γ-oscillations.

4.3.7 Grouped patient IgG samples

The results above raised the possibility that patient IgG may have an effect on γ-oscillation power in the mEC: although γ power is clearly not stable over prolonged periods as indicated in the literature, the decline in power in the patient IgG groups appeared more pronounced than in the vehicle or control IgG groups. Also, in the slices exposed to Pt3 IgG, γ-power was significantly lower than in slices perfused only with vehicle or with cIgG.

This possible effect should be related to the presence of NMDAR-Abs in the patient IgG samples, as control IgG had a less pronounced effect on γ-power. It is not possible to quantify the concentration of NMDAR-Ab in purified IgG samples, and this will be different in each preparation. Any effect of the NMDAR-Abs will be related to the total amount used in each experiment, which is unknown. Using set concentrations of 10 and 30μg/ml may therefore have been rather artificial. As shown for Pt2 and 3 IgG, there were no statistically significant differences in power between the slices exposed to each of the IgG concentrations. This would suggest that at the two relatively low concentrations used here (1:500 and 1:1200 dilution, compared to 1:10 to 1:100 used by other groups (Hughes *et al.*, 2010), no concentration-effect could be detected. The results of three patient samples have therefore been pooled to form a larger patient IgG group (pIgG, n=38). At the end of the one-hour perfusion with IgG, the reduction in peak power of γ-oscillations was greater in the pIgG group compared to the vehicle, cIgG and Fab groups (one-way ANOVA, $F(4, 69) = 2.513$, $p = 0.0494$), but not the DC group (see Table 4.14). The latter is likely to be related to the small sample size and large variation of the SD group.

Table 4.14 Change in mEC γ-oscillation power and frequency in the five groups studied.

	P by ANOVA	pIgG (n=38)	Vehicle (n=8) P by uncorrected Fisher's LSD vs. pIgG	cIgG (n=13) P by uncorrected Fisher's LSD vs. pIgG	Fab (n=11) P by uncorrected Fisher's LSD vs. pIgG	DC (n=4) P by uncorrected Fisher's LSD vs. pIgG
Change in peak power (%)	*	41.31 ±27.54	17.24 ±35.49 *	20.67 ±30.65 *	17.88 ±27.48 *	33.45 ±41.31
Change in area power (%)	*	35.96 ±22.82	5.13 ±40.61 **	21.30 ±19.46	22.02 ±16.44	27.67 ±33.0
Change in frequency (%)	ns	4.9 ±11.84	-0.24 ±4.65	3.36 ±4.48	1.18 ±5.47	2.93 ±3.08

The decline in area power of γ-oscillations was greater in the pIgG group compared to vehicle only (one-way ANOVA, $F(4, 68) = 3.115$, $p = 0.0205$). Change in frequency was minimal and similar across groups (see Table 4.14 and Figure 4.15**Error! Reference source not found.**).

Changes in power and frequency at 90 minutes (at the end of a 30 minute washout period) were not compared across groups as the significant reduction in power at 90 minutes in the vehicle group suggests that deterioration in slice health might confound any effect of IgG.

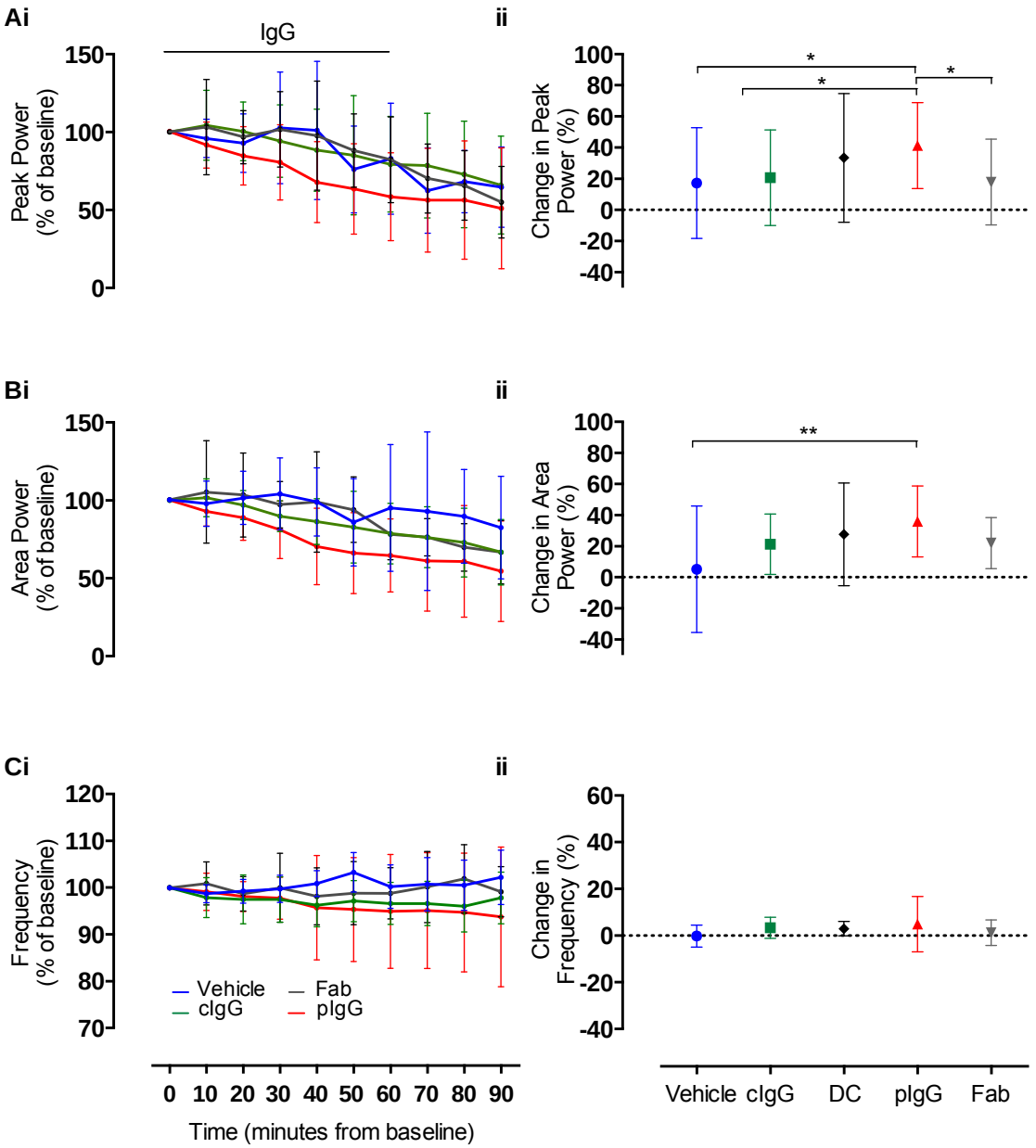

Figure 4.15 Change in power and frequency of mEC γ-oscillations in slices exposed to vehicle, cIgG, Fab or pIgG.
The average time course of peak power (Ai), area power (Bi) and frequency (Ci) are presented as mean ±S.D. Peak and area power decline in all groups during the active perfusion period. There is no recovery during the washout phase. Frequency remains stable. The change in peak power is greater in the pIgG group than in the other groups except disease control (DC) (Aii, mean ± S.D.). The change in area power in pIgG is greater only than that in vehicle (Bii). There is no difference in frequency change among groups.

4.4 Discussion

The first aim of this research project was to determine if NMDAR-Abs could disrupt γ-oscillations in the mEC *in vitro* in a manner similar to NMDAR antagonists. This would lend support to their pathogenic potential and suggest a possible mechanism for the neuropsychiatric symptoms experienced by patients with NMDAR encephalitis. One of the first findings of this study was a gradual decline in γ-oscillation power over time under normal conditions. Indeed, γ-oscillations defined as stable by electrophysiological criteria over 40 minutes remained so for only a further 30-40 minutes. After this a visible reduction in peak and area power occurred, which became significant at 90 minutes for peak power.

The power of γ-oscillations is predicted by the size and synchrony of the IPSPs impinging onto principal cells (and also inhibitory interneurons through recurrent inhibitory connections), and thus phase-locking their output (Cunningham *et al.*, 2003a; Cunningham *et al.*, 2006). The size of these IPSPs is itself related to the excitatory drive, in the form of excitatory post-synaptic potentials (EPSPs) onto the fast-spiking interneurons that generate the oscillation. This excitatory drive has several sources. Activity in the gap-junctionally coupled axonal plexus of excitatory principal cells constitutes an important part (Cunningham *et al.*, 2004), but the relatively low frequency of phasic EPSPs recorded in fast-spiking interneurons suggests tonic drive is also required (Cunningham *et al.*, 2003a). Thus, there are several mechanisms by which the power of an oscillation might decline even without pharmacological intervention. Significant cell death among either the principal neurons or interneurons in the slice would lead respectively to a reduction in the excitatory drive to interneurons or the size of the IPSPs invading principal cells. Endogenous adenosine, the levels of which increase with kainate application in the slice preparation used here, is also known to depress excitatory glutamatergic and cholinergic transmission and therefore reduces γ-oscillation power (Pietersen *et al.*, 2009).

The observed reduction in oscillation power in control conditions meant that it was not possible to simply compare power before and after perfusion with patient or control IgG. Instead, statistical comparisons were made with reference to relevant endpoints in control conditions (60 minutes after the onset

of perfusion with the active compound and after 30 minutes of active compound washout).

When the results of the slices exposed to each of the three patient IgG samples were grouped, the decline in γ-oscillation power was greater than that related to factors endogenous to the slice preparation. Indeed the reduction in the pIgG slices was greater than the reduction in any of the other groups examined and there were no significant differences between vehicle, cIgG, Fab and DC IgG. This would suggest that the difference in reduction is related to the NMDAR-Abs, which are unique to the pIgG group. Purification of the NMDAR-Abs from patient IgG has so far not been possible. This would be required for the definitive demonstration that the reduction in γ-oscillation power seen in these experiments was due to the NMDAR-Abs in the IgG. However, the patient serum from which the IgG was purified has been shown not to bind other neurotransmitter receptors and ion channels as part of the diagnostic process. The purification process will also have removed other putative agents such as anti-epileptic medication for example. Furthermore, to show that there were no other detectable neuronal surface antibodies in the IgG preparation, adsorption of the antibodies by NMDAR-expressing cells was shown for each of the IgG preparations (Pettingill, unpublished).

As expected from the literature (Cunningham *et al.*, 2006), NMDAR-Ab containing IgG had no effect on hippocampal γ-oscillations. Immunohistochemistry using CSF or serum containing NMDAR-abs reveals that staining is most intense in the HPC, and this is related to the very high concentration of NMDAR in this region (Moscato *et al.*, 2014). In view of the effect of NMDAR-abs on mEC γ-oscillations shown above, and the likely pathogenic role of the antibodies, it is likely that a change in NMDAR-mediated neurotransmission in HPC would occur *in vivo* after exposure to NMDAR-abs. However, γ-oscillations the HPC-mEC slice preparation do not allow detection of such a change. Other electrophysiological measurements such as NMDAR-mediated EPSP or LTP in the HPC are likely to be more conducive to this.

The disease control IgG was purified from the serum of a patient with limbic encephalitis and antibodies to LGI-1. LGI-1 is a secreted protein that interacts with several synaptic scaffolding proteins and complexes with the Kv1.1

subtype of voltage-gated potassium channels, thereby preventing its inactivation (Schulte *et al.*, 2006). Electrophysiological slice studies from LGI-1 knockout mice have demonstrated increased frequency of miniature excitatory postsynaptic currents in hippocampal pyramidal cells compared to wild-type mice, reflecting increased glutamate release (Yu *et al.*, 2010). Similar increases in neurotransmitter release and hyperexcitability have been demonstrated as a consequence of inactivation or loss of Kv1.1 potassium channels (Schulte *et al.*, 2006; Simeone *et al.*, 2013), with consequent reduced spike-timing precision in pyramidal cells in the hippocampus of Kv1.1 knock-out mice (Simeone *et al.*, 2013). Pyramidal cell hyperexcitability, reduced spike-timing precision, and hyperglutamatergic states adversely affect network organisation into oscillatory patterns.

It is therefore likely that the DC IgG used here would impair γ-oscillations and perhaps cause epileptiform activity to emerge as seen in other studies (Yu *et al.*, 2010; Lalic *et al.*, 2011). This would mitigate its usefulness as a control for the effects of NMDAR-abs. We did indeed observe an apparent reduction in γ-power in the mEC but not the HPC, but no epileptiform activity was recorded. The ambivalent effect may be related to the high dilution and/or small sample size used in this study, in contrast to Lalic *et al.* (2011), where the concentration of IgG used was ten times higher. These points highlight the fact that γ-oscillations are a sensitive assay of perturbations of neuronal function, synaptic transmission and the balance of inhibition and excitation, but not a very specific one. Indeed, γ-oscillations are impaired in a number of neuropsychiatric conditions.

One of the limitations of this study is a lack of mechanistic explanation for the observed decrease in mEC γ-oscillation power. In pharmacological experiments using ketamine, reduction in γ-power is due to fewer and smaller IPSPs reaching principal cells, indicating a disruption in the γ-output of the interneurons that govern the locally recorded oscillations (Cunningham *et al.*, 2006; Middleton *et al.*, 2008). In the acute setting, this is likely to be related to the loss of the powerful NMDAR-mediated drive to fast-spiking interneurons in layer II of the mEC (Jones and Buhl, 1993). To determine if this is the case with NMDAR-Abs, intracellular recordings from both principal cells and interneurons

during γ-oscillations would be required. I have not obtained sufficient good quality intracellular recordings from principal cells during γ-oscillations to justify their inclusion here, but it is at least reassuring that patient IgG did not cause cell death during intracellular recordings, ruling out a direct toxic effect.

It is unlikely that NMDAR-Abs have a direct antagonistic effect at the NMDAR complex. Indeed, if that were the case, the experiments with patient Fab fragments should have yielded similar results to the pIgG experiments as the binding moiety of the antibody is preserved in Fab. However, there is a significant difference in oscillation power in slices exposed to Fab and pIgG. Furthermore, no acute antagonistic effect has been found using other methods: the amplitude of NMDAR-mediated currents in cultured hippocampal neurons is not affected by exposure to patient CSF for 30 minutes or purified patient Fab for 24 hours (Moscato *et al.*, 2014). Instead, the proposed mechanism of action of NMDAR-Abs is by cross-linking bound receptors and causing their internalisation (Hughes *et al.*, 2010). The observed lack of effect of Fab, which cannot crosslink antigen (Hughes *et al.*, 2010), would support internalisation as the cause of the reduction seen here. However, the reported time frame for internalisation may be outwith the duration of our experiments. Indeed, significant loss of surface NR1 immunofluorescence due to NMDAR-Ab-mediated internalisation in hippocampal neuron cultures only occurred after 12 hours of exposure to patient CSF (Moscato *et al.*, 2014). On the other hand, Mikasova *et al.* (2012) found that significant internalisation had occurred by two hours in cultures and also showed that patient antibodies removed synaptic NR2A-containing NMDAR from synapses and caused internalisation of extra-synaptic NR2B-containing NMDAR within that time as well, significantly changing the functional cellular distribution of NMDARs. It could therefore be hypothesised, that small changes in surface and synaptic NMDAR density, particularly in the exquisitely NMDA-sensitive fast-spiking interneurons that generate γ-oscillations in the superficial mEC (Jones and Buhl, 1993), could have functionally relevant implications whilst remaining undetectable by immunofluorescence.

Finally, one study has found that acute exposure to NMDAR-Abs in patient CSF prolongs the open time of NMDARs compared to control CSF in the presence of glutamate and glycine (Gleichman *et al.*, 2012). The Abs are unlikely to cause

the channels to open as there was no effect on closed time. It is not clear what the functional effect of this prolonged opening time might be, especially as the same group found no difference in the amplitude of NMDAR-mediated current in cultured hippocampal neurons exposed to patient or control CSF (Moscato *et al.*, 2014). An enhancement of NMDAR-mediated excitation is possible although unlikely in our slice preparation where NMDAR activity is already promoted by the use of low-Mg^{2+} aCSF and kainate-induced depolarisation of neuronal membrane potentials. Indeed, one study found that adding NMDA to the perfusion medium during kainate-induced oscillations had a concentration-dependent effect with very low concentrations (1μM) causing an increase in power whilst higher concentrations (2μM and above) massively reduced γ-oscillation power (Hall, 2012). It is therefore more likely that desensitisation would occur. NMDA receptors are characterised by their slow kinetics and slow and complex desensitisation mechanisms (Sun *et al.*, 2002), such that small prolongations of opening time would not necessarily cause desensitisation. However, it is conceivable that calcium-dependent desensitisation could be increased by the Ab-mediated stabilisation of the open state. Additionally, even in non-calcium-dependent desensitisation, the rate of desensitisation is higher from the open state than the closed state (Lin and Stevens, 1994).

The lack of effect of patient IgG on hippocampal γ-oscillations is in keeping with the literature (Cunningham *et al.*, 2006) and also suggests that the effect in the mEC is not mediated through toxicity.

Unlike the changes caused by ketamine and D-AP5, the decrease in power observed with pIgG was not reversible with washout. Reversibility is a useful feature of pharmacological experiments, as it indicates the effect is specific to the drug used and not related to cell death or deterioration of the slice. There are a number of potential explanations for the lack of reversibility seen with pIgG: NMDAR-Abs in pIgG may have caused internalisation of surface NMDARs, with the duration of the washout phase insufficient for membrane insertion of new receptors (Nong *et al.*, 2003). Alternatively, it may simply be that the antibodies are not easily washed out of the slice once bound to their antigen and so do not “free up” glutamate binding sites during the washout phase. Finally, it has been shown that intracerebral infusion of CSF from patients with NMDAR-Ab encephalitis increases the extracellular concentration

of glutamate in the hippocampus of rats *in vivo.* This was accompanied by a disruption of NMDA-mediated synaptic regulation of glutamate (Manto *et al.*, 2010). Hyperglutamatergic states are known to cause excitotoxicity and reduced neuronal excitability, which could responsible for the progressive reduction in γ-oscillations beyond the application of patient IgG.

4.4.1 Further work

There are two important weaknesses of the data presented here. Firstly, the effects seen with pIgG cannot be unequivocally linked to the presence of NMDAR-Abs. This is because purified IgG contains the whole range of antibodies found in a healthy human being in addition to NMDAR-Abs. All three patients had high titres of NMDAR-Abs as detected by CBA, and so we can presume that NMDAR-Ab concentration far exceeded that of any other antibody, especially at the high dilutions used in these experiments. However, to be certain that the effect on γ-power was NMDAR-Ab related, oscillating slices should be exposed to IgG from which the NMDAR-Abs have been pre-absorbed. If the oscillation power in these slices followed a course similar to that seen in the vehicle/cIgG groups, it could be concluded that the effect seen here are due to NMDAR-Abs.

Secondly, the mechanisms by which NMDAR-Abs might cause a decline in γ-power have not been investigated. A number of intracellular recordings from pyramidal cells in both oscillating and non-oscillating conditions were obtained, but very few were of satisfactory quality and no reliable conclusions could be drawn from them.

The effect seen in these experiments was small and confounded by the large variation in γ-power from one slice to the next as well as the natural decline in oscillation power over time in the mEC. It would have been better to use lower dilutions of IgG guided by normal IgG concentration in CSF and binding on CBA instead of relying on previous electrophysiological data obtained from the mEC with the attendant confounding factors mentioned above. Some indication of the validity of the results described above could be given by the detection of human IgG or its downstream effects in the slices used for electrophysiology and this will be the focus of the next chapter.

Chapter 5 The search for human Immunoglobulin binding in rodent brain slices

5.1 Introduction

NMDAR-Ab positive CSF has been shown to bind very strongly to the hippocampal neuropil (the areas of the hippocampus containing axons, dendrites and glial processes but not cell bodies (Dalmau *et al.*, 2007; Irani *et al.*, 2010b)). Binding is also present throughout the forebrain cortex, in the striatum and in the granule cell layer of the cerebellum, albeit much less intensely. This difference has been shown to be due to the high NMDAR content of the hippocampus (Moscato *et al.*, 2014). Additionally, the staining pattern seen with patient CSF coincides with that obtained using commercial NR1 antibodies (Moscato *et al.*, 2014), confirming it is due to NMDAR-Abs in the CSF. In the hippocampus, intense staining is present in both the medial and lateral blades of the molecular layer of the dentate gyrus, in the stratum oriens and throughout the molecular layers of the CA1-3 hippocampal subfields, with subtly reducing intensity in stratum radiatum and stratum lacunosum moleculare in CA3. The polymorph layer of the dentate gyrus (or hilus) is spared as are the pyramidal cell layers of CA1-3 (Dalmau *et al.*, 2007; Irani *et al.*, 2010b) This pattern is easily recognised and will be used in the coming sections to determine if NMDAR-Ab binding has taken place, although it should be appreciated that there are antibodies to other neuronal proteins that give similar staining patterns in the hippocampus. Immunohistochemically, AMPAR-Abs and GABAR-Abs can be differentiated from NMDAR-Abs by the differences in neocortical and cerebellar staining patterns.

The binding pattern described above has been obtained by incubating thin sections (<10μM) of both fixed and fresh frozen normal rodent brain tissue with patient CSF. Similar reactivity has also been demonstrated in the brains of mice exposed to NMDAR-Ab positive patient CSF by continuous intracerebroventricular infusion over two weeks (Planagumà *et al.*, 2014) and 48 hours following a single intraventricular injection of purified patient IgG (Wright *et al.*, 2015b). NMDAR-Abs in patient CSF and serum bind to the surface of the cell membrane of cultured rodent live hippocampal neurons after 1 hour's incubation, but binding in live rodent brain slices has not been reported. Only two published studies applying CSF or purified serum IgG from patients with NMDAR-Ab or VGKC-Ab encephalitis respectively to acute rodent brain slices exist (Lalic *et al.*, 2011; Q. Zhang *et al.*, 2012), and in neither was binding of

human IgG in the slices sought. To my knowledge, this is therefore the first attempt at developing a method to detect human IgG bound to rodent brain in the acute brain slice preparation commonly used in electrophysiology.

5.2 Methods

Sections for immunofluorescence were obtained from two sources. Firstly, the technique was learnt on horizontal naïve rat brain slices. Then, the slices from the electrophysiology (EP) experiments in chapter 3 were used. The immunofluorescence technique in fresh frozen tissue was based on protocols suggested by Dr P Pettingill of the Nuffield Department of Clinical Neuroscience, Oxford University.

For the naïve brain slices, the PBS-perfused and snap-frozen brain of a male Wistar rat was used. On a cryostat, 10µm horizontal sections were prepared and collected on to slides and allowed to air-dry overnight before storing at -20˚C. For staining, the slides were thawed for one hour at room temperature and blocked in 0.1 M Phosphate-buffered saline (PBS) with 10% normal goat serum (10% NGS/PBS) for one hour at room temperature. Sections were then incubated with NMDAR-antibody positive CSF diluted 1:10 in 3%-NGS/PBS or a commercial NR1 Ab (rat NMDAR1 aa. 660-811 recombinant protein, BD pharmingen) diluted 1:200 in 3%NGS-PBS overnight at 4˚C. Sections were washed three times in 300ml of PBS and specific IgG binding was detected using Alexa Fluor goat anti-human IgG secondary antibody (1:2000, Invitrogen, USA) for 1 hour at room temperature. Slides were washed three times in PBS, air dried and mounted with DAKO fluorescent mounting medium containing DAPI.

For the sections obtained from EP experiments, slices were removed from the recording chamber by lifting the filter paper on which they were resting using forceps at the end of the experiments. They were placed on a second piece of rigid filter paper covered with a thin layer of OCT compound (Tissue-Tek) to keep them flat during the freezing process. This was plunged into liquid nitrogen-chilled isopentane and then stored at -80˚C until slicing**.** On a cryostat, 12µm or 20µm sections were prepared (thickness depending on quality of frozen tissue and amount of tissue loss whilst slicing). The staining protocol was adjusted several times in order to optimize signal:noise ratios and cannot

therefore be summarized here. Briefly, the blocking step was either performed with 10% NGS/PBS or omitted. The AlexaFluor goat anti-human IgG secondary antibody (both 488 and 568 fluorescence bandwidth were used) was then applied to the slice at various dilutions and for different incubation periods. Slides were then washed three times for durations ranging from 30 seconds to 10 minutes in PBS, air-dried, and mounted with DAKO fluorescent mounting medium containing DAPI. The exact protocol used will be described in the results section.

The slides were then examined on a fluorescence microscope and pictures of areas of interest taken using the QCapture Pro Software (Qimaging, Canada**).**

For experiments using fixed tissue, slices were fixed in 4% paraformaldehyde (PFA) immediately after EP experiments, and preserved in 4% PFA until IF was carried out (<1 week). On the day of IF, the slices were cryoprotected in 30% sucrose in PBS, then re-sectioned to 40μm thickness on a freezing stage microtome. In some slices, antigen retrieval was carried out using just-boiled 10mM Sodium Citrate at pH 6.00, and both the blocking step and incubation with secondary antibody were performed in the presence of 0.05% Tween for mild permeabilisation. The sections were examined by confocal microscopy.

5.3 Results

5.3.1 Naïve rat brain sections

As horizontal hippocampal slices were used in the electrophysiological experiments described above, the binding pattern of NMDAR-Ab positive CSF in naïve horizontal rat brain sections was investigated in the first instance. Control slices incubated in 10% normal goat serum (NGS) only before adding the fluorescent secondary anti-human IgG antibody showed minimal non-specific background staining only (see **Error! Reference source not found.** A). In sections exposed to patient CSF (1:10) binding was observed in the hippocampus in the predicted pattern (see **Error! Reference source not found.** B-D). The molecular layer of the DG was the most intensely stained area (**Error! Reference source not found.** C). Within the DG molecular layer, the inner third was more strongly labelled than the middle and outer third, consistent with unpublished observations from the neuroimmunology laboratory

in Oxford (Dr. P. Pettingill). No binding was detected in the DG hilus. The stratum oriens and molecular layers of the CA subfields were also strongly labelled, with more intense labelling at the borders of the stratum pyramidale (**Error! Reference source not found.** D). Some staining was also seen in the mEC and the cerebellum (**Error! Reference source not found.** Biii and E). Similar patterns were seen with the CSF from two patients with NMDAR-Ab encephalitis, and when sagittal rat brain slices were exposed to a commercial NR1 Ab, although permeabilisation with 1% Triton was required for the commercial antibody (see Figure 5.2). In unpermeabilised section, the commercial NR1 antibody bound to individual cell bodies in the cortex, the pyramidal layers of HPC, the granule cell layer and hilus of the DG.

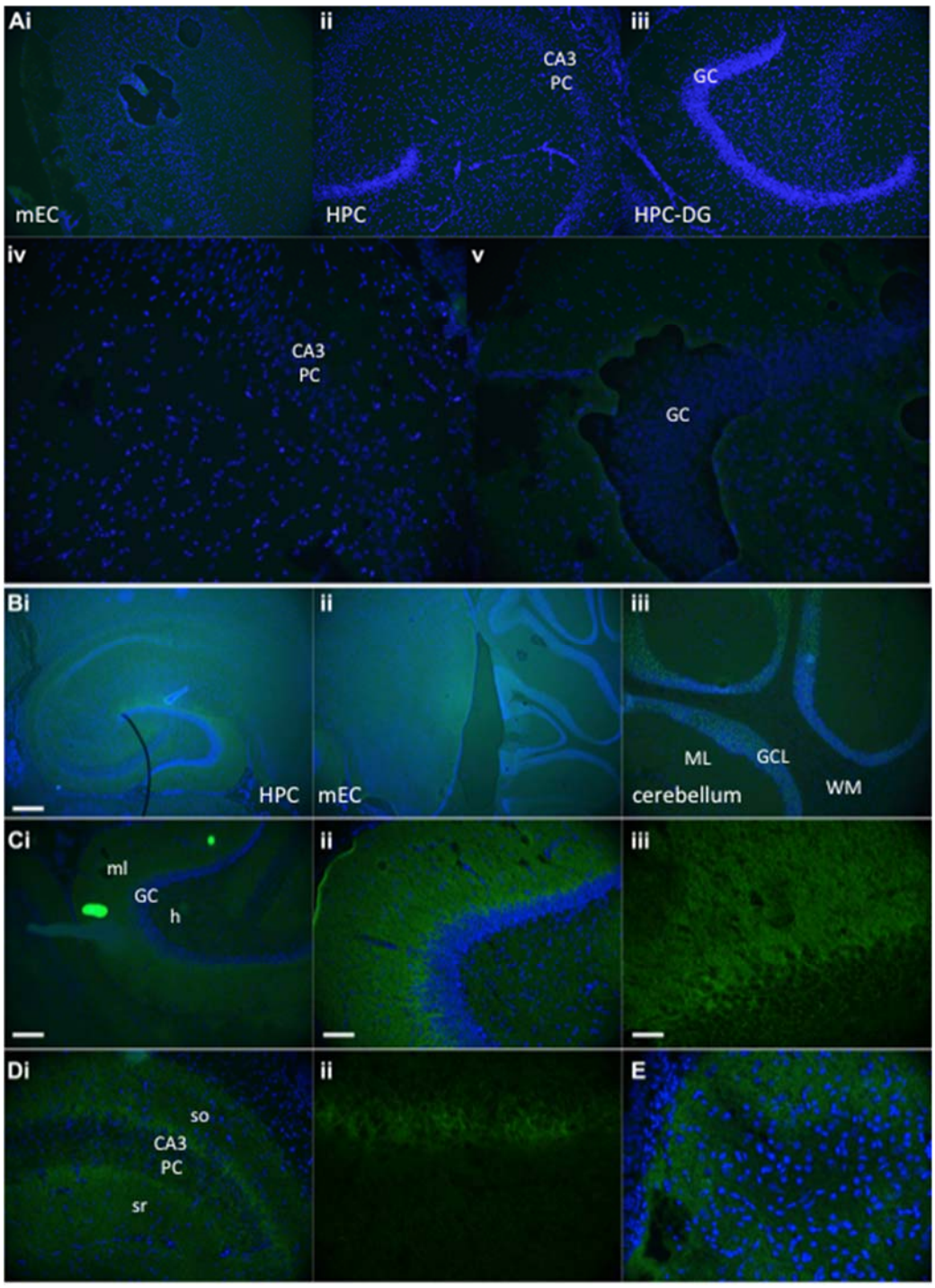

Figure 5.1 NMDAR-Ab positive CSF binds strongly to the molecular layers of hippocampal (HPC) subfields and dentate gyrus (DG).

A i-v shows the negative control naïve horizontal brain slices incubated with fluorescent anti-human IgG antibody. Only DAPI fluorescence is visible in the HPC and mEC. Ai mEC x10 – DAPI+anti-IgG, ii CA3 x10 – DAPI+anti-IgG, iii DG x10 – DAPI+anti-IgG. iv CA3 x20 – DAPI+anti-IgG, v DG x20 – DAPI+anti-IgG. B, C, D, and E show sections stained with patient CSF. Note the strong staining of the hippocampal neuropil (ml, so, sr) with sparing of the dentate gyrus hilus (h) (Bi, HPC x5 - DAPI+anti-IgG; Ci dentate gyrus x10, Di CA3 x20). Binding can also be seen in the mEC and cerebellum granule cell layer (gcl; Bii - mEC and cerebellum x5, Biii cerebellum x10). At larger magnification, the punctate cell-membrane staining is better appreciated: Cii - DG x20, iii – DG x40 anti-IgG alone; Dii CA3 x40 anti-IgG alone; E - superficial mEC x20 merge. GC: granule cells of DG; gcl: granule cell layer of cerebellum; h: hilus; ml: molecular layer; PC: pyramidal cell layer; so: stratum oriens; sr: stratum radiatum, WM: white matter.

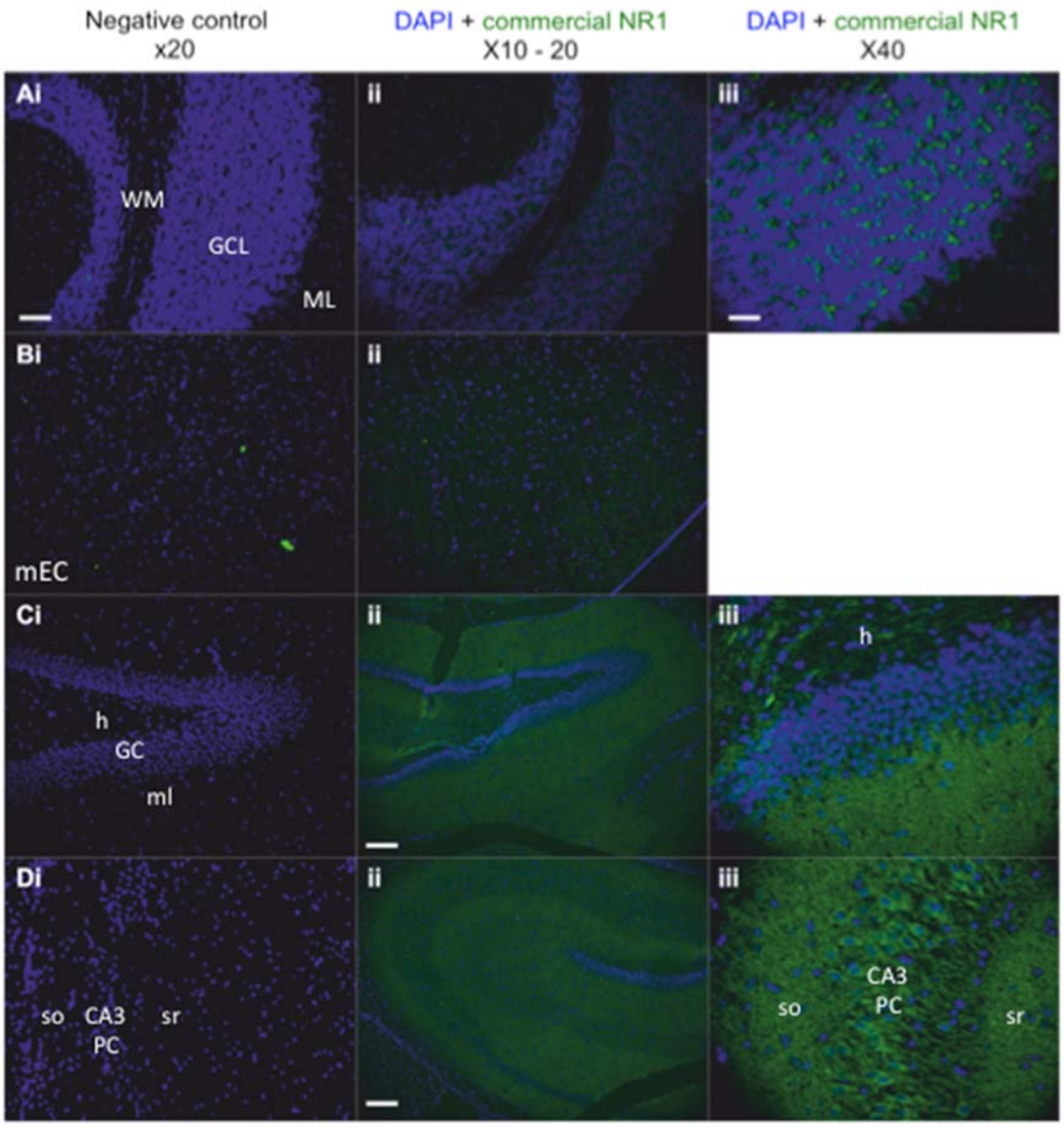

Figure 5.2 Commercial NR1 antibody binding distribution is similar to that of patient antibodies but requires permeabilisation.
Each row represents a different area of the brain. Cerebellar staining is shown in A, entorhinal cortex in B, dentate gyrus in C, and CA1-3 in D (Diii shows a x40 magnification of CA3). Note that unlike patient CSF, the commercial antibody binds to cell bodies in CA3 pyramidal layer and DG hilus in addition to the neuropil. Scale bars: 40μm in x10 images (Cii and Dii), 20μm in x20 images (Ai-Di and Aii and Bii), 10μm in x40 images (Aiii-Diii).

5.3.2 Electrophysiology control slices

In control EP slices (holding chamber or recording chamber but exposed to KA only) the results were not as clear as in the naïve horizontal sections. The background staining in the negative control sections appeared much stronger. In the sections incubated with patient CSF, the staining was much less bright and much “flatter”. The punctate pattern of staining was not seen at high magnification. The appearance of the neuropil was also less healthy: the surface of the sections appeared irregular with numerous small tears, giving it the appearance of cracked glass (see Figure 5.3). This was felt to represent freezing artefacts. This tissue damage is likely to be responsible for the high background in the negative control slices.

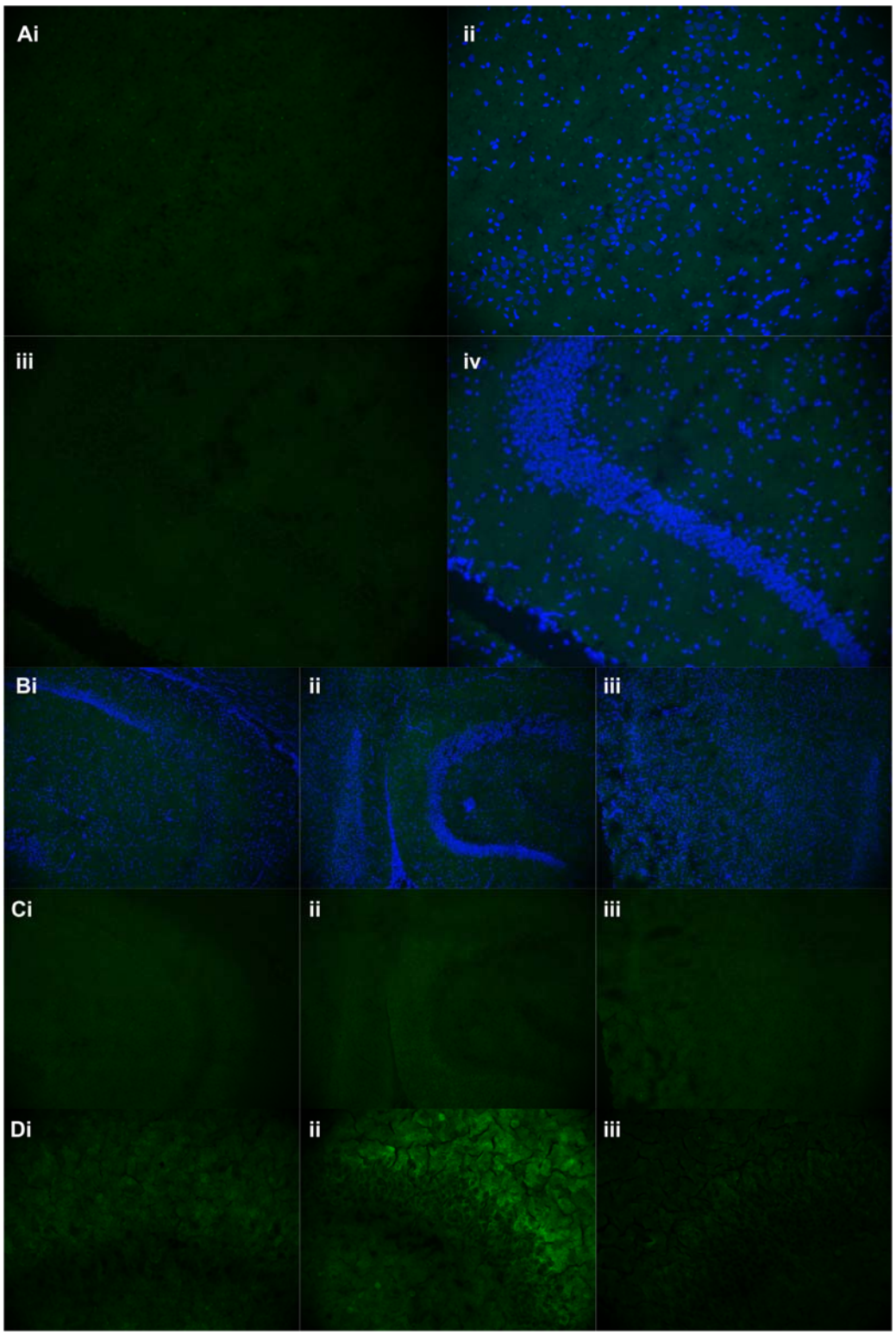

Figure 5.3 Patient CSF staining of slices used during electrophysiology experiments.

Negative control slices are shown in Ai-iv. Note the uniform background staining (A, CA3 x20, i: anti-human IgG IF alone, ii: merged DAPI and IgG IF; DG x20, iii: anti-human IgG IF alone, iv: merge with DAPI). Control EP slices incubated in patient CSF are shown in B-D. Low magnification images of the HPC and mEC (Bi-iii, x10, merged DAPI and IgG IF; Ci-iii corresponding anti-human IgG Ab IF only) show background staining only of the hippocampal neuropil. Higher magnification (x40) images of the same areas suggest there may be some specific NMDAR-Ab binding in the molecular layer of the DG in some sections (Dii, CSF 1:10) but not others (Diii, CSF 1:5). There does not appear to be any specific staining in CA3 (Di: CA3 x40, CSF 1:10)

5.3.3 The search for human IgG in slices used in electrophysiology experiments

Snap-frozen fresh tissue

In the first instance, the same protocol as above was used to attempt detection of IgG in EP slices. As the effect on the staining of the blocking step was uncertain, some sections underwent a one-hour blocking step in 10% NGS prior to incubation with fluorescent anti-human IgG, whilst others were simply incubated in 1:2000 secondary antibody overnight at 4°C.

For the patient IgG-exposed slices, a slice from a typical one-hour experiment as described in Chapter 4 was used. Briefly, this slice had been perfused with aCSF+KA containing 30μg/ml Pt3 IgG for one hour followed by a 30-minute wash in aCSF+KA. To investigate the effect of more prolonged exposure to patient IgG, a slice pre-incubated with 30μg/ml Pt3 IgG for 5 hours at room temperature and then placed on the EP rig and perfused with 10μg/ml Pt3 IgG for 3 hours at 32°C was also used. The control slice used had been stored in the holding chamber before being frozen and had therefore not been exposed to either KA or human IgG.

There was no NMDAR-specific staining pattern comparable to the CSF staining described in section 5.3.1 in either section (see Figure 5.4 A). The presence of the blocking step did not seem to impact the staining, with similar non-specific background staining in the two groups of slices.

The experiment was repeated with a short fixation step (3% formaldehyde for 2 minutes) in half the sections prior to incubation with anti-human IgG antibody because of concerns that the washing steps following the incubation with secondary antibody might lead to loss of subtle NMDAR-specific staining. The secondary antibody incubation period was also shortened (30 minutes at room temperature) to reduce non-specific staining. Similar slices were chosen for the staining. Again, there was no NMDAR-specific staining in any of the patient IgG-exposed sections, whether fixed or not (images not shown). In fact, non-specific background staining was brighter and more obtrusive in the sections that had undergone light fixation.

To prevent loss of bound antigen-secondary antibody complexes in the absence of fixation, the washes following the incubation in secondary antibody were shortened significantly to three thirty-second washes. The secondary antibody used was changed to a red-fluorescent goat anti-human IgG (AlexaFluor 568) as it was felt this may reduce the intensity of the background staining, and several dilutions of this antibody were trialled.

Sections from a slice exposed to 30µg/ml Pt3 IgG for one hour (ca. 40% reduction in gamma-frequency oscillation power) and from a slice exposed to HC2 IgG 10µg/ml were incubated in 1:700, 1:2000 or 1:6000 Alexa Fluor 568 goat anti-human IgG. No NMDAR-specific staining was detected in the Pt3-perfused slices. The secondary antibody dilution did not appear to affect the intensity of the non-specific staining (see Figure 5.4 B).

Finally, a very prolonged incubation in the secondary antibody was undertaken. Sections prepared from slices perfused with 30µg/ml Pt3 IgG and 10µg/ml HC1 IgG were incubated for 72 hours at 4°C with fluorescent goat anti-human IgG at either 1:2000 or 1:6000 dilution. This also failed to detect any NMDAR-specific labelling in the patient IgG-perfused slices (see Figure 5.4 C).

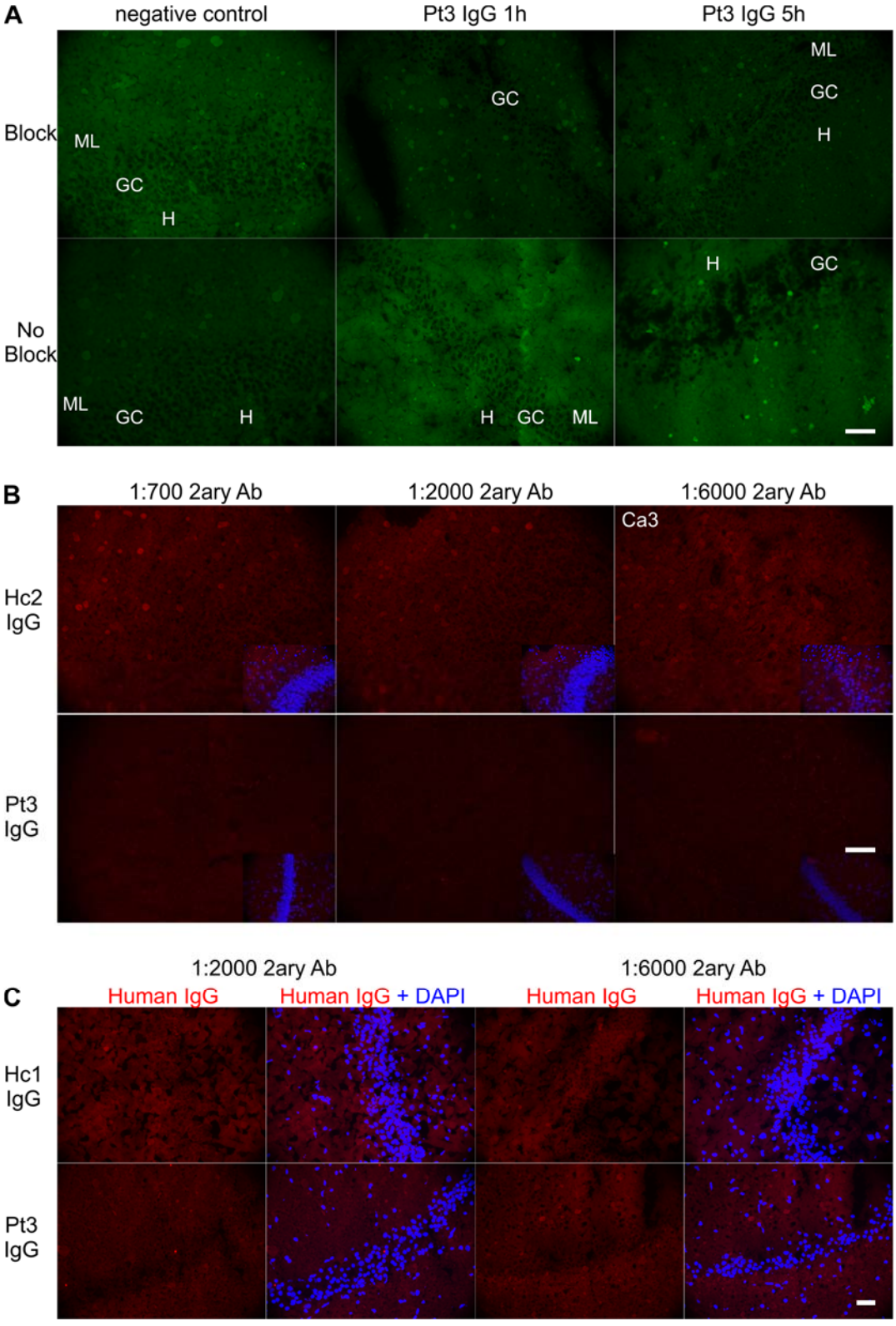

Figure 5.4 No anti-human IgG antibody binding is present in snap-frozen slices from EP experiments.
All images are from dentate gyrus unless otherwise indicated. The results of the standard protocol are illustrated in A: there was no NMDAR-Ab specific staining in slices exposed to pIgG for 1-5 hours, and removing the blocking step had no effect. Using a secondary antibody with a different excitation wavelength, varying the duration of incubation in 2°Ab (both B), and prolonging incubation time (C) also had no effect. GC: granule cell layer of DG, H: hilus, ML: molecular layer. X40 magnification, scale bars 10μm.

Table 5.1 Summary of changes to standard immunofluorescence protocol and their effect

Steps in IF protocol	Basic Protocol	Adaptations	Reason	Effect
In control tissue from whole perfused fresh-frozen brain				
Slice thickness	≤10μM	12-20 μM	To minimise tissue loss	No difference in patient CSF binding pattern
In EP slices				
Fixation	None	3% PFA 1-2 minutes in some slices	To reduce antigen loss	⇑ non-specific background
Block	10% normal serum	Not done in some slices	To minimise steps preceding 2°Ab incubation	No effect
Washes	PBS 10 minutes x3	⇓ to 30 seconds x3	To reduce antigen loss	No effect
Secondary antibody				
Dilution	1:2000	1: 700; 1:2000: 1:6000	⇓ dilution to improve detection of subtle binding	No effect
			⇑dilution to reduce non-specific binding	No effect
Incubation Time	Overnight at 4°C	15 and 30 minutes at room temperature	⇓ duration to reduce non-specific binding and ⇑ temperature to reach equilibrium of antigen-antibody reaction faster	No effect
		72 hours at 4°C	⇑ duration to saturate antigen with antibody	No effect

Fixed tissue

The quality of the tissue used for the immunofluorescence experiments is of paramount importance in obtaining valid results. As mentioned above, there was a clear difference in the quality of the sections obtained from the snap-frozen whole brain of a naïve rat and the EP slices. The whole brain was much easier to slice and the sections displayed very little damage. On the other hand, the frozen EP slices were often not flat despite efforts and therefore difficult to re-section on the cryostat, resulting in tissue loss and tears. This “geographical” damage rendered the sections prone to presenting uneven staining patterns. Also there was often marked freezing artefact in the EP slices, presumably caused by the slices being frozen whilst wet (straight off the perfusion chamber). The artefact was not present in slices from the whole brain, the surface of which has remained relatively “dry” during the perfusion process. The freezing artefact gave the tissue an appearance like cracked glass and also resulted in irregular background staining. Whether human IgG could be detected in fixed tissue was therefore investigated, as fixation might circumvent both the tissue damage and loss caused by snap-freezing and subsequent cryostat slicing, and the possible loss of antigen during the IF process. Here, slices were fixed in 4% paraformaldehyde (PFA) immediately after EP experiments, cryoprotected in 30% sucrose, then re-sectioned to 40μm thickness on a freezing stage microtome before being incubated with the anti-human IgG antibody. The sections were examined by confocal microscopy.

Using this technique, anti-human IgG binding was detected in scattered cells in cortex and hippocampus (see Figure 5.5 and 5.6). The binding appeared to be located in the cytoplasm of the cells. This staining was faint and present in both cIgG and pIgG-exposed slices but not in control slices (n=5 Pt3 IgG slices, n=3 HC2 IgG). No clear pattern of binding was noted: the visual intensity of staining as well as the number of bound cells varied from section to section, but did occasionally appear brighter in cIgG-exposed slices (see Figure 5.7). No systematic analysis of binding intensity was undertaken as the staining was very subtle. The areas with the greatest density of cells with bound IgG were the perirhinal cortex and auditory cortex as well as the hilus of the dentate gyrus. Cells were less often detected in entorhinal cortex and pyramidal layers of the HPC. No cells were seen in the granule cell layer of the DG. This

distribution is unlikely to be related to the orientation of the slice in the perfusion chamber as this varied for each experiment and also would not explain the presence of bound cells in both peripheral (e.g. perirhinal cortex) and central areas of the slice (e.g. hilus of DG). Both antigen retrieval and lower dilutions of the secondary antibody (1:200) resulted in brighter staining, albeit in the same distribution as described above. The typical neuropil pattern of staining was not detected. No double-labelling was performed so the nature of the cells taking up human IgG is not known.

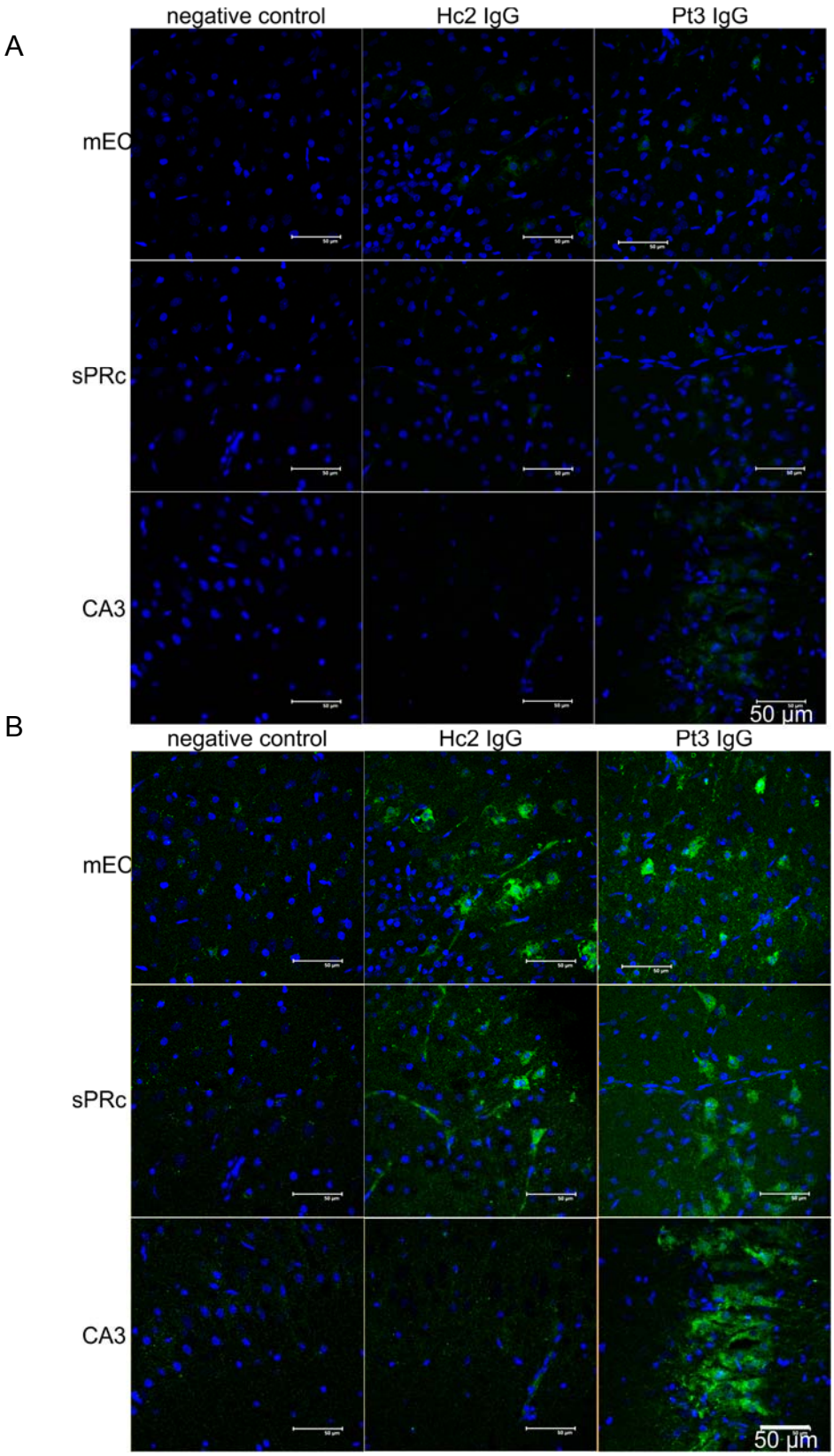

Figure 5.5 Intracellular binding of anti-human IgG antibody in EP experiment slices in fixed tissue.
Unadjusted images are shown in A and corresponding enhanced images in B for clarity. Subtle staining of individual cells is visible in several areas of the neocortex and as well as pyramidal layer of HPC. Bound cells are present equally in neocortex sections from slices exposed to cIgG and pIgG; in HPC human IgG reactivity appears limited to slices exposed to pIgG. Magnification x63; scale bars 50µm; mEC-medial entorhinal cortex, sPRc-superficial perirhinal cortex, CA3-Cornu Ammonis 3 subfield of HPC.

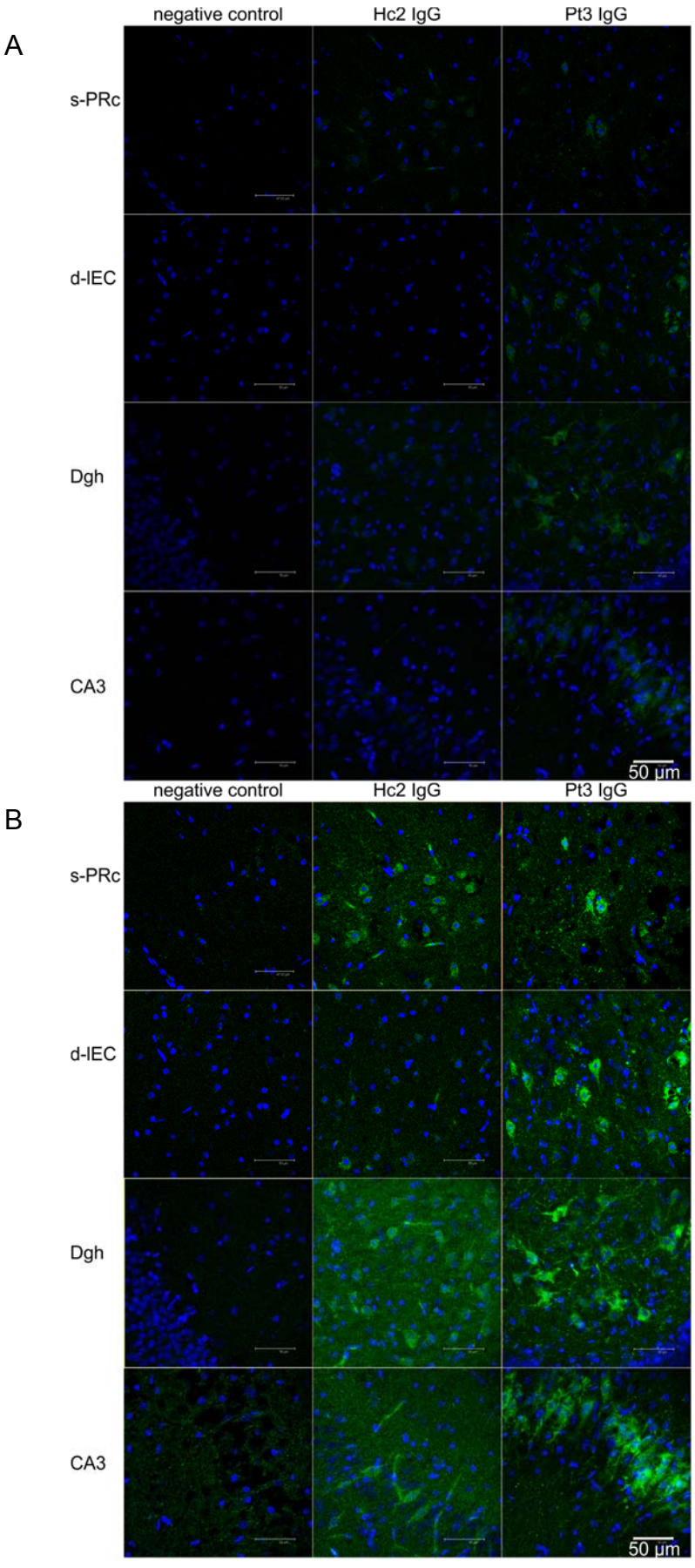

Figure 5.6 Intracellular binding of anti-human IgG antibody in EP experiment slices in fixed tissue. Unadjusted images are shown in A and corresponding enhanced images in B for clarity. Subtle staining of individual cells is visible in several areas of the neocortex and as well as pyramidal layer of HPC and hilus of DG. Bound cells are perhaps more prominent in sections from slices exposed to pIgG. Magnification x63; scale bars 50µm; sPRc-superficial perirhinal cortex, d-lEC- deep lateral entorhinal cortex, DGh – dentate gyrus hilus, CA3-Cornu Ammonis 3 subfield of HPC.

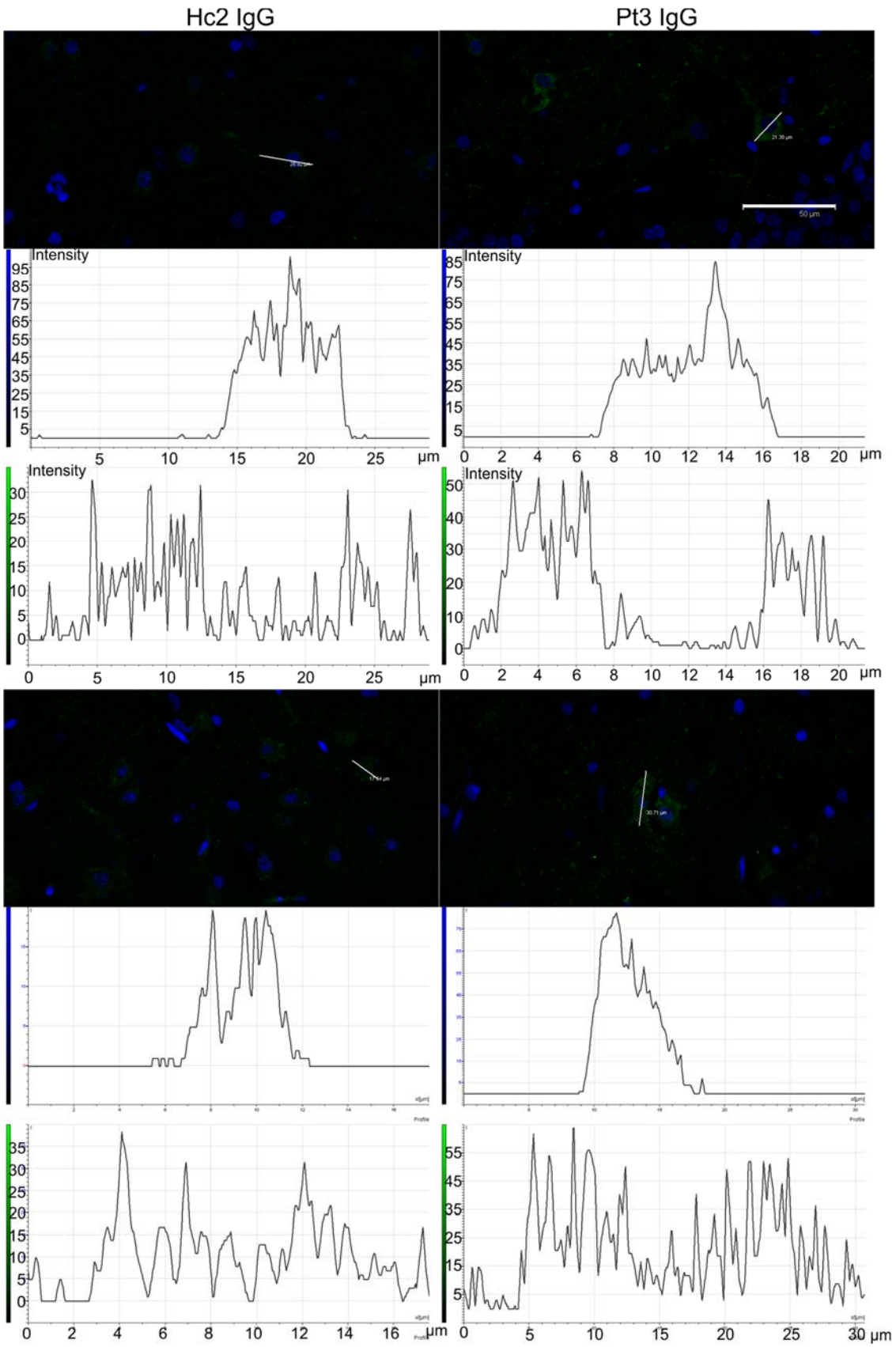

Figure 5.7 Brighter intensity of staining in cells in pIgG-exposed slices. Measurement of pixel intensity in a random selection of cells exhibiting intracellular binding of anti-human IgG antibody reveals brighter staining in pIgG slices although this has not been performed systematically. Scale bar 50µm.

5.4 Conclusion

5.4.1 Remarks on fresh-frozen tissue IF

No binding to human IgG was detected in slices snap-frozen immediately after EP experiments. As mentioned in Chapter 4, the IgG concentrations used in the EP experiments were low when compared to those used in studies describing the binding pattern of NMDAR-Abs in patient CSF or serum (Hughes *et al.*, 2010).

Several methodological factors may influence the detection of subtle specific staining by immunofluorescence. The concentration of the antigen against which the secondary antibody is raised is obviously pertinent. The experience of the Oxford lab is that incubating control rodent brain section with CSF from patients with NMDAR-Ab encephalitis gives much stronger and more specific fluorescence patterns than using serum or purified IgG. This is probably related to the more propitious NMDAR antibody:total immunoglobulin ratio in CSF than serum. Whilst the IgG concentration in serum and CSF are around 10,000µg/ml and 25µg/ml respectively, that is a 400-fold difference, titration studies have shown that the NMDAR antibody concentration may only be around 10-fold lower in CSF than serum (Prof. A Vincent, personal communication). The smaller NMDAR antibody:total immunoglobulin ratio in the purified IgG used to perfuse the slices may mean that a smaller proportion of NMDAR in the EP slices are bound compared to control slices exposed to NMDAR-Ab-positive patient CSF.

Several attempts at reducing background staining or antigen loss by varying the blocking step, the concentration and duration of incubation with secondary antibody, the duration of washes or introducing a brief post-fixation step all failed to reveal the presence of anti-human IgG in the EP slices.

This may be because perfusion for one hour with relatively low concentrations of IgG was not sufficient to allow penetration of the antibodies into the slice and binding with NMDARs. Gamma-frequency oscillations are recorded by placing the tip of the recording electrode on the surface of the slice, causing as little damage to the tissue as possible, so that only slice surface binding should be required to see an effect on oscillation parameters. The other more likely explanation is that the lack of staining was related to the poor quality of the

fresh-frozen tissue used here. Indeed, there was significant freezing artefact and tissue loss in the sections obtained from re-sectioning the EP slices on a cryostat. This was associated with increased background staining and absence of the typical NMDAR-Ab binding pattern in slices exposed to patient CSF in comparison to sections from snap-frozen perfused whole-brain.

5.4.2 Remarks on fixed tissue IF

In slices re-sectioned from PFA-fixed EP tissue, human IgG was detected in the cytoplasm of individual cells in both pIgG and cIgG-exposed slices. This was not the pattern expected with NMDAR-Abs, which bind surface NDMARs. However, binding in the EP slices may not follow the pattern predicted by *in vitro* experiments due to cross-linking and internalisation of the antibody-antigen complex (Hughes *et al.*, 2010; Mikasova *et al.*, 2012). Nevertheless, the presence of human IgG in both pIgG and cIgG-exposed slices suggested this might also represent non-specific binding.

Indeed, in addition to the NMDAR-Ab concentration and perfusion duration issues discussed above, another major barrier to detecting NMDAR-Ab binding in EP slices is the damage to the surface of each slice caused by the cutting process. Each EP slice has a layer of dead and damaged cells on both the rig-contacting surface and the surface exposed to the perfusion medium. In order to reach and bind to NMDAR on live neurons in the slices, NMDAR-abs in the purified IgG would need to diffuse through these layers. It is likely that IgG binding to, and diffusion or uptake through, damaged cell membranes on the surface of the EP slices would take place. This would be detected by the anti-human IgG secondary antibody in both pIgG- and cIgG-exposed slices, potentially concealing any specific NMDAR-Ab binding in the pIgG slices.

Immunoglobulin uptake into neurons has not been extensively studied but recent studies have demonstrated this in neuronal cultures, organotypic slice cultures and human brain biopsy material (Hill *et al.*, 2009; Geis *et al.*, 2010; Congdon *et al.*, 2013; Iffland *et al.*, 2013). Hill *et al.* (2009) found IgG from healthy individuals in the dendrites and processes of cerebellar Purkinje cells after 4 hours of incubation and within the cell body cytoplasm and nuclei by 24 hours in organotypic cultures of rat cerebellum. This did not affect the viability of the Purkinje cells. Other cell types in the cultures were not reported to

incorporate IgG. Congdon *et al.* (2013) demonstrated much faster neuronal IgG uptake, showing that maximal internalisation of IgG occurred within 30 minutes of incubation of organotypic hippocampal slice cultures prepared from 400μm mouse hippocampus sections. The uptake was concentration-dependent, saturable and temperature dependent, with a significant reduction if the temperature was reduced to 4°C. However, the internalised IgG consisted mostly of specific antibodies targeting intracellular antigens (in this case Tau antibody in cultures from mice with high levels of intracellular tau). Intracellular control IgG was found in both wild-type and high-tau mice, but the levels were 91% lower than those of tau antibody in slices from the high-tau line. The authors felt this might partly be related to more rapid clearance of unbound IgG out of neurons. Of note, about a third of the uptake was through damaged cell membranes, caused by sectioning the HPC into 400μm sections.

Similar results have been obtained by others (Geis *et al.*, 2010; Greenlee *et al.*, 2014): IgG internalisation was seen with sera or purified IgG containing intracellularly-directed antibodies, and much less so with control IgG or serum from which intracellularly-directed antibodies had been pre-adsorbed. The antibodies targeting intracellular antigens in these preparations cannot have been preferentially internalised by an epitope-dependent mechanism, as the epitopes were internal and therefore invisible. It is therefore likely that targeted and untargeted IgG had both been taken up and the same mechanism of clearance of unbound internalised IgG had occurred.

The relevance of the intracellular human IgG detected in EP slices is therefore still unclear. The nature of these cells remains to be determined, as does the role of cell membrane damage due to slicing. Other unanswered questions pertain to the epitope-specificity of the process: is the uptake at the level expected for control IgG internalisation in the studies above? Does it reflect retention of antibodies against cytoplasmic or nuclear antigens in the two samples? Of note, neither of the two samples had anti-nuclear antibodies. Visually, the intensity of staining appeared somewhat brighter in the pIgG slices although this was not examined systematically.

5.4.3 Further work

It was not possible to detect human IgG in the NMDAR-Ab-specific pattern in the slices exposed to pIgG in EP experiments. Some intracellular human IgG was found in fixed and permeabilised slices exposed to pIgG and cIgG, but the functional relevance of this is unknown. This latter finding may be worth some further attention. The nature of the cells taking up the IgG could be determined using double-labelling studies and the functional consequence of IgG internalisation could be examined by Western blot analysis of NR1 content in the slices. However, at this juncture, a modest reduction in γ-power in the mEC *in vitro* and no definite NMDAR-Ab binding have been observed. It therefore seemed important to develop a method that would definitively deliver NMDAR-Abs to the target tissue and allow enough time for receptor internalisation to take place. In the next chapter, the effect of intracerebral injection of pIgG on γ-frequency oscillations *in vitro* 1-3 days after injection will be examined.

Chapter 6 The effect of subacute exposure to NMDAR antibodies on γ-frequency oscillations *in vitro*

6.1 Introduction

The acute exposure of rodent brain slices to NMDAR-Abs as performed in Chapters 4 and 5 did not result in unequivocal binding to NMDARs. There are several potential reasons for this finding. Firstly, the combination of the large size of immunoglobulin G molecules and the thickness of the slices (450μm) may preclude sufficient diffusion of the antibodies through the slice in the space of a one-hour experiment. Secondly, the concentration of NMDAR-Ab in 10 or 30μg/ml purified IgG may well be too low to reveal the typical reactivity pattern seen in 10μm section incubated with patient CSF at 1:10 dilution (especially relative to the much larger number of NMDAR in a 400μm thick slice). Finally, rather than the surface binding detected by immunofluorescence in frozen slices, IgG internalisation may be taking place in the live rodent brain slices used in this study. An additional factor to contend with is the mechanism of action of the NMDAR-Abs in the acute slices. Whilst a subtle (19%) but significant amount of NMDAR internalisation has been observed in cultured hippocampal neurons incubated with highly dilute patient CSF (1:300) after two hours in one study (Mikasova *et al.*, 2012), (but see Moscato *et al.* (2014) for contrast), these neurons have much better access to the NMDAR-Abs in the incubation medium than neurons in brain slices. Not only are cells more densely packed in the brain slice preparation, the cutting process damages cells on the surface of the slices so that any perfused agent has to diffuse through a layer of dead or unhealthy cells before reaching viable targets for its action. The occurrence of functionally significant internalisation over the one-hour period of perfusion in the acute experiments is therefore in question. Therefore, in order to provide more certain and more prolonged antibody delivery to the mEC, animals were subjected to a single intracranial injection of NMDAR-Abs in the form of patient's purified plasma IgG.

Several rodent passive transfer studies of autoimmune CNS disorders exist, showing variable and incomplete reproduction of clinical syndromes. Geis et al (Geis *et al.*, 2010; Geis *et al.*, 2012) showed that several intrathecal injections of IgG from patient with amphiphysin antibodies over 16 days resulted in stiffness, muscle spasms and anxiety in rats. Amphiphysin antibody binding to relevant

brain structures was also demonstrated. Shorter injection protocols have also shown promise, with a single intracerebroventricular injection of glycine-receptor antibodies, in the form of IgG purified from the serum of patients with progressive encephalomyelitis with rigidity and myoclonus, resulting in anxiety-like behaviours in mice (Carvajal *et al.*, 2015). A single intrathecal injection of antibodies against the metabotropic glutamate receptor type 1 has also been shown to cause acute and reversible ataxia in mice with strong binding throughout the cerebellum (Sillevis Smitt *et al.*, 2000). Finally, a single intracerebroventricular injection of NMDAR-Ab positive IgG decreased the seizure threshold of mice and was associated with significant NMDAR-Ab binding in structures surrounding the ventricle, including dentate gyrus and CA3, in the pattern expected for NMDAR-Abs 48 hours after the injection (Wright *et al.*, 2014).

It therefore seemed sensible to investigate whether a similar intervention in rats would lead to changes in γ-frequency oscillations in the mEC. Intracerebroventricular injections of pIgG and cIgG were performed in rats using increasing volumes of IgG, but no binding in structures adjacent to the ventricle was noted. Furthermore, the distance from the ventricle to the mEC is sizeable. Because of concerns that diffusion of the antibodies to the mEC would not occur even if larger volumes of IgG were used, intraventricular injections were abandoned in favour of direct intra-entorhinal injections.

Direct intracerebral injection of IgG has also been shown to have both functional and behavioural effects in passive transfer models of CNS autoimmune diseases. Saadoun et al (2010) found that injections of aquaporin-4 antibody-containing IgG with complement into one cerebral hemisphere caused axonal injury with myelinolysis after a single injection and full neuromyelitis optica lesions on the injected side after three injections. This was accompanied by preferential ipsilateral turning of the mice. Coesman et al (2003) delivered metabotropic glutamate type 1 receptor-antibody positive patient IgG to the flocculus of the cerebellum of mice by osmotic minipump and observed an eye movement disorder. Finally, acute infusion of NMDAR-Abs over five minutes into the prefrontal area of the rat neocortex has been shown to increase extracellular glutamate concentration within 30 minutes of infusion (Manto *et al.*, 2010) consistent with disinhibition of excitatory neurons as seen

with NMDAR antagonists Moghaddam *et al.* (1997). This last finding in particular is of relevance to this study, as it suggests an effect on GABA-ergic inhibitory interneurons, which are essential in the generation of γ-oscillations. Indeed, if significant internalisation of NMDARs occurs in the mEC of animals injected with pIgG, one might predict reduced excitatory drive to these interneurons. This in turn would lead to less efficient recruitment to γ-rhythmogenesis, and therefore less powerful oscillations.

First, the distribution of human IgG following a single intra-entorhinal injection of patient or control IgG will be described. Then, effects on baseline γ-oscillations in entorhinal cortex and their NMDAR-sensitivity will be examined. Finally, NMDAR-mediated synaptic transmission will be investigated using sharp-electrode intracellular recordings.

6.2 Methods

Male Wistar rats weighing 250-280g received a single intra-entorhinal IgG injection as described in Chapter 2. 5μL of either pIgG or cIgG (undiluted, concentration around 12mg/ml for all samples used) was injected at a rate of 0.250μL/minute. A very small volume of fluorescent beads was co-injected to permit rapid localisation of the injection site both visually during EP experiments and for IF. Injections were carried out blinded for IgG type but in pairs so that the first the first cohort of rats received either Pt2 or HC2 IgG, and the second cohort received either Pt3 or HC1 IgG.

Slices for electrophysiological experiments were prepared as previously described 1-3 days after the intra-entorhinal injection. Only slices containing a visible injection site in the mEC were used. Slices from the un-injected right side were used as controls. Entorhinal cortex γ-oscillations were generated by adding KA to the perfusion medium (aCSF) to a concentration of 400nM. Once oscillations had stabilised (power and frequency values in four consecutive recordings within 30 minutes changing by less than 20%), 50μM D-AP5 was added to test the NMDAR sensitivity of the oscillations.

For intracellular recordings, non-oscillating slices were used. Here, a bipolar stimulating electrode was placed in the most medial portion of the mEC in the same layer as the injection site. The position of the stimulating electrode was

adjusted so that the distance between the stimulating and recording electrode remained constant in each slice. Cells were identified from their electrophysiological properties and this was later matched to their morphological characteristics using biocytin immunocytochemistry. Baseline membrane properties were examined as well as the size of the NMDAR-mediated component of evoked EPSPs. These were obtained by blocking other components of the membrane response to stimulation (AMPA/KA receptor-mediated portion of EPSP blocked by 20μM NBQX, $GABA_A$ and $GABA_B$ IPSPs following the EPSP blocked with 1μM Gabazine and 1μM CGP55845 respectively). The cell membrane potential was held at -70mV during the EPSP recordings. Stimuli were delivered at 1Hz for 10 seconds for each stimulus voltage used (1, 2, 5, 7, 10, 12, 15 Volts) and the recording set up so that each one-second sweep was averaged with the previous sweeps so that a single averaged EPSP was obtained for each stimulus voltage. Peak amplitude (mV) and slope (mV/s) during the initial segment were measured. For EPSPs, once the stimulus was large enough to elicit a spike, it was no longer possible to reliably measure amplitude or slope and these EPSPs were excluded from the analysis. Occasionally, it was clear that spiking only occurred after 1 or only a few stimuli. In these cases, the stimuli were repeated individually and measurements were taken only when the stimulus was not followed by a spike.

To determine the distribution of human IgG in the injected slices, slices were placed in 4% PFA immediately after an EP experiment. On the day of the IF procedure, the slice was cryoprotected in 30% sucrose, re-sectioned on a freezing-stage microtome, washed and then incubated with anti-human IgG antibody overnight, before being mounted in DAPI-containing fluorescent mounting-medium and coverslipped. For colocalisation studies, primary antibodies to CAMKII, PV, calretinin, calbindin, somatostatin, GAD 67 and GABA were used before incubation with appropriate secondary antibodies as well as anti-human IgG Ab.

6.3 Results

6.3.1 Accuracy of injection and surgical complications

In total 62 male Wistar rats weighing 250-280g received a single intracerebral injection into the left mEC. The first two animals were injected with FITC-

conjugated dextran (molecular weight (m.w.) 500000 Da; compared to IgG: m.w. 150000 Da) to examine the extent of diffusion of large molecular weight molecules in brain *in vivo*. Both animals received 10μL at a rate of 250nL/min. One animal did not recover from anaesthesia and it was felt that the large volume of the injection may have caused pressure on the brainstem and thus reduced respiratory drive. After this, the injection volume was first reduced to 3 μL and then increased to 5μL in all experimental animals, as this was well tolerated. The animals responded well to being returned to their home-cage post-operatively and no aggressive behaviour towards cage-mates was noted. No obvious change in behaviour and no visible seizures occurred whilst the animals were observed (during examinations and during cage-cleans and cage-changes by animal housing unit staff). Mild weight loss took place in the day or two following surgery in half the animals, but this did not exceed 10% of pre-surgery body mass and recovered in those animals not killed before post-operative day 2.

Figure 6.1 shows the distribution of FITC-dextran dye in the brain following a single intra-entorhinal injection on the left. This image is from the brain of the animal that died during the procedure and thus was not perfused with PBS prior to removal of the brain. Despite the blood vessels, a yellow discoloration of the whole ventro-caudal pole of the forebrain can be seen on the left. In the insets are images taken during slicing of the brain of the animal that survived the procedure. Here, the yellow discolouration caused by the FITC-conjugated dextran can again be seen with the naked eye. It is present throughout the medial portion of the mEC where the injection is sited and spreads laterally along the white matter separating the HPC and neocortex.

The injection was misplaced in four of the 56 animals whose brains were used in EP or IHC experiments. In two animals no injection site was visible and in another two, it was too rostral, either in the subiculum or in the white matter separating the cortex and hippocampus. These four animals were excluded from the study. In the remaining 54 animals, the location of the injection site within the entorhinal cortex varied, presumably because of variation in the size of each individual rat. The position of the injection varied both along the medio-lateral axis and rostro-caudal axis (i.e. layer of mEC) but all animals in which the injection was sited within the mEC were kept in the study. For γ-oscillation

assessments, recordings were made in layers II and III only, irrespective of the layer in which the injection site was found. For intracellular recordings, the electrode was placed as close as possible to the injection site.

6.3.2 Detection of human IgG in injected rat brains

NMDAR-Ab negative control IgG bound to individual neurons and neuropil surrounding the injection site one to three days after injection, but no binding and no fluorescent beads were detected on the un-injected side (Figure 6.1). In five of nine animals studied, anti-human IgG immunofluorescence was present as a faint rim around the injection site, extending radially by about 20-30 μm. Occasionally, faintly labeled cell bodies were also visible near the injection site (see Figure 6.1 Cii). In one animal (day 3 post injection), such faintly labeled cell bodies were seen further afield as well. In two animals no anti-human IgG binding could be detected. In a further two animals strong anti-human IgG reactivity was detected around the injection site with some strongly bound cell bodies within 20-30 μm from the injection site and some weakly labeled cells further afield (e.g. Figure 6.1 Di and ii).

A similar pattern of binding was detected in slices from animals injected with pIgG (Figure 6.2). There were no beads and no fluorescence in the uninjected side (see Figure 6.2 C). Anti-human IgG antibody fluorescence was present as a rim around the injection site in nine of the ten animals studied. In one rat, no anti-human IgG was detected by IF. In six animals the reactivity was faint, and accompanied by faintly stained cells extending up to 50μm from the injection site (Figure 6.2, Ai-iii), as well some faintly stained cells further afield (in three animals, e.g., in deeper layers of the mEC and in one case in the subiculum below the mEC, see Figure 6.3). In the remaining three animals (of note, these had all received Pt3 IgG), brightly stained cells could be seen around the injection site and also extending down below the injection site into the deeper cortical layers. These cells had the appearance of neurons, with visible apical or basal dendrites. These dendrites were also moderately brightly stained and could be followed as they extended into the superficial layers of the mEC (Figure 6.2 B).

A number of brains were not used for EP experiments, but were snap-frozen after PBS perfusion. No difference in staining pattern between fixed tissue and

fresh-frozen tissue was noted, confirming that the reactivity seen in fixed slices was not due to fixation of unbound antigen. Also, no differences in distribution of human IgG in brains examined at days 1 to 3 could be detected in either cIgG or pIgG-exposed animals.

Overall, the intensity of human IgG antibody-binding appeared highest in sections from pIgG-exposed animals, although this difference was entirely attributable to the binding pattern seen in Pt3-exposed slices. Similarly, labelled dendrites were only seen in Pt3 IgG slices. In all other slices, variable intensity of binding in the area immediately surrounding the injection site was noted.

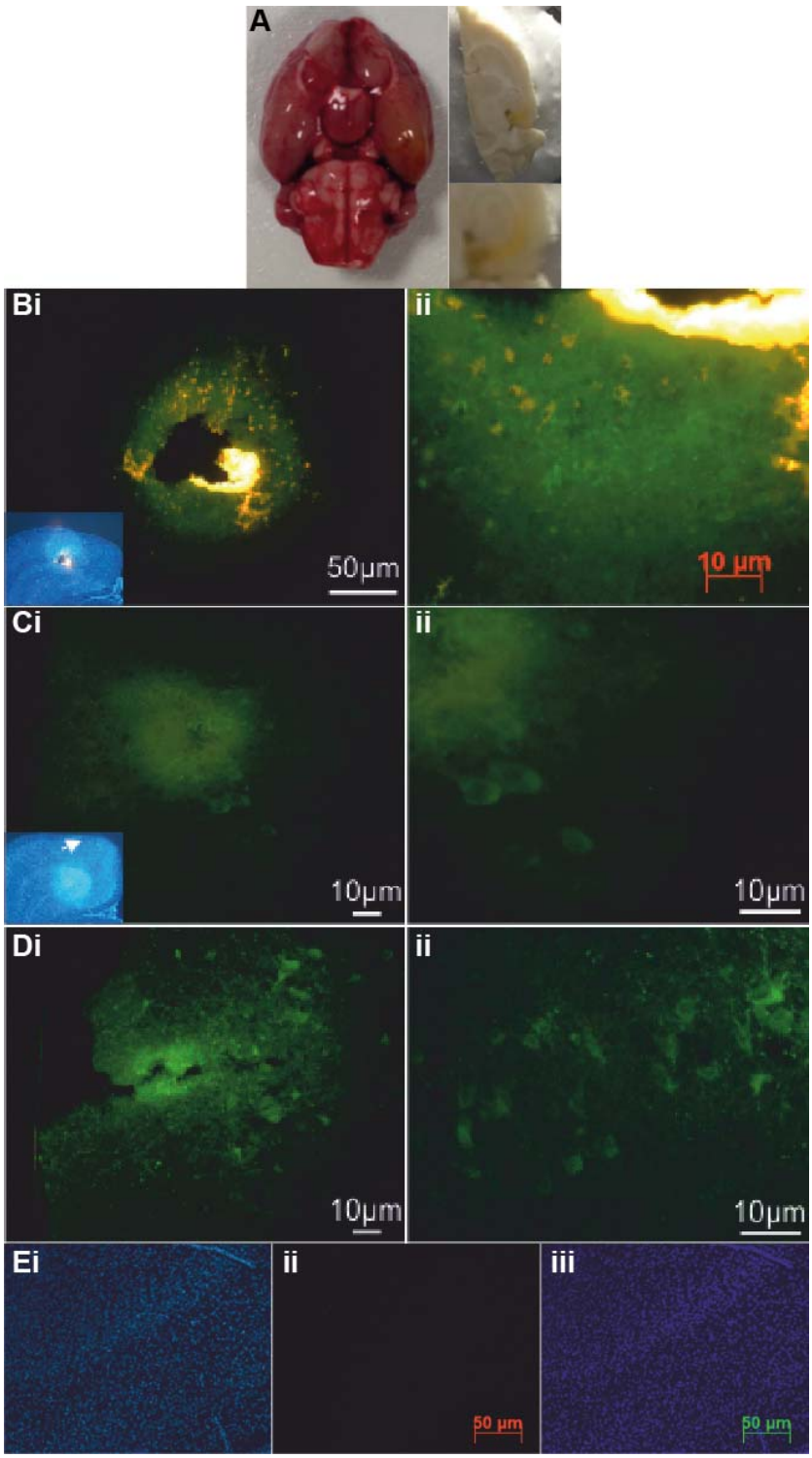

Figure 6.1 cIgG binds to individual neurons and neuropil surrounding the injection site.
Injection of large molecular weight fluorescent dye (A) suggested good diffusion throughout the mEC. In most animals receiving cIgG, anti-human IgG fluorescence is present as a faint rim extending 20-30µm around the injection site (B and C, Bi x10 with inset showing injection in layer 3 mEC, yellow= fluorescent beads, Bii x40, Ci x20 with inset showing injection in layer 1 (white arrow)) with occasional faintly stained cell bodies nearby (Cii, x40). In some animals the anti-human IgG fluorescence was very strong with intensely stained cell bodies around the injection site (Di, layer 1 injection site (outer aspect of mEC to left of photograph)) as well more weakly stained cells further afield (Dii – x40 of cells in layer 2 lateral to injection site). No human IgG was detected in the un-injected side of the brain (layers 1-4 mEC, Ei DAPI x10, ii anti-human IgG x10, iii merge).

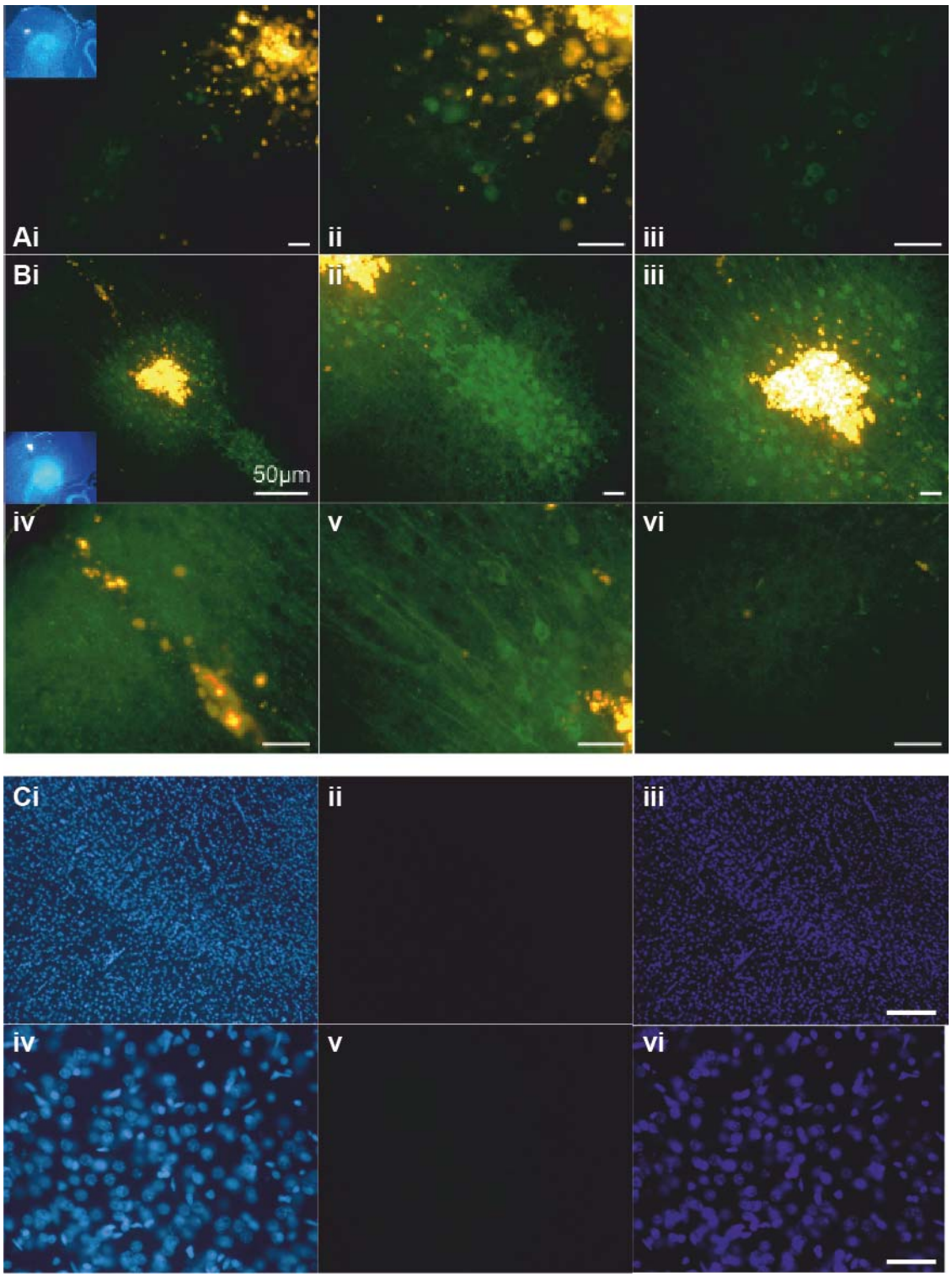

Figure 6.2 pIgG binds to cell bodies and neuropil surrounding the injection site. In most animals with pIgG injections, the anti-human IgG fluorescence is weak (Ai x20, with inset showing injection site in LII/III. Stained cells are visible around and below the injection site (Aii and iii, x40). In a few animals intense immunofluorescence can be seen in cells surrounding the injection site and extending below into deeper cortical layers (Bi, x10 with inset showing injection site in LII/III, ii and iii are x20, iv-vi are x40). Biv and v show bound axo-dendritic trees of the these neurons extending towards the brain surface with strong binding in layer I. vi illustrates the rapid decline in binding as distance from binding site increases. No human IgG is detected in the un-injected mEC (Ci-vi, i-iii are x10 and iv-vi are x40, i+iv are DAPI, ii+v are anti-human IgG IF, iii+vi are merge). Scale bars: 50μm on x10 images, 10μm on x20 and x40 images.

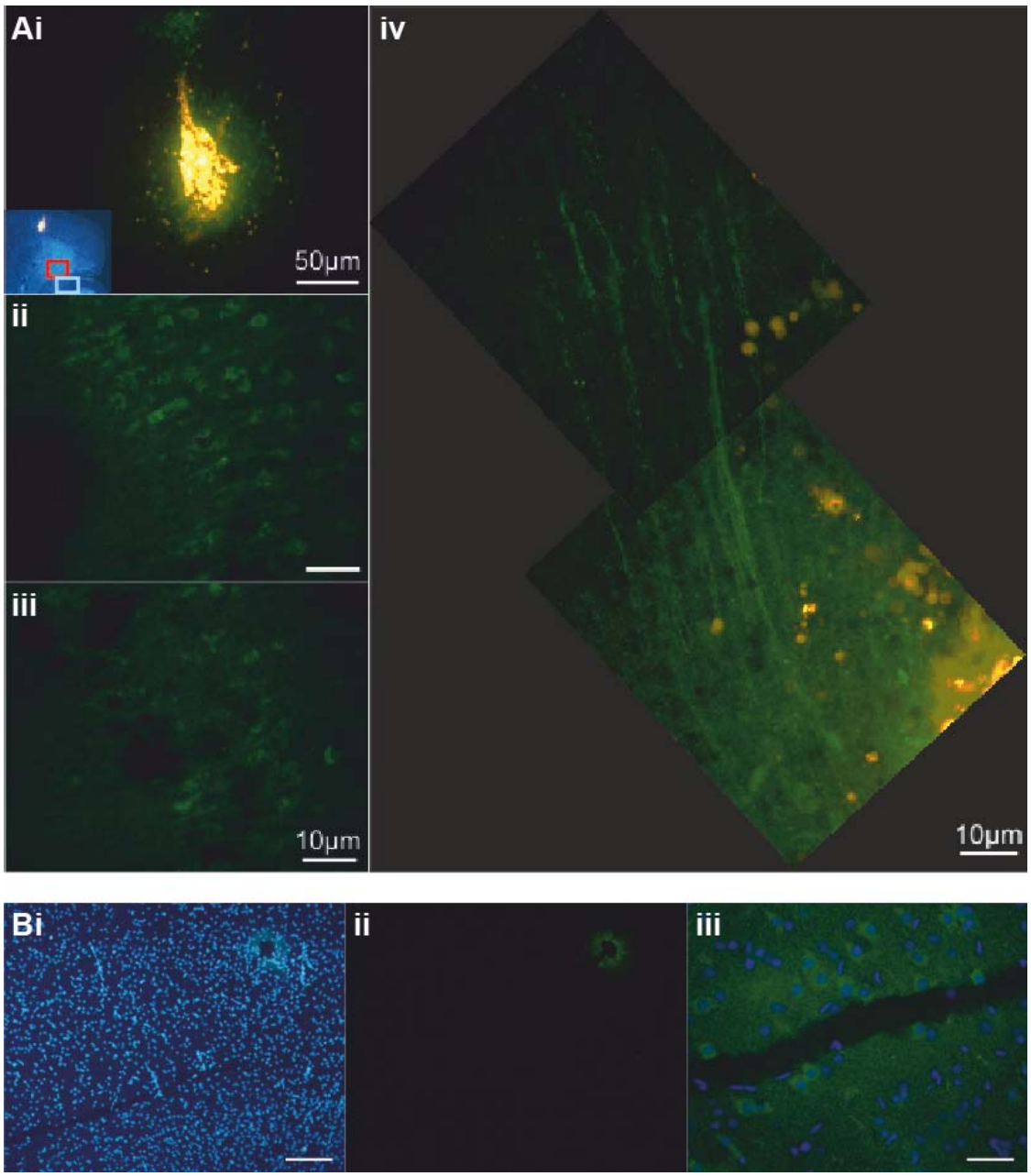

Figure 6.3 pIgG binds to cells distant from injection site and axo-dendritic tree of cells near injection site.

In some animals, faintly stained cells could be detected over 100μms away from injection site, as in A, where moderately bright IF can be seen within 50μm from the injection in layer 2 of mEC (i) and faintly stained cells were seen in the subiculum (ii) and molecular layer of DG (iii), indicated by red and blue rectangle respectively on the inset in Ai. Axons and dendrites running towards the superficial layers of the mEC are also bound near the injection site (Aiv, x40). Images in B show the same phenomenon in an animal with very faint anti-human IgG fluorescence after pIgG injection into layer 3 mEC.

6.3.3 γ-frequency oscillations in brain slices sub-acutely exposed to NMDAR-Abs

Baseline γ-oscillation characteristics

KA perfusion (400nM) generated γ-oscillations in 123 slices from 24 animals injected with either pIgG or cIgG. To compare the characteristics of γ-oscillations in pIgG and cIgG brains, the peak power, area power and frequency of γ-activity were recorded one hour after addition of KA to the perfusion medium. This time point was chosen as oscillation power and frequency had been observed to peak around this time in previous experiments. Oscillations with a peak power greater than 100μV^2/Hz were excluded from the analysis as outliers. Seventy-two of the slices were from the left side of the brain (injected side) and 51 from the un-injected right side. Pt2 (n=21 left-sided slices from 6 rats) and Pt3 IgG (n=21 left-sided slices from 7 rats) were used as a source of NMDAR-Abs, and both HC1 (n=16 left-sided slices from 6 rats) and HC2 (n=14 left-sided slices from 5 rats) as cIgG. For controls, slices from the un-injected right side of the brain dissected at the same level as the left-sided slices used (n=26 from pIgG brains, 12 rats; n=25 from cIgG brains, 10 rats), as well as 6 slices from two naïve animals were used. Experiments were carried out blinded to the nature of the IgG used in each animal. From here, left-sided slices from pIgG brains will be referred to as pIgG slices, left-sided slices from cIgG brains as cIgG slices and right-sided slices as control slices. There was no statistical difference between right-sided slices from pIgG and cIgG brains in peak power (unpaired t-test, t(21) = 0.2925, *p*=0.77), area power (t(21) = 0.697, *p*=0.49), or frequency (t(21) = 1.446, *p*=0.16).

The first cohort of rats received either Pt2 (n=21 slices from 6 rats) or HC2 IgG (n=14 left-sided slices from 5 rats, see Table 6.1 and Figure 6.4 A-C). Peak power in pIgG slices was lower than in control slices but not cIgG slices. There was also a trend towards lower area power in pIgG slices than control slices. There was no difference in oscillation frequency between the three groups.

Table 6.1 mEC γ-oscillation parameters in slices from animals exposed to Pt2 IgG, HC2 IgG and control slices

	pIgG (median ± *IQR*)	cIgG (median ± *IQR*)	Control (median ± *IQR*)	Kruskal-Wallis *H*	P	Dunn's MCT*	P
Peak power $\mu V^2/Hz$	3.6 ± 2.34-13.24	11.2 ± 3.99-38.9	10.94 ± 6.35-32.87	7.022	0.03	pIgG vs. control	0.035
Area power $\mu V^2/Hz.kHz$	0.143 ± 0.057-0.32	0.324 ± 0.116-0.833	0.343 ± 0.134-0.977	5.843	0.054	pIgG vs. control	0.066
Frequency Hz	45.86 ±12.79[$]	45.80 ±11.92[$]	48.11 ±11.06[$]	F(2, 55) = 0.253[§]	0.777		

* multiple comparisons test; [$] Mean ± standard deviation: [§] one-way ANOVA

Visual inspection of the pooled power spectrum obtained by averaging the power spectrum at 1 hour of KA perfusion for each Pt2 IgG slice revealed a wider spread of frequencies at half-maximal power (31.74 Hz) than in HC2 IgG slices (25.64Hz) or control slices (23.5Hz, see Figure 6.4 B and D), raising the possibility of diminished synchrony, although it was not possible to investigate this further due to time constraints.

The second cohort of rats received either Pt3 (n=21 slices from 7 rats) or HC1 IgG (n=16 slices from 6 rats, see Table 6.2 and Figure 6.4 D and E). Peak power in pIgG slices was larger than in control slices but not cIgG slices. There was no difference in area power between pIgG slices and either cIgG or control slices however. There was no difference in oscillation frequency between the three groups.

Table 6.2 mEC γ-oscillation parameters in slices from animals exposed to Pt3 IgG, HC1 IgG and control slices

	pIgG (mean ± *SD*)	cIgG (mean ± *SD*)	Control (mean ± *SD*)	ANOVA *F*	P	Tukey's MCT*	P
Peak power $\mu V^2/Hz$	29.62 ± 19.58	21.06 ± 15.25	15.79 ± 12.78	F(2, 62) = 4.582	0.014	pIgG vs. control	0.01
Area power $\mu V^2/Hz.kHz$	0.561 ± 0.443	0.568 ± 0.408	0.281	F(2, 63)= 2.613	0.081		
Frequency Hz	53.94 ±5.81	52.91 ±6.79	55.58 ±5.3	F(2, 63) = 1.150	0.323		

* multiple comparisons test

The apparent effect of subacute exposure to pIgG was therefore to disrupt γ-power in one cohort and potentiate it in the other (see Figure 6.4). When the two cohorts were combined (Figure 6.5 Ai-Ci), these effects cancelled each other out so that there were no differences in peak power, area power or frequency of mEC γ-oscillations between groups (see Table 6.3).

Table 6.3 mEC γ-oscillation parameters in slices from animals exposed to grouped pIgG, grouped cIgG and control slices

	pIgG (median ± *IQR*)	cIgG (median ± *IQR*)	Control (median ± *IQR*)	Kruskal-Wallis *H*	P
Peak power $\mu V^2/Hz$	13.24 ± 3.59-32.38	14.22 ± 5.95-38.54	13.00 ± 6.35-26.84	0.494	0.78
Area power $\mu V^2/Hz.kHz$	0.234 ± 0.110-0.514	0.394 ± 0.145-0.871	0.309 ± 0.140-0.535	2.135	0.344
Frequency Hz	49.99 ±10.56[$]	49.59 ±10.03$	52.21 ±9.12[$]	1.354[§]	0.508

[$] Mean ± standard deviation: [§] one-way ANOVA *F*

As mentioned above, the location of the injection site within the mEC varied because of the size of each animal. The immunofluorescence studies above demonstrated generally limited diffusion of the IgG around the mEC. Thus, NMDAR-Abs injected into the deep layers (layers IV-VI mEC) may not have reached the γ-generating fast-spiking interneurons in LII of the mEC. Baseline γ-oscillation power and frequency from pIgG slices with a superficial injection (LI-III, n=24 pIgG exposed slices) and a deep injection (LIV-VI, n=16 pIgG slices) were therefore compared (see Table 6.4 and Figure 6.5 Aii-Cii). There were no differences in peak power, area power, or frequency between slices with superficial or deep injection sites.

Table 6.4 Baseline γ-characteristics in pIgG slices (grouped Pt 2 and 3 slices) by layer of injection site

Location of injection site	LI-III (n=24)	Layer IV-VI (n=16)	Mann-Whitney *U*	P value
Peak Power $\mu V^2/Hz$ (median±IQR)	16.34 ± 5.18-38.92	10.88 ± 3.82-21.27	164	0.448
Area Power $\mu V^2/Hz.kHz$ (median±IQR)	0.34 ± 0.108-0.654	0.224 ± 0.127-0.482	175	0.644
Frequency Hz (mean ± SD)	52.16 ±7.15	50.81 ±9.82	t(38)= 0.506[§]	0.616

[§] unpaired t-test

Similarly, increasing time from injection was felt to potentially diminish any effect caused by the NMDAR-Abs because of active clearance of IgG. However, there were no differences in power or frequency in pIgG slices prepared 1 to 3 days after injection (Table 6.5 and Figure 6.5 Aiii-Ciii).

Table 6.5 Baseline γ-characteristics in pIgG slices (grouped Pt2 and 3 slices) by days since injection

Day after injection	Day 1 (n=4)	Day 2 (n=16)	Day 3 (n=17)	P value
Peak Power $\mu V^2/Hz$ (median±IQR)	10.27 ±2.97-69.44	10.08 ±3.44-17.99	17.89 ±5.35-37.39	0.3 Kruskal-Wallis (H=2.403)
Area Power $\mu V^2/Hz.kHz$ (median±IQR)	0.305 ±0.067-1.463	0.275 ±0.093-0.482	0.214 ±0.113-0.534	0.99 Kruskal-Wallis (H=0.028)
Frequency Hz (mean ± SD)	46.84 ±8.89	49.00 ±8.8	54.35 ±6.78	0.09 ANOVA (F(2, 34)=2.569

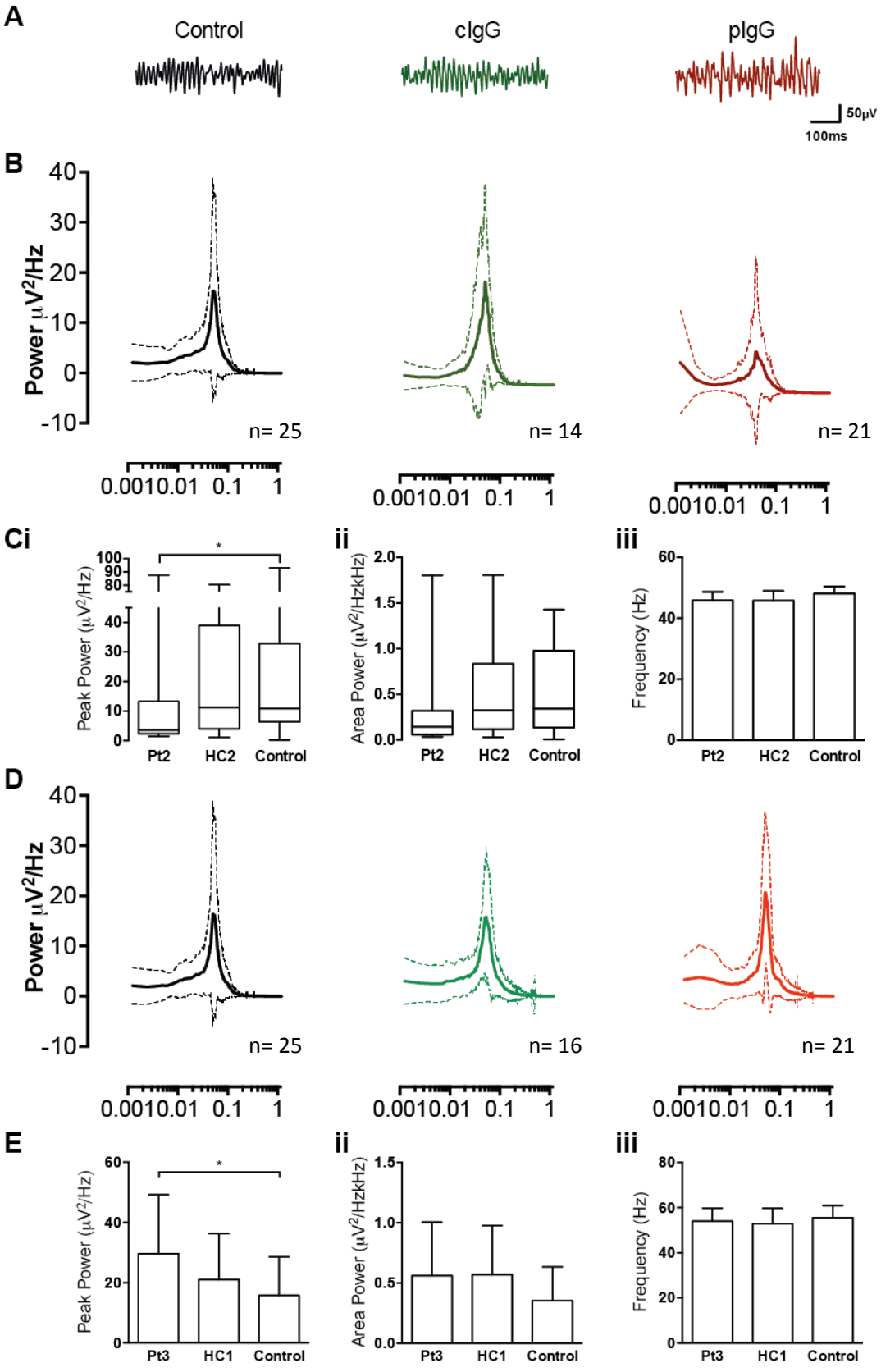

Figure 6.4 Differential effect of Pt2 and Pt3 IgG on γ-oscillation power in mEC after subacute exposure.
Peak power (Ci, median ±IQR (box) ±min-max (whiskers)) but not frequency (Ciii, mean ±SD) was reduced in slices from animals injected with Pt2 IgG compared to control slices, whereas it was increased in animals injected with Pt3 IgG (Ei, mean ±SD), with no effect on frequency (Eiii). In both cases, there were no differences when compared to HC IgG. Traces in A are illustrative examples of extracellular field

recordings in slices from brains injected with HC2 IgG (green) or Pt 2 IgG (red), and a control slice from the right-side of an injected brain (black). Note the latter trace appears somewhat less rhythmical. B and D show the average power spectrum (solid line ± SD in dashed line) obtained from 1-minute recordings done 1h after the start of KA perfusion in each group of brain slices (Pt2 IgG: B dark red n=21 slices; HC2: B dark green n=14 slices; control slices from Pt2+HC2 brains: black n=25; Pt3 IgG: D red n=21 slices; HC1: D green n=16 slices; control slices from Pt2+HC2 brains: black n=25).

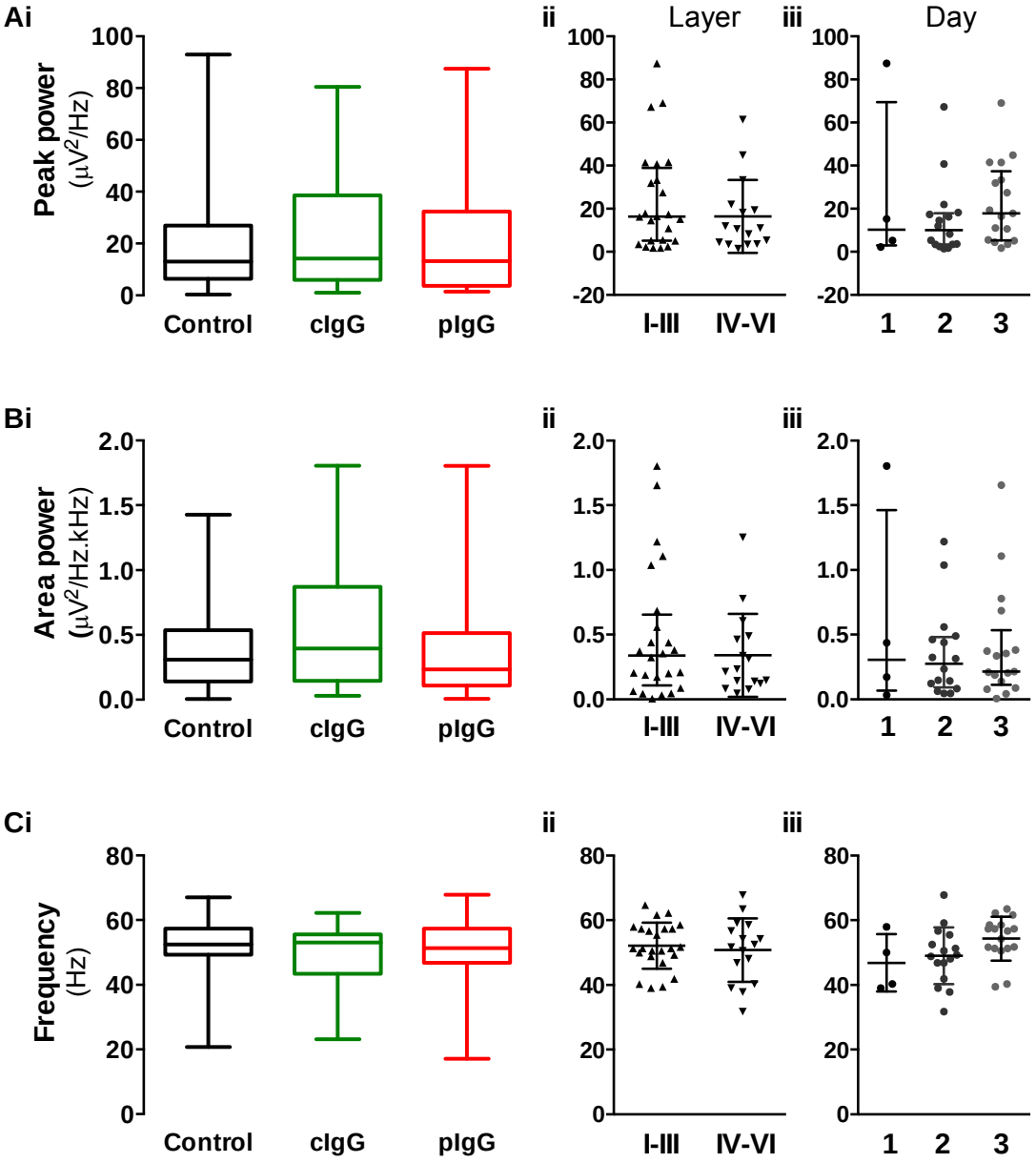

Figure 6.5 Subacute exposure to pIgG has no effect on γ-oscillation characteristics.
When the results from the two cohorts of injected animals (Pt2 and HC2 IgG + Pt3 and HC1 IgG) are pooled, no effect on γ power or frequency is detected (Ai to Bi, median ± IQR (box) ± min-max (whiskers). The absence of changes after subacute exposure to pIgG (n=42 slices from 13 rats) was not related to the location of the injection (Aii peak power, Bii area power *versus* location of injection: median ± IQR; Cii frequency *vs.* location of injection: mean ± SD) or the number of days since the injection (Aiii peak power, Biii area power *vs.* number of days after injection: median ± IQR; Ciii frequency *vs.* days after injection: mean ± SD). cIgG: n= 30 slices from 11 rats, control: n= 50 slices from 24 rats).

Response to NMDAR antagonism

Next, sensitivity to NMDA receptor antagonism was investigated. Diminished response to NMDAR antagonism might be expected in slices from animals exposed to NMDAR-abs for 24-48 hours, as significant internalisation of surface and synaptic NMDARs should have occurred after 12 hours (Moscato *et al.*, 2014). The selective and competitive NMDAR antagonist D-AP5 at the standard concentration of 50μM was used to test this hypothesis.

D-AP5 (50μM) was added to the perfusion medium once oscillations had stabilised as described in Chapter 4, and washed out after 40 minutes. Stabilisation occurred in 19 slices from pIgG brains (9 slices from 6 animals injected with Pt2 IgG, and 10 slices from 6 animals injected with Pt3 IgG), 14 slices from cIgG brains (6 slices from 4 animals injected with HC2 IgG, and 8 slices from 4 animals injected with HC1 IgG), and 20 naïve slices (14 slices from the un-injected side of the brain of experimental animals and 6 slices from naïve animals). This constitutes just less than half the slices exposed to KA in each group, which compares well with previous experience with naïve brain slices.

D-AP5 caused a non-significant reduction in peak power in the three groups of slices (see Table 6.6). Area power was reduced significantly, but only in the pIgG slices. Frequency decreased significantly in the three groups of slices with D-AP5 perfusion. There was no effect of IgG treatment on the changes seen in any of these parameters (2-way ANOVA; frequency: IgG type $F(2, 50)= 2.284$, $p=0.112$; area power: IgG type $F(2, 50)= 0.676$, $p=0.513$; peak power: IgG type $F(2, 50) =0.433$, $p=0.651$, see Figure 6.6).

Table 6.6 Response to D-AP5 in slices from animals exposed to pIgG, cIgG and control slices

Reduc-tion in:	pIgG (mean ± *SD*)	cIgG (mean ± *SD*)	Control (mean ± *SD*)	Two-way ANOVA *F*	P	Tukey's MCT*	P
Peak power %	26.54 ±46.88	6.33 ±70.64	14.62 ±63.76	F(2, 100)= 2.876	0.061		
Area power %	23.55 ±34.62	7.069 ±56.21	15.35 ±40.97	F(2, 100)= 4.249	0.017	pIgG baseline vs. D-AP5	<0.05
Freq-uency %	13.10 ±10.66	22.07 ±11.52	16.93 ±15.10	F(2, 100)= 61.12	<0.0001	baseline vs. D-AP5 all groups	<0.0001

* multiple comparisons test

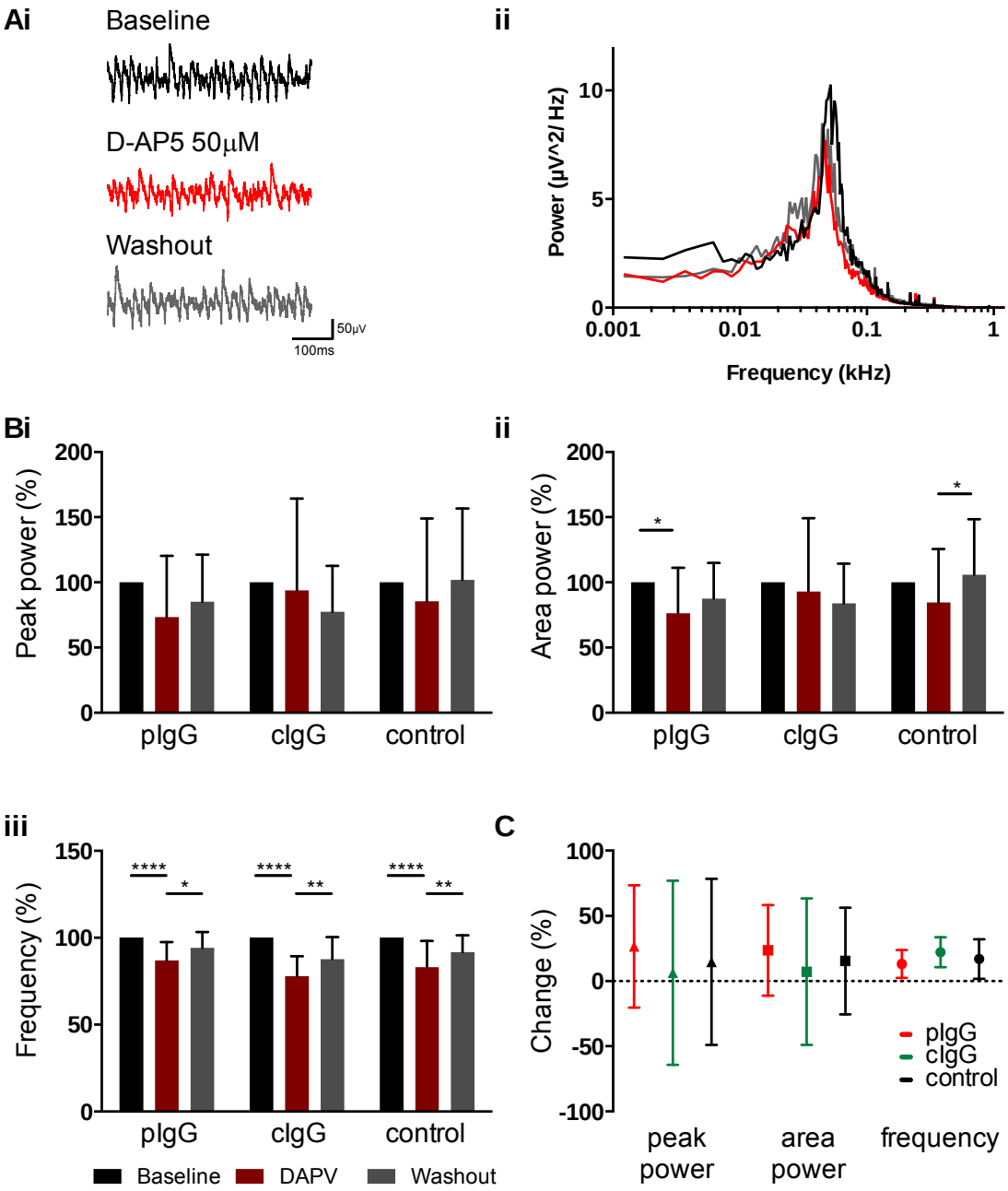

Figure 6.6 There is no effect of IgG treatment on sensitivity to NMDAR antagonism in oscillating slices.

D-AP5 induced a reduction in power and frequency of γ-oscillations in superficial mEC in slices from animals sub-acutely exposed to pIgG or cIgG and in control slices as expected (Bi-iii). Example field potential recordings from a Pt2 IgG slice before addition of D-AP5 (black), after addition of D-AP5 (red) and after D-AP5 washout (grey) are shown in Ai with corresponding power spectra in ii, illustrating the small decline in power and frequency, which partially recovers. Unlike earlier pharmacological experiments, the reduction in power was not significant (except area power in pIgG slices, Bii). However, the nature of the injected IgG does not affect the magnitude of the reduction (C).

6.3.4 NMDAR synaptic function in animals sub-acutely exposed to NMDAR-Abs

Although γ-oscillations in the mEC and other cortical areas are clearly sensitive to pharmacological blockade or genetic alterations of NMDAR (Cunningham *et al.*, 2006; Middleton *et al.*, 2008; Carlen *et al.*, 2011), no direct evidence for NMDAR dysfunction in slices exposed to NMDAR-Abs can be obtained from extracellular field recordings of γ-oscillations. There is little doubt that NDMAR-mediated drive to fast-spiking parvalbumin positive interneurons is an essential component of γ-rhythmogenesis (Middleton *et al.*, 2008; Carlen *et al.*, 2011). To determine if NMDAR-mediated synaptic transmission is disrupted in animals exposed to NMDAR-Abs would require intracellular recordings from such fast-spiking interneurons. The contribution of NMDAR-mediated drive to the phasic output of these cells during γ-oscillations could then be quantified in the presence and absence of NMDAR-Abs. However, finding interneurons using sharp microelectrodes and obtaining sufficiently long recordings are both difficult. Patch-clamping techniques, which allow visualisation of the neurons in slices, and more recently optogenetic systems allowing stimulation or inhibition of selected interneuron subtypes can circumvent these issues, but were not available for this study.

It is possible to obtain indirect evidence of a specific effect on interneurons by examining the IPSPs invading excitatory principal cells during γ-rhythms. A reduction in their size and synchrony concomitant with a decline in local field γ-power would suggest that the latter is related to the former, especially in the presence of unchanged EPSPs in the recorded principal cell.

Since no effect on γ-oscillation power or sensitivity to pharmacological NMDAR blockade was found in the mEC of rats having received a local NDMAR-Ab injection, it was futile to look for any of these changes during γ-oscillations in these animals. Instead, a simple direct assay of NMDAR function in cells near the injection site was used. There is no evidence to suggest that NMDAR-Abs bind preferentially to NMDAR on interneurons (Moscato *et al.*, 2014); although the reduction in γ-oscillations with NMDAR antagonists is a result of a specific effect on fast-spiking interneurons, this is a reflection of their essential role in generating this rhythm and their much higher sensitivity to NMDAR antagonism

compared to pyramidal cells (Grunze *et al.*, 1996). If NMDAR-Abs were able to bind and cause the internalisation of NMDARs in principal cells near the injection site, a reduction in the NMDAR-mediated component of evoked EPSPs might result. This was investigated using sharp intracellular electrode recordings from neurons near the injection site in slices prepared from animals exposed to either cIgG or pIgG. Because of time constraints, few good quality recordings from neurons in naïve animals were obtained, but where possible will be shown as well.

Cell characterisation and inclusion criteria

Recordings were obtained from a total of seventeen cells. Nine were stellate cells and 8 were pyramidal cells. The nature of the cells was determined based on electrophysiological characteristics and then confirmed post-hoc by immunohistochemistry of biocytin-filled cells (see Figure 6.7). Stellate cells are the most numerous cell type in layer II of the mEC and can be recognised electrophysiologically by their response to depolarising and hyperpolarising current pulses (Alonso and Klink, 1993): the membrane potential peaks and then sags to a steady-state level (Figure 6.7 B). If suprathreshold depolarising current steps are given, firing occurs early due to the peak in membrane potential (Figure 6.7C). Other characteristics include a marked depolarising afterpotential (DAP) following each action potential, a shorter action potential duration than pyramidal cells, and the presence of an intrinsic membrane potential oscillation in the theta range (Figure 6.7 A) (Alonso and Klink, 1993). Pyramidal cells, on the other hand, have a much subtler current-induced sag, and firing after threshold depolarisation occurs late due slowly rising membrane potential. DAPs are very small if visible at all and no subthreshold oscillatory activity of the membrane potential is visible (Alonso and Klink, 1993).

Three cells had to be excluded from the analysis because the stimulating electrode was misplaced, usually too far from - and in a deeper layer than - the recording electrode. This resulted in no or only minuscule EPSPs being recorded even with high stimulation power. For 2 cells, only baseline characterisation was available, the cells being lost before the stimulation protocol was commenced. These 2 cells were included in the intrinsic membrane properties analysis. Thus, a total of 5 pyramidal cells (2 cIgG and 3

pIgG) and 7 stellate cells (5 cIgG and 2 pIgG) were available for evoked EPSP analysis (see Table 6.7).

Table 6.7 Summary of recorded cells included in intrinsic membrane properties and evoked EPSP analysis.

Cell type	cIgG			pIgG		
	Injection location	**Day post-injection**	**Excluded from EPSP/ comment**	**Injection location**	**Day post-injection**	**Excluded from EPSP/ comment**
Pyramidal cells	LII mid-mEC	1		LII lateral mEC	1	
	LII/III mid-mEC	1	Only characterisation; stimulating electrode misplaced	LII mid-mEC	1	Only characterisation available
	L6 medial mEC	2		LIII mid-mEC	1	
				LIV-V mid-mEC	2	
				LVI lateral mEC/WM	3	Completely excluded: injection location and stimulating electrode misplaced
Stellate Cells	LIII lateral mEC	1		LII lateral mEC	1	
	LIII mid-mEC	1		LII mid-mEC	1	Only characterisation available
	LV lateral mEC	2		LII mid-mEC	1	
	LIII medial mEC	3				
	LIV medial mEC	3				
	L2	3	Only characterisation; stimulating electrode misplaced			

Intrinsic membrane properties

Pyramidal cells

There were no differences in either resting membrane potential (RMP) or firing threshold (FT) between the cIgG (n=3) and pIgG (n=4) exposed cells or naïve cells (n=3, see Figure 6.8). RMP was -58.83 ±12.35mV in naïve cells, -63.50 ± 7.4 mV in cIgG-exposed rats and -67.5 ± 4.8 mV in pIgG-exposed rats (one-way ANOVA $F(2, 7)=0.933$, $p=0.437$). FT was -51.17 ±3.33mV in naïve cells, -54.17 ± 1.44 mV in cIgG exposed slices and -56.75 ±3.40 mV in pIgG exposed slices ($F(2, 7)= 1.065$, $p=0.111$).

There was also no difference in membrane input resistance (R_{in}) between the three groups of cells (one-way ANOVA: naïve 80.24 ±48.41 MΩ, cIgG 115.5 ±13.00 MΩ, pIgG 93.29 ±43.20 MΩ, $F(2, 7)=0.633$, $p=0.56$).

Inter-spike interval (ISI) at firing threshold however, was longer in cIgG-exposed cells and naïve cells than pIgG-exposed cells with significant differences between each group (median ± IQR: naïve 0.676 ±0.55-0.89s, n=221 APs; cIgG 0.897 ±0.48-1.688s n=174 APs; pIgG 0.318 ±0.228-0.5705s n=456 APs, $H = 58.80$, $p<0.0001$; Dunn's multiple comparisons test $p<0.01$ for each comparison).

To further investigate this apparent difference in firing rate, input-frequency curves were constructed by counting the number of APs on each depolarising step from 0.1 to 0.4 nA for each cell. This is a more controlled method for examining firing rate and thus excitability as the membrane potential is controlled. There was no difference between groups in the number of APs on each step (2-way ANOVA, effect of size of depolarising current $F(3, 108)= 53.16$, $p<0.0001$, effect of antibody treatment $F(2, 108)= 0.289$, $p=0.75$).

The change in membrane potential (MP) in response to injection of a brief current step (IV curve) differed significantly between the groups, with a greater change in membrane potential at each step in cells from slices exposed to cIgG compared to pIgG, but greater change in pIgG cells compared to naïve cells suggesting these differences are related to random sampling error caused by the small number of cells in each group (2-way ANOVA: effect of step size

F(6,102) = 16811, p <0.0001; effect of IgG type F(6, 102) = 9.81, p =0.0023, Sidak's post-hoc multiple comparisons p<0.001 for each step).

Stellate cells

Recordings from only two naïve stellate cells were obtained, and so the results from these are not included in the analysis below, but they are shown on the graphs in Figure 6.9 for completeness.

RMP and FT were similar in the cIgG and pIgG exposed cells. RMP was -61.78 ±7.14 mV in cIgG-exposed cells and -65.00 ±2.65 mV in pIgG-exposed cells (cIgG n=6, pIgG n=3; unpaired t-test t(7)=0.734, p=0.487, see Figure 6.9). Naïve cell RMP was -72.00 ± 1.41 mV (n=2). Firing threshold was -60.95 ±2.12 mV in cIgG exposed slices and -58.33 ±3.51 mV in pIgG exposed slices (unpaired t-test t(7)=1.426, p=0.197). Naïve cell FT was -63.75 ±1.06 mV.

There was also no difference in membrane R_{in} between cIgG and pIgG cells (unpaired t-test: cIgG 75.00 ±17.69 MΩ, pIgG 76.71 ±9.61 MΩ, t(7)=0.152, p=0.88). R_{in} of naïve stellate cells was 71.25 ±30.27 MΩ.

In contrast to pyramidal cells, ISI at firing threshold was longer in pIgG-exposed cells than cIgG-exposed cells (median ± IQR: cIgG 0.269 ±0.192-0.462 s, n=218 APs from 6 cells; pIgG 1.194 ±0.602-2.157s, n=82 APs from 3 cells; Mann-Whitney test, U = 2358, p<0.0001). Naïve cell ISI at FT was 0.096 ±0.072-0.12 s. When the input-frequency data were examined, there was also an effect of antibody treatment on number of APs per 100ms step (2-way ANOVA: effect of step size F(3, 100)= 86.27, p<0.0001; effect of antibody treatment F(1, 100)= 6.15, p=0.015), but this was only present at the 0.2nA step (uncorrected Fisher's least significant difference test: 0.2nA step cIgG *vs.* pIgG t(100)=2.014, p=0.047; p>0.05 at 0.1, 0.3 and 0.4 steps).

The IV curve of the stellate cells differed significantly between the two groups, with a greater change in membrane potential at most steps in cells from slices exposed to pIgG compared to cIgG (2-way ANOVA: effect of step size F(8,207) = 11042, p <0.0001; effect of IgG type F(1, 207) = 4.78, p =0.03, Sidak's post-hoc multiple comparisons test p<0.001 for -0.3, -0.2, 0.2, 0.3, 0.4 steps; p>0.05 for -0.4, -0.1 and 0.1 steps). Note that this is the opposite as the difference seen in pyramidal cells.

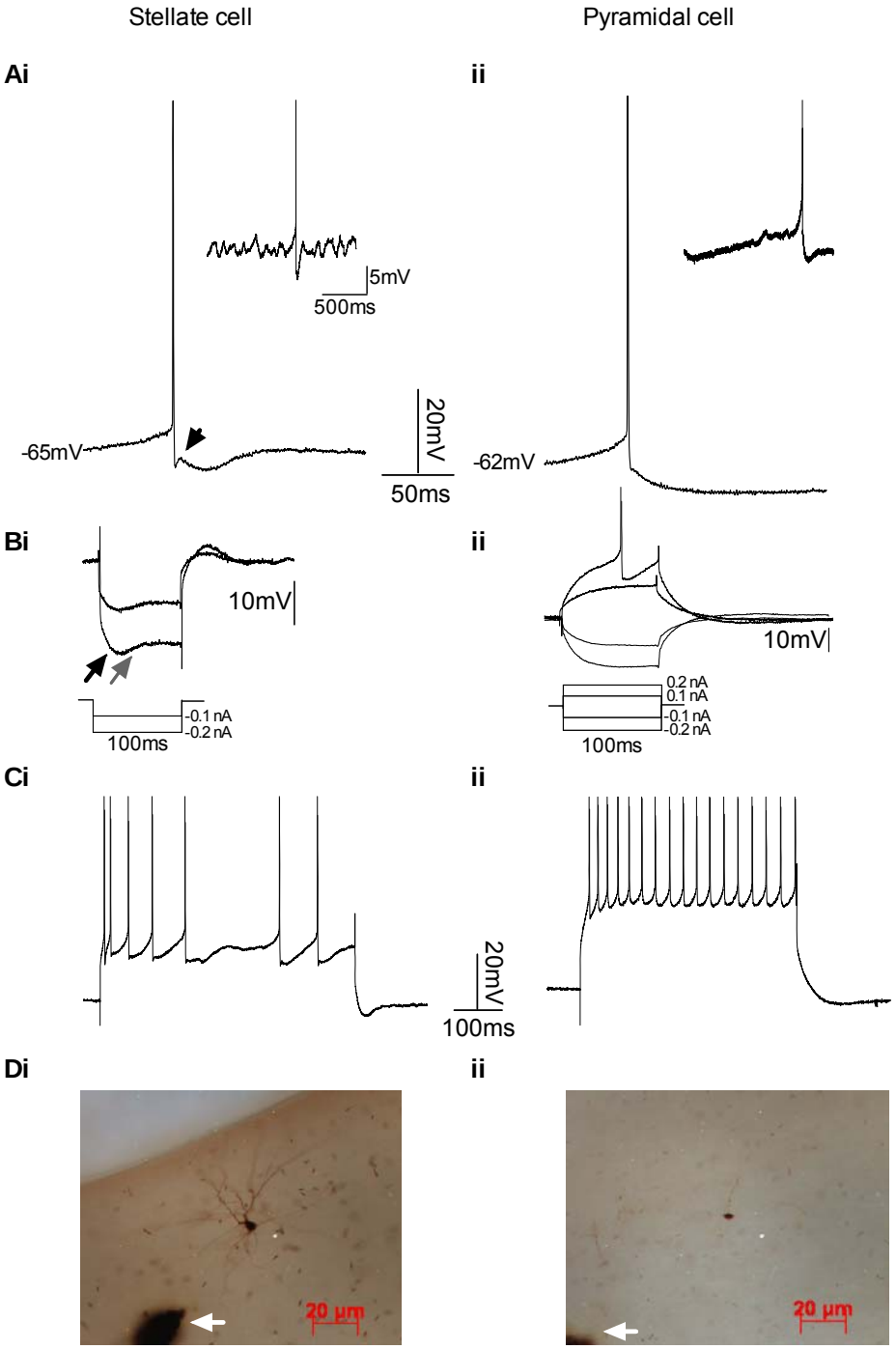

Figure 6.7 Cell type identification by electrophysiological and morphological characteristics.
Stellate neuron (i) and pyramidal neuron (ii) action potentials are shown in A. The distinct DAP of stellate cells is indicated by the black arrowhead. Insets show the slow intrinsic membrane oscillation present in stellate cells but absent in pyramidal cells (APs truncated). The membrane response to hyperpolarising and depolarising current injections is shown in B. The peak (black arrow) and sag (grey arrow) becomes more pronounced with the magnitude of the input in stellate cells (i), but is absent in pyramidal cells (ii, AP truncated). The response to a longer depolarising step (C, APs truncated) demonstrates the characteristic early firing with rapid accommodation of firing rate in stellate cells in contrast to the later firing (see also Bii, 0.2nA step) with minimal accommodation in pyramidal cells. Examples of biocytin-filled recorded cells are shown in D. Note the extensive lateral dendritic arborisation of the stellate cell (i). Unfortunately, only one filled pyramidal cell was successfully stained and little anatomical detail is visible. The injection site is indicated by white arrows.

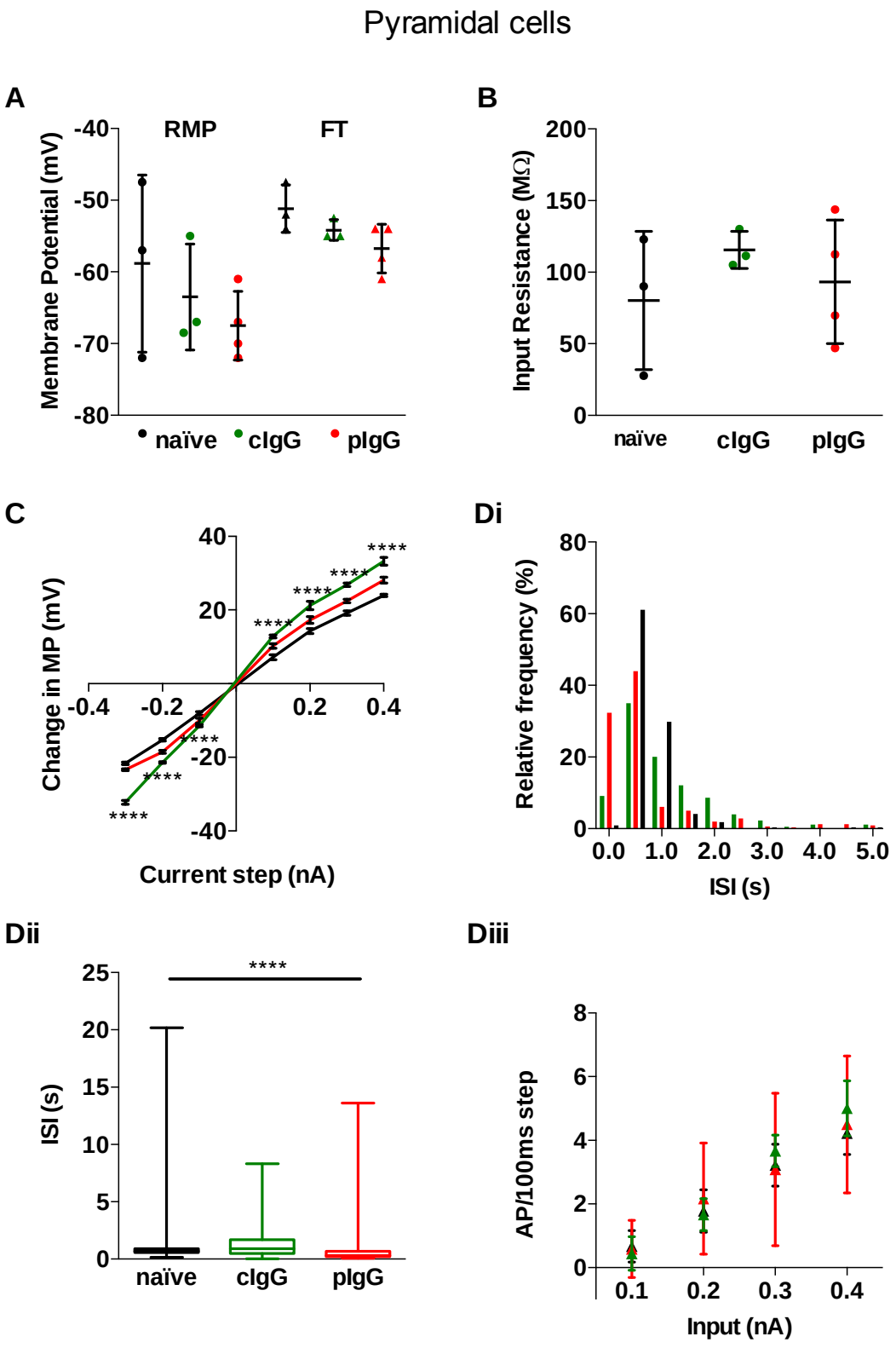

Figure 6.8 Intrinsic membrane properties of naïve, cIgG and pIgG exposed pyramidal neurons.
There was no difference in resting membrane potential (RMP, A), firing threshold (FT, A) or input resistance (B) between the three groups, although membrane potential change to incremental 0.1nA current injections (I-V curve, C) appeared larger in cIgG cells. However, the IV curve of pIgG cells was steeper than that of naïve cells. Interspike interval (ISI, s) at FT is shown in Di and Dii. There appeared to be a significant difference with higher firing rates in pIgG cells, but this was not borne out when membrane potential was controlled (Diii).

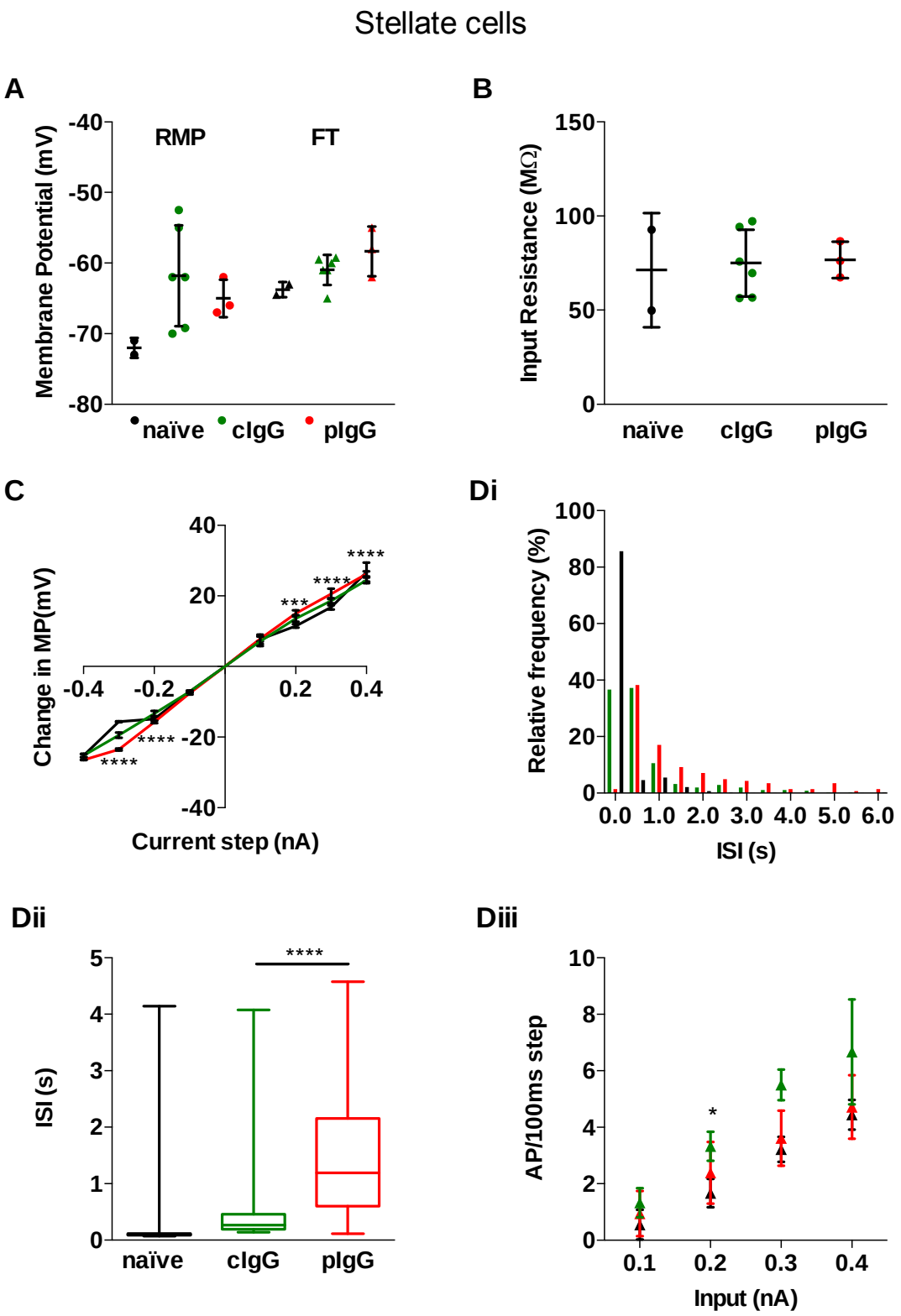

Figure 6.9 Intrinsic membrane properties of naïve, cIgG and pIgG exposed stellate cells.
There was no difference in resting membrane potential (RMP, A), firing threshold (FT, A) or input resistance (B) between the pIgG and cIgG cells, although membrane potential change to incremental 0.1nA current injections (I-V curve, C) appeared larger in pIgG cells at the larger current steps. Interspike interval (ISI, s) at FT is shown in Di and Dii. There appeared to be a significantly lower firing rate in pIgG cells, and this was also present when membrane potential was controlled (Diii). Only two naïve stellate cells were recorded; the values obtained are shown above but were not included in statistical analysis.

Evoked EPSP analysis

EPSPs were elicited in the presence of 20μM NBQX, 1μM CGP55845, and 1μM Gabazine to block the AMPAR-mediated component of the EPSP and any contribution of GABA-mediated inhibition to the shape of the EPSP. To confirm that the resultant EPSP were wholly NMDAR-mediated, D-AP5 (50μM) was added to the perfusion medium and the stimulation protocol repeated. As expected, EPSPs were completely abolished (Figure 6.10).

Pyramidal cells

EPSPs were obtained from 2 cIgG, 3 pIgG and only one naïve pyramidal cells at stimulus voltages from 1-25V. The 1 and 2 V stimuli rarely gave rise to a visible membrane potential deflection. A complete data set is only available for stimuli of 5,7, and 10V.

On average, EPSP peak amplitude and slope were greater in cIgG cells than pIgG cells (Figure 6.11 A and B). However, the number of cells in each group is very small and the variability within groups was large, such that it is not possible to interpret this difference. An ANOVA showed, as expected, that it did not reach statistical significance (2-way ANOVA for peak amplitude: effect of stimulus size $F(3, 11) = 1.57$, $p = 0.25$; effect of IgG type $F(1,11) = 0.617$, $p = 0.45$. 2-way ANOVA for slope : stimulus $F(5, 17) = 2.17$, $p = 0.11$; IgG $F(1, 17) = 2.89$, $p = 0.11$).

Stellate cells

EPSPs were obtained from 4 cIgG, 2 pIgG and no naive stellate cells at stimulus voltages from 1-25V. The 1 V stimulus rarely gave rise to a visible membrane potential deflection. A complete data set is only available for stimuli of 1, 2, 5, and 7V.

On average, EPSPs peak amplitude and slope were greater in cIgG cells than pIgG cells at each stimulus (Figure 6.11 C and D). However, the number of cells in each group is very small and the variability within groups was large, such that interpreting this difference is difficult. An ANOVA showed the difference did not reach statistical significance (2-way ANOVA for peak amplitude: effect of stimulus size $F(3, 16) = 3.750$, $p = 0.033$; effect of IgG type $F(1,16) = 0.923$, p

=0.35. 2-way ANOVA for slope : stimulus F(3, 16) = 2.48, p =0.099; IgG F(1, 16) =0.267, p =0.613).

Large depolarisation events

Occasionally, a stimulus would be followed by a large and/or prolonged depolarisation event, usually after a stimulus larger than that of a magnitude sufficient to cause spiking had been exceeded. These large depolarisation events were seen in both pyramidal and stellate cells and in both pIgG and cIgG injected animals. The duration, area under the curve and coastline of these events were compared to determine if NMDAR-abs had any effect on the characteristics of the events by altering the excitability of the cells.

Pyramidal cells

Pyramidal cells appeared relatively resistant to producing large or prolonged depolarisation after stimulation, with one of two cIgG and one of three pIgG-exposed cells exhibiting this behaviour. In both cells, the events consisted of a large membrane depolarisation superimposed with multiple action potentials. There was progressive failure of action potential repolarisation, leading to a large depolarisation of membrane potential. If spike repolarisation was completely abolished, as in the cIgG cell in the top panel of Figure 6.12, a rhythmic membrane potential oscillation became apparent on the depolarised membrane plateau. It is not possible to compare the two events statistically, but they appeared of similar duration and coastline.

Stellate cells

All the stellate cells recorded exhibited prolonged depolarisations with repetitive firing upon suprathreshold stimulation (Figure 6.12). In some cells, this occurred only with large stimuli, e.g. above 20V, but in others, this was present at low voltage stimulation on the first of ten stimuli only. Figure 6.12 shows the first depolarisation event recorded from each stellate cell (the characteristics of the events did not change markedly within cells as stimulation voltage increased), and summarises the events' characteristics.

The events were highly heterogeneous with some events displaying failure of spike repolarisation and consequent marked membrane depolarisation with intrinsic membrane oscillations as seen in the pyramidal cells, whilst others

consisted of smaller recurrent membrane depolarisations triggering firing of a single spike or a small cluster of APs. Finally, some had features of both of the above. Statistical comparison seemed inappropriate in view of the small number of events and the heterogeneity. Of note, the events in the pIgG-exposed stellate cells appeared longer than in their cIgG counterparts (1.53 ±0.69s *vs.* 0.852 ±0.146s), suggesting perhaps an inhibition deficit. In contrast, the coastline of the pIgG cell events was smaller, indicating the events were less complex despite their longer duration.

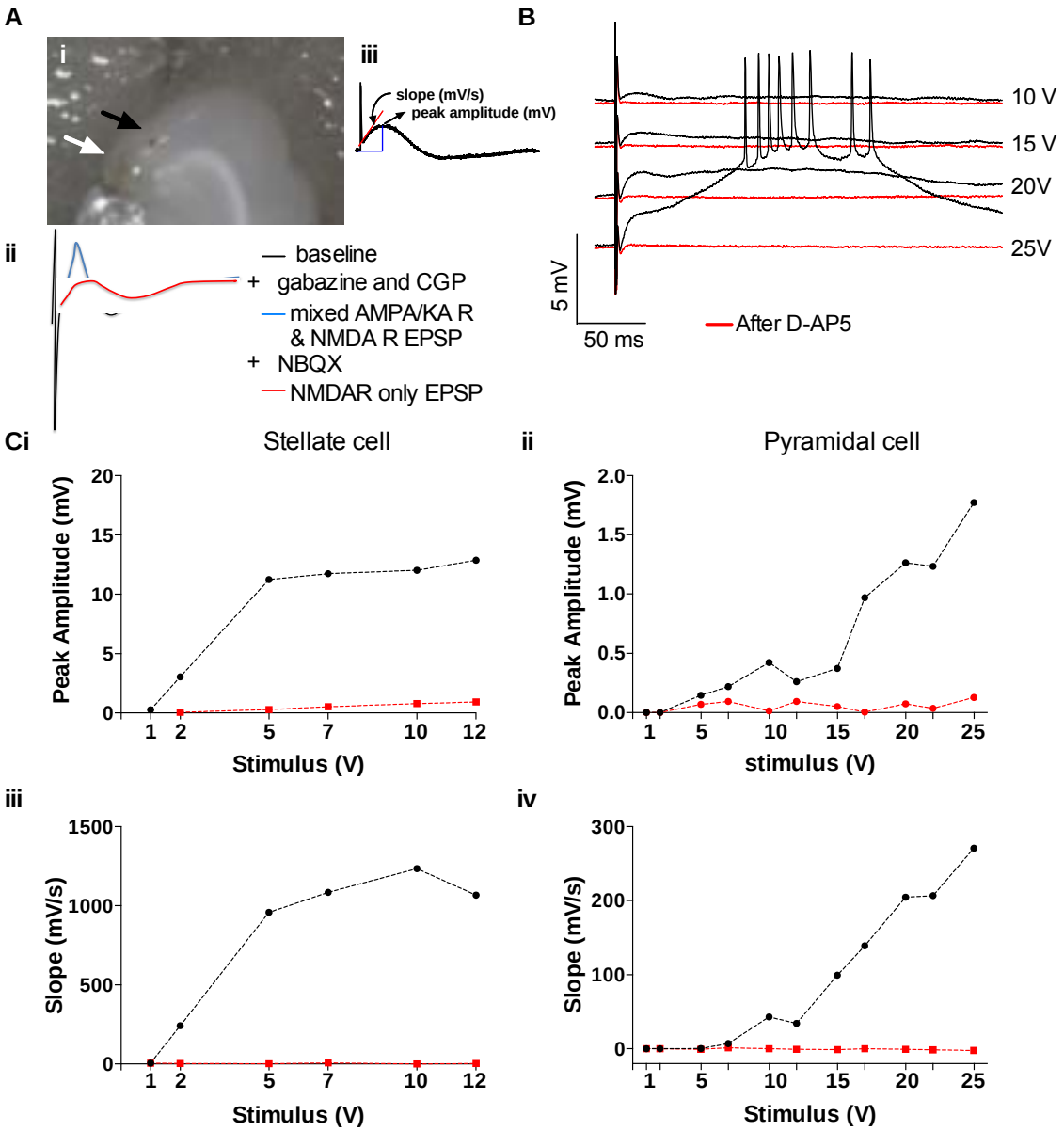

Figure 6.10 EPSP characterisation and response to D-AP5.
A - EPSPs were recorded by electrically stimulating neurons at a set distance from the recording electrode (black arrow, Ai) using a bipolar electrode (white arrow, Ai). The injection site can be seen as a red dot in LII/III of mEC (Ai). The NMDAR-mediated component of the EPSP was isolated by adding 1μM Gabazine and CGP55845 to block GABAR-mediated inhibition and 20μM NBQX to block AMPA/KA receptor mediated excitation (schematic in ii). The peak amplitude and slope of the EPSP was then measured (iii). The NMDA-R mediated nature of the resultant EPSPs was confirmed by perfusing a slice with D-AP5, causing the remaining EPSPs to be abolished (B). Ci-iv demonstrate the complete absence of EPSPs once NMDARs have been blocked in both stellate cells(i and iii) and pyramidal cells (ii and iv).

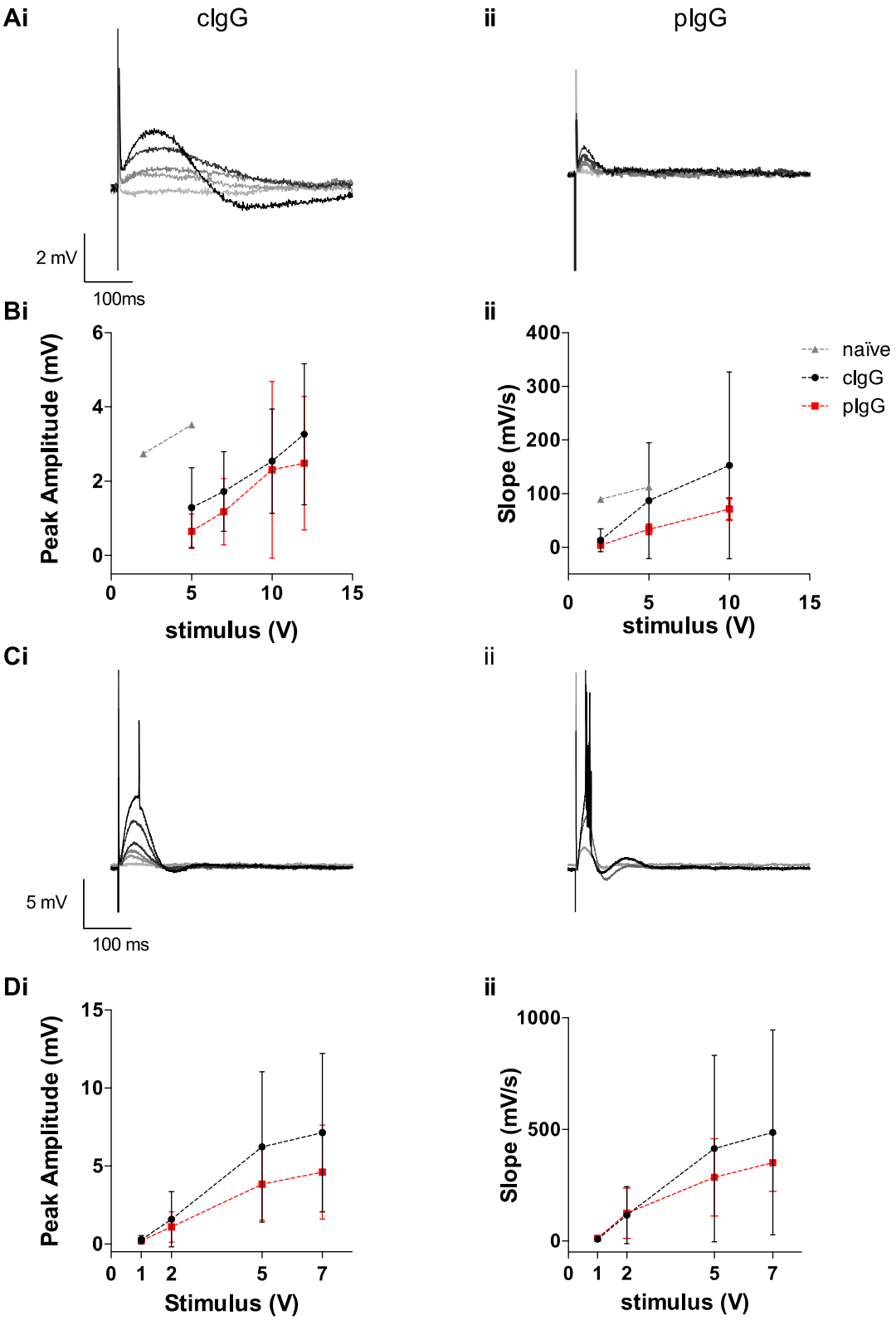

Figure 6.11 EPSPs recorded in pyramidal and stellate cells from cIgG brains are larger than those recorded from pIgG slices.
Example recordings from pyramidal cells (Ai and ii) and stellate cells (Ci and ii) illustrate the larger EPSPs evoked in cIgG than pIgG cells (increasing stimulus intensity illustrated by darker grey response). Average values (±SEM) for peak amplitude (Bi and Di) and slope (Bii and Dii) show the large variability in EPSP size between cells. No statistical comparison has been performed (pyramidal cIgG n=2 Ai and B, pyramidal pIgG n=3 Aii and B (naïve pyramidal n=1); stellate cIgG n=4 Ci and D, stellate pIgG n=2 Cii and D).

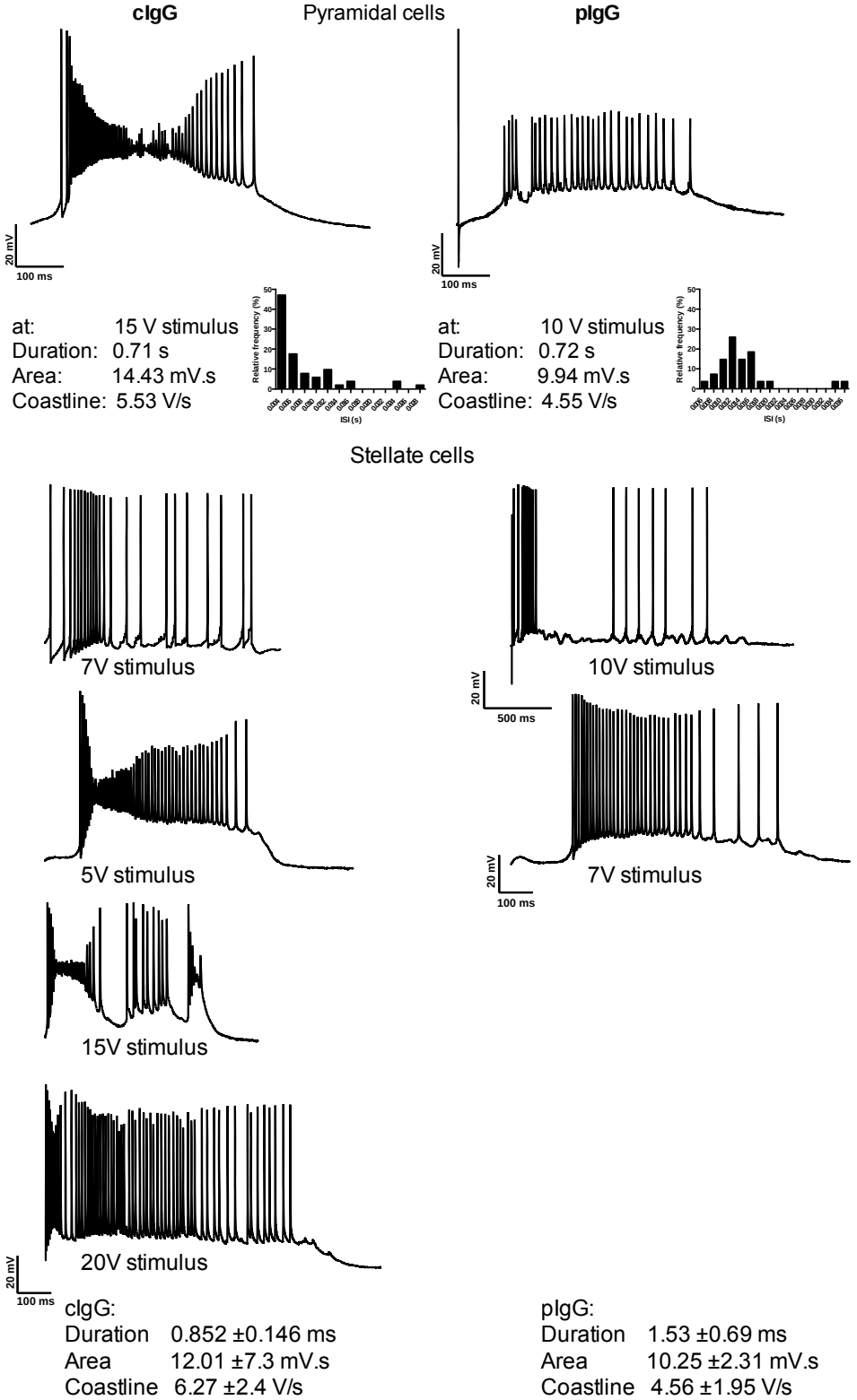

Figure 6.12 Large depolarisation events elicited by suprathreshold stimulation of pyramidal and stellate cells.

Pyramidal cell events are shown in the first row and stellate cell events below this. Events in cIgG cells occupy the left panel and those in pIgG cells the right panel. Most events consist of repeated small depolarisation, which trigger one or more APs. In some cells, spike repolarisation fails and a plateau depolarisation is reached where intrinsic membrane oscillations are visible (e.g. cIgG pyramidal cell and 5 and 15V stellate cIgG cell.

6.3.5 Histological findings in mEC sub-acutely exposed to NMDAR-Abs

Nature of the cell bodies containing internalised IgG

Anti-human IgG antibody binding was detected in slices from both cIgG and pIgG brains used during EP experiments, as described in section 6.3.2. The binding seemed to be within the cytoplasm of the cells, and occasionally also along the axo-dendritic tree of presumed neurons, albeit this only appeared to be the case for pIgG brain sections. The nature of these cells was investigated using double-labelling for intracellular proteins specific to neuron subtypes of interest. Unfortunately, the double-staining process led to significant loss of anti-human IgG antibody binding, such that it was difficult to confirm double-staining.

Co-localisation with excitatory principal cells

Antibodies against the α isoform of calcium/calmodulin-dependent protein kinase II (CAMKIIα) were used to label excitatory principal neurons. CAMKIIα is exclusively expressed in excitatory neuronal populations in rodent cerebral cortex and hippocampus (Liu and Murray, 2012).

PIgG and cIgG injections did not appear to disrupt excitatory cell distribution in any of the slices examined (Figure 6.13). Colocalisation of human IgG with CAMKIIα was seen in slices from 2 animals only, both having received Pt3 IgG. In both these animals, the injection was located superficially in LI/II and human IgG binding within cells was visible in LII, where CAMKII positive excitatory neurons are located. In other animals the human IgG-positive cells and CAMKII-positive cells did not appear to colocalise (Figure 6.13 and Figure 6.14). However, in these animals the pIgG injection was situated in slightly deeper layers (II and III) and the IgG-bound cells tended to cluster below the injection site (Figure 6.15).

Co-localisation with inhibitory interneurons

No co-localisation was seen with Parvalbumin, GABA or GAD67 (Figure 6.16). Co-localisation with interneurons of subtypes other than parvalbumin was not directly investigated in view of the results with GABA and GAD67. It is noteworthy that both GABA and GAD67 immunofluorescence was often weak and that human IgG binding was less marked in double-stained slices.

Furthermore, bleed-through of the interneuron marker immunofluorescence into human IgG immunofluorescence occurred, increasing the difficulty of interpreting the results.

Effect of IgG injection on Parvalbumin-positive interneuron numbers

A reduction in the number of parvalbumin-positive interneurons in the cerebral cortex and hippocampus following chronic pharmacological NMDAR blockade or partial genetic NMDAR ablation has been noted in several animal models of schizophrenia.(Keilhoff *et al.*, 2004; Rujescu *et al.*, 2006; Gandal *et al.*, 2012) Parvalbumin-positive cell bodies in the mEC of injected rats were therefore counted and compared to the number on the uninjected side. Cells were counted in the whole mEC in order to avoid spurious results caused by variation in size of the injection site and expressed as number of cells/mm^2. There was no difference in the number of PV-positive cell bodies in the whole mEC of the naïve (n=16) or cIgG (n=8) and pIgG (n=8) injected slices (mean ± SD: naïve 53.91 ±12.05 cells/mm^2, cIgG 42.52 ±22.34 cells/mm^2, pIgG 42.00 ±23.67 cells/mm^2, ANOVA: $F(2, 28)=1.624$, $p= 0.215$). There were also no differences between cIgG and pIgG slices when LII, LIII and the deep layers (V and VI) were considered separately, although there were significantly more PV-positive cells in LIII of uninjected slices (naïve 25.12 ±4.69 cells/mm^2, cIgG 16.84 ±11.27 cells/mm^2, pIgG 17.10 ±10.42 cells/mm^2, ANOVA: $F(2, 28)= 3.465$, $p= 0.045$; Uncorrected Fisher's Least Significant Difference test $t(28)=2.211$, $p=0.035$ naïve *vs.* pIgG, $t(28)= 2.059$, $p=0.049$ naïve *vs.* cIgG) presumably because of the absence of tissue disruption/damage related to the injection (Figure 6.17)

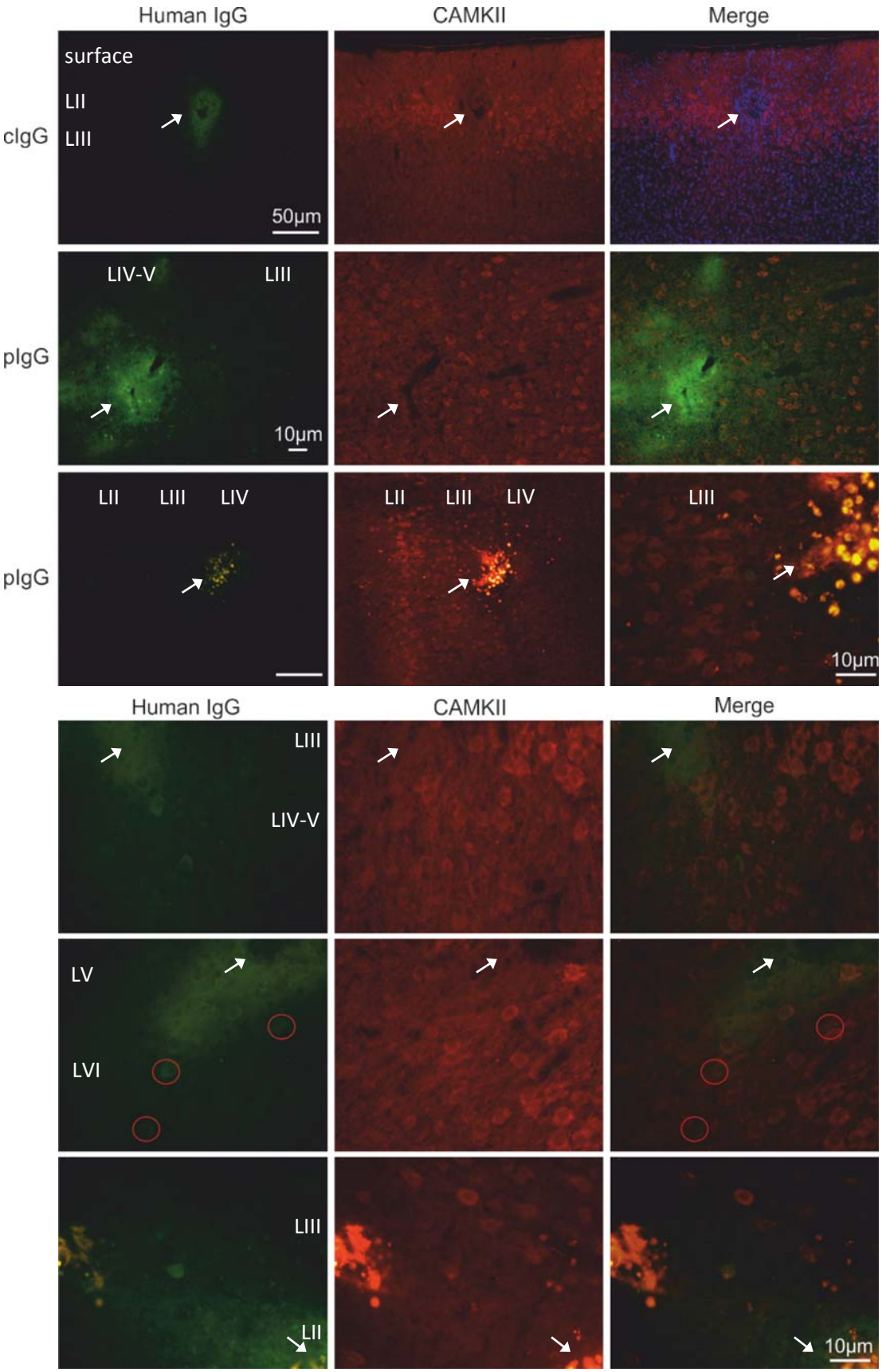

Figure 6.13 cIgG and pIgG do not disrupt excitatory cell distribution in mEC and cIgG does not co-localise with CAMKIIα.
Top row (x40) shows an injection of cIgG into layer II of mEC (1 day after injection). The DAPI and CAMKII merge show very limited disruption of the excitatory cell distribution in layer II at the site of the injection. The second (x20) and third (x20 and x40) rows show a similar pattern of apparently even excitatory cell distribution very

close to pIgG injection sites (fluorescent beads in third row). The bottom panel shows human IgG and CAMKII binding in cIgG slices. Few cells with bound anti-human IgG antibody are present, but they do not co-localise with CAMKII (e.g. circled cells in middle row). Injection sites indicated by arrows. Layers 1-6 indicated by notation LI to LVI.

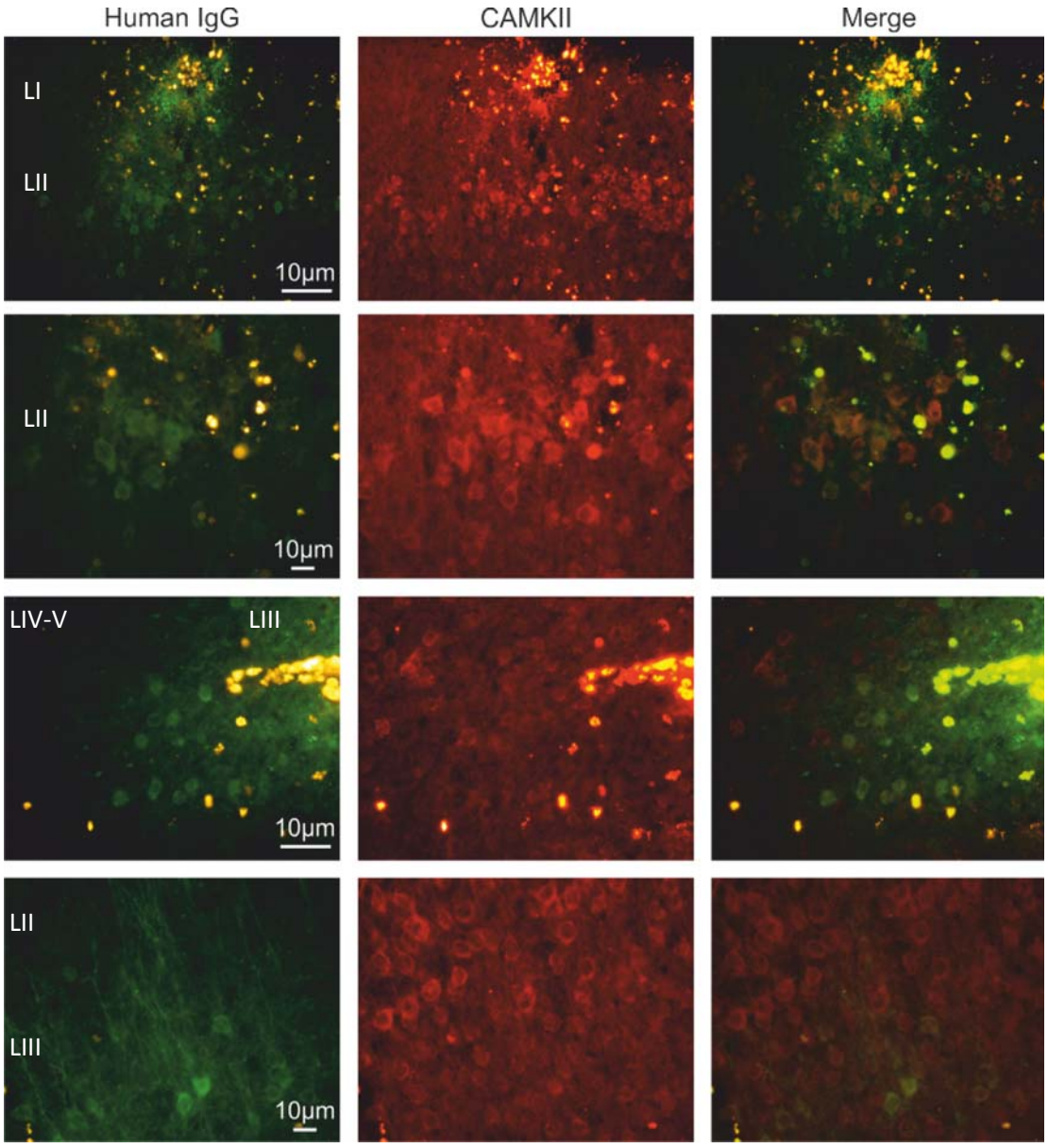

Figure 6.14 Co-localisation of pIgG and CAMKIIα is occasionally seen.
Human IgG and CAMKII co-localisation was seen in two animals only (see top row (x20) and second row (x40 of top row). In other animals the cells with human IgG binding and CAMKII-positive cells did not appear to colocalise (bottom two rows). However, in these animals the pIgG injection was situated in slightly deeper layers (II and III) and the human IgG-positive cells tended to cluster below the injection site, where fewer CAMKII positive cells were seen. In one animal, there was marked dendritic binding (bottom row). The labeled dendrites appeared to contact CAMKII-positive cells in LII and III, where CAMKII-negative IgG-bound cells were also present (see merge panel).

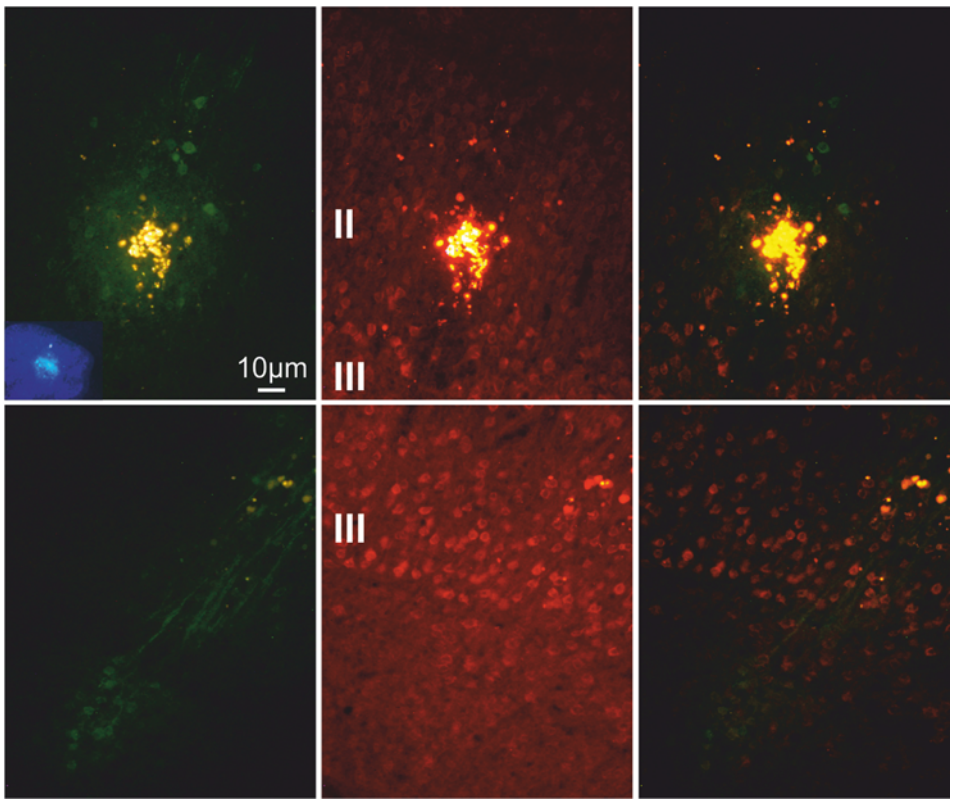

Figure 6.15 Human IgG-positive cells appear to be located in a different layer to the CAMKII-positive cells in pIgG slices
In this animal, the pIgG injection was located in LII of the mEC (see inset in first row). CAMKII-positive excitatory cells are seen around and just below the injection site (yellow fluorescent beads). Photographs in the bottom row are taken below the injection site (injection towards top right of pictures). The bottom of layer III is denoted by the presence of CAMKII-positive cells. Below this is layer IV or lamina dissecans. The human IgG-bound cells appear to be within layer V and have labelled dendrites that extend upwards towards layer III. The human IgG-positive cells are not CAMKII positive.

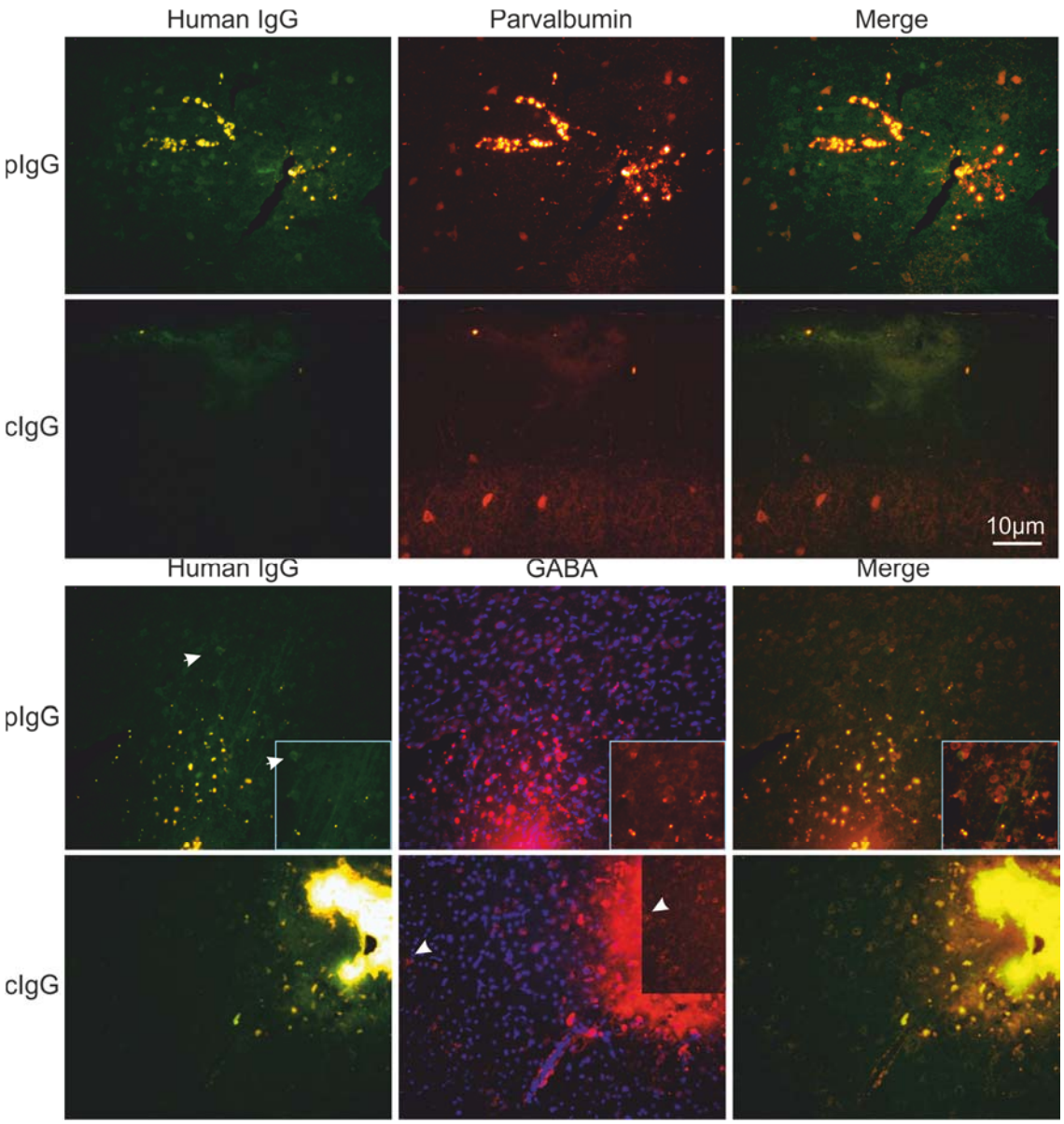

Figure 6.16 human IgG does not co-localise with inhibitory interneuron markers. The top panel shows Parvalbumin immunofluorescence with PV-positive cells present in the proximity of pIgG (top) and cIgG (bottom row) with no colocalisation with human IgG antibody. GABA-positive cells are much more numerous than PV cells as they comprise other interneuron subtype as well. No colocalisation is seen. For both PV and GABA, some bleedthrough of immunofluorescence into the human IgG channel has occurred. The white arrowheads in the bottom panel denote cells used as landmarks in the higher magnification insets.

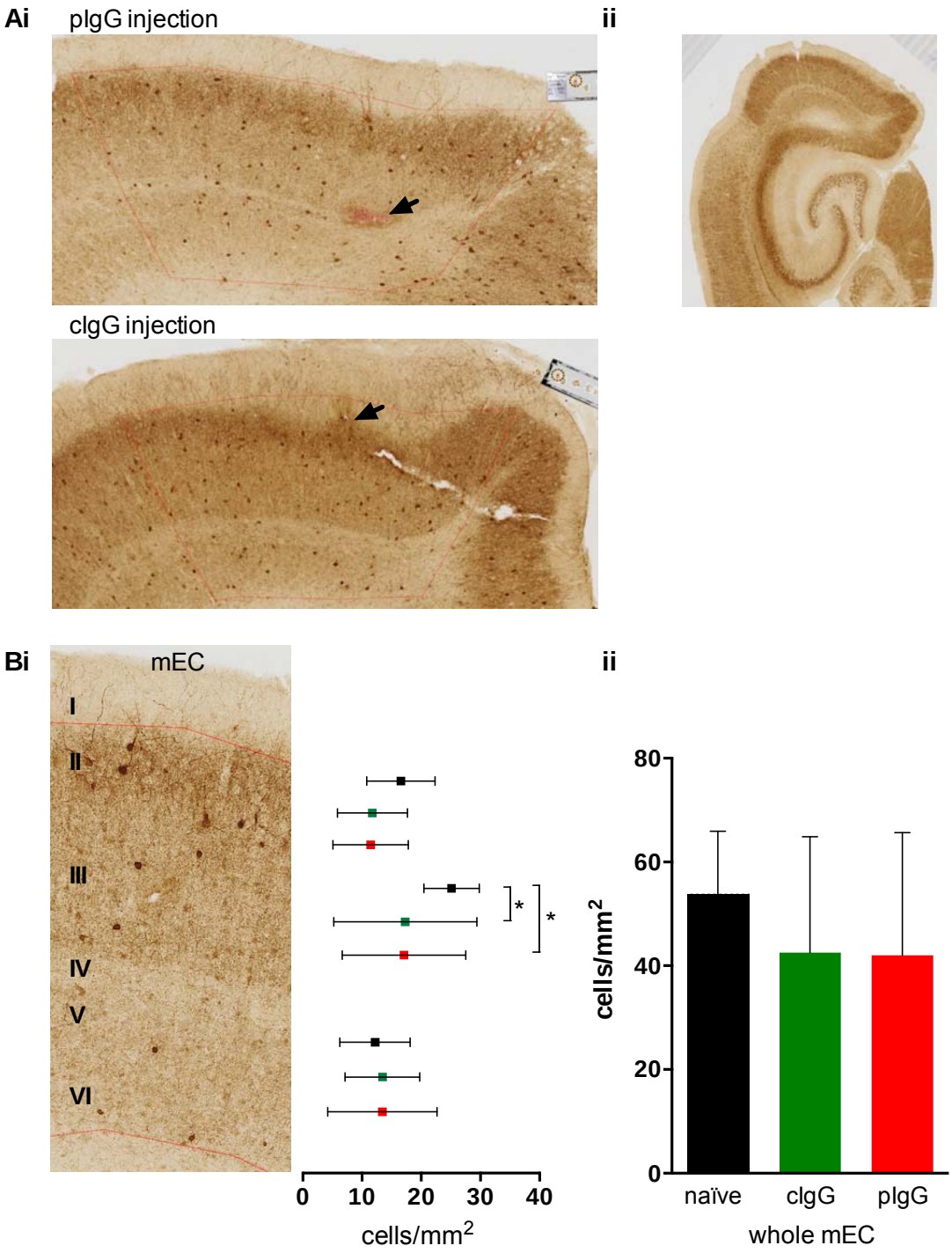

Figure 6.17 There is no reduction in Parvalbumin-positive interneurons in slices from animals sub-acutely exposed to NMDAR-Abs.
Example microphotographs of mEC sections stained for PV are shown in A. Ai shows the apparently normal distribution of PV-positive cells around pIgG and cIgG injection sites. A lower magnification image in Aii shows the normal distribution of PV-positive interneurons in mEC and HPC, with intense staining related to dendritic arborisation in LII of mEC and throughout the pyramidal layers of the HPC. The deeper layers of MEC as well as the peri-rhinal cortical areas have less intense staining. PV-positive interneurons were less numerous in both cIgG and pIgG injected brain slices compared to the contralateral un-injected, slice but there was no difference between the two treatment groups.

6.4 Discussion

6.4.1 The distribution of human IgG in rodent brain slices after injection

The diffusion and binding pattern of the injected human IgG was not as widely distributed as expected. Neuropil staining by anti-human IgG antibody was only detected within 50μm of the injection site and yet FITC-conjugated dextran dye, with a molecular weight far surpassing that of IgG molecules (500 kDa versus 150 kDa) was detectable throughout the mEC and within the ipsilateral lateral ventricle 24 hours after injection. Moreover, contrary to expectations, most of the binding of human IgG that was seen appeared to be intracellular and very faintly stained cells were sometimes noted some 100-200 μm away from the injection site, suggesting that some sub-detection threshold diffusion had taken place. In a small minority of pIgG-injected animals axo-dendritic localisation of human IgG appeared quite prominent.

This reactivity pattern contrasts with that seen in mice having received a single injection of 10μL purified pIgG, where strong binding of anti-human IgG antibody was observed in the molecular layers of the dentate gyrus, CA1 and CA3, as predicted by NR1 subunit immunofluorescence, up to 48 hours after injection with no intracellular binding (Wright *et al.*, 2015b). In that study, anti-human IgG immunofluorescence following healthy control IgG injection was minimal and limited to the injection site.

Antibody diffusion after direct intracerebral injection *in vivo* has only very recently received attention (Daniel J. Wolak *et al.*, 2015). The authors showed that non-targeted IgG diffusion in the extracellular space (ECS) of rat neocortex is reduced by a factor of ten compared to that in a free medium and is much slower than that of other large molecules such as transferrin (80 kDA). This is in agreement with older studies showing that an antibody against amyloid-β remained localised to the injection site for up to one week with little binding of amyloid-β plaques not in the immediate vicinity of the injection (Wilcock *et al.*, 2003).

A number of factors influence the diffusion of molecules through the ECS of the brain (D. J. Wolak and Thorne, 2013). The size of the molecule is of course

important, as ECS width has been measured at around 40-60nm, but other factors such as hindrance by non-specific binding to cellular or extracellular matrix constituents, cellular obstacles and electrical charge all play a part. Binding to Fcγ receptors was shown to play a significant part in hindering antibody diffusion in rodent brain ECS, as adding excess Fc fragments or unlabelled antibody increased the diffusion of fluorescently labelled antibody (Daniel J. Wolak *et al.*, 2015). Fcγ receptors are present on most cell types in the central nervous system, including astrocytes, oligodendrocytes, microglia, neurons and brain capillary endothelial cells (Okun *et al.*, 2010). Some non-specific binding is therefore likely to have taken place after the injection. Assessing the distribution of binding using NMDAR-Fab fragments may clarify this.

Furthermore, IgG removal from brain is rapid. Y. Zhang and Pardridge (2001) found that IgG efflux following a single intracortical injection had a half-time of 48 minutes, considerably faster than the egress of a 70 kDA dextran used as control, the levels of which remained essentially unaltered over the 90-minute experiments. Similar rapid elimination has been demonstrated after intra-cisternal antibody infusion in rats, with an antibody CSF half-life of 24 minutes in the early phase and 12.8 hours in the late phase, leaving 0.1% of the initial antibodies in the CSF at 90 minutes (O'Hear and Foote, 2006), although some medium-term survival of antibody occurred by diffusion into brain parenchyma after administration into CSF. The rapid efflux from brain parenchyma found by Y. Zhang and Pardridge (2001) was nearly entirely mediated by Fcγ receptors, most likely situated on the abluminal membrane of brain capillary endothelium, as the addition of unlabelled Fc, intact IgG, but not Fab abolished the efflux.

The presence of intracellular human IgG in the slices in this study is consistent with the findings of studies described in Chapter 5, which demonstrated internalisation of intracellular antigen-targeted but also non-targeted or healthy control IgG into neurons (Hill *et al.*, 2009; Geis *et al.*, 2010; Congdon *et al.*, 2013; Iffland *et al.*, 2013). As both control and patient IgG appeared intracellularly located, it is likely that a portion of the uptake occurred through non-specific Fc receptor binding, rather than through binding to the NMDA receptors.

In view of the limited diffusion and rapid elimination of IgG in brain, the restricted and inconsistent binding seen here is perhaps less surprising than the striking NR1-like distribution of immunofluorescence after single intracerebroventricular injection of NMDAR-Ab positive IgG in mice. CSF turnover rate is high in rodents, occurring up to 12 times per day in rats, and elimination of antibodies via choroid plexus cells is also expected. However, both Daniel J. Wolak *et al.* (2015) (2mg/ml) and Y. Zhang and Pardridge (2001) used much lower IgG concentrations than either this study (5μL of IgG at around 12 mg/ml, so total 60 μg administered) or in Wright *et al.* (2015b)(10μL at around 25mg/ml, so 250μg of IgG). Y. Zhang and Pardridge (2001) determined that addition of 1.5 μg unlabelled non-specific IgG completely blocked labelled IgG efflux, such that it is plausible that the much higher IgG concentrations used in the Oxford study could have saturated the Fc receptor-mediated efflux mechanism and therefore prolonged the half-life and diffusivity of NMDAR-abs following ventricular injection.

A reduction in NMDAR-Ab titre in the IgG preparations used over time may also be relevant. Indeed, immunofluorescence intensity and distribution deteriorated over consecutive mouse cohorts in the Oxford study (personal communication, Dr S. Wright, NDCN, Oxford University). The IgG administered during intracerebral injections in this study had been prepared one (Pt 3 IgG) to two (Pt 2 IgG) years previously. If NMDAR-Ab concentration in the IgG decreased over that time, the likelihood of obtaining neuropil staining in the NR1 pattern would be much lower, whereas non-specific internalisation would still be present.

The co-localisation studies were rather unsuccessful and did not resolve the nature of the cells taking up the IgG. Co-localisation with CAMKIIα, a marker of excitatory cortical neurons, could only be ascertained in slices from two animals that had received Pt3 IgG injections. The distribution of the stained cells in these sections was striking however: as well as being present around the injection site, the human IgG-positive cell bodies clustered vertically below the injection site into the deeper layers. Processes assumed to be apical dendrites travelled vertically up towards layer II, reminiscent of the columnar-like arrangement of the entorhinal cortex, where dendrites and axons of layer III and V pyramidal cells gather into bundles that travel up towards the superficial layers, separating layer II cells into islands (Ikeda *et al.*, 1989; Witter and

Moser, 2006). These columns are thought to mediate connectivity between deep and superficial layers of the mEC. Although it was encouraging that no co-localisation was detected in slices from animals with cIgG injections, it is noteworthy that anti-human IgG antibody immunofluorescence was lost in the double-staining process. Additionally, co-localisation with microglia, astrocytes and oligodendrocytes was not investigated. These cells also express FCγ receptors and microglial uptake of foreign IgG would be expected (Okun *et al.*, 2010).

Even if IgG uptake occurred mostly in neuronal cells, the functional effect on surface or total NMDAR levels was not assessed here. Reduction in surface NMDARs would be expected in order for network or single cell effects to take place, as demonstrated by the lack of effect of incubation with Fab fragments or short incubation with patient CSF on surface NMDAR density and NMDAR-mediated currents in cultured hippocampal neurons (Moscato *et al.*, 2014). No difference in total NR1 was found 22 or 46 days after a single intracerebroventricular injection of patient IgG or control IgG in mice (Pettingill, 2013), but a reduction in surface NR1 protein concentration was noted in the hippocampi of mice receiving a 14-day infusion of patient CSF (Planagumà *et al.*, 2014) with accompanying memory deficits and anhedonic behaviours. On the other hand, 48 hours after a single injection of 10μL of patient IgG (Wright *et al.*, 2015b), there was no apparent NMDAR loss, despite increased seizure susceptibility in the mice, which correlated with the amount of IgG bound to the hippocampus.

6.4.2 Network activity in brain slices from animals sub-acutely exposed to NMDAR-Abs

No effect on γ-oscillation power or frequency, or sensitivity to NMDAR antagonism was noted, and the lack of effect did not appear to be related to either variability in injection location or time elapsed since antibody administration. This was probably due to the restricted diffusion of antibodies directly injected into the mEC and rapid clearance described above. Additionally, no effect on the number of PV-positive interneurons was seen here, in contrast to studies of chronic NMDAR hypofunction in rodents (Keilhoff *et al.*, 2004; Rujescu *et al.*, 2006; Gandal *et al.*, 2012).

As can be seen in Figure 6.17, although the number of PV-positive interneurons in layer II of the entorhinal cortex is quite low (16.58 ± 5.75 cells/mm^2), especially in comparison to the excitatory principal cells, the axonal arborisation is dense, and it is known that multiple interneurons synapse onto individual principal cells and provide recurrent inhibitory synapses onto other interneurons (Jones and Buhl, 1993). Even if successful binding of NMDAR-Abs and consequent internalisation of NMDARs in the small areas where neuropil and cell body binding was seen is assumed, this is unlikely to reduce NMDAR-mediated drive to a sufficient number of PV-positive interneurons to disrupt γ-rhythmogenesis.

6.4.3 NMDAR-mediated synaptic function in slices from animals sub-acutely exposed to NMDAR-Abs

Intrinsic membrane properties of neurons such as resting membrane potential and apparent input resistance, are generally determined by permeability to ions, chiefly Na^+, K^+, and Cl^-, and this in turn correlates to the number of open ion channels in the cell membrane. These ion channels are generally voltage-gated and not related to glutamate or GABA receptors. A change in these properties in the presence of NMDAR-Abs would therefore not be expected unless there was a toxic effect on the membrane from the IgG. Furthermore, NMDARs are usually quiescent at normal resting membrane potentials, as both ligand binding and depolarisation of the cell membrane are required to open the ion channel and remove the Mg^{2+} block. The contribution of NMDARs to baseline excitatory neurotransmission is therefore small.

Some statistically significant differences in intrinsic membrane properties of neurons in animals administered cIgG or pIgG were found however. Firing rate appeared higher in pIgG-exposed pyramidal cells although this was not confirmed by the input-frequency curve, and slower in pIgG-exposed stellate cells. Surprisingly, although resting membrane potential and input resistance were similar, the change in membrane potential to increasing magnitude current steps were different in cIgG and pIgG cells, albeit in opposing direction for the two cell types. The validity of these differences is questionable in view of the low number of cells in the analysis. Additionally, the differences in I-V curve may be a consequence of the analysis method: the response to each current step was measured three times in each neuron and the average and standard

deviation (which was always very small) for each step were pooled for all the neurons in each category. This resulted in a much smaller standard deviation at each step than if a single value from each neuron had been used, in which case the inter-neuron standard deviation would have been calculated rather than a pool of the intra-neuron standard deviation. The IV curve shape, that is the magnitude of change in membrane potential resulting from different current steps, is related to voltage-sensitive ionic conductances in the cell membranes and not to neurotransmitter receptor activity, such that it is difficult to reconcile the changes seen here in pIgG cells with what is known about the electroresponsiveness of stellate and pyramidal cells in the entorhinal cortex (Klink and Alonso, 1993).

The reduction in pIgG stellate cell firing rate appears somewhat more robust, as it was confirmed by the input-frequency results, where membrane potential is controlled. Again, it is difficult to envisage a simple explanation for this. A reduction in firing rate could result from an increase in the inhibition: excitation ratio experienced by the cell. Cells in layers II, III, and V of mEC are exposed to continuous spontaneous excitation through tonic glutamatergic activity (Berretta and Jones, 1996; Greenhill *et al.*, 2014): This is mostly AMPA receptor driven although there is evidence for both spontaneous discrete pure NMDAR activation and mixed spontaneous AMPA and NMDAR synaptic activity, more frequent in deeper layers.

Internalisation of NMDARs might lead to a reduction in excitation, thus increasing the inhibition: excitation ratio. However, such an explanation is too simplistic, as it does not take into account the effect of antibodies on NMDARs on inhibitory cells, and probably exaggerates the role of NMDAR-driven excitation in the firing of principal cells. In fact, spontaneous inhibition dominates synaptic responses in all layers of the mEC, with increasing inhibition-to-excitation ratios from layer V to layer II (Greenhill *et al.*, 2014). Layer II interneurons with extensive axonal and dendritic arborisation in layers I and II have powerful NMDAR-mediated activation relative to the faster AMPA receptor-driven response (Jones and Buhl, 1993), such that an NMDAR-related change in the inhibition: excitation ratio at individual layer II stellate cells will more likely reflect alterations of inhibitory tone. Internalisation of NMDAR on interneurons would predict a reduction in inhibition, which should lead to the

opposite effect on firing rate. The situation is made yet more complex because the link between spontaneous miniature synaptic activity and firing rate is not a given: firing rate appeared related to network connectivity rather than intrinsic excitability in one study of the mEC (Quilichini *et al.*, 2010) and high layer II cell firing rates in the mEC have been recorded *in vivo* despite the dominant inhibition seen both in spontaneous and evoked synaptic responses (see discussion in Jones (1994)).

The small number of cells from which EPSPs were obtained precluded statistical analysis and prevents firm conclusions from being drawn, but encouragingly, the trend appears to be in the hypothesised direction with, on average, smaller evoked NMDAR-mediated EPSPs in stellate and pyramidal cells from slices exposed to pIgG. Stimulation paradigms such as the one used here have been shown to elicit monosynaptic NMDAR responses, so that a reduction in EPSP amplitude will likely relate directly to NMDAR content or activity at the synapse (Jones, 1994). Here, other sources of excitation and inhibition have been removed pharmacologically so that the generally elevated synaptic inhibition discussed above is not relevant.

The large depolarisation events resulting from supra-threshold stimulation in stellate cells resembled the epileptiform discharges seen *in vitro* after pharmacological blockade of $GABA_A$ and $GABA_B$-mediated inhibition (Jones, 1994). $GABA_A$ and $GABA_B$ inhibition is blocked in these slices, but the epileptogenic potential of this intervention is mitigated by the concurrent inhibition of fast excitatory transmission through AMPA and KA receptors. Instead, these events only occurred when electrical stimulation depolarised the recorded cell sufficiently to remove the NMDAR Mg^{2+} block and promote action potential firing, thus circumventing the AMPAR block. The greater degree of depolarisation, as indicated by the area under the curve, and the greater complexity of the response being related to a higher number of membrane NMDAR in the cIgG stellate cells is an attractive hypothesis, but cannot be verified by the data obtained here. Similarly, the depolarisation events recorded in pyramidal cells strongly resembled reported epileptiform paroxysmal depolarising events that emerge during early network synchronisation induced by loss of $GABA_A$ inhibition, and the same mechanism as above can presumably be invoked. Layer III and layer V pyramidal neurons are very

susceptible to producing these network-driven discharges, presumably because of the lower inhibition: excitation ratio found in these layers, but also because of the relatively high probability of recurrent connections between pyramidal cells in these layers (Dhillon and Jones, 2000). The recurrent excitatory postsynaptic potentials recorded at these connection are AMPA and NMDAR-mediated. The relative resistance of pyramidal cells in this study to producing these epileptiform discharges was therefore somewhat surprising, but it is important to remember that the experiments were not set up in such a way as to study this phenomenon and a number of other factors may have affected the outcome, such as distance between recording and stimulating electrode and tissue disruption due to the injection.

6.4.4 Further work

This chapter describes an attempt at establishing a passive transfer model that would allow investigation of the effects of NMDAR-abs on NMDAR-mediated transmission. Because the IgG injections were intra-entorhinal, the model was always going to be very limited and there was no expectation that it would result in any of the clinical features of NMDAR-Ab encephalitis. Unfortunately, this model was marred by limitations related to immunoglobulin availability and binding within brain matter after a single intracerebral infusion. The lack of effect of pIgG injections on γ-oscillations is therefore likely to be a result of the limitations of this particular model rather than an indication that NMDAR-abs are not pathogenic. The encouraging preliminary intracellular NMDAR-mediated EPSP recording results and the findings in Chapter 4 support this view.

To validate the use of this model, it would be important to determine whether the NMDAR-Ab injection was associated with a reduction in surface or total NMDARs. Without this key information, the link between the injections and any electrophysiological changes recorded can only be surmised. Along this line, it would also be important to determine if the IgG uptake seen in these slices is into microglia or neurons.

However, the low diffusivity of antibodies through brain extracellular space (Daniel J. Wolak *et al.*, 2015) and rapid clearance into blood by reverse transcytosis (Y. Zhang and Pardridge, 2001) would suggest that a single intracerebral injection is not the ideal model to study the effect of NMDAR-Abs

on network or single-cell activity. A more prolonged infusion of a relatively high IgG concentration (or addition of Fc fragments to patient IgG to saturate the Fc receptor-mediated efflux mechanism) seems like a more reliable method to obtain significant binding of NMDAR-Abs and some functional effect on NMDAR density has already been demonstrated using this technique (Planagumà *et al.*, 2014).

Finally, effects of NMDAR-Abs at the single cell level, where factors that may introduce variability such as fluctuations in cell membrane potential can be controlled, need to be firmly established before progressing to investigating changes in network activity. This could be achieved using sharp microelectrode intracellular recordings as done here or by patch-clamp recordings. Obtaining sufficient recordings from interneurons may remain a challenge, but animal models with reduced NR1 expression on PV-positive interneurons (Korotkova *et al.*, 2010) or optogenetic systems that allow selective stimulation or inhibition of PV-positive interneurons (Sohal *et al.*, 2009) may circumvent this issue.

Chapter 7 General Discussion

7.1 Overview

NMDAR-Ab encephalitis is a recently identified disorder that raises many unanswered issues in terms of the best diagnostic tests, the mechanisms of antibody-induced disease, and the best treatment strategies. The work reported here first compared four different assays used for the detection of NMDAR-Abs in patients with suspected NMDAR-Ab encephalitis. The rest of the Thesis describes the acute and sub-acute effects of exposure to NMDAR-Abs from patients with NMDAR-Ab encephalitis on γ-frequency oscillations in the medial entorhinal cortex of rats. Entorhinal cortex oscillations were chosen as a model of a cognitively relevant rhythm that relies partly on normal NMDAR function (Cunningham *et al.*, 2006).

7.2 What is the most accurate diagnostic assay for the detection of NMDAR-Abs?

For serum samples, the study undertaken as part of this thesis confirmed the high sensitivity of the live cell-based assay developed by Oxford (l-CBA, sensitivity 100%) but highlighted its low specificity (28.57%), limiting its usefulness as a single test for the presence of relevant antibodies in serum. The specificity of the l-CBA is likely to be underestimated in this study because of the deliberate over-representation of patients with known non-immune pathology and positive NMDAR-Abs by l-CBA.

Several methods for improving l-CBA specificity have been suggested, including addition of a control step in positive samples to detect co-localisation with a commercial NR1 antibody, and performing a further study of the addition of CSF assays to serum testing. Addition of a more specific assay, such as IHC, which was found to be 100% specific and 85.71% sensitive, would also be helpful although this may not distinguish well between different CNS antibodies, in particular NMDAR, $GABA_BR$, and AMPAR antibodies. Indeed, the pattern of binding in the hippocampus for these three antigens is very similar (Dalmau *et al.*, 2008; Lai *et al.*, 2009; Lancaster *et al.*, 2010). AMPAR-Ab and $GABA_BR$-Ab binding in the cortex, basal ganglia, and in particular in the cerebellum differ markedly from that of NMDAR-Abs (Lai *et al.*, 2009; Lancaster *et al.*, 2010), and

should therefore allow differentiation of the antibody when there is discrepancy between CBA and IHC result.

It is important to note that the use of the terms sensitivity and specificity is somewhat premature here. The sensitivity and specificity of a diagnostic test can only be assessed in the presence of a gold standard for diagnosis, and this is not yet available for NMDAR-Ab encephalitis, although clinical criteria are expected to be published soon (A. Vincent, personal communication). The results of this study have been expressed as sensitivity and specificity for each test for practical purposes, although it may have been more correct to report only preliminary true-positive, true-negative, false-positive and false-negative rates. The diagnosis for patients included was classified by the treating physician as “definite”, “probable”, “possible”, and “unlikely” NMDAR-Ab encephalitis based on their experience and also using a diagnostic aid (see Appendix B) we prepared for this purpose. The robustness and reliability of this classification is therefore arguable, and has not been validated.

For a definite diagnosis, the patient had to meet the following criteria: one of inflammatory CSF or teratoma; three of psychiatric symptoms, dysautonomic features, movement disorder, or seizures and/or EEG epileptiform abnormalities; and two of the five following additional features (encephalopathy, altered consciousness, improvement with immunotherapy or tumour removal, MRI changes, or tumour other than teratoma). The fallibility of these criteria is exemplified in the discussion of the clinical history of patient 3 in Appendix B, and further work to improve these and test their validity would be required.

Insufficient samples were available to determine the sensitivity and specificity of the assays studied for CSF, and to examine whether NMDAR-Abs are present in all patients with NMDAR-Ab encephalitis, and thus if CSF testing should be preferred to serum testing.

The commercial antibody detection kit developed by Euroimmun (Euf-CBA) had the lowest sensitivity (74.04%) but high specificity (92.86%), rendering it of limited usefulness. This finding contrasts with those reported by Wandinger *et al.* (2011), but is in keeping with previous unpublished experience at the Oxford Neuroimmunology laboratory. The poor sensitivity is unlikely to be due to problems with the execution of the assay or interpretation of the results in this

study as some serum samples with negative Euf-CBA scores scored highly on at least two of the other methods. It may be related to a factor intrinsic to the assay such as the over-fixation of the cells used to allow durability.

The fixed cell based assay used in Barcelona (f-CBA) also requires combination with IHC and testing of CSF to be useful (Gresa-Arribas *et al.*, 2014) and therefore offered no additional advantage over l-CBA in this study. It had lower sensitivity (71.43%) but higher specificity (85.71%) than l-CBA.

Overall, combining IHC with l-CBA, and paying particular attention to IHC results when there is a discrepancy in results, may be the most accurate diagnostic assay approach. L-CBA has advantages over f-CBA for serum samples, as it is faster to perform, and f-CBA is associated with marked non-specific background staining of all cells on the coverslip and also a lower density of cells on the coverslip. It is not possible to state whether CSF testing is necessary for the accurate diagnosis of NMDAR-Ab encephalitis from this study.

The degree of discordance between assays in this study was surprisingly high. The design of the study and the time available to perform it did not allow investigation of the causes of this. The amount of antigen available for the NMDAR-abs to bind might be one relevant factor, and the assay with the most NR1 protein would be predicted to be the most sensitive. The amount of NR1 protein in each preparation could be assessed using Western blot, and is likely to be higher in the CBAs than in IHC due to virally-driven expression of NR1 (and NR2B). Fixation and permeabilisation are also likely to impact the amount of NR1 protein in the CBAs. However, contrary to expectation, IHC was more sensitive than both l-CBA and Euf-CBA. Additionally, end-titres were highest with IHC. The good sensitivity and los threshold of detection of IHC for both serum and CSF is thus still difficult to explain. It is worth noting that the discordance among assays was much more marked for serum samples than CSF, suggesting that non-specific binding plays a role in the discrepancies between assays.

7.3 Improving the NMDAR-ab assay comparison study

One significant limitation of the comparison study performed here is the fact that the Barcelona f-CBA could only be approximated. Indeed, the permeabilisation step as well as the dilutant used for the samples and the washes had to be altered in order to reduce background staining with serum and obtain usable result. The Barcelona laboratory presumably does not experience the same level of background staining, as this would render their assay difficult to interpret and less time efficient, both essential qualities for a diagnostic test. A preferable approach would therefore have been for the Barcelona group to perform the f-CBA and IHC and score the results as part of a collaboration, such that their results could be compared with the results of the l-CBA performed at Oxford and the Euf-CBA performed as per *Euroimmun* instructions.

The ideal comparison study should also be performed prospectively rather than retrospectively as done here, and a control group should be included comprising healthy controls, patients with other types of autoimmune encephalitis, and non-immune pathologies.

7.4 Insights into the neurobiological impact of NMDAR-Abs

Anterograde amnesia and other cognitive deficits occur early in NMDAR-Ab encephalitis and persist throughout the illness. They are likely to result from impaired function of the hippocampus and parahippocampal region, including the entorhinal cortex (Zola-Morgan *et al.*, 1994), which lies at a critical juncture between the hippocampus and sensory cortices. The vast majority of cortico-hippocampal inputs pass through the entorhinal cortex and an intact entorhinal cortex is required for correct encoding of spatial context in the hippocampus (Lu *et al.*, 2013), and learning and retention of spatial tasks (Steffenach *et al.*, 2005). During the course of this thesis, memory impairments have been demonstrated in mice exposed to NMDAR-Abs intracerebroventricularly after a single injection (Pettingill, 2013) and prolonged infusion (Planagumà *et al.*, 2014). In both studies the performance of mice on memory tasks improved after cessation of administration of antibodies. Planagumà *et al.* (2014) were able to demonstrate parallel memory deficits and recovery and reduction followed by

recovery of total and synaptic NMDAR cluster density in the hippocampus of mice exposed to NMDAR-Abs.

In view of the proposed mechanism of action of NMDAR-Abs being internalisation and degradation of cross-linked surface NMDAR, these findings would suggest a link between the NMDAR-mediated transmission and the memory deficits described. However, no study so far has satisfactorily examined the neural mechanisms underlying these changes or established a clear deficit of NMDAR-mediated transmission in neuronal networks.

To establish whether NMDAR-Abs affect NMDAR-mediated neurotransmission, and in particular, if the function of NMDAR on parvalbumin-positive interneurons is altered, we examined the power and frequency of γ-frequency oscillations in the mEC of rats.

7.4.1 Findings from acute application experiments *in vitro*

Acute exposure to NMDAR-Abs by perfusion of live entorhinal-hippocampal brain slices with purified IgG from three patients with NMDAR-Ab encephalitis for one hour resulted in a reduction in γ-oscillation power, which persisted despite washout. No change in frequency was noted. Smaller declines in γ-power were seen in naïve slices exposed to vehicle only, slices exposed to healthy control IgG, disease control IgG containing VGKC-Abs, and NMDAR-Ab Fab. The decreases in these groups of controls slices were very similar, suggesting that although there is an attrition in the population taking part in oscillatory activity over time in brain slices, the larger reduction in slices exposed to patient IgG is likely to be due to the NMDAR-Abs.

No specific extracellular binding of patient IgG to the brain slices used in electrophysiological experiments was detected. Both patient and control IgG could be detected in the cytoplasm of individual cells in all regions of the slices, indicating that some IgG internalisation had occurred during the 1-hour electrophysiology experiments. It is unclear whether this is relevant to the electrophysiological findings, as some degree of non-specific IgG uptake by neurons is expected (Hill *et al.*, 2009; Geis *et al.*, 2010; Congdon *et al.*, 2013; Iffland *et al.*, 2013; Greenlee *et al.*, 2014), particularly in brain slices where membrane damage to superficial cells is prevalent.

7.4.2 Findings from rats administered NMDAR-Abs intracerebrally

To determine if more marked effects could be obtained by prolonged exposure to NMDAR-Abs, the spontaneous activity and pharmacologically induced γ-oscillations in slices from animals having received an intracerebral injection of concentrated NMDAR-Abs were examined. No epileptiform or rhythmic activity was noted in pharmacologically unchallenged slices, suggesting there was no widespread loss of inhibition or toxicity from the IgG. There were no changes in power or frequency of γ-oscillations and no differences in the sensitivity to NMDAR antagonism in the mEC of rats having received a single intra-entorhinal injection of patient IgG up to three days previously. It is worth noting that the two patient IgG samples used produced opposite effects on γ-power however, with lower baseline power in animals administered Pt2 IgG and higher power in those given Pt3 IgG, raising the possibility that Pt3 IgG had lost activity over time. Evoked NMDAR-mediated excitatory post-synaptic potentials in pyramidal and stellate cells surrounding the injection site also appeared smaller in animals exposed to NMDAR-Abs in Pt2 IgG, although only a small number of cells was available for this analysis. Human IgG was detected in a small area around the injection site and within cells in close proximity. In two patient IgG-treated animals this reactivity appeared brighter and was present in several cells below the injection site, which also stained positive for CAMKII, identifying them as excitatory neurons. No co-localisation with markers of inhibitory interneurons and no reduction in the numbers of parvalbumin-positive cells were detected however, in keeping with the lack of change in γ-oscillation parameters.

7.5 Strengths and weaknesses

All in all, the results are not unequivocal. Patient IgG was able to reduce γ-oscillation power and appeared to also diminish the NMDAR-mediated component of evoked synaptic responses. Both these findings support the presence of a reduction in inhibitory tone in functional cortical networks exposed to NMDAR-Abs. Using the reduction in the magnitude of the evoked NMDAR-mediated synaptic response in pyramidal and stellate cells as evidence supporting a reduction in inhibitory tone may seem counter-intuitive, but it is worth remembering that during physiological activity, the inhibition:excitation ratio is strongly in favour of inhibition. Interneurons in the entorhinal cortex and

other cortical areas are highly sensitive to NMDAR antagonism (Jones and Buhl, 1993; Homayoun and Moghaddam, 2007; Middleton *et al.*, 2008; Carlen *et al.*, 2011), and it is conceivable that if an antibody-mediated reduction in the NMDAR-mediated component of evoked responses is present in principal cells, it is also present in interneurons, where it will have much more dramatic effects on network activity and oscillatory rhythms.

Several limitations of the techniques used in this study may have impacted the magnitude of the changes recorded. In the acute exposure experiments low NMDAR-Ab concentrations were used, compounding the likely slow and incomplete diffusion of antibodies through the slices. It is also not clear if incubation with NMDAR-Abs for one hour is sufficient to allow significant binding and internalisation of NMDAR. The findings of Mikasova *et al.* (2012), who demonstrated significant levels of internalisation after two hours in neuronal cultures, and of Congdon *et al.* (2013), who found that maximal neuronal IgG uptake had occurred within 30 minutes of incubation in hippocampal organotypic slice cultures, would suggest that at least some degree of specific binding and internalisation is possible within the duration of our experiments. This may also explain the lack of recovery in γ-oscillation power during the washout phase.

In the subacute exposure experiments, the diffusion of patient IgG around the injection site was noted to be limited, even in animals examined three days after the injection. This is in keeping with the slow diffusion of IgG through brain extracellular space (Daniel J. Wolak *et al.*, 2015) and rapid elimination of IgG by transcytosis after intraparenchymal injection (Y. Zhang and Pardridge, 2001). A single intraparenchymal IgG injection may therefore not have provided sufficiently prolonged and widespread exposure to NMDAR-Abs within the mEC to cause obvious network changes.

One of the features of NMDAR hypofunction models of schizophrenia is reduced inhibition-to-excitation balance with, in particular, lower numbers of parvalbumin-positive interneurons (Gandal *et al.*, 2012). Pyramidal neuron excitability is increased in NR1 knock-down mice in the hippocampus (Gandal *et al.*, 2012) and in the prefrontal cortex of rats treated with an NMDAR antagonist (Homayoun and Moghaddam, 2007). In keeping with the essential

role of inhibitory activity by PV+ fast-spiking interneurons in the generation of γ-oscillations, stimulus-evoked γ-oscillations are also impaired in NR1 knock-down mice (Gandal *et al.*, 2012) and mice with NR1 deletions from PV+ interneurons (Carlen *et al.*, 2011). Whether a similar link exists between Ab-mediated reduction in NMDAR and preferential deficits in inhibition remains unresolved, but is supported by our findings of reduced γ-power and NMDAR-mediated evoked synaptic responses (see above). The early occurrence of seizures in NMDAR-Ab encephalitis supports the possibility of relative inhibition impairment although it is also possible that early inflammatory and possibly destructive histopathological changes in NMDAR-Ab encephalitis could mediate this. More recently, an increased susceptibility to seizure following PTZ administration was found in mice given a single bolus of NMDAR-Ab-positive IgG compared to mice receiving control IgG (Wright *et al.*, 2015a). No increase in apoptosis markers had been noted in these animals, and although direct measures of neuronal excitability were not performed, it is therefore likely that the seizures reflected an impairment of inhibition. Moscato et al (Moscato *et al.*, 2014) have reported similar degrees of internalisation of NMDAR on excitatory and inhibitory neurones in hippocampal neurone cultures and also found that the amplitude and frequency of miniature inhibitory post-synaptic currents (mIPSCs) were similar in cultured hippocampal neurones treated with patient or control CSF for 24 hours. Instead, the density of inhibitory synapses onto excitatory neurons was reduced, which the authors considered to be a homeostatic response to the lower NMDAR concentration at synapses.

However, using mIPSCs as a measure of GABA-ergic neurotransmission is misleading. mIPSCs are recorded in the presence of tetrodotoxin, a Na^+ channel blocker that blocks action potentials generation. mIPSCs are caused by quantal release of neurotransmitter rather than action potential-mediated mechanisms, and therefore do not estimate use-dependent GABA release. A reduction in synaptic NMDAR content in interneurons might be expected to cause a reduction in principal cell inhibition when glutamate is present to activate glutamatergic synapses but not in the resting state when there is minimal input to interneurons (note that mIPSCs were recorded in the presence of an AMPAR antagonist). This is supported by the findings of Li et al (Li *et al.*, 2002), who showed that the NMDAR antagonist MK-801 reduced the frequency

and amplitude of spontaneous and evoked IPSCs in pyramidal cells in the posterior cingulate and retrosplenial cortices, but had no effect on mIPSCs, such that the effect of MK-801 on interneurons relied on action potential dependent mechanisms.

In this study, the use of γ-oscillations and evoked responses in brain slices circumvented these issues by providing functional networks with endogenous glutamate in which to observe use-dependent physiologically relevant responses. A significant excess reduction in γ-power in the mEC was found after slice perfusion with patient IgG compared to control IgG. This would be in keeping with a greater effect on PV+ fast-spiking cells, whose activity synchronises principal cell firing in γ-oscillations, however no direct proof of this is available at present. No reduction in PV+ interneurons was found in the injected animals and evoked IPSPs were obtained in too few cells to allow meaningful comparison. Proof would require intracellular recordings ideally from interneurons to examine the nature and strength of NMDAR and AMPAR-driven synaptic inputs, or from principal cells, where the pattern of invading IPSPs and EPSPs could be scrutinised to determine relative deficits.

7.6 Future studies

A number of studies would need to be carried out to explain and complete the findings in this thesis. Firstly, γ-oscillation recordings in the presence of patient IgG from which NMDAR-Abs have been pre-absorbed would be required to confirm the effect seen in this thesis is NMDAR-Ab related. Secondly, the mechanisms underlying the reduction could be investigated using intracellular recordings as described above. Finally, an effect on surface NMDAR density or synaptic content would need to be demonstrated. This is likely to be complex in brain slices were techniques based on surface protein biotinylation have been shown to be unreliable (Grosshans *et al.*, 2002a; Grosshans *et al.*, 2002b). Future studies should be performed using a more reliable method of antibody delivery to the brain parenchyma, such as prolonged infusions. The effect of antibodies at a single-cell level should also be firmly established before moving on to network activity although both mediums are important to develop an understanding of the neurobiological mechanisms underlying temporal lobe dysfunction in NMDAR-Ab encephalitis. Studies using optogenetic activation on

specific neuronal subtypes such as PV+ interneurons and genetic models such as mice lacking NR1 expression in PV+ interneurons are likely to be useful in that endeavour.

NMDAR-Ab binding detected immunohistochemically in rodent brain slices is strongest in the hippocampus due to the high concentration of NMDAR in this brain region (Moscato *et al.*, 2014). This in itself is likely to be indicative of its importance in memory and learning. Long-term infusion of CSF from patients with NMDAR-Abs into the cerebral ventricles of mice has been shown to cause intense NMDAR-Ab deposition in the hippocampus (Planagumà *et al.*, 2014). This region therefore seems to be a strong candidate for assays of the effects of NMDAR-abs on NMDAR-dependent synaptic transmission and network activity.

After the submission of this thesis, a further study demonstrating just such an effect was published (Planaguma *et al.*, 2016), closing the gap between reduced surface NMDAR loss and behavioural changes in the partial animal model described above (Planagumà *et al.*, 2014). In their (2016) study, the authors replicated their work showing memory impairments paralleling the course of NMDAR-Ab deposition in the hippocampus of mice receiving an intracerebral infusion of CSF from patients with NMDAR-abs. They also performed slice electrophysiology experiments *ex vivo* examining LTP in the hippocampus. They found that short-term plasticity, assayed using a paired pulse protocol, was similar in animals receiving patient or control CSF, indicating that pre-synaptic transmitter release probability was unaffected. However, LTP as indicated by an increase in the slope of the evoked field EPSP in CA1, was markedly reduced in animals having received patient CSF compared to control CSF.

LTP at the Schaffer collateral-CA1 synapses is NMDAR-dependent, and a mouse model with NR1 loss restricted to the CA1 area of the hippocampus has previously demonstrated absent CA1 LTP and selectively impaired spatial memory (Tsien *et al.*, 1996). It is therefore very likely that the antibody-mediated reduction in surface and synaptic NMDAR content demonstrated by Planaguma *et al.* (2016) throughout the hippocampus of the mice receiving patient CSF was responsible for the LTP deficit in these mice.

Additionally, they elegantly demonstrate the first potentially relevant non-immune-based translational therapeutic strategy. Indeed, Mikasova *et al.* (2012) had shown that the interaction between NMDAR and Ephrin B2 receptors was weakened by NMDAR-abs, leading to removal of NMDARs from the synapses and subsequent internalisation. Activating Ephrin B2 receptors using Ephrin B2 prevented the loss of NMDARs. Indeed, Ephrin B2 receptors are felt to stabilise and cluster NMDAR at excitatory synapses. Planaguma *et al.* (2016) added Ephrin B2 to the CSF infused in half the mice receiving patient and control CSF, and found that this prevented the memory impairment, the reduction in surface and synaptic NDMAR density and the loss of LTP. Although translating such a finding for use in the human disease will require much more work, including developing a fuller animal model of NMDAR-Ab encephalitis, it is an encouraging example of hypothesis-led laboratory discoveries finding practical and potentially therapeutic applications.

7.7 Summary

Publication of the results of the studies undertaken as part of this thesis are planned as follows:

7.7.1 Assay study

- Poor agreement between assays for serum sample results
- Good agreement when using CSF
- Performance of assays calculated using available clinical data (data collection still on-going, as is comparison of assays using a larger cohort of samples) shows:
    - Good performance of IHC with satisfactory “sensitivity” and excellent “specificity”
    - L-CBA also has good sensitivity, but at the expense of specificity
    - Euf-CBA has good specificity at the expense of sensitivity
    - Overall all tests require careful interpretation if performed using serum, in the light of clinical details and laboratories using Euf-

CBA should send away negative samples for re-testing on IHC and a CBA at a reference laboratory.

7.7.2 Electrophysiology

- Patient IgG reduces γ-oscillation power in acute slices in the mEC but not hippocampus
- Further experiments using a lower dilution on IgG will hopefully confirm this and allow construction of a dose-response curve
- At present, no mechanistic explanation for this effect is available but it is likely to be related to NMDAR internalisation in the slices.
- The results of the intracerebral injection studies will not be included in the publication, as the model did not appear to result in sufficient antibody binding to NMDARs.

Appendix

Appendix A Clinical details of patient samples used in this thesis

Patient 2

Patient 2 was a 25-year-old woman who developed headache and non-specific flu-like symptoms with a sore throat one week before becoming confused, disorientated and febrile. There also appeared to be intermittent anisocoria. Over the following 24 hours, the confusion worsened and was accompanied by anxiety and paranoid thoughts. She was admitted to hospital and started on antiviral therapy and antibiotics, as well as antiepileptic medication.

Lumbar puncture revealed a lymphocytosis with 120 lymphocytes per mm^3. CSF protein was modestly raised. Extensive virological investigations were negative. Over the next two days she became increasingly agitated and displayed catastrophic thinking. This was promptly followed by somnolence and reduced responsiveness. On the 6^{th} day of her admission, she responded only to pain and MRS score was 5. She was also diagnosed with a pulmonary embolism, which was treated with anticoagulation on a high dependency unit. Brain imaging with MRI showed bilateral hippocampal signal change.

On the 7^{th} day of admission, she developed periodic grimacing movements. EEG showed no evidence of epileptiform activity during these however. Abdominal distension was also noted.

As there had been no response to antiviral treatment with acyclovir, ganciclovir and ribavirin and viral PCR studies had been negative, anti-neuropil antibodies were looked for and NMDAR-Abs were detected. Imaging of chest, abdomen and pelvis with CT showed no abnormalities.

On day 10 of admission she developed excessive secretions from nose and mouth.

Pulsed intravenous methylprednisolone was commenced on day 25 of the illness, followed by high-dose oral prednisolone. She also received a course of intravenous immunoglobulin but failed to respond. An ovarian teratoma was not found, but she eventually underwent oophorectomy on day 160 of the illness as

she had failed to respond to treatments. She died on day 190, having remained at MRS 5 during the entire course of her illness.

Patient 3

Patient 3 initially presented in 2006 at the age of 15 with an acute onset of frequent complex partial seizures, visual hallucinations, agitation with aggressive outbursts, intermittent drowsiness and reversal of sleep-wake cycle. There was high signal in the right insular cortex on brain imaging with MRI and a CSF lymphocytosis with normal protein and glucose. EEG revealed diffuse slow wave activity over the right hemisphere. CSF PCR studies were negative for herpes viruses. Treatment with intravenous acyclovir and anticonvulsants did not lead to any improvement and she was therefore given a course of intravenous immunoglobulin for a presumptive immune-mediated encephalitis. Seizures and agitation settled, but she continued to be significantly cognitively impaired.

She re-presented in 2009 with a 4-day history of acute agitation, auditory halllucinations, reversal of sleep-wake cycle, and impulsive behaviours. No seizures or focal neurological signs were noted. Brain imaging with MRI and CSF studies were normal. CSF viral PCR studies were negative. EEG findings were similar to her previous admission with mild slowing over the right hemisphere but no epileptiform activity.

On this occasion, NMDAR-Ab encephalitis was suspected and the diagnosis was confirmed on serum assay. No teratoma was detected using CT scanning of chest, abdomen and pelvis as well as pelvic ultrasound.

She received intravenous immunoglobulin and high dose oral prednisolone with little benefit initially. She started to improve after plasma exchange. Slow improvement continued after this with a progressive decline in NMDAR-Ab level. She was treated with azathioprine as a steroid-sparing agent from 2010. There have been no further relapses, and she slowly recovered to a score of 96/100 on the Addenbrooke's cognitive examination. She is currently working full-time and is no longer on immunosuppressing medication, but she continues to have a low positive NMDAR-Ab titre.

Appendix B Clinical decision aid devised for the assay comparison study

Table B.1 Features required for a clinical diagnosis of NMDAR-Ab encephalitis

CORE FEATURES	SPECIFIC FEATURES	ADDITIONAL FEATURES
Inflammatory CSF	Psychiatric symptoms	Encephalopathy
Teratoma	Dysautonomic features	Altered consciousness (form stupor to coma)
	Movement disorders	Improvement with immunotherapy/tumour removal
	Seizures and/or EEG epileptiform abnormalities	MRI alterations
		Tumour other than teratoma

DIAGNOSIS	Core features	Specific features	Additional Features
DEFINITE	1/2	3/4	2/5
PROBABLE	1/2	<3	2/5
	or		
	0	3/4	2/5
POSSIBLE	1/2	1/4	<2
	or		
	0	2/4	2/5
UNLIKELY	0	<2	Irrelevant

For example, patient 2 above would score 1/2 on the core features (inflammatory CSF) and 3/4 on specific features (psychiatric symptoms, movement disorder, and dysautonomic features all present). She had 3 of the 5 additional features (encephalopathy, altered consciousness, and MRI abnormalities). She therefore qualifies for a definite clinical diagnosis of NMDAR-Ab encephalitis.

For patient 3, both episodes need to be considered together in order for a probable diagnosis to be made. When both episodes are considered together, 1 of the 2 core features were present (inflammatory CSF; first episode), as were 2 of the 4 specific features (psychiatric symptoms and seizures), and 3 of the 5 additional features (encephalopathy, improvement with immunotherapy, and MRI abnormalities). In this case, the presence of autoimmune encephalitis was

strongly suspected from the course of the first episode. The second episode was characterised by encephalopathy and psychiatric features, which on their own would be insufficient for anything above a possible NMDAR-Ab encephalitis diagnosis. However, the presence of a previous episode with clearer encephalitic features and the patient's age and sex, render any other diagnosis very unlikely.

References

Alexopoulos, H., Kosmidis, M. L., Dalmau, J. and Dalakas, M. C. (2011) 'Paraneoplastic anti-NMDAR encephalitis: long term follow-up reveals persistent serum antibodies', *J Neurol*, 258(8), pp. 1568-70.

Alonso, A. and Klink, R. (1993) 'Differential electroresponsiveness of stellate and pyramidal-like cells of medial entorhinal cortex layer II', *Journal of Neurophysiology*, 70(1), pp. 128-143.

Anderson, W. W., Anderson, W. W., Lewis, D. V., Scott Swartzwelder, H. and Wilson, W. A. (1986) 'Magnesium-free medium activates seizure-like events in the rat hippocampal slice', *Brain Research*, 398(1), pp. 215-219.

Bartos, M., Vida, I. and Jonas, P. (2007) 'Synaptic mechanisms of synchronized gamma oscillations in inhibitory interneuron networks', *Nat Rev Neurosci*, 8(1), pp. 45-56.

Bataller, L., Kleopa, K. A., Wu, G. F., Rossi, J. E., Rosenfeld, M. R. and Dalmau, J. (2007) 'Autoimmune limbic encephalitis in 39 patients: immunophenotypes and outcomes', *Journal of Neurology Neurosurgery and Psychiatry*, 78, pp. 381-385.

Batra, R., Pang, Y. and Friedman, M. T. 'Therapeutic plasma exchange in anti-N-methyl-D-aspartate-receptor (anti-NMDA-R) encephalitis associated with benign ovarian teratoma', *Journal of Clinical Apheresis*, 27(4), pp. 227-8.

Belforte, J. E., Zsiros, V., Sklar, E. R., Jiang, Z., Yu, G., Li, Y., Quinlan, E. M. and Nakazawa, K. (2010) 'Postnatal NMDA receptor ablation in corticolimbic interneurons confers schizophrenia-like phenotypes', *Nat Neurosci*, 13(1), pp. 76-83.

Berretta, N. and Jones, R. S. (1996) 'A comparison of spontaneous EPSCs in layer II and layer IV-V neurons of the rat entorhinal cortex in vitro', *J Neurophysiol*, 76(2), pp. 1089-100.

Bien, C. G., Schulze-Bonhage, A., Deckert, M., Urbach, H., Helmstaedter, C., Grunwald, T., Schaller, C. and Elger, C. E. (2000) 'Limbic encephalitis not associated with neoplasm as a cause of temporal lobe epilepsy', *Neurology*, 55, pp. 1823-1828.

Bliss, T. V. P. and Collingridge, G. L. (1993) 'A synaptic model of memory: Long-term potentiation in the hippocampus', *Nature*, 361(6407), pp. 31-39.

Bragin, A., Jando, G., Nadasdy, Z., Hetke, J., Wise, K. and Buzsaki, G. (1995) 'Gamma (40-100 Hz) oscillation in the hippocampus of the behaving rat', *Journal of Neuroscience*, 15(1 I), pp. 47-60.

Buckley, C., Oger, J., Clover, L., Tüzün, E., Carpenter, K., Jackson, M. and Vincent, A. (2001) 'Potassium channel antibodies in two patients with reversible limbic encephalitis', *Ann Neurol*, 50, pp. 73-78.

Buhl, E. H., Halasy, K. and Somogyi, P. (1994) 'Diverse sources of hippocampal unitary inhibitory postsynaptic potentials and the number of synaptic release sites', *Nature*, 368, pp. 823-828.

Buzsaki, G. and Draguhn, A. (2004) 'Neuronal oscillations in cortical networks', *Science*, 304(5679), pp. 1926-9.

Camdessanché, J. P., Streichenberger, N., Cavillon, G., Rogemond, V., Jousserand, G., Honnorat, J., Convers, P. and Antoine, J. C. (2011) 'Brain immunohistopathological study in a patient with anti-NMDAR encephalitis', *European Journal of Neurology*, 18(6), pp. 929-931.

Cardin, J. A., Carlen, M., Meletis, K., Knoblich, U., Zhang, F., Deisseroth, K., Tsai, L. H. and Moore, C. I. (2009) 'Driving fast-spiking cells induces gamma rhythm and controls sensory responses', *Nature*, 459(7247), pp. 663-7.

Carlen, M., Meletis, K., Siegle, J. H., Cardin, J. A., Futai, K., Vierling-Claassen, D., Ruhlmann, C., Jones, S. R., Deisseroth, K., Sheng, M., Moore, C. I. and Tsai, L. H. (2011) 'A critical role for NMDA receptors in parvalbumin interneurons for gamma rhythm induction and behavior', *Mol Psychiatry*.

Carvajal, A., Jacobson, L., Clover, L., Lang, B., Upton, L. and Vincent, A. (2015) 'Passive transfer of glycine receptor-antibody IgG induces anxiety-like behaviour in mice', *Americal Academy of Neurology*. Neurology.

Castro-Alamancos, M. A. and Connors, B. W. (1996) 'Spatiotemporal properties of short-term plasticity sensorimotor thalamocortical pathways of the rat', *J Neurosci*, 16(8), pp. 2767-79.

Chapman, A. G. (1998) 'Glutamate receptors in epilepsy', *Prog Brain Res*, 116, pp. 371-83.

Chrobak, J. J. and Buzsaki, G. (1996) 'High-frequency oscillations in the output networks of the hippocampal-entorhinal axis of the freely behaving rat', *J Neurosci*, 16(9), pp. 3056-66.

Coesmans, M., Sillevis Smitt, P. A., Linden, D. J., Shigemoto, R., Hirano, T., Yamakawa, Y., Van Alphen, A. M., Luo, C., Van Der Geest, J. N., Kros, J. M., Gaillard, C. A., Frens, M. A. and De Zeeuw, C. I. (2003) 'Mechanisms underlying cerebellar motor deficits due to mGluR1-autoantibodies', *Annals of Neurology*, 53(3), pp. 325-336.

Congdon, E. E., Gu, J., Sait, H. B. and Sigurdsson, E. M. (2013) 'Antibody uptake into neurons occurs primarily via clathrin-dependent Fcgamma receptor endocytosis and is a prerequisite for acute tau protein clearance', *J Biol Chem*, 288(49), pp. 35452-65.

Cunningham, M. O., Davies, C. H., Buhl, E. H., Kopell, N. and Whittington, M. A. (2003a) 'Gamma Oscillations Induced by Kainate Receptor Activation in the Entorhinal Cortex In Vitro', *Journal of Neuroscience*, 23(30), pp. 9761-9769.

Cunningham, M. O., Davies, C. H., Buhl, E. H., Kopell, N. J. and Whittington, M. (2003b) 'Gamma oscillations induced by kainate receptor activation in the entorhinal cortex *in vitro*', *The Journal of Neuroscience*, 23(30), pp. 9761-9769.

Cunningham, M. O., Hunt, J., Middleton, S., LeBeau, F. E. N., Gillies, M. G., Davies, C. H., Maycox, P. R., Whittington, M. A. and Racca, C. (2006) 'Region-specific reduction in entorhinal gamma oscillations and parvalbumin-immunoreactive neurons in animal models of psychiatric illness', *Journal of Neuroscience*, 26(10), pp. 2767-2776.

Cunningham, M. O., Whittington, M. A., Bibbig, A., Roopun, A., LeBeau, F. E. N., Vogt, A., Monyer, H., Buhl, E. H. and Traub, R. D. (2004) 'A role for fast rhythmic bursting neurons in cortical gamma oscillations in vitro', *Proc Natl Acad Sci U S A*, 101(18), pp. 7152-7157.

Dahm, L., Ott, C., Steiner, J., Stepniak, B., Teegen, B., Saschenbrecker, S., Hammer, C., Borowski, K., Begemann, M., Lemke, S., Rentzsch, K., Probst, C., Martens, H., Wienands, J., Spalletta, G., Weissenborn, K., Stocker, W. and Ehrenreich, H. (2014) 'Seroprevalence of autoantibodies against brain antigens in health and disease', *Ann Neurol*, 76(1), pp. 82-94.

Dale, R. C., Pillai, S. and Brilot, F. (2013) 'Cerebrospinal fluid CD19(+) B-cell expansion in N-methyl-D-aspartate receptor encephalitis', *Developmental Medicine & Child Neurology*, 55(2), pp. 191-3.

Dalmau, J. (2017) 'In vitro effects of a human monoclonal antibody against the N-methyl-d-aspartate receptor', *Brain*, 140(Pt 2), p. e9.

Dalmau, J., Gleichman, A. J., Hughes, E. G., Rossi, J. E., Peng, X., Lai, M., Dessain, S. K., Rosenfeld, M. R., Balice-Gordon, R. and Lynch, D. R. (2008) 'Anti-NMDA-receptor encephalitis: case series and analysis of the effects of antibodies', *The Lancet Neurology*, 7(12), pp. 1091-1098.

Dalmau, J., Lancaster, E., Martinez-Hernandez, E., Rosenfeld, M. R. and Balice-Gordon, R. (2011) 'Clinical experience and laboratory investigations in patients with anti-NMDAR encephalitis', *The Lancet Neurology*, 10(1), pp. 63-74.

Dalmau, J. and Rosenfeld, M. R. (2008) 'Paraneoplastic syndromes of the CNS', *The Lancet Neurology*, 7(4), pp. 327-340.

Dalmau, J., Tuzun, E., Wu, H. Y., Masjuan, J., Rossi, J. E., Voloschin, A., Baehring, J. M., Shimazaki, H., Koide, R., King, D., Mason, W., Sansing, L. H., Dichter, M. A., Rosenfeld, M. R. and Lynch, D. R. (2007) 'Paraneoplastic anti-N-methyl-D-aspartate receptor encephalitis associated with ovarian teratoma', *Ann Neurol*, 61(1), pp. 25-36.

de Toledo-Morrell, L., Goncharova, I., Dickerson, B., Wilson, R. S. and Bennett, D. A. (2000) 'From healthy aging to early Alzheimer's disease: in vivo detection of entorhinal cortex atrophy', *Ann N Y Acad Sci*, 911, pp. 240-53.

de Witte, L. D., Hoffmann, C., van Mierlo, H. C., Titulaer, M. J., Kahn, R. S. and Martinez-Martinez, P. (2015) 'Absence of N-Methyl-D-Aspartate Receptor IgG Autoantibodies in Schizophrenia: The Importance of Cross-Validation Studies', *JAMA Psychiatry*, 72(7), pp. 731-3.

Dhillon, A. and Jones, R. S. (2000) 'Laminar differences in recurrent excitatory transmission in the rat entorhinal cortex in vitro', *Neuroscience*, 99(3), pp. 413-22.

Dingledine, R., Borges, K., Bowie, D. and Traynelis, S. F. (1999) 'The glutamate receptor ion channels', *Pharmacol Rev*, 51(1), pp. 7-61.

Du, F., Whetsell, W. O., Jr., Abou-Khalil, B., Blumenkopf, B., Lothman, E. W. and Schwarcz, R. (1993) 'Preferential neuronal loss in layer III of the entorhinal cortex in patients with temporal lobe epilepsy', *Epilepsy Res*, 16(3), pp. 223-33.

Duncan, G. E., Inada, K., Koller, B. H. and Moy, S. S. (2010) 'Increased sensitivity to kainic acid in a genetic model of reduced NMDA receptor function', *Brain research*, 1307, pp. 166-176.

Duncan, G. E., Moy, S. S., Perez, A., Eddy, D. M., Zinzow, W. M., Lieberman, J. A., Snouwaert, J. N. and Koller, B. H. (2004) 'Deficits in sensorimotor gating and tests of social behavior in a genetic model of reduced NMDA receptor function', *Behav Brain Res*, 153(2), pp. 507-19.

Ego-Stengel, V. and Wilson, M. A. (2010) 'Disruption of ripple-associated hippocampal activity during rest impairs spatial learning in the rat', *Hippocampus*, 20(1), pp. 1-10.

Eichenbaum, H., Yonelinas, A. P. and Ranganath, C. (2007) 'The medial temporal lobe and recognition memory', *Annu Rev Neurosci*, 30, pp. 123-52.

EUROIMMUN Medizinische Labordiagnostika AG (2011) *Anti-glutamate receptor (type NMDA) IFA test instructions* (Version 17.06.2011, FA_112d-51_A_US_D03.doc) (Accessed: 29.09.2015).

Farmilo, A. J. and Stead, R. H. (2001) 'Fixation', in Boenisch, T. (ed.) *Handbook Immunochemical Staining Methods*. Third Edition edn. California, USA: DakoCytomation.

Fell, J., Klaver, P., Lehnertz, K., Grunwald, T., Schaller, C., Elger, C. E. and Fernandez, G. (2001) 'Human memory formation is accompanied by rhinal-hippocampal coupling and decoupling', *Nat Neurosci*, 4(12), pp. 1259-64.

Finke, C., Kopp, U. A., Prüss, H., Dalmau, J., Wandinger, K. P. and Ploner, C. J. (2012) 'Cognitive deficits following anti-NMDA receptor encephalitis', *Journal of Neurology, Neurosurgery and Psychiatry*, 83(2), pp. 195-198.

Fisahn, A., Contractor, A., Traub, R. D., Buhl, E. H., Heinemann, S. F. and McBain, C. J. (2004) 'Distinct roles for the kainate receptor subunits GluR5 and GluR6 in kainate-induced hippocampal gamma oscillations', *J Neurosci*, 24(43), pp. 9658-68.

Fisahn, A., Pike, F. G., Buhl, E. H. and Paulsen, O. (1998) 'Cholinergic induction of network oscillations at 40 Hz in the hippocampus *in vitro*', *Nature*, 394, pp. 186-189.

Florance, N. R., Davis, R. L., Lam, C., Szperka, C., Zhou, L., Ahmad, S., Campen, C. J., Moss, H., Peter, N., Gleichman, A. J., Glaser, C. A., Lynch, D. R., Rosenfeld, M. R. and Dalmau, J. (2009) 'Anti-N-methyl-D-aspartate receptor (NMDAR) encephalitis in children and adolescents', *Annals of Neurology*, 66(1), pp. 11-18.

Frechette, E. S., Zhou, L., Galetta, S. L., Chen, L. and Dalmau, J. (2011) 'Prolonged follow-up and CSF antibody titers in a patient with anti-NMDA receptor encephalitis', *Neurology: Clinical Practice*, 76(Supplement 2), pp. S64-S66.

Fuchs, E. C., Zivkovic, A. R., Cunningham, M. O., Middleton, S., Lebeau, F. E., Bannerman, D. M., Rozov, A., Whittington, M. A., Traub, R. D., Rawlins, J. N. and Monyer, H. (2007) 'Recruitment of parvalbumin-positive interneurons determines hippocampal function and associated behavior', *Neuron*, 53(4), pp. 591-604.

Fyhn, M., Molden, S., Witter, M. P., Moser, E. I. and Moser, M.-B. (2004) 'Spatial Representation in the Entorhinal Cortex', *Science*, 305(5688), pp. 1258-1264.

Gabilondo, I., Saiz, A., Galán, L., González, V., Jadraque, R., Sabater, L., Sans, A., Sempere, A., Vela, A., Villalobos, F., Viñals, M., Villoslada, P. and Graus, F. (2011) 'Analysis of relapses in anti-NMDAR encephalitis', *Neurology*, 77(10), pp. 996-999.

Gandal, M. J., Sisti, J., Klook, K., Ortinski, P. I., Leitman, V., Liang, Y., Thieu, T., Anderson, R., Pierce, R. C., Jonak, G., Gur, R. E., Carlson, G. and Siegel,

S. J. (2012) 'GABAB-mediated rescue of altered excitatory-inhibitory balance, gamma synchrony and behavioral deficits following constitutive NMDAR-hypofunction', *Transl Psychiatry*, 2, p. e142.

Gao, X. M., Sakai, K., Roberts, R. C., Conley, R. R., Dean, B. and Tamminga, C. A. (2000) 'Ionotropic glutamate receptors and expression of N-methyl-D-aspartate receptor subunits in subregions of human hippocampus: effects of schizophrenia', *Am J Psychiatry*, 157(7), pp. 1141-9.

Geis, C., Grünewald, B., Weishaupt, A., Wultsch, T., Toyka, K. V., Reif, A. and Sommer, C. (2012) 'Human IgG directed against amphiphysin induces anxiety behavior in a rat model after intrathecal passive transfer', *Journal of Neural Transmission*, 119(8), pp. 981-985.

Geis, C., Weishaupt, A., Hallermann, S., Grunewald, B., Wessig, C., Wultsch, T., Reif, A., Byts, N., Beck, M., Jablonka, S., Boettger, M. K., Uceyler, N., Fouquet, W., Gerlach, M., Meinck, H. M., Siren, A. L., Sigrist, S. J., Toyka, K. V., Heckmann, M. and Sommer, C. (2010) 'Stiff person syndrome-associated autoantibodies to amphiphysin mediate reduced GABAergic inhibition', *Brain*, 133(11), pp. 3166-80.

Gleichman, A. J., Spruce, L. A., Dalmau, J., Seeholzer, S. H. and Lynch, D. R. (2012) 'Anti-NMDA receptor encephalitis antibody binding is dependent on amino acid identity of a small region within the GluN1 amino terminal domain', *Journal of Neuroscience*, 32(32), pp. 11082-11094.

Graus, F., Cordon-Cardo, C. and Posner, J. B. (1985) 'Neuronal antinuclear antibody in sensory neuronopathy from lung cancer', *Neurology*, 35(4), pp. 538-543.

Gray, C. M. and Singer, W. (1989) 'Stimulus-specific neuronal oscillations in orientation columns of cat visual cortex', *Proc Natl Acad Sci U S A*, 86(5), pp. 1698-702.

Greenhill, S. D., Chamberlain, S. E., Lench, A., Massey, P. V., Yuill, K. H., Woodhall, G. L. and Jones, R. S. (2014) 'Background synaptoc activity in rat entorhinal cortex shows a progressively greater dominance of inhibition over excitation from deep to superficial layers', *PLoS One*, 9(1), p. e85125.

Greenlee, J. E., Clawson, S. A., Hill, K. E., Wood, B., Clardy, S. L., Tsunoda, I., Jaskowski, T. D. and Carlson, N. G. (2014) 'Neuronal uptake of anti-Hu antibody, but not anti-Ri antibody, leads to cell death in brain slice cultures', *J Neuroinflammation*, 11, p. 160.

Grenier, F., Timofeev, I. and Steriade, M. (2003) 'Neocortical very fast oscillations (ripples, 80-200 Hz) during seizures: intracellular correlates', *J Neurophysiol*, 89(2), pp. 841-52.

Gresa-Arribas, N., Titulaer, M. J., Torrents, A., Aguilar, E., McCracken, L., Leypoldt, F., Gleichman, A. J., Balice-Gordon, R., Rosenfeld, M. R., Lynch, D., Graus, F. and Dalmau, J. (2014) 'Antibody titres at diagnosis and during follow-up of anti-NMDA receptor encephalitis: a retrospective study', *The Lancet Neurology*, 13(2), pp. 167-177.

Grosshans, D. R., Clayton, D. A., Coultrap, S. J. and Browning, M. D. (2002a) 'Analysis of glutamate receptor surface expression in acute hippocampal slices', *Science"s STKE [electronic resource] : signal transduction knowledge environment*, 2002(137).

Grosshans, D. R., Clayton, D. A., Coultrap, S. J. and Browning, M. D. (2002b) 'LTP leads to rapid surface expression of NMDA but not AMPA receptors in adult rat CA1', *Nat Neurosci*, 5(1), pp. 27-33.

Grunze, H. C., Rainnie, D. G., Hasselmo, M. E., Barkai, E., Hearn, E. F., McCarley, R. W. and Greene, R. W. (1996) 'NMDA-dependent modulation of CA1 local circuit inhibition', *J Neurosci*, 16(6), pp. 2034-43.

Gulyás, A. I., Szabó, G. G., Ulbert, I., Holderith, N., Monyer, H., Erdélyi, F., Szabó, G., Freund, T. F. and Hájos, N. (2010) 'Parvalbumin-containing fast-spiking basket cells generate the field potential oscillations induced by cholinergic receptor activation in the hippocampus', *The Journal of neuroscience : the official journal of the Society for Neuroscience*, 30(45), pp. 15134-15145.

Hachiya, Y., Uruha, A., Kasai-Yoshida, E., Shimoda, K., Satoh-Shirai, I., Kumada, S., Kurihara, E., Suzuki, K., Ohba, A., Hamano, S. and Sakuma, H. (2013) 'Rituximab ameliorates anti-N-methyl-D-aspartate receptor encephalitis by removal of short-lived plasmablasts', *Journal of Neuroimmunology*, 265(1-2), pp. 128-30.

Haenschel, C., Baldeweg, T., Croft, R. J., Whittington, M. and Gruzelier, J. (2000) 'Gamma and beta frequency oscillations in response to novel auditory stimuli: A comparison of human electroencephalogram (EEG) data with in vitro models', *Proc Natl Acad Sci U S A*, 97(13), pp. 7645-50.

Hafting, T., Fyhn, M., Molden, S., Moser, M. B. and Moser, E. I. (2005) 'Microstructure of a spatial map in the entorhinal cortex', *Nature*, 436(7052), pp. 801-6.

Hájos, N., Pálhalini, J., Mann, E. O., Nèmeth, B., Paulsen, O. and Freund, T. F. (2004) 'Spike timing of distinct types of GABAergic interneuron during hippocampal gamma oscillations in vitro', *Journal of Neuroscience*, 24(41), pp. 9127-9137.

Hakami, T., Jones, N. C., Tolmacheva, E. A., Gaudias, J., Chaumont, J., Salzberg, M., O'Brien, T. J. and Pinault, D. (2009) 'NMDA receptor hypofunction leads to generalized and persistent aberrant gamma oscillations independent of hyperlocomotion and the state of consciousness', *PLoS One*, 4(8), p. e6755.

Hall, S. (2012) *An examination into the impact of cross-fostering on entorhinal-hippocampal gamma rhythmogenesis*. Newcastle University.

Hanslmayr, S., Spitzer, B. and Bauml, K. H. (2009) 'Brain oscillations dissociate between semantic and nonsemantic encoding of episodic memories', *Cereb Cortex*, 19(7), pp. 1631-40.

Hara, M., Morita, A., Kamei, S., Yamaguchi, M., Homma, T., Nemoto, N., Sugita, K., Yamamoto, T. and Dalmau, J. (2011) 'Anti-N-methyl-D-aspartate receptor encephalitis associated with carcinosarcoma with neuroendocrine differentiation of the uterus', *J Neurol*, 258(7), pp. 1351-3.

Hebb, D. O. (1949) *The Organization of Behavior*. New York: John Wiley.

Hill, K. E., Clawson, S. A., Rose, J. W., Carlson, N. G. and Greenlee, J. E. (2009) 'Cerebellar Purkinje cells incorporate immunoglobulins and immunotoxins in vitro: implications for human neurological disease and immunotherapeutics', *J Neuroinflammation*, 6, p. 31.

Höftberger, R., Sabater, L., Marignier, R., Aboul-Enein, F., Bernard-Valnet, R., Rauschka, H., Ruiz, A., Blanco, Y., Graus, F., Dalmau, J. and Saiz, A. (2013) 'An Optimized Immunohistochemistry Technique Improves NMO-IgG Detection: Study Comparison with Cell-Based Assays', *PLoS ONE*, 8(11), p. e79083.

Homayoun, H. and Moghaddam, B. (2007) 'NMDA receptor hypofunction produces opposite effects on prefrontal cortex interneurons and pyramidal neurons', *J Neurosci*, 27(43), pp. 11496-500.

Howard, M. W. (2003) 'Gamma Oscillations Correlate with Working Memory Load in Humans', *Cerebral Cortex*, 13(12), pp. 1369-1374.

Hughes, E. G., Peng, X., Gleichman, A. J., Lai, M., Zhou, L., Tsou, R., Parsons, T. D., Lynch, D. R., Dalmau, J. and Balice-Gordon, R. J. (2010) 'Cellular and synaptic mechanisms of anti-NMDA receptor encephalitis', *J Neurosci*, 30(17), pp. 5866-75.

Hull, C., Isaacson, J. S. and Scanziani, M. (2009) 'Postsynaptic mechanisms govern the differential excitation of cortical neurons by thalamic inputs', *J Neurosci*, 29(28), pp. 9127-36.

Iffland, P. H., Carvalho-Tavares, J., Trigunaite, A., Man, S., Rasmussen, P., Alexopoulos, A., Ghosh, C., Jørgensen, T. N. and Janigro, D. (2013) 'Intracellular and circulating neuronal antinuclear antibodies in human epilepsy', *Neurobiology of disease*, 59, pp. 206-219.

Iizuka, T., Sakai, F., Ide, T., Monzen, T., Yoshii, S., Iigaya, M., Suzuki, K., Lynch, D. R., Suzuki, N., Hata, T. and Dalmau, J. (2008) 'Anti-NMDA receptor encephalitis in Japan: Long-term outcome without tumor removal', *Neurology*, 70(7), pp. 504-511.

Ikeda, J., Mori, K., Oka, S. and Watanbe, Y. (1989) 'A columnar arrangement of dendritic processes of entorhinal cortex neurons revealed by a monoclonal antibody', *Brain Res*, 505(1), pp. 176-9.

Inta, D., Monyer, H., Sprengel, R., Meyer-Lindenberg, A. and Gass, P. (2010) 'Mice with genetically altered glutamate receptors as models of schizophrenia: a comprehensive review', *Neurosci Biobehav Rev*, 34(3), pp. 285-94.

Irani, S. R., Alexander, S., Waters, P., Kleopa, K. A., Pettingill, P., Zuliani, L., Peles, E., Buckley, C., Lang, B. and Vincent, A. (2010a) 'Antibodies to Kv1 potassium channel-complex proteins leucine-rich, glioma inactivated 1 protein and contactin-associated protein-2 in limbic encephalitis, Morvan's syndrome and acquired neuromyotonia', *Brain*, 133(9), pp. 2734-48.

Irani, S. R., Bera, K., Waters, P., Zuliani, L., Maxwell, S., Zandi, M. S., Friese, M. A., Galea, I., Kullmann, D. M., Beeson, D., Lang, B., Bien, C. G. and Vincent, A. (2010b) 'N-methyl-d-aspartate antibody encephalitis: Temporal progression of clinical and paraclinical observations in a predominantly non-paraneoplastic disorder of both sexes', *Brain*, 133(6), pp. 1655-1667.

Irani, S. R., Pettingill, P., Kleopa, K. A., Schiza, N., Waters, P., Mazia, C., Zuliani, L., Watanabe, O., Lang, B., Buckley, C. and Vincent, A. (2012) 'Morvan syndrome: clinical and serological observations in 29 cases', *Annals of Neurology*, 72(2), pp. 241-55.

Ishiura, H., Matsuda, S., Higashihara, M., Hasegawa, M., Hida, A., Hanajima, R., Yamamoto, T., Shimizu, J., Dalmau, J. and Tsuji, S. (2008) 'Response of

anti-nmda receptor encephalitis without tumor to immunotherapy including rituximab', *Neurology*, 71(23), pp. 1921-1923.

Jantzen, S. U., Ferrea, S., Wach, C., Quasthoff, K., Illes, S., Scherfeld, D., Hartung, H. P., Seitz, R. J. and Dihné, M. (2013) 'In vitro neuronal network activity in NMDA receptor encephalitis', *BMC Neuroscience*, 14.

Jones, R. S. (1994) 'Synaptic and intrinsic properties of neurons of origin of the perforant path in layer II of the rat entorhinal cortex in vitro', *Hippocampus*, 4(3), pp. 335-53.

Jones, R. S. and Buhl, E. H. (1993) 'Basket-like interneurones in layer II of the entorhinal cortex exhibit a powerful NMDA-mediated synaptic excitation', *Neuroscience Letters*, 149, pp. 35-39.

Kalev-Zylinska, M. L., Symes, W., Young, D. and During, M. J. (2009) 'Knockdown and overexpression of NR1 modulates NMDA receptor function', *Mol Cell Neurosci*, 41(4), pp. 383-96.

Kandel, E. R., Kupfermann, I. and Iversen, S. (2000) 'Learning and Memory', in Kandel, E. R., Schwartz, J. H. and Jessell, T. M. (eds.) *Principles of Neural Science*. Fourth Edition edn. McGraw-Hill, pp. 1227-1247.

Kann, O., Papageorgiou, I. E. and Draguhn, A. (2014) 'Highly energized inhibitory interneurons are a central element for information processing in cortical networks', *J Cereb Blood Flow Metab*, 34(8), pp. 1270-82.

Kataoka, H., Dalmau, J. and Ueno, S. (2008) 'Paraneoplastic encephalitis associated with ovarian teratoma and N-methyl-d-aspartate receptor antibodies [4]', *European Journal of Neurology*, 15(1), pp. e5-e6.

Keilhoff, G., Becker, A., Grecksch, G., Wolf, G. and Bernstein, H. G. (2004) 'Repeated application of ketamine to rats induces changes in the hippocampal expression of parvalbumin, neuronal nitric oxide synthase and cFOS similar to those found in human schizophrenia', *Neuroscience*, 126(3), pp. 591-8.

Klausberger, T., Magill, P. J., Marton, L. F., Roberts, J. D. B., Cobden, P. M., Buzsaki, G. and Somogyi, P. (2003) 'Brain-state- and cell-type-specific firing of hippocampal interneurons *in vivo*', *Nature*, 421, pp. 844-848.

Klink, R. and Alonso, A. (1993) 'Ionic mechanisms for the subthreshold oscillations and differential electroresponsiveness of medial entorhinal cortex layer II neurons', *J Neurophysiol*, 70(1), pp. 144-57.

Korotkova, T., Fuchs, E. C., Ponomarenko, A., von Engelhardt, J. and Monyer, H. (2010) 'NMDA receptor ablation on parvalbumin-positive interneurons impairs hippocampal synchrony, spatial representations, and working memory', *Neuron*, 68(3), pp. 557-69.

Kreye, J., Wenke, N. K., Chayka, M., Leubner, J., Murugan, R., Maier, N., Jurek, B., Ly, L. T., Brandl, D., Rost, B. R., Stumpf, A., Schulz, P., Radbruch, H., Hauser, A. E., Pache, F., Meisel, A., Harms, L., Paul, F., Dirnagl, U., Garner, C., Schmitz, D., Wardemann, H. and Pruss, H. (2016) 'Human cerebrospinal fluid monoclonal N-methyl-D-aspartate receptor autoantibodies are sufficient for encephalitis pathogenesis', *Brain*, 139(Pt 10), pp. 2641-2652.

Krystal, J. H., Karper, L. P., Seibyl, J. P., Freeman, G. K., Delaney, R., Bremner, J. D., Heninger, G. R., Bowers Jr, M. B. and Charney, D. S. (1994) 'Subanesthetic effects of the noncompetitive NMDA antagonist, ketamine, in

humans: Psychotomimetic, perceptual, cognitive, and neuroendocrine responses', *Archives of General Psychiatry*, 51(3), pp. 199-214.

Kurian, M., Fluss, J. and Korff, C. 'Anti-NMDA receptor encephalitis: the importance of early diagnosis and aggressive immunotherapy in tumor negative pediatric patients', *European Journal of Paediatric Neurology*, 16(6), pp. 764-5.

Kwon, J. S., O'Donnell, B. F., Wallenstein, G. V., Greene, R. W., Hirayasu, Y., Nestor, P. G., Hasselmo, M. E., Potts, G. F., Shenton, M. E. and McCarley, R. W. (1999) 'Gamma frequency-range abnormalities to auditory stimulation in schizophrenia', *Arch Gen Psychiatry*, 56(11), pp. 1001-5.

Lahti, A. C., Koffel, B., LaPorte, D. and Tamminga, C. A. (1995) 'Subanesthetic doses of ketamine stimulate psychosis in schizophrenia', *Neuropsychopharmacology*, 13(1), pp. 9-19.

Lahti, A. C., Weiler, M. A., Tamara Michaelidis, B. A., Parwani, A. and Tamminga, C. A. (2001) 'Effects of ketamine in normal and schizophrenic volunteers', *Neuropsychopharmacology*, 25(4), pp. 455-67.

Lai, M., Hughes, E. G., Peng, X., Zhou, L., Gleichman, A. J., Shu, H., Mata, S., Kremens, D., Vitaliani, R., Geschwind, M. D., Bataller, L., Kalb, R. G., Davis, R., Graus, F., Lynch, D. R., Balice-Gordon, R. and Dalmau, J. (2009) 'AMPA receptor antibodies in limbic encephalitis alter synaptic receptor location', *Ann Neurol*, 65(4), pp. 424-34.

Lalic, T., Pettingill, P., Vincent, A. and Capogna, M. (2011) 'Human limbic encephalitis serum enhances hippocampal mossy fiber-CA3 pyramidal cell synaptic transmission', *Epilepsia*, 52(1), pp. 121-31.

Lancaster, E., Lai, M., Peng, X., Hughes, E., Constantinescu, R., Raizer, J., Friedman, D., Skeen, M. B., Grisold, W., Kimura, A., Ohta, K., Iizuka, T., Guzman, M., Graus, F., Moss, S. J., Balice-Gordon, R. and Dalmau, J. (2010) 'Antibodies to the GABA(B) receptor in limbic encephalitis with seizures: case series and characterisation of the antigen', *Lancet Neurol*, 9(1), pp. 67-76.

Lawley, A. (2009) *Anti-NMDA receptor antibodies: implications for the disruption of cortical gamma-frequency oscillations*. Dissertation thesis. Newcastle University.

Leite, M. I., Jacob, S., Viegas, S., Cossins, J., Clover, L., Morgan, B. P., Beeson, D., Willcox, N. and Vincent, A. (2008) 'IgG1 antibodies to acetylcholine receptors in 'seronegative' myasthenia gravis', *Brain*, 131(Pt 7), pp. 1940-52.

Leypoldt, F., Armangue, T. and Dalmau, J. (2015) 'Autoimmune encephalopathies', *Ann N Y Acad Sci*, 1338, pp. 94-114.

Li, Q., Clark, S., Lewis, D. V. and Wilson, W. A. (2002) 'NMDA receptor antagonists disinhibit rat posterior cingulate and retrosplenial cortices: a potential mechanism of neurotoxicity', *J Neurosci*, 22(8), pp. 3070-80.

Liguori, R., Vincent, A., Clover, L., Avoni, P., Plazzi, G., Cortelli, P., Baruzzi, A., Carey, T., Gambetti, P., Lugaresi, E. and Montagna, P. (2001) 'Morvan's syndrome: peripheral and central nervous system and cardiac involvement with antibodies to voltage-gated potassium channels', *Brain*, 124(Pt 12), pp. 2417-26.

Lin, F. and Stevens, C. F. (1994) 'Both open and closed NMDA receptor channels desensitize', *J Neurosci*, 14(4), pp. 2153-60.

Liu, X.-B. and Murray, K. D. (2012) 'Neuronal excitability and calcium/calmodulin-dependent protein kinase type II: Location, location, location', *Epilepsia*, 53, pp. 45-52.

Llinas, R. and Ribary, U. (1993) 'Coherent 40-Hz oscillation characterizes dream state in humans', *Proc Natl Acad Sci U S A*, 90, pp. 1078-2081.

Low, C.-M. and Wee, K. S.-L. (2010) 'New Insights into the Not-So-New NR3 Subunits of N-Methyl-d-aspartate Receptor: Localization, Structure, and Function', *Molecular Pharmacology*, 78(1), pp. 1-11.

Lu, L., Leutgeb, J. K., Tsao, A., Henriksen, E. J., Leutgeb, S., Barnes, C. A., Witter, M. P., Moser, M. B. and Moser, E. I. (2013) 'Impaired hippocampal rate coding after lesions of the lateral entorhinal cortex', *Nat Neurosci*, 16(8), pp. 1085-93.

Mackay, G., Ahmad, K., Stone, J., Sudlow, C., Summers, D., Knight, R., Will, R., Irani, S., Vincent, A. and Maddison, P. (2012) 'NMDA receptor autoantibodies in sporadic Creutzfeldt-Jakob disease', *Journal of Neurology*, 259(9), pp. 1979-1981.

Malter, M. P., Helmstaedter, C., Urbach, H., Vincent, A. and Bien, C. G. (2010) 'Antibodies to glutamic acid decarboxylase define a form of limbic encephalitis', *Ann Neurol*, 67(4), pp. 470-8.

Mann, E. O. and Mody, I. (2010) 'Control of hippocampal gamma oscillation frequency by tonic inhibition and excitation of interneurons', *Nat Neurosci*, 13(2), pp. 205-212.

Mann, E. O., Suckling, J. M., Hajos, N., Greenfield, S. A. and Paulsen, O. (2005) 'Perisomatic feedback inhibition underlies cholinergically induced fast network oscillations in the rat hippocampus in vitro', *Neuron*, 45(1), pp. 105-117.

Mansbach, R. S. and Geyer, M. A. (1989) 'Effects of phencyclidine and phencyclidine biologs on sensorimotor gating in the rat', *Neuropsychopharmacology*, 2(4), pp. 299-308.

Manto, M., Dalmau, J., Didelot, A., Rogemond, V. and Honnorat, J. (2010) 'In vivo effects of antibodies from patients with anti-NMDA receptor encephalitis: further evidence of synaptic glutamatergic dysfunction', *Orphanet J Rare Dis*, 5, p. 31.

Manto, M., Dalmau, J., Didelot, A., Rogemond, V. and Honnorat, J. (2011) 'Afferent facilitation of corticomotor responses is increased by IgGs of patients with NMDA-receptor antibodies', *J Neurol*, 258(1), pp. 27-33.

Martinez-Hernandez, E., Horvath, J., Shiloh-Malawsky, Y., Sangha, N., Martinez-Lage, M. and Dalmau, J. (2011) 'Analysis of complement and plasma cells in the brain of patients with anti-NMDAR encephalitis', *Neurology*, 77(6), pp. 589-593.

Masdeu, J. C., Gonzalez-Pinto, A., Matute, C., Ruiz De Azua, S., Palomino, A., De Leon, J., Berman, K. F. and Dalmau, J. (2012) 'Serum IgG antibodies against the NR1 subunit of the NMDA receptor not detected in schizophrenia', *Am J Psychiatry*, 169(10), pp. 1120-1.

Middleton, S., Jalics, J., Kispersky, T., Lebeau, F. E., Roopun, A. K., Kopell, N. J., Whittington, M. A. and Cunningham, M. O. (2008) 'NMDA receptor-dependent switching between different gamma rhythm-generating microcircuits in entorhinal cortex', *Proc Natl Acad Sci U S A*, 105(47), pp. 18572-7.

Mikasova, L., De Rossi, P., Bouchet, D., Georges, F., Rogemond, V., Didelot, A., Meissirel, C., Honnorat, J. and Groc, L. (2012) 'Disrupted surface cross-talk between NMDA and Ephrin-B2 receptors in anti-NMDA encephalitis', *Brain*, 135(5), pp. 1606-1621.

Miltner, W. H. R., Braun, C., Arnold, M., Witte, H. and Taub, E. (1999) 'Coherence of gamma-band EEG activity as a basis for associative learning', *Nature*, 397, pp. 434-436.

Moghaddam, B., Adams, B., Verma, A. and Daly, D. (1997) 'Activation of glutamatergic neurotransmission by ketamine: a novel step in the pathway from NMDA receptor blockade to dopaminergic and cognitive disruptions associated with the prefrontal cortex', *J Neurosci*, 17(8), pp. 2921-7.

Mohn, A. R., Gainetdinov, R. R., Caron, M. G. and Koller, B. H. (1999) 'Mice with reduced NMDA receptor expression display behaviors related to schizophrenia', *Cell*, 98(4), pp. 427-436.

Monyer, H., Burnashev, N., Laurie, D. J., Sakmann, B. and Seeburg, P. H. (1994) 'Developmental and regional expression in the rat brain and functional properties of four NMDA receptors', *Neuron*, 12(3), pp. 529-540.

Monyer, H., Sprengel, R., Schoepfer, R., Herb, A., Higuchi, M., Lomeli, H., Burnashev, N., Sakmann, B. and Seeburg, P. H. (1992) 'Heteromeric NMDA receptors: Molecular and functional distinction of subtypes', *Science*, 256(5060), pp. 1217-1221.

Moscato, E. H., Peng, X., Jain, A., Parsons, T. D., Dalmau, J. and Balice-Gordon, R. J. (2014) 'Acute mechanisms underlying antibody effects in anti-N-methyl-D-aspartate receptor encephalitis', *Ann Neurol*, 76(1), pp. 108-19.

Nakazawa, K., Sun, L. D., Quirk, M. C., Rondi-Reig, L., Wilson, M. A. and Tonegawa, S. (2003) 'Hippocampal CA3 NMDA Receptors are crucial for memory acquisition of one-time experience', *Neuron*, 38, pp. 305-315.

Niewoehner, B., Single, F. N., Hvalby, O., Jensen, V., Meyer zum Alten Borgloh, S., Seeburg, P. H., Rawlins, J. N., Sprengel, R. and Bannerman, D. M. (2007) 'Impaired spatial working memory but spared spatial reference memory following functional loss of NMDA receptors in the dentate gyrus', *Eur J Neurosci*, 25(3), pp. 837-46.

Nokura, K., Yamamoto, H., Okawara, Y., Koga, H., Osawa, H. and Sakai, K. (1997) 'Reversible limbic encephalitis caused by ovarian teratoma', *Acta Neurol Scand*, 95(6), pp. 367-73.

Nong, Y., Huang, Y.-Q., Ju, W., Kalia, L. V., Ahmadian, G., Wang, Y. T. and Salter, M. W. (2003) 'Glycine binding primes NMDA receptor internalization', *Nature*, 422(6929), pp. 302-307.

NyÍri, G., Stephenson, F. A., Freund, T. F. and Somogyi, P. (2003) 'Large variability in synaptic n-methyl-d-aspartate receptor density on interneurons and a comparison with pyramidal-cell spines in the rat hippocampus', *Neuroscience*, 119(2), pp. 347-363.

O'Hear, C. and Foote, J. (2006) 'Antibody Buffering in the Brain', *Journal of Molecular Biology*, 364(5), pp. 1003-1009.

Okamura, H., Oomori, N. and Uchitomi, Y. (1997) 'An acutely confused 15-year-old girl', *Lancet*, 350(9076), p. 488.

Okun, E., Mattson, M. P. and Arumugam, T. V. (2010) 'Involvement of Fc receptors in disorders of the central nervous system', *Neuromolecular Med*, 12(2), pp. 164-78.

Pantev, C., Makeig, S., Hoke, M., Galambos, R., Hampson, S. and Gallen, C. (1991) 'Human auditory evoked gamma-band magnetic fields', *Proc Natl Acad Sci U S A*, 88(20), pp. 8996-9000.

Parwani, A., Duncan, E. J., Bartlett, E., Madonick, S. H., Efferen, T. R., Rajan, R., Sanfilipo, M., Chappell, P. B., Chakravorty, S., Gonzenbach, S., Ko, G. N. and Rotrosen, J. P. (2000) 'Impaired prepulse inhibition of acoustic startle in schizophrenia', *Biol Psychiatry*, 47(7), pp. 662-9.

Penfield, W. (1947) 'Some observations on the cerebral cortex of man', *Proc R Soc Lond B Biol Sci*, 134(876), pp. 329-47.

Pettingill, P. (2013) *Investigating the pathogenic effects of antibodies against the Voltage-Gated-Potassium-Channel-complex and N-methyl-D-aspartate receptor in CSN disorders*. Universoty of Oxford.

Pietersen, A. N., Lancaster, D. M., Patel, N., Hamilton, J. B. and Vreugdenhil, M. (2009) 'Modulation of gamma oscillations by endogenous adenosine through A1 and A2A receptors in the mouse hippocampus', *Neuropharmacology*, 56(2), pp. 481-92.

Planaguma, J., Haselmann, H., Mannara, F., Petit-Pedrol, M., Grunewald, B., Aguilar, E., Ropke, L., Martin-Garcia, E., Titulaer, M. J., Jercog, P., Graus, F., Maldonado, R., Geis, C. and Dalmau, J. (2016) 'Ephrin-B2 prevents N-methyl-D-aspartate receptor antibody effects on memory and neuroplasticity', *Ann Neurol*, 80(3), pp. 388-400.

Planagumà, J., Leypoldt, F., Mannara, F., Gutiérrez-Cuesta, J., Martín-García, E., Aguilar, E., Titulaer, M. J., Petit-Pedrol, M., Jain, A., Balice-Gordon, R., Lakadamyali, M., Graus, F., Maldonado, R. and Dalmau, J. (2014) 'Human N-methyl D-aspartate receptor antibodies alter memory and behaviour in mice', *Brain*.

Pouille, F. and Scanziani, M. (2001) 'Enforcement of temporal fidelity in pyramidal cells by somatic feed-forward inhibition', *Science*, 293(5532), pp. 1159-63.

Pozo-Rosich, P., Clover, L., Saiz, A., Vincent, A. and Graus, F. (2003) 'Voltage-gated potasssium channel antibodies in limbic encephalitis', *Annals of Neurology*, 54, pp. 530-533.

Quilichini, P., Sirota, A. and Buzsaki, G. (2010) 'Intrinsic circuit organization and theta-gamma oscillation dynamics in the entorhinal cortex of the rat', *J Neurosci*, 30(33), pp. 11128-42.

Reiber, H. (1998) 'Cerebrospinal fluid--physiology, analysis and interpretation of protein patterns for diagnosis of neurological diseases', *Mult Scler*, 4(3), pp. 99-107.

Rodriguez, E., George, N., Lachaux, J.-P., Martinerie, J., Renault, B. and Varela, F. J. (1999) 'Perception's shadow: long-distance synchronization of human brain activity', *Nature*, 397, pp. 430-433.

Roopun, A. K., Cunningham, M. O., Racca, C., Alter, K., Traub, R. D. and Whittington, M. A. (2008) 'Region-specific changes in gamma and beta2

rhythms in NMDA receptor dysfunction models of schizophrenia', *Schizophr Bull*, 34(5), pp. 962-973.

Roopun, A. K., Middleton, S. J., Cunningham, M. O., LeBeau, F. E., Bibbig, A., Whittington, M. A. and Traub, R. D. (2006) 'A beta2-frequency (20-30 Hz) oscillation in nonsynaptic networks of somatosensory cortex', *Proc Natl Acad Sci U S A*, 103(42), pp. 15646-50.

Rosenmund, C., Feltz, A. and Westbrook, G. L. (1995) 'Synaptic NMDA receptor channels have a low open probability', *J Neurosci*, 15(4), pp. 2788-95.

Rubio-Agustí, I., Dalmau, J., Sevilla, T., Burgal, M., Beltrán, E. and Bataller, L. (2011) 'Isolated hemidystonia associated with NMDA receptor antibodies', *Movement Disorders*, 26(2), pp. 351-352.

Rujescu, D., Bender, A., Keck, M., Hartmann, A. M., Ohl, F., Raeder, H., Giegling, I., Genius, J., McCarley, R. W., Moller, H. J. and Grunze, H. (2006) 'A pharmacological model for psychosis based on N-methyl-D-aspartate receptor hypofunction: molecular, cellular, functional and behavioral abnormalities', *Biol Psychiatry*, 59(8), pp. 721-9.

Saadoun, S., Waters, P., Bell, B. A., Vincent, A., Verkman, A. S. and Papadopoulos, M. C. (2010) *Intra-cerebral injection of neuromyelitis optica immunoglobulin G and human complement produces neuromyelitis optica lesions in mice*.

Sansing, L. H., Tüzün, E., Ko, M. W., Baccon, J., Lynch, D. R. and Dalmau, J. (2007) 'A patient with encephalitis associated with NMDA receptor antibodies', *Nature Clinical Practice Neurology*, 3(5), pp. 291-296.

Schulte, U., Thumfart, J.-O., Klöcker, N., Sailer, C. A., Bildl, W., Biniossek, M., Dehn, D., Deller, T., Eble, S., Abbass, K., Wangler, T., Knaus, H.-G. and Fakler, B. (2006) 'The Epilepsy-Linked Lgi1 Protein Assembles into Presynaptic Kv1 Channels and Inhibits Inactivation by Kvβ1', *Neuron*, 49(5), pp. 697-706.

Sederberg, P. B., Schulze-Bonhage, A., Madsen, J. R., Bromfield, E. B., McCarthy, D. C., Brandt, A., Tully, M. S. and Kahana, M. J. (2007) 'Hippocampal and neocortical gamma oscillations predict memory formation in humans', *Cereb Cortex*, 17(5), pp. 1190-6.

Seki, M., Suzuki, S., Iizuka, T., Shimizu, T., Nihei, Y., Suzuki, N. and Dalmau, J. (2008) 'Neurological response to early removal of ovarian teratoma in anti-NMDAR encephalitis', *J Neurol Neurosurg Psychiatry*, 79(3), pp. 324-6.

Sillevis Smitt, P., Kinoshita, A., De Leeuw, B., Moll, W., Coesmans, M., Jaarsma, D., Henzen-Logmans, S., Vecht, C., De Zeeuw, C., Sekiyama, N., Nakanishi, S. and Shigemoto, R. (2000) 'Paraneoplastic cerebellar ataxia due to autoantibodies against a glutamate receptor', *N Engl J Med*, 342(1), pp. 21-7.

Simeone, T. A., Simeone, K. A., Samson, K. K., Kim, D. Y. and Rho, J. M. (2013) 'Loss of the K(v)1.1 potassium channel promotes pathologic sharp waves and high frequency oscillations in in vitro hippocampal slices', *Neurobiology of disease*, 54, pp. 68-81.

Singer, W. (2001) 'Consciousness and the binding problem', *Ann N Y Acad Sci*, 929, pp. 123-46.

Singer, W. and Gray, C. M. (1995) 'Visual feature integration and the temporal correlation hypothesis', *Annual Review of Neuroscience*, 18, pp. 555-586.

Sohal, V. S., Zhang, F., Yizhar, O. and Deisseroth, K. (2009) 'Parvalbumin neurons and gamma rhythms enhance cortical circuit performance', *Nature*, 459(7247), pp. 698-702.

Spencer, K. M., Nestor, P. G., Perlmutter, R., Niznikiewicz, M. A., Klump, M. C., Frumin, M., Shenton, M. E. and McCarley, R. W. (2004) 'Neural synchrony indexes disordered perception and cognition in schizophrenia', *Proc Natl Acad Sci U S A*, 101(49), pp. 17288-93.

Squire, L. R. (2009) 'The Legacy of Patient H.M. for Neuroscience', *Neuron*, 61(1), pp. 6-9.

Steffenach, H. A., Witter, M., Moser, M. B. and Moser, E. I. (2005) 'Spatial memory in the rat requires the dorsolateral band of the entorhinal cortex', *Neuron*, 45(2), pp. 301-13.

Steiner, J., Teegen, B., Schiltz, K., Bernstein, H. G., Stoecker, W. and Bogerts, B. (2014) 'Prevalence of N-methyl-D-aspartate receptor autoantibodies in the peripheral blood: healthy control samples revisited', *JAMA Psychiatry*, 71(7), pp. 838-9.

Steiner, J., Walter, M., Glanz, W., Sarnyai, Z., Bernstein, H. G., Vielhaber, S., Kastner, A., Skalej, M., Jordan, W., Schiltz, K., Klingbeil, C., Wandinger, K. P., Bogerts, B. and Stoecker, W. (2013) 'Increased prevalence of diverse N-methyl-D-aspartate glutamate receptor antibodies in patients with an initial diagnosis of schizophrenia: specific relevance of IgG NR1a antibodies for distinction from N-methyl-D-aspartate glutamate receptor encephalitis', *JAMA Psychiatry*, 70(3), pp. 271-8.

Steriade, M., Contreras, D., Curro Dossi, R. and Nunez, A. (1993) 'The slow (< 1 Hz) oscillation in reticular thalamic and thalamocortical neurons: scenario of sleep rhythm generation in interacting thalamic and neocortical networks', *J Neurosci*, 13(8), pp. 3284-99.

Strüber, M., Jonas, P. and Bartos, M. (2015) 'Strength and duration of perisomatic GABAergic inhibition depend on distance between synaptically connected cells', *Proceedings of the National Academy of Sciences of the United States of America*, 112(4), pp. 1220-1225.

Sun, Y., Olson, R., Horning, M., Armstrong, N., Mayer, M. and Gouaux, E. (2002) 'Mechanism of glutamate receptor desensitization', *Nature*, 417(6886), pp. 245-53.

Tallon-Baudry, C. and Bertrand, O. (1999) 'Oscillatory gamma activity in humans and its role in object representation', *Trends in Cognitive Sciences*, 3(4), pp. 151-162.

Tallon-Baudry, C., Kreiter, A. and Bertrand, O. (1999) 'Sustained and transient oscillatory responses in the gamma and beta bands in a visual short-term memory task in humans', *Visual Neuroscience*, 16(03), pp. 449-459.

Taylor, R. B., Mason, W., Kong, K. and Wennberg, R. (1999) 'Reversible paraneoplastic encephalomyelitis associated with a benign ovarian teratoma', *Can J Neurol Sci*, 26(4), pp. 317-20.

Thieben, M. J., Lennon, V. A., Boeve, B. F., Aksamit, A. J., Keegan, M. and Vernino, S. (2004) 'Potentially reversible autoimmune limbic encephalitis with neuronal potassium channel antibody', *Neurology*, 62, pp. 1177-1182.

Thomas, A., Rauschkolb, P., Gresa-Arribas, N., Schned, A., Dalmau, J. O. and Fadul, C. E. (2013) 'Anti-N-methyl-D-aspartate receptor encephalitis: a patient with refractory illness after 25 months of intensive immunotherapy', *JAMA Neurology*, 70(12), pp. 1566-8.

Tiitinen, H., Sinkkonen, J., Reinikainen, K., Alho, K., Lavikainen, J. and Näätänen, R. (1993) 'Selective attention enhances the auditory 40-Hz transient response in humans', *Nature*, 364, pp. 59-60.

Titulaer, M. J., McCracken, L., Gabilondo, I., Armangué, T., Glaser, C., Iizuka, T., Honig, L. S., Benseler, S. M., Kawachi, I., Martinez-Hernandez, E., Aguilar, E., Gresa-Arribas, N., Ryan-Florance, N., Torrents, A., Saiz, A., Rosenfeld, M. R., Balice-Gordon, R., Graus, F. and Dalmau, J. (2013) 'Treatment and prognostic factors for long-term outcome in patients with anti-NMDA receptor encephalitis: an observational cohort study', *The Lancet Neurology*, 12(2), pp. 157-165.

Tonomura, Y., Kataoka, H., Hara, Y., Takamure, M., Naba, I., Kitauti, T., Saito, K. and Ueno, S. (2007) 'Clinical analysis of paraneoplastic encephalitis associated with ovarian teratoma', *Journal of Neuro-Oncology*, 84(3), pp. 287-292.

Traub, R. D., Cunningham, M. O., Gloveli, T., LeBeau, F. E., Bibbig, A., Buhl, E. H. and Whittington, M. A. (2003) 'GABA-enhanced collective behavior in neuronal axons underlies persistent gamma-frequency oscillations', *Proc Natl Acad Sci U S A*, 100(19), pp. 11047-52.

Traub, R. D., Jefferys, J. G. R. and Whittington, M. A. (1997) 'Simulation of gamma rhythms in networks of interneurons and pyramidal cells', *Journal of Computational Neuroscience*, 4(2), pp. 141-150.

Traub, R. D., Whittington, M. A., Buhl, E. H., LeBeau, F. E., Bibbig, A., Boyd, S., Cross, H. and Baldeweg, T. (2001) 'A possible role for gap junctions in generation of very fast EEG oscillations preceding the onset of, and perhaps initiating, seizures', *Epilepsia*, 42(2), pp. 153-70.

Tsien, J. Z., Huerta, P. T. and Tonegawa, S. (1996) 'The essential role of hippocampal CA1 NMDA receptor-dependent synaptic plasticity in spatial memory', *Cell*, 87, pp. 1327-1338.

Turkdogan, D., Orengul, A. C., Zaimoglu, S. and Ekinci, G. 'Anti-N-methyl-d-aspartate (Anti-NMDA) receptor encephalitis: rapid and sustained clinical improvement with steroid therapy starting in the late phase', *Journal of Child Neurology*, 29(5), pp. 684-7.

Tuzun, E., Zhou, L., Baehring, J. M., Bannykh, S., Rosenfeld, M. R. and Dalmau, J. (2009) 'Evidence for antibody-mediated pathogenesis in anti-NMDAR encephalitis associated with ovarian teratoma', *Acta Neuropathol*, 118(6), pp. 737-43.

Uhlhaas, P. J., Haenschel, C., Nikolic, D. and Singer, W. (2008) 'The role of oscillations and synchrony in cortical networks and their putative relevance for the pathophysiology of schizophrenia', *Schizophr Bull*, 34(5), pp. 927-43.

van Strien, N. M., Cappaert, N. L. and Witter, M. P. (2009) 'The anatomy of memory: an interactive overview of the parahippocampal-hippocampal network', *Nat Rev Neurosci*, 10(4), pp. 272-82.

Vincent, A. (2002) 'Unravelling the pathogenesis of myasthenia gravis', *Nat Rev Immunol*, 2(10), pp. 797-804.

Vincent, A. and Bien, C. G. (2008) 'Anti-NMDA-receptor encephalitis: a cause of psychiatric, seizure, and movement disorders in young adults', *The Lancet Neurology*, 7, pp. 1074-1075.

Vincent, A., Buckley, C., Schott, J. M., Baker, I., Dewar, B.-K., Detert, N., Clover, L., Parkinson, A., Bien, C. G., Omer, S., Lang, B., Rossor, M. N. and Palace, J. (2004) 'Potassium channel antibody-associated encephalopathy: a potentially immunotherapy-responsive form of limbic encephalitis', *Brain*, 127, pp. 701-712.

Vismer, M. S., Forcelli, P. A., Skopin, M. D., Gale, K. and Koubeissi, M. Z. (2015) 'The piriform, perirhinal, and entorhinal cortex in seizure generation', *Front Neural Circuits*, 9, p. 27.

Vitaliani, R., Mason, W., Ances, B., Zwerdling, T., Jiang, Z. and Dalmau, J. (2005) 'Paraneoplastic encephalitis, psychiatric symptoms, and hypoventilation in ovarian teratoma', *Annals of Neurology*, 58(4), pp. 594-604.

Voltz, R. (2002) 'Paraneoplastic neurological syndromes: an update on diagnosis, pathogenesis, and therapy', *The Lancet Neurology*, 1(5), pp. 294-305.

Wandinger, K. P., Saschenbrecker, S., Stoecker, W. and Dalmau, J. (2011) 'Anti-NMDA-receptor encephalitis: a severe, multistage, treatable disorder presenting with psychosis', *J Neuroimmunol*, 231(1-2), pp. 86-91.

Wang, H. X. and Gao, W. J. (2009) 'Cell type-specific development of NMDA receptors in the interneurons of rat prefrontal cortex', *Neuropsychopharmacology*, 34(8), pp. 2028-40.

Wasterlain, C. G., Naylor, D. E., Liu, H., Niquet, J. and Baldwin, R. (2013) 'Trafficking of NMDA Receptors During Status Epilepticus: Therapeutic Implications', *Epilepsia*, 54(0 6), pp. 78-80.

Waxman, E. A. and Lynch, D. R. (2005) 'N-methyl-D-aspartate receptor subtypes: multiple roles in excitotoxicity and neurological disease', *Neuroscientist*, 11(1), pp. 37-49.

Whittington, M., Traub, R. D. and Jefferys, J. G. R. (1995) 'Synchronized Oscillations in Interneuron Networks Driven by Metabotropic Glutamate Receptor Activation', *Nature*, 373, pp. 612-615.

Wilcock, D. M., DiCarlo, G., Henderson, D., Jackson, J., Clarke, K., Ugen, K. E., Gordon, M. N. and Morgan, D. (2003) 'Intracranially administered anti-Abeta antibodies reduce beta-amyloid deposition by mechanisms both independent of and associated with microglial activation', *J Neurosci*, 23(9), pp. 3745-51.

Wiltgen, B. J., Brown, R. A., Talton, L. E. and Silva, A. J. (2004) 'New circuits for old memories: the role of the neocortex in consolidation', *Neuron*, 44(1), pp. 101-8.

Witter, M. P. and Moser, E. I. (2006) 'Spatial representation and the architecture of the entorhinal cortex', *Trends Neurosci*, 29(12), pp. 671-8.

Wolak, D. J., Pizzo, M. E. and Thorne, R. G. (2015) 'Probing the extracellular diffusion of antibodies in brain using in vivo integrative optical imaging and ex vivo fluorescence imaging', *Journal of Controlled Release*, 197(0), pp. 78-86.

Wolak, D. J. and Thorne, R. G. (2013) 'Diffusion of macromolecules in the brain: implications for drug delivery', *Mol Pharm*, 10(5), pp. 1492-504.

Wright, S., Hacohen, Y., Jacobson, L., Agrawal, S., Gupta, R., Philip, S., Smith, M., Lim, M., Wassmer, E. and Vincent, A. (2015a) 'N-methyl-D-aspartate receptor antibody-mediated neurological disease: results of a UK-based surveillance study in children', *Arch Dis Child*, 100(6), pp. 521-6.

Wright, S., Hashemi, K., Pettingill, P., Lang, B., Vincent, A. and Upton, L. (2014) 'Poster 98: Autoantibodies to the N-methyl-D-aspartate receptor and seizure susceptibility in mice', *The Lancet*.

Wright, S., Hashemi, K., Stasiak, L., Bartram, J., Lang, B., Vincent, A. and Upton, L. (2015b) 'Epileptogenic effects of NMDAR-antibodies in a passive transfer mouse model', *Brain*, November, *In Press*.

Wulff, P., Ponomarenko, A. A., Bartos, M., Korotkova, T. M., Fuchs, E. C., Bahner, F., Both, M., Tort, A. B., Kopell, N. J., Wisden, W. and Monyer, H. (2009) 'Hippocampal theta rhythm and its coupling with gamma oscillations require fast inhibition onto parvalbumin-positive interneurons', *Proc Natl Acad Sci U S A*, 106(9), pp. 3561-6.

Yu, Y. E., Wen, L., Silva, J., Li, Z., Head, K., Sossey-Alaoui, K., Pao, A., Mei, L. and Cowell, J. K. (2010) 'Lgi1 null mutant mice exhibit myoclonic seizures and CA1 neuronal hyperexcitability', *Human Molecular Genetics*.

Zandi, M. S., Irani, S. R., Lang, B., Waters, P., Jones, P. B., McKenna, P., Coles, A. J., Vincent, A. and Lennox, B. R. (2011) 'Disease-relevant autoantibodies in first episode schizophrenia', *Journal of Neurology*, 258(4), pp. 686-688.

Zandi, M. S., Paterson, R. W., Ellul, M. A., Jacobson, L., Al-Diwani, A., Jones, J. L., Cox, A. L., Lennox, B., Stamelou, M., Bhatia, K. P., Schott, J. M., Coles, A. J., Kullmann, D. M. and Vincent, A. (2015) 'Clinical relevance of serum antibodies to extracellular N-methyl-D-aspartate receptor epitopes', *J Neurol Neurosurg Psychiatry*, 86(7), pp. 708-13.

Zhang, Q., Tanaka, K., Sun, P., Nakata, M., Yamamoto, R., Sakimura, K., Matsui, M. and Kato, N. (2012) 'Suppression of synaptic plasticity by cerebrospinal fluid from anti-NMDA receptor encephalitis patients', *Neurobiol Dis*, 45(1), pp. 610-615.

Zhang, Y. and Pardridge, W. M. (2001) 'Mediated efflux of IgG molecules from brain to blood across the blood-brain barrier', *J Neuroimmunol*, 114(1-2), pp. 168-72.

Zhang, Z. J. and Reynolds, G. P. (2002) 'A selective decrease in the relative density of parvalbumin-immunoreactive neurons in the hippocampus in schizophrenia', *Schizophr Res*, 55(1-2), pp. 1-10.

Zola-Morgan, S., Squire, L. R. and Ramus, S. J. (1994) 'Severity of memory impairment in monkeys as a function of locus and extent of damage within the medial temporal lobe memory system', *Hippocampus*, 4(4), pp. 483-95.